N° d'ordre: 40909

UNIVERSITÉ LILLE 1 SCIENCES ET TECHNOLOGIES

THÈSE

Présentée à

L'ÉCOLE DOCTORALE SCIENCES POUR L'INGÉNIEUR

Spécialité Micro et Nanotechnologies, Acoustique et Télécommunications

par

Chang Wu

Dispositif microfluidique utilisant la technologie d'électromouillage sur isolant dédié à la préparation d'échantillons pour des analyses biologiques : Application au suivi en ligne de bioprocédés

soutenue publiquement le 23 Novembre 2012

Rapporteur	Mme. Anne-Marie Gué	Directeur de Recherche CNRS, LAAS, Toulouse
Rapporteur	Mr. Tijani Gharbi	Professeur, Université de Franche-Comté, Besançon
Examinateur	Mr. Tuami Lasri	Professeur, Université de Lille 1, Lille
Examinateur	Mr. Frédéric Reymond	General Manager, DiagnoSwiss S.A., Monthey
Examinateur	Mr. Rénato Froidevaux	Maitre de conférences, HDR, Université de Lille 1, Lille
Directeur de thèse	Mr. Vincent Senez	Directeur de Recherche CNRS, IEMN, Lille

ACKNOWLEDGEMENT

First and foremost, I would like to thank my supervisor, ***Vincent Senez*** for his scientific and academic guidance through my graduate studies. You always challenged me to be passionate, positive and hardworking. Thank you very much for regular work discussions and for helping me in writing the articles and thesis. I would like to thank you for the numerous opportunities to share my work at international conferences and collaborate with other research groups in the NANOBE project.

I would like to thank ***Farida Bendriaa*** who is my technology advisor. Thank you for helping me in the cleanroom work and in the fabrication problems solving. I am also grateful to ***Vincent Thomy*** for his very fruitful discussions about EWOD characterization. You gave me a lot of active suggestions in the research.

Many thanks to ***Maxime Harnois*** for his technical advices with fabrications, his assistance in building the valve control and experimental platform set up. I really appreciate your suggestions for my research during our discussions. Thank you for your continuous encouragement and help in completing the challenging NANOBE project.

I would especially like to thank ***Thomas Borel*** for his assistance in building the EWOD program and ***François Brunelle*** for his kind assistance with reagent preparation. Special thanks also go to ***Florian Lapierre*** for his help in image analysis by Image J software and valuable advices. I would also like to thank ***Xianglei Han*** for his exceptional skills with SEM.

I would like to thank all colleagues in BioMEMS group who make my work and life a wonderful memory: ***Alexis Vlandas***, ***Anthony Treizebré***, ***Timothée Houssin***, ***Damien Debuisson***, ***Florian Lapierre***, ***Thi Phuong Nhung Nguyen***, ***Romuald Lejard***, ***Magalie De Ville***, ***François Brunelle***, ***Guillaume Perry***, ***Renaud Dufour***, ***Simon Laurette***, ***Alfred Dibao-Dina***, ***Sebastien Lamant***, and ***Alain Agboton***.

I would like to thank you all the partners in NANOBE project:

a) VTT: ***Juha-Pekka Pitkänen***, ***Päivi Heimala***, ***Sami Holmstrom***

b) Galilaeus: ***Ari Batsman***

c) IBA: ***Karen Lemke***, ***Andreas Grodrian***, ***Robert Roemer***;

d) IMTEK: ***Junichi Miwa***;

e) Presens: ***Christian Krause***

f) Microsaic: ***Peter Edwards***;

g) Diagnoswiss: ***Frédéric Reymond***, ***Christine Vollet***;

h) EPFL: ***Harald van Lintel***, ***Guillaume Mernier***;

I would like to thank all the friends at IEMN, who help me a lot and shared a lot of joyful time together. I would also like to thank the engineers at IEMN for their help and technology support.

I would like to acknowledge the members of my Ph.D. committee, ***Anne-Marie Gué***, ***Tijani Gharbi***, ***Tuami Lasri***, ***Frédéric Reymond***, and ***Rénato Froidevaux***, for their comments and valuable advices. Special thanks to Dr ***Anne-Marie Gué*** and Professor ***Tijani Gharbi***, for reviewing my thesis and providing me with useful guidance. Thanks to Professor ***Alain Cappy***, former IEMN director and Dr ***Lionel Buchaillot***, current IEMN director for their authorization to work in the laboratory at IEMN.

My acknowledgement goes to the China Scholarship Council (CSC) from China Government for the scholarship support. My acknowledgement also goes to E.U. (FP7) which supports the NANOBE project n°227243 (nano and microtechnology based analytical devices for online measurements of bioprocesses).

Finally and most importantly, I would like to thank my parents (***Zhengyong Wu*** and ***Xiaobin Wang***) and my husband (***Xianglei Han***) for their endless love, support and encouragement.

CONTENT

CONTENT

GENERAL INTRODUCTION

1. Motivation of this thesis

The rapid development in biotechnology during the last few years is enhanced by progress in genetic engineering, and the advancement of bioprocess monitoring will play a crucial role to meet the future requirements of bioprocess technology [1][2]. The increasing number of production organisms and bioprocesses sets demands for fast and versatile product measurement tools. The aim of the NANOBE project (n°227243 supported by the E.U. (FP7)) is to construct a versatile tool for real-time analysis of several compounds and biomarker in bioreactor processes. This thesis is aiming at developing a microfluidic tool for the preparation of intra/extra cellular compounds of yeast cells before their analysis by external analytical micro-tools, which is part of NANOBE project. The tasks of this microfluidic tool (*i.e.*, sample preparation unit) include: a) automatic and continuous preload of samples, b) independent manipulation of several sample droplets, c) recombination and exportation of samples to external analysis/detection fluidic modules.

Manipulating discrete aliquots of samples and reagents on the micro-scale in active control is an emerging field, defined as digital microfluidics (DMF). With droplets, the possibility of manipulating numerous samples and reagents as individual packets becomes feasible. One common actuation method for digital microfluidic is electrowetting-on-dielectric (EWOD) where an electric field can control the wettability of liquids on a dielectric solid surface [3][4][5][6]. EWOD technique can allow precise control of multiple reagents without the need of a complex network of micro-valves. This method facilitates the integration of numerous elemental fluidic operations (transporting, merging, mixing and splitting) by programming electrodes. Its programmable and reconfigurable architecture permits maximum operational flexibility. Thus, the sample preparation unit integrated in the NANOBE system uses EWOD technology to control the displacement of droplets. However, EWOD technology suffers from

the lack of continuous-supply of reagents and the impossibility to export sample in continuous flow format. To address this issue, it is a desirable goal to integrate inlet/outlet interfaces on EWOD-based device to couple with external fluidic modules. To achieve the sample preparation unit, our work joins a small group of studies that have combine micro-channels and EWOD-based digital microfluidics in a single chip. This method put forward a new flexible plan toward fully integrated on-line sample preparation and off-chip post-processing.

2. Aim of this thesis

The aim of this thesis is comprised of three major tasks.

The first part of this thesis is to understand the opportunities and limitations of EWOD-based DMF system, and focus on stating the desirable need for development of interfaces coupled to external fluidic modules. We present the classification and point out the important of inlet and outlet interface integration on EWOD chip. Based on the integrated level of the interfaces, our classification distinguishes between inlet interface integration, outlet interface integration, and full interfaces integration. It contains examples which are selected as fitting to our proposed classification. The aim is to illustrate the many efforts in struggling the compatibility of EWOD-based DMF chip with interfaces for complex biomedical applications. Among them, the full interfaces integration can fully automatically process the required operations from the sample loading to the sample detection. This method allows to reducing dead volume and thus the volume of the sample is reduced. Full interfaces integration is subdivided into fully integrated hybrid EWOD chip (with on-chip detection/analysis) and fully integrated sample preparation unit (with off-chip detection/analysis). High-levels of integration and automation have been realized in fully integrated hybrid EWOD chip. However, due to the special design, the scope of applications is limited. While, fully integrated sample preparation unit works as a central fluid transceiver module in an integrated system. This method put forward a new flexible plan toward fully integrated on-line sample preparation and off-chip post-processing.

The second part of this thesis is aiming at developing a fully integrated sample preparation

unit. The accomplishment of this device is stated, from concept to a proof-of-concept. We develop two generations of microfluidics devices based on combining the EWOD functionalities and channel-based continuous microfluidic technique: (a) 'AD/DA microfluidics converter' with a three layers PSP (Pyrex-Silicon-Pyrex) configuration, and (b) 'Sample Preparation Unit' with a bilayer PS (Pyrex-Silicon) configuration. In our first work, a three layers PSP (Pyrex-Silicon-Pyrex) configuration with hydrophobic liquid-solid interfaces is employed. The fabrication is based on deep reactive ion etching of silicon and low temperature full wafer adhesive bonding. It is believed that the fabrication technology can be used in diverse MEMS applications. However, our preliminary device suffers from a key limitation: the difficulty in droplet formation. To address this limitation, we develop a new sample preparation unit with a bilayer PS (Pyrex-Silicon) configuration with superhydrophobic liquid-solid interfaces. A method of silicon nanostructures (SiNSs) surface fabrication using chemical modification of silicon wafer is employed to realize the superhydrophobic top plate. In our second design, the fundamental fluid operations (droplet formation, transport, merging and mixing, and delivery) are validated. We discuss about several parameters that are critical for droplet formation and for accurate droplet volume tuning. Besides, high speed camera technique is used to observe water droplet transport, which is very useful for the displacement and velocity study of the receding and advancing edge.

In the third part of this thesis, the sample preparation unit is used for real-time analysis of several compounds and biomarker in online bioreactor processes. First, a short introduction on the motivation and scope of the NANOBE project is given. With the help of sample preparation unit, the advantage of 'digital' preconditioning can allow individual control of multiple reagents without the need of a complex network of micro-valves, and the reprocessed 'continuous' format makes it ideal for interfacing to downstream analytical and detection instruments (ELISA and coupling CE-MS module). As in the central part of the whole integrated system, sample preparation unit is a key module which affects the success rate of the complete operation of the integrated system. Thus, the first period work is to validate the

sample preparation unit by using real samples needed in the final integrated test, including the movement feasibility and fluid operations. The operation procedures controlled by our homemade LabVIEW program is described. Then, coupling tests between the sample preparation unit and other fluidic modules are presented. Finally, full analysis test cycles are carried out with the integrated system.

3. Outline of this thesis

The development of EWOD-based digital microfluidics has been stated in the **Chapter 1**, including EWOD theory, principle, fluidic operations and configurations. The significances of inlet/outlet interfaces developments to couple EWOD chip with external fluidic modules are pointed out and the classifications are presented. It contains examples which are selected as fitting to our proposed classification.

Chapter 2 represents experimental methodology used. We developed two generations of microfluidics devices, 'AD/DA microfluidics converter' and 'Sample Preparation Unit'. Details concern the device design and fabrication. The material presented in this chapter has been published in *Microelectronic Engineering 88 (2011) 1878–1883*.

Chapter 3 proposes the 'Sample Preparation Unit' used in NANOBE integrated system for online bioprocesses monitoring. The material presented in this chapter has been published in *15th International Conference on Miniaturized Systems for Chemistry and Life Sciences in Seattle in 2011 (micro-TAS)* and *the 25th International Conference on Micro Electro Mechanical Systems in Paris in 2012 (IEEE MEMS)*.

The overall summary and outlook are presented in **Conclusion and Perspective**. The detailed experimental process documents and LabVIEW program guide are included in **Appendix**.

References

[1] K. Schügerl, "Progress in monitoring, modeling and control of bioprocesses during the last 20 years", *Journal of Biotechnology*, vol. 85, pp. 149–173, 2001.

[2] F. Clementschitsch and K. Bayer, "Improvement of bioprocess monitoring: development of novel concepts", *Microb Cell Fact*, vol. 5, no. 19, pp. 1–11, 2006.

[3] S.-Y. Teh, R. Lin, L.-H. Hung, and A. P. Lee, "Droplet microfluidics", *Lab Chip*, vol. 8, pp. 198–220, 2008.

[4] R. B. Fair, "Digital microfluidics: is a true lab-on-a-chip possible?", *Microfluidics and Nanofluidics*, vol. 3, pp. 245–281, 2007.

[5] M. Abdelgawad and A. R. Wheeler, "The Digital Revolution: A New Paradigm for Microfluidics", *Advanced Materials*, vol. 21, pp. 920–925, 2009.

[6] M. J. Jebrail and A. R. Wheeler, "Let's get digital: digitizing chemical biology with microfluidics", *Current Opinion in Chemical Biology*, vol. 14, pp. 574–581, 2010.

1. DEVELOPMENT OF EWOD-BASED DIGITAL MICROFLUIDICS

Content

1.1. Microfluidics development

Microfluidics is a multidisciplinary field intersecting engineering, physics, chemistry, micro-technology and biotechnology. In approximately two decades, the development of microfluidics has been a steady increase in its interest and development by the scientific and industrial communities. Microfluidics is established very well in academia and industry as a toolbox which has given rise to the development of new methods and products from chemical synthesis and biological analysis to optics and information technology [1][2][3][4]. Microfluidic technology holds great promise as it can perform typical laboratory operations using a fraction of the volume of reagents in significantly less time [5].

The revolution of microfluidics is illustrated in **Figure 1.1**. At the really beginning, microfluidics was continuous-flow microfluidics (CMF). CMF is based on the manipulation of continuous liquid flow through channels, where actuation of liquid flow is implemented either by external pressure sources, external mechanical pumps, integrated mechanical micro-pumps, or by combinations of capillary forces and electrokinetic mechanisms [6][7]. Continuous-flow devices are adequate for many well-defined and simple biochemical applications [8] (*e.g.*, chemical separation), but these closed-channel systems are inherently difficult to integrate and scale. Scaling up is a big challenge for CMF as the size of devices scales almost linearly with the number of parallel experiments.

Therefore, an alternative approach (*i.e.*, discrete microfluidics) that enables manipulation of discrete droplets is currently developed. It classified into two types, channel-based droplet microfluidics and surface-based digital microfluidics. First attempt of discrete microfluidics was droplet-based microfluidics, which focuses on creating and transporting discrete volumes in a continuous flow with the use of immiscible phases through closed microchannels [5][9][10]. However, its one-dimension simultaneous motion and passive pressure driven model are yet match the need for complex multifunction operations. To address this issue, surface-based digital microfluidics (DMF) has emerged, where droplets are actuated by surface acoustic wave (SAW) or electrowetting-on-dielectric (EWOD) technique. The surface-based digital microfluidics comes up with a high flexibility since liquid processing

can be freely programmed. SAW technology transfers momentum to droplet placed on the chip. The SAW pulse hits the droplet, leading the droplet deformation and transport. While, droplet transport driven by EWOD is due primarily to a gradient in interfacial tension between the droplet and an insulator surface. Though both SAW and EWOD techniques are programmable, there is a limit of SAW technique in individual actuation of droplets. EWOD technique can individually manipulate discrete droplet-format samples, thus it is better match for array-based biochemical applications thanks to its programmable and reconfigurable architecture [5][11][12][13].

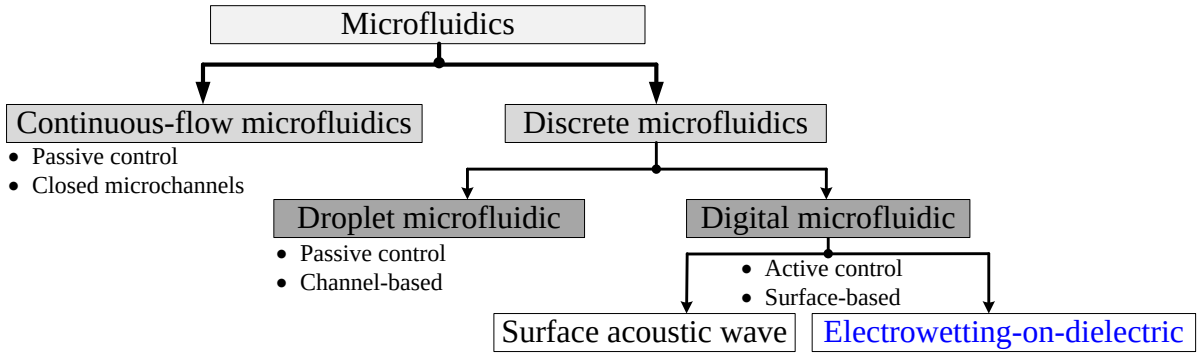

Figure 1.1 Scheme of microfluidics development.

In the following sections, the fundamentals of EWOD-based DMF system will be stated, including EWOD theory, principle, fluidic operations and configurations. Then, we will present the strengths of coupling EWOD chip with external fluidic modules. It contains examples which are selected as fitting to our proposed classification. The aim is to illustrate the many efforts in struggling the compatibility of EWOD-based DMF chip with interfaces for complex biomedical applications.

1.2. EWOD-based DMF system

1.2.1. Theoretical background

1.2.1.1. Static electrowetting

1.2.1.1.1. Lippmann-Young Law

As early as 1875, French physicist Gabriel Lippmann observed that the capillary depression of mercury in contact with electrolyte solutions could be varied in the presence of electric charges between the two liquids, and advanced the principle of electro-capillarity as described by an equation which is now called the Lippmann law [14]. More than 100 years later, Beni et al. [15] replaced the liquid mercury electrode with a solid electrode and introduced the electrowetting phenomenon. It relates to the change in solid-electrolyte contact angle by the application of a potential difference between the solid and the electrolyte. To prevent electrolysis of the liquid, Bruno Berge in the 1990s presented a configuration where the electrode was covered with a thin dielectric film on top of the electrode [16][17] and described this phenomenon which named electrowetting on dielectrics (EWOD) by the Lippmann-Young law. The Lippmann-Young law expresses the change in contact angle of a liquid as a function of applied voltage, which combined the Lippmann law with the Young law. A change in the solid-liquid apparent interfacial tension is related to the Lippmann law

$$\gamma_{SL}(V) = \gamma_{SL,0} - \frac{C}{2}V^2 \qquad \textbf{(1.1)}$$

The relationship between the surface tension and the contact angle is described in the Young law (**Equation 1.2**)

$$\gamma_{LG}\cos\theta_0 = \gamma_{SG} - \gamma_{SL,0}; \qquad \textbf{(1.2-a)}$$

$$\gamma_{LG}\cos\theta = \gamma_{SG} - \gamma_{SL}(V) \qquad \textbf{(1.2-b)}$$

By substituting the Young law (**Equation 1.2**) into the Lippmann law (**Equation 1.1**), the Lippmann-Young law is obtained

$$\cos\theta = \cos\theta_0 + \frac{C}{2\gamma_{LG}}V^2 \quad \textbf{(1.3)}$$

where θ and θ_0 are the contact angles with and without an applied potential V, respectively; γ_{SG}, γ_{SL}, γ_{LG} indicate the interfacial tension between solid/gas, solid/liquid, and liquid/gas, respectively; C is the capacitance of the dielectric layer. As described by **Equation (1.3)**, when the voltage is applied, the electric charge changes the free energy on the dielectric surface and reduces the interfacial tension, thus inducing a change in wettability on the surface and contact angle of the droplet.

A typical EWOD experimental example is shown in **Figure 1.2** [18]. It shows that: a) the relation between the contact angle θ and the applied voltage V fits the Lippman-Young Law, limited to the minimum and the maximum actuation voltage, b) contact angle saturation corresponds to the phenomenon when the electric potential is above the maximum actuation voltage there is no more gain in contact reduction, and c) contact angle hysteresis corresponds to the phenomenon when the electric potential is beyond the minimum actuation voltage the contact angle becomes independent of the applied voltage.

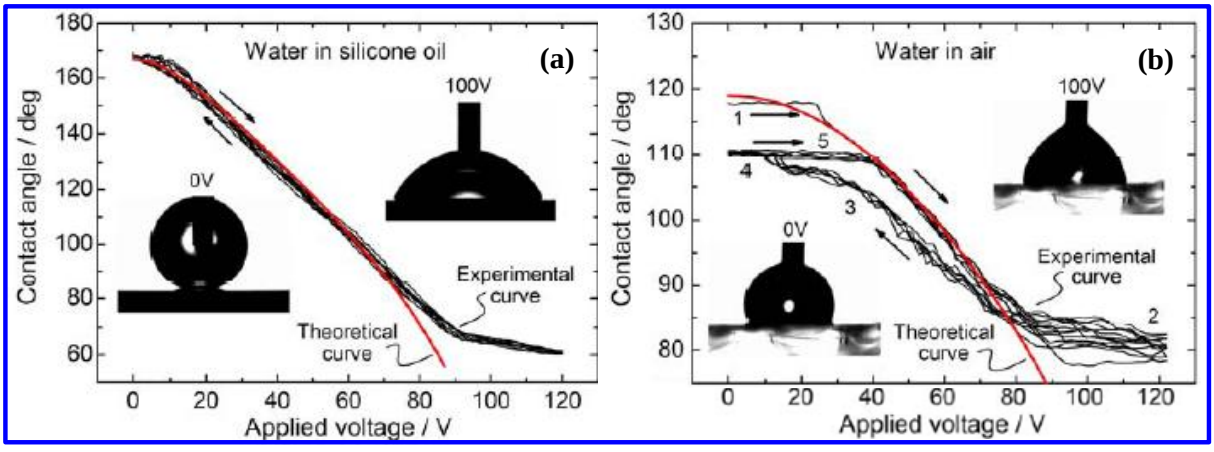

Figure 1.2 Contact angle vs. voltage electrowetting curves for water droplets sitting on a Telfon AF surface for (a) silicone oil and (b) air as the surrounding fluid (copy from [18]). The theoretical curve (in red) is calculated from the Young-Lippmann's theoretical equation.

1.2.1.1.2. Contact angle saturation: modified Lippmann-Young Law

As shown in **Figure 1.2**, due to the saturation effect, the contact angle does not decrease below a certain limit although higher voltages are applied. To date, the physical properties of

contact angle saturation have been explained by several mechanisms, yet it is still a matter of debate. These explanations are based on very different physical phenomena, like charge trapping, zero effective solid-liquid surface tension, increase of the liquid electric resistance, leakage due to dielectric breakdown, or air ionization near the triple line [19].

In the year 1905, Langevin took into account the saturation and modified the Lippmann-Young law by a Langevin's function (described by **Equation (1.4)**).

$$L(\chi) = \coth(\chi) - \frac{1}{3\chi} \quad \textbf{(1.4)}$$

Langevin's function is closely approximated by the linear relation $L(\chi) = \chi$ at the origin and has the asymptote $L(\chi) = 1 \text{ when } \chi \to \infty$. Hence take into account the saturation into Lippman-Young Law, the law can be written as

$$\frac{\cos\theta - \cos\theta_0}{\cos\theta_s - \cos\theta_0} = L\left(\frac{CV^2}{2\gamma_{LG}(\cos\theta_s - \cos\theta_0)}\right) \quad \textbf{(1.5)}$$

where L is the Langevin function, and θ_s is the saturation angle. **Equation (1.5)** is called modified Lippmann-Young law, which shows a linear dependence between $\cos\theta$ and V^2 at low electric potential and while the contact angle has an asymptote at large electric potentials.

1.2.1.1.3. Static contact angle hysteresis

It is widely observed that the droplet spreads on the substrate (corresponding to an advancing contact angle) or the droplet shrinks on the substrate (corresponding to a receding contact angle) following an increase or a decrease of the actuation voltage. **Figure 1.2** shows one example of this phenomenon. The notion of the contact angle hysteresis is approximately defined as the vertical shift between the two curves [20]. However, the shift between the two curves is not strictly constant and some variations exist as the electric potential changes. It is also noteworthy that [18], by varying the voltage back and forth from 0 to 120V, the contact angle hysteresis of water droplets is much higher in air (shown in **Figure 1.2 (b)**) than in silicone oil (shown in **Figure 1.2 (a)**). This can explain the reason that in some EWOD

applications oil is used to encapsulate the droplets to reduce the hysteresis pattern of the electrowetting curve.

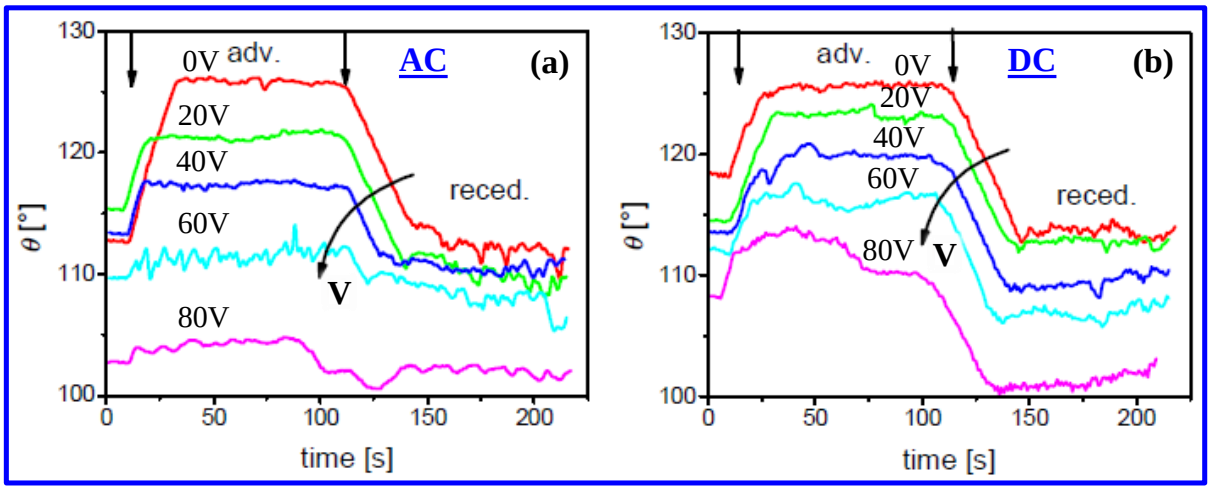

Figure 1.3 Advancing and receding contact line for (a) AC voltage at f=1 kHz and (b) DC voltage (copy from [21]). The applied voltage (V) increases from top to bottom: 0, 20, 40, 60, 80V.

Besides, the contact angle hysteresis for droplet also differs from the control voltage using either alternating (AC) or direct (DC) voltage. F. Li and F. Mugele demonstrated that [21] the contact angle hysteresis for sessile drops in electrowetting almost disappears with increasing AC voltage. As a consequence (shown in **Figure 1.3(a)**), at the high voltages, both θ_a and θ_r decrease so that the contact angle hysteresis ($\alpha = \theta_a - \theta_r$) reduces as the voltage increases. In contrast, for DC voltage (shown in **Figure 1.3(b)**), both θ_a and θ_r decrease in the same way upon increasing V that the contact angle hysteresis remains constant.

1.2.1.2. Dynamic of droplet transport

1.2.1.2.1. No contact angle hysteresis

Droplet transport is the most basic EWOD operation, performed by sequential application of a potential to one electrode to the adjacent one. The principle of droplet motion is due to an 'apparent wettability gradient' between an actuated and a non-actuated electrode [19]. A model of droplet actuation proposed by Song et al. [22] is used to study the effects of contact angle hysteresis during droplet transport in a systematic manner.

A cross-section of a typical droplet movement under EWOD actuation is illustrated in **Figure 1.4**. The droplet is placed between two parallel plates with hydrophobic surfaces, and the space between two parallel plates with a medium of air or silicon oil. The electrodes are covered with the insulating layer and connected to a voltage source. In initially status (**Figure 1.4(1)**), the droplet is on the non-actuated left electrode with a static contact angle θ_0. When the right electrode is actuated, the droplet is transported from the left electrode to the right one under EWOD. Considering that there is no hysteresis, during transport (**Figure 1.4(2)**), the droplet maintains a dynamic contact angle θ_d. When the droplet is completely moved to the right electrode (**Figure 1.4(3)**), the droplet becomes stationary with a new static contact angle $\theta(V)$.

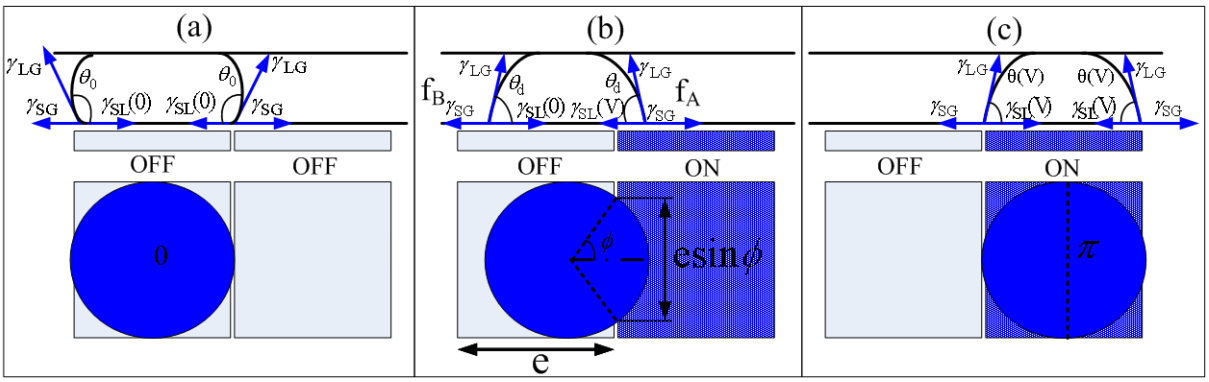

Figure 1.4 Side-view and top-view show voltage-actuated contact angle changes and key dimensions. The droplet moves toward the right electrode: (a) the droplet on the left non-actuated electrode, (b) the droplet during transport considering that there is no hysteresis, and (c) the droplet stationary over the right actuated electrode.

In initially status and when the droplet is stationary over the right electrode, surface tension forces along the triple line are balanced between solid, liquid, and gas. During the droplet transport, the force balance is illustrated in **Figure 1.4(2)**. Under the influence of a wetting force (f_A), a droplet moves and expresses an angle of advancement (ϕ). Along the droplets triple line, the force balance per unit length over the right actuated electrode is expresses as:

$$f_A = \gamma_{SG} - \gamma_{LG}\cos\theta_d - \gamma_{SL}(V) \qquad \textbf{(1.6)}$$

The force balance per unit length along the droplets triple line over the left non-actuated is

presented as:

$$f_B = \gamma_{SL}(0) + \gamma_{LG}\cos\theta_d - \gamma_{SG} \quad \textbf{(1.7)}$$

Then, the driving force per unit length is the sum of these two forces:

$$f_{total} = f_A + f_B = \gamma_{SL}(0) - \gamma_{SL}(V) \quad \textbf{(1.8)}$$

The integration of the driving force per unit length (f_{total}) over the contact line of a droplet of diameter (e), yields the total force on the droplet:

$$F_{total} = f_{total}\, e\sin\phi \quad \textbf{(1.9)}$$

In this simplified analysis only the projected length of the droplet matters. The angle of advancement (ϕ) increases from 0 to π as the droplet moves to the next electrode (shown in **Figure 1.4**). Therefore, the driving force for the droplet changes as it moves from one electrode to the next one.

1.2.1.2.2. With contact angle hysteresis

It is known that contact angle hysteresis (α), caused by random pinning forces, introduces an obstacle to droplet transport manifested as a threshold voltage [19]. In this regard, the receding triple line during droplet transport can maintain a contact angle of $\theta_0 - \alpha$ while the advancing triple line can maintain the contact angle of $\theta_0 + \alpha$. Thus, the total force per unit length on a droplet in **Equation 1.8** is written as follows:

$$f_{total} = f_A + f_B = \gamma_{SL}(0) - \gamma_{SL}(V) = \gamma_{LG}\cos[\theta(V) + \alpha] - \gamma_{LG}\cos(\theta_0 - \alpha) \quad \textbf{(1.10)}$$

Using a trigonometric identity and the Lippmann-Young equation (**Equation 1.3**), the driving force per unit length is estimated as:

$$f_{total} = \gamma_{LG}\cos\alpha[\cos\theta(V) - \cos\theta_0)] - \gamma_{LG}\sin\alpha[\sin\theta(V) + \sin\theta_0] \quad \textbf{(1.11)}$$

$$f_{total} = \cos\alpha \frac{C}{2} V^2 - \gamma_{LG} \sin\alpha [\sin\theta(V) + \sin\theta_0] \quad \textbf{(1.12)}$$

It is seen that the driving force per unit length is modified by contact angle hysteresis, which highly depends on the combination of the substrate surface, droplet liquid, and the filler fluid. Thus, from **Equation 1.9** the total estimated force on an actuated droplet becomes:

$$F_{total} = e \sin\Phi \left\{ \cos\alpha \frac{C}{2} V^2 - \gamma_{LG} \sin\alpha [\sin\theta(V) + \sin\theta_0] \right\} \quad \textbf{(1.13)}$$

1.2.2. EWOD device configurations

There are two general approaches of EWOD device configurations: two-plate (closed) configuration and single-plate (open) configuration. In closed EWOD devices, the ground electrode and actuation electrodes are positioned in the top and bottom plate, respectively. While in open EWOD devices, the ground electrode is positioned in the same plate as the actuation electrodes. In both configurations an insulating dielectric layer covers the bottom-plate electrodes and all surfaces are covered by a hydrophobic coating [23].

1.2.2.1. Two-plate configuration

In two-plate architecture, the droplet is sandwiched between two plates and surrounded by silicone oil or other immiscible liquid or gas, where the bottom plate carries the actuation electrode array while the top plate comprises a single ground electrode or ground electrode array.

This two-plate configuration for EWOD actuation requires electrodes on both plates, either asymmetrically or symmetrically. **In asymmetrically arrangement**, the top plate contains a single continuous reference/ground electrode which is either electrically insulated from (**Figure 1.5 (a)**) or directly in contact with the droplet (**Figure 1.5 (b)**) [24], while the bottom plate contains an array of independently addressable control electrodes. Both surfaces are covered with thin hydrophobic layers (*e.g.*, Teflon® or CYTOP®) [25]. Once a sufficient electrical potential is applied between the top reference/ground electrode and one electrode on

the bottom plate overlapping a portion of the droplet, the resulting surface pressure gradient (due to the contact angle changes between liquid and solid) induces the droplet to move toward the charged electrode.

In symmetrically arrangement (shown in **Figure 1.5 (c)**), both the top and bottom plates contained rows of electrodes which can be actuation or ground electrodes, depending on the desired direction of droplet translation [26][27]. However, this design is probably the most complex to fabricate and to control, despite it is expected to be the most efficient due to achieve two-dimensional droplet translation with fewer electrodes.

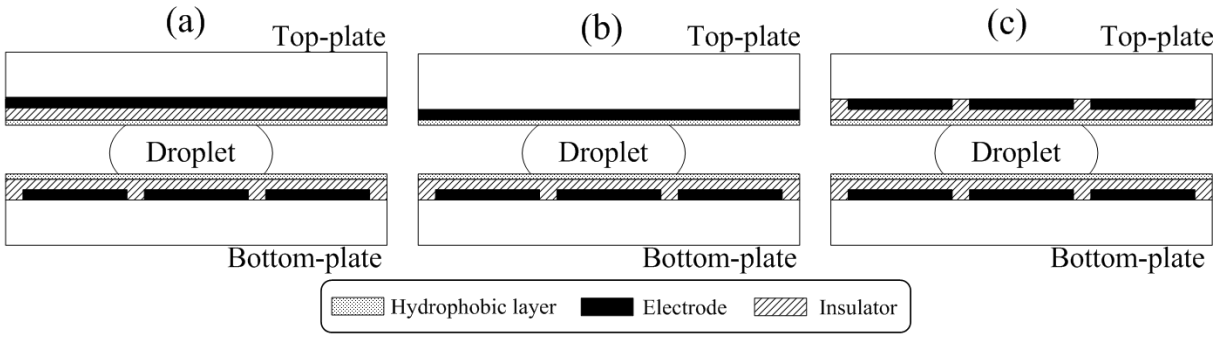

Figure 1.5 Alternative two-plate architectures.

Two-plate devices are often operated in air, although substitution with other filler media (*e.g.*, silicon oil) is possible. When operated in air, to prevent bio-molecular adsorption on surface, low concentration of surfactants can be used as a solution additive to facilitate the actuation of droplets [28][29]; On the other hand, when operated in silicon oil [30], the droplet is isolated from the surface and thus the required actuation voltage for droplet movement can be reduced.

1.2.2.2. Single-plate configuration

Alternatively, in single-plate configuration, droplets are actuated on a single plate which carries both the actuation and grounding. A wide range of the grounding electrodes/wires have been reported in the literature [31][32][33][34][35][36] for droplet manipulation in the single-plate configuration, illustrated in **Figure 1.6**. In these designs, the grounding

electrodes/wires may be passing through the droplet [14], on top of the dielectric layer by surrounding [15] or upward [16] the actuation electrodes, or coplanar as a continuous network located in the spaces between [18] or within the control electrodes [17][19]. Abdelgawad et al. [37] proposed a combination of numerical simulations and experimental tests to estimate the actuation forces among the above six different geometries, illustrated in **Figure 1.6**. It explains that the position of the grounding electrodes/wires impacts the intensity and distribution of the electric field in the vicinity of the droplet, which determines the actuation force on the droplet. In **Figure 1.6-(b)**, the actuation line force is given by the equation ($f_x = {}^1/_2\, CV^2$) agreed with electromechanical modeling on the assumption that the droplet lies in the path of the electric field lines between the active and ground electrodes.

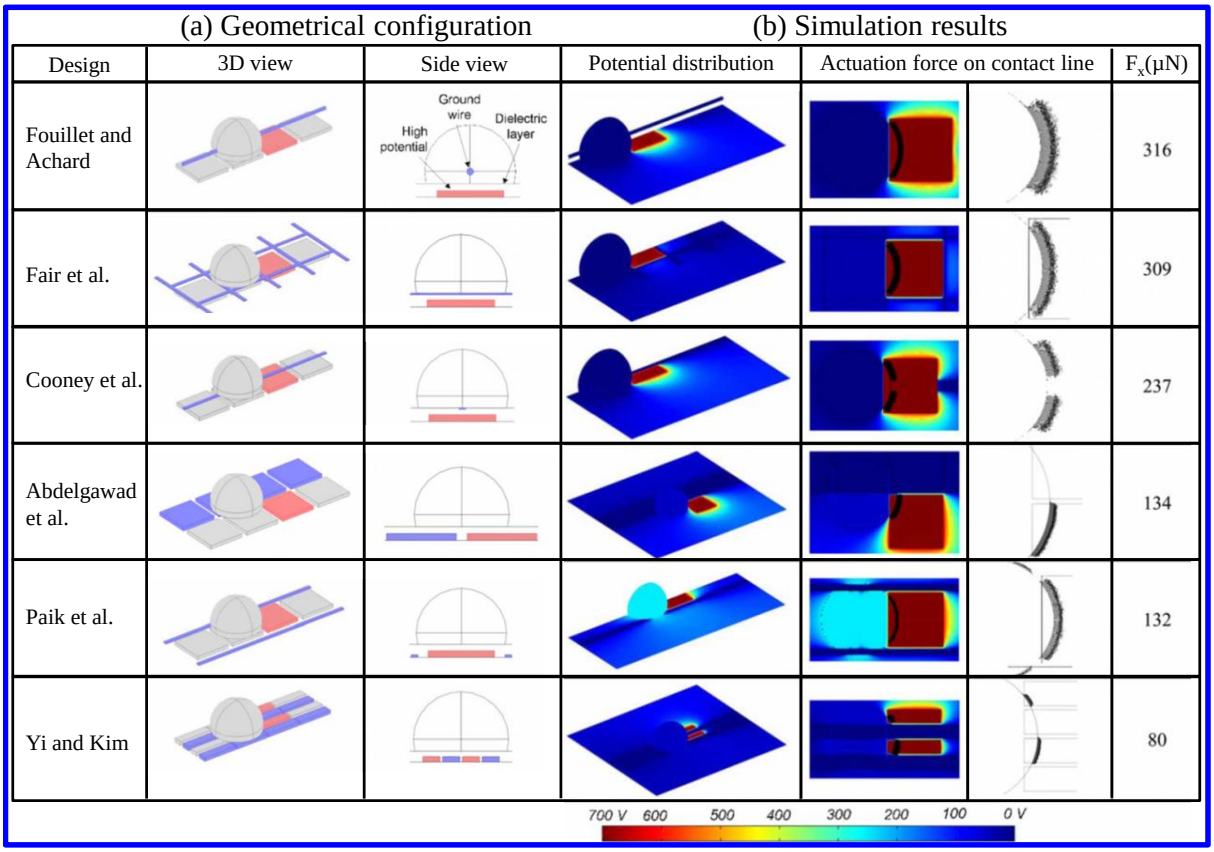

Figure 1.6 The actuation force models among the various designs reported in the literature for single-plate droplet manipulation (copy from [37]). (a) Geometrical configuration: energized electrodes are colored red, ground electrodes/wires are colored blue, and floating electrodes are colored grey. (b) Results of the numerical modeling: colors represent electric potential, and short black arrows (shown on the third column) are actuation forces.

In the top three grounded designs (*i.e.*, the droplet is in direct contact with the grounding

wire electrode without a dielectric coating in between), forces are higher than the bottom three non-grounded designs. **In grounded designs**, electrodynamic forces are based on a large fraction of the three-phase contact line overlaps the energized electrode. The prediction actuation force of Cooney et al. design is not accurately predicted by electromechanical modeling, because the ground wire is positioned between the droplet and the active electrode. However, its lower force compared with the others can be explained as the ground wire covered the center part of the energized electrode and masked it from the contact line. While, **in non-grounded designs**, electrodynamic forces are inversely proportional to the droplet potential which floated to a value between that of the energized electrode and ground electrode. Thus, this actuation force model can be a reasonable criterion for evaluation single-plate device design.

Overall, both configurations have advantages which can be employed in a particular application. Although the operation principles are similar, two-plate devices can enable a wider range of operations (including dispensing, moving, splitting, and merging), either in air or other filler media. Conversely, single-plate devices are incapable of splitting and dispensing, but they can be more easily fabricated and allow implementation of rapid mixing schemes.

1.2.3. EWOD fundamental operations

1.2.3.1. Droplet dispensing from on-chip reservoirs

Droplet dispensing is an elementary operation of aliquoting a large volume of liquid into small unit droplets on EWOD-based systems. Controlled droplet dispensing on chip can occur by extruding a liquid finger from the on-chip reservoir through activation of adjacent serial electrodes [11]. Dispensing consists of three steps [19]:

a) Small volumes of liquid extrude from the on-chip reservoir onto the electrode row by activating a series of adjacent electrodes. When the liquid overlaps the actuated electrode where the droplet is to be formed, all the remaining electrodes are switched off. At this moment, a liquid neck is formed.

b) A pinching effect shrinks the liquid filament at the level of the intermediated switched-off electrodes.

c) In order to effectively separate a droplet from the reservoir, a 'back pumping' step (*i.e.*, re-actuation of electrode underneath the reservoir) is used to extract the droplet. The role of back-pumping is to decrease the droplet pressure, causing the neck to be broken, thus forming a droplet.

1.2.3.2. Droplet splitting and merging

Droplet splitting is based on the similar strategy as droplet dispensing. Splitting occurs when the electrodes near the opposite ends of a droplet are activated, and the central one underneath the droplet is grounded. The droplet is pulled towards actuated electrodes on both ends. As a result, the droplet is pinched off and divided in the middle. Merging of two droplets is a straightforward operation, whereas two aqueous droplets are displaced towards the same electrode and their coalescence is immediate.

1.2.3.3. Droplet mixing

Mixing of analytes and reagents is manipulated on a EWOD-based device for sample preparation, sample dilution or a specific reaction. With successive splitting and merging operations, a variety of mixing and dilution strategies can be implemented. Also, mixing of two droplets can be simply achieved by merging them and then moving the merged droplet along a programmed path. Improved mixing in EWOD devices is enabled by the ability to create chaotic flow patterns within the droplet which promotes mixing efficiency. In closed EWOD platform, the studies of mixing motion consists of three types[19]: (1) a back and forth motion on a linear row of electrodes, (2) successive division and merging operations on a linear row of electrodes, and (3) a loop motion on square rows of electrodes.

1.2.4. Applications

The EWOD-based DMF chip is an attractive platform for biochemical applications. A short

representation of applications is introduced as follows (illustrated in **Figure 1.7**).

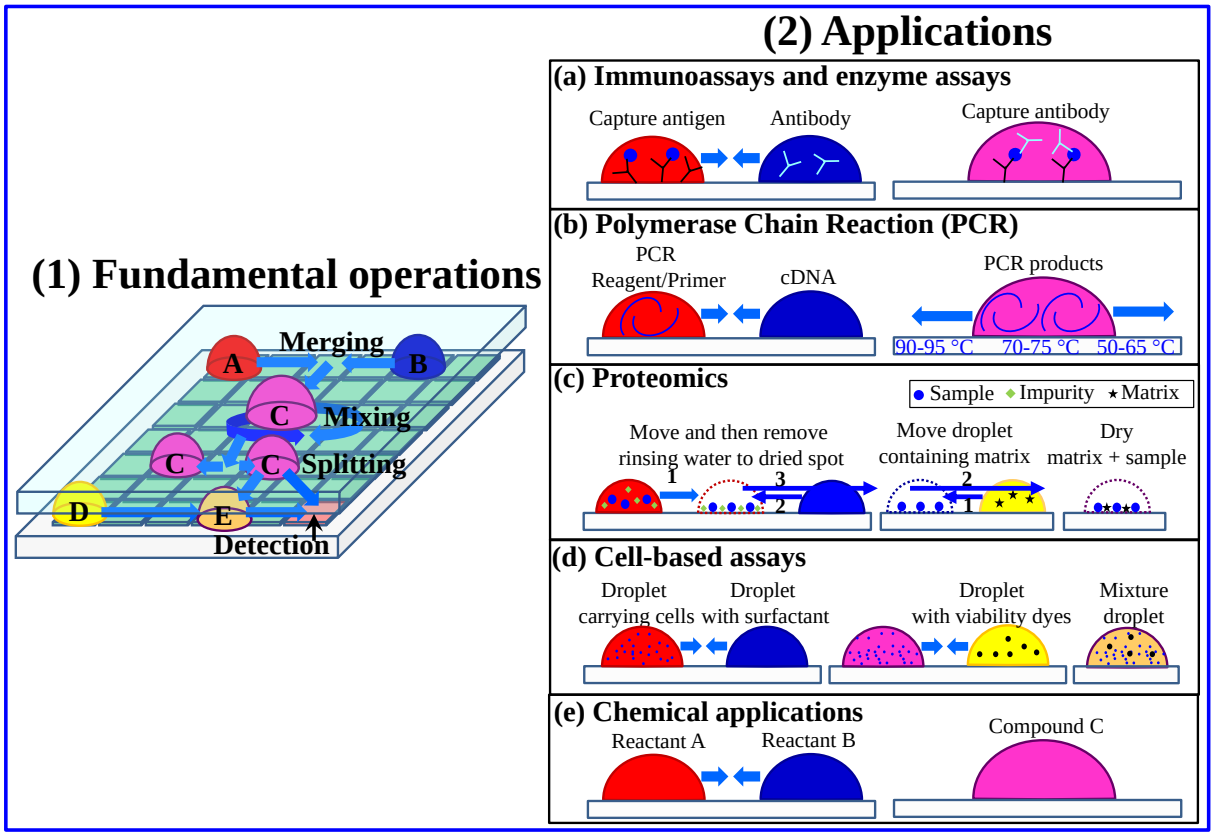

Figure 1.7 (1) Fundamental operations of EWOD chip (transport, merging, mixing, and splitting); (2) Diverse applications based on the type of operative sample droplets.

(a) Immunoassays and enzyme assays

The immunoassay is widely used in clinical diagnostics and environmental monitoring. The most popular immunoassay method is enzyme linked immunosorbent assay (ELISA) [38]. ELISA requires the antibody or antigen to be immobilized on a fixed surface so that the unbound molecules can easily be washed away. The major enzyme assay is magnetic bead-assisted, involving the following steps [40]: (1) mixing a droplet containing magnetic beads with the capture antigen with another droplet containing the antibody, (2) splitting and merging the mixture droplet in order to improve binding efficiency, (3) formatting the capture antibody-antigen complex, (4) immobilizing the magnetic beads with a magnet, (5) washing away the unbounded material, (6) performing a specific number of serial dilution-based wash steps, and (7) transporting analyte droplets to the detection place. EWOD-based DMF chips

are well suited to immunoassays (illustrated in **Figure 1.7-2(a)**), because mixing of droplets decreases the amount of time required for the target molecules to come into contact with the capture antibody [39].

(b) Polymerase Chain Reaction (PCR)

However, the results of immunoassays depend on many factors, especially antibody quality, which might become false-positive. Polymerase chain reaction (PCR) has probably eliminated the complication, due to the target sequence (DNA or RNA) with an ultimate alternative in improving specificity [38]. PCR is a method for creating copies of a specific portion of a DNA molecule to produce large quantities of DNA (DNA amplification) [11][41]. In order to achieve the PCR on a EWOD-based chip (illustrated in **Figure 1.7-2(b)**), the following operations must be successively performed: (1) merging and mixing of a droplet containing PCR-mix with another droplet containing sample, (2) submitting the mixture to the temperature cycles, and (3) detecting the reaction results.

(c) Proteomics

Proteomics is the study of the expression, function and interaction of proteins in health and disease [42]. The typical processing pipeline for proteomics involves the following steps [43]: (1) selection and/or extraction of the particular proteins to be analyzed, (2) protein separations by sorting complex protein mixtures into nearly purified components, (3) digestion of the protein sample, and (4) mass spectral analysis of the digests. The EWOD-based chip has a great potential for protein analysis covering a sequence of reactions and purification steps [39] (illustrated in **Figure 1.7-2(c)**).

(d) Cell-based assays

Because cells are likely to adsorb onto hydrophobic surfaces which increases the challenge in droplet movement feasibility on EWOD device, there are a few attempts involving cells with EWOD technology. One aspect is to combine EWOD cell-based assays with

fluorescence micro-plate reader detection that it can be used on manipulation and analysis of cells [44] (illustrated in **Figure 1.7-2(d)**). Another inverted aspect is to generate cell patterns on a hydrophobic dielectric surface, either by programming selectively switching on microelectrode arrays to cause a local EWOD effect to localize cell adhesion on the surface [45], or as micro-patches of bio-molecules allowing cells to be arrayed as cell clusters or as single cells on the controlled bio-functionalization EWOD chip surface [46].

(e) Chemical application

With the possibility of performing the elementary operations like displacement, merging and mixing of droplets, droplets handled EWOD system can be used as micro-reactors for chemical synthesis in small volumes (illustrated in **Figure 1.7-2(e)**). Through rapid mixing and combining with temperature compatibility, EWOD platform provides highly precise control of reaction conditions and improved reaction speeds and selectivity compared to macro scale approaches [47].

1.3. Coupling EWOD-based DMF chip to external fluidic modules

The individual EWOD fluidic operations have been largely demonstrated in experiments. However, the EWOD chip still relies on some manual steps on: (a) loading samples on chip, and (b) exporting samples off chip for post-processing. These manual steps can be slow, inefficient, and even impractical, as the number of input and output ports increases. Thus, it is a desirable goal to integrate inlet and outlet interfaces on EWOD chip, coupling to external fluidic modules [48][49][50][51][52][53][54][55].

1.3.1. Inlet interface: Analog-to-Digital

Typically, samples are pipetted loaded onto on-chip reservoirs of EWOD chip. This method is slow and inefficient. Another key drawback of this loading method is a lack of a continuous supply external source which keeps the on-chip reservoirs full [11]. Thus, it is necessary to integrate an Analog-to-Digital (A/D) inlet interface on EWOD-chip to address

the loading drawback. The inlet interface integration is challenging due to the difference in the scales of samples between external fluidic modules (tens of microliters to milliliters) and EWOD chip (nanoliters to microliters) [11].

The simple way for loading samples from off-reservoirs to the input port is through a loading hole in the top plate (shown in **Figure 1.8-1**) (2004)[30](2004)[56]. This method involves the following steps: (1) A small volume of sample is pipetted or injected with the assistance of external pressure into a loading hole in the top plate; (2) on-chip reservoir is primed by turning on the reservoir via purely EWOD force; (3) A series of electrodes adjacent to the reservoir electrode are activated so that a liquid column is extruded from the on-chip reservoir; (4) Once the liquid column overlaps the electrode used for the droplet forming, the intermediated electrodes are deactivated to pinch-off a droplet.

Another path for the inlet interface integration is droplet dispensing system. Droplet dispensing system is controlled by a capacitance or impedance feedback. **Ren et al.** presented a sample loading/dosing system mated to an oil-filled EWOD platform (shown in **Figure 1.8-2(a)**) (2004)[57]. The volume of droplet can be automatically controlled by using this dosing system. The capacitance (between the droplet and a reference electrode) is monitored by an electronic system and a feedback loop shut off the liquid source when the desired volume (related to a constant capacitance) is achieved. Similar, **Ding el al.** demonstrated an accurate on-demand reagent dispensing system with impedance-based threshold sensing for air-filled chip (shown in **Figure 1.8-2(b)**) (2011) [58]. The volume of droplet is precise on the order of ~1μL or less.

The third method combines channel-based CMF with EWOD-based DMF, proposed by **Malloggi et al.** (2007)[59] and **Kedzierski et al.** (2009) [60]. This method not only harvests the power of both CMF and EWOD-based DMF, but also offers the capability of addressing their limitations. A water drop can be generated by using electrowetting actuation in an oil micro-channel where multiple EWOD electrodes are integrated (shown in **Figure 1.8-3**). Thus this microfluidic structure opens up new opportunities for automated droplet generation.

Heikenfeld and Papautsky groups demonstrated a method for electronic transport of

liquid in programmable formation of virtual microfluidic channels (*i.e.*, a continuous array of electrowetting posts) (shown in **Figure 1.8-4(a)**) (2010)[61]. Due to posts, once the aqueous contact line touches the next set of posts, a ratcheting forward of the aqueous liquid indefinitely continues. Their work in inlet interface module work in oil-filled chip. This approach allows for introduction of aqueous liquid into an electrowetting chip without need for syringe-pump pressure, making the inlet interface simple. Late, they demonstrated reconfiguration of 'post-less' virtual channels which can be switched on-demand between multiple inputs and outputs. It allows wide access to multiple microfluidic functions (shown in **Figure 1.8-4(b)**) (2012)[62].

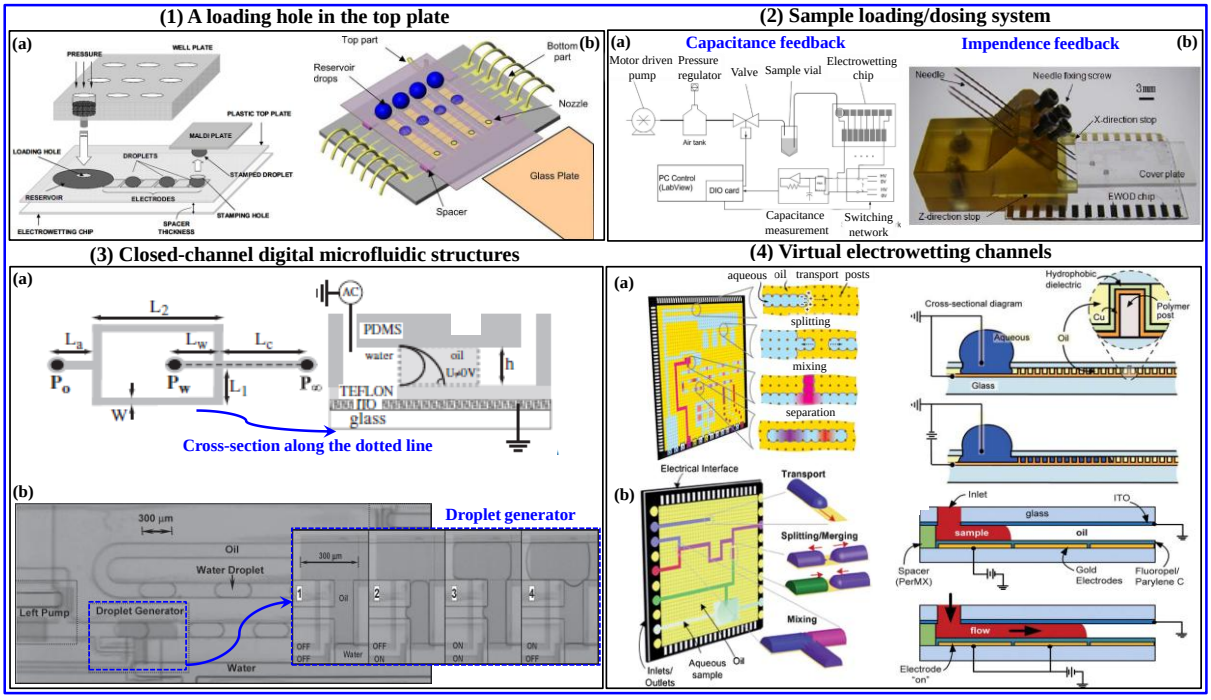

Figure 1.8 (1) Sample from off-reservoirs to the input port is through a loading hole in the top plate (copy from [30][56]); (2) The loading/dosing system mated to (a) oil-filled (copy from [57]) or (b) air-filled (copy from [58]) EWOD platform; (3) Closed-channel digital microfluidic structures (copy from [59][60]); and (4) Virtual electrowetting channels (copy from [61][62]).

1.3.2. Outlet interface coupling with post-processing components

Integration of outlet interface on EWOD chip mainly considers the fluidic formate of samples coupling with the post-processing. Due to the fluidic formate as droplet-based or continuous-flow, the outlet interface is classified into two groups: (a) Digital-to-Digital (D/D)

and (b) Digital-to-Analog (D/A).

1.3.2.1. Digital-to-Digital outlet interface

Table 1.1 Applications and detection techniques in Digital-to-Digital outlet interface module

#	Detection			Application	Integration	Group	Ref.
	Type	Mode	Method				
Off-line detection							
1	MS		MALDI-MS	Chemical applications	A stamping interface	Fair	[30]
2	MS		MALDI-MS	Proteomics	Purified using a ZipTip	Wheeler	[63]
3	MS		MALDI-TOF MS	Chemical	An electrohydrodynamic (EHD) mixing scheme	Nichols and Gardeniers	[64]
4	MS	Matrix-assisted	MALDI-MS	Proteomics	A 'box-to-box' electrode to overcome the surface biofouling problem	Garrell and Kim	[65] [66] [67] [42]
5	MS		MALDI-MS	Proteomics	Joule heating and thermistor elements	Kim	[68]
6	MS		MS ELISA	Cell-based assays	The liquid-liquid extraction zone bounded by a photoresist "wall"	Wheeler and Casper	[69]
7	MS	Matrix-free	DIOS-MS	Proteomics	A surface-assisted desorption-ionization (SALDI) silicon nanowire-based interface	Our group	[70]
8	Optical	Label-Assisted	Gel electrophoresis	PCR	A micro temperature sensor and two micro heaters	Lee	[41]
9	Optical	Label-Assisted On-line; Label-Assisted	UV spectrophotometer Image based concentration measurement	Proteomics	Combining dielectrophoretic forces	Moon	[71]
On-line detection							
1	Optical		A green LED and a PD	Chemical applications	Glucose is measured using a colorimetric enzyme-kinetic method based on Trinder's reaction.	Fair	[72]
2	Optical	Label-Assisted	Violet InGaN LEDs and fluorescence microscope	Wave guide	Fabricated on a large planar waveguide substrate	Heikenfeld and Steckl	[73]
3	Optical		Fluorescence detector	Chemical applications	Combining chaotic advection created by surface acoustic waves for mixing	Marchand et al.	[74]
4	Optical	Label-free	SPRi and CCD array detector	PCR	A SPR-supporting top plate with defined Au detection spots	Malic et al.	[75]
5	Electrochemical	On-line	Potentiostat	Chemical applications	Two Au catenaries	Marchand and Vaultier	[76]
6	Electrochemical	On-line	Potentiostat	Chemical applications	A Au working wire, a Ag reference wire and a Pt auxiliary wire	Tuantranont	[77]
7	Electrochemical	On-line	Capacitor feedback patch-clamp	Chemical applications	Integrated three pairs of Ag/AgCl electrodes	Poulos et al.	[78]
8	Electrochemical	On-line	Capacitor feedback patch-clamp	Chemical applications	Two opposite coplanar EWOD device and a middle silicon plate holding an aperture	Fan	[79]

The first attempt in coupling EWOD-based DMF with external detection modules is by integrating Digital-to-Digital (D/D) outlet interface. The coupling to external detection modules can perform either: (a) sample preparation for post-processing on-chip and then

taken off-chip for detection, or (b) integrating detection components (*e.g.*, optical sensors) on-chip for on-line detection. Several efforts are made to couple existing detection methods (summarized in **Table 1.1**): mass spectrometry, optical detection, and electrochemical detection.

1.3.2.1.1. Mass spectrometry (MS)

(1) Matrix-assisted

EWOD chip has the capability to perform various multiplexing processes, thus it is empowered to perform sample preparations for matrix-assisted laser desorption ionization mass spectrometry (MALDI-MS) [80]. EWOD chip coupling to MALD-MS are used following two protocols. First, taken-off-chip: samples are manipulated by EWOD, then collected with a pipette and dispensed onto a stainless steel target. After samples are mixed with a matrix solution, and allowed to dry. Second, dry-on-chip: sample droplet and matrix droplet are moved, merged, and mixed by EWOD and then the mixture is allowed to dry on the surface.

a) Taken-off-chip

The preliminary results establishing the feasibility of coupling EWOD device with MALDI-MS detection was presented by **Fair group** (shown in **Figure 1.9(1)**). They developed a EWOD-based platform with a stamping interface to transfer protein samples onto a MALDI-MS substrate for MS analysis (2004)[30]. Droplets encapsulated with a thin film of silicone oil are dispensed manually onto chip, transported by EWOD, and passively stamped through the top plate to a MALDI plate. However, some dead volume is left behind in the hole. To eliminate the residual dead volume, **Yi and Kim** replaced the stamping interface with a ‘soft printing’ mechanism. This ‘soft printing’ method is performed through contact between liquid droplets (inside hydrophobic microchannels) and a solid hydrophilic printing surface without any solid-to-solid contact or ejection of a droplet (2004)[56]. As a result, multiple water or DNA (~100nL) droplets without encapsulation in a thin film of silicone oil can be

successfully spotted on glass plates with no dead volume remaining in the reservoirs. In these two methods, the stamped or spotted droplets are correctly identified in the mass spectrum. These results establish the feasibility of transporting droplets from the EWOD-based system to the mass spectrometer.

Wheeler group reported an enhanced integrated EWOD-based method for implementing three discrete proteomic sample processing steps, including reduction, alkylation, and enzymatic digestion (shown in **Figure 1.9(2)**) (2009)[63].After every step of EWOD-driven processing, each sample was purified using a ZipTip (*i.e.*, a 10 μL pipette tip with a 0.6 or 0.2 μL bed of chromatography media fixed at its end with no dead volume.) and then qualitatively evaluated by **MALDI-MS**. The results demonstrated that EWOD-based DMF is a robust tool capable of implementing all of the key steps in proteomic processing with high reproducibility.

There are a variety of spectroscopy techniques available for investigation reaction kinetics which requires a chromophore. However, matrix-assisted laser desorption/ionization time-of-flight mass spectrometry (MALDI-TOF MS) allows for the determination of rate constants regardless of the incorporation of a chromophore. **Nichols and Gardeniers** demonstrated a lab-on-a-chip system for the study of pre-steady-state chemical kinetics using a EWOD device incorporated an electrohydrodynamic (EHD) mixing scheme, coupling with time-stepped MALDI-TOF MS measurements (2007)[64]. In this system, droplets are dispensed from four on-chip reservoirs (an enzyme, a substrate, a quench, and a matrix-forming solution) and transported to **MALDI-TOF MS** analysis by using an external robotic droplet dispenser (shown in **Figure 1.9(3)**).

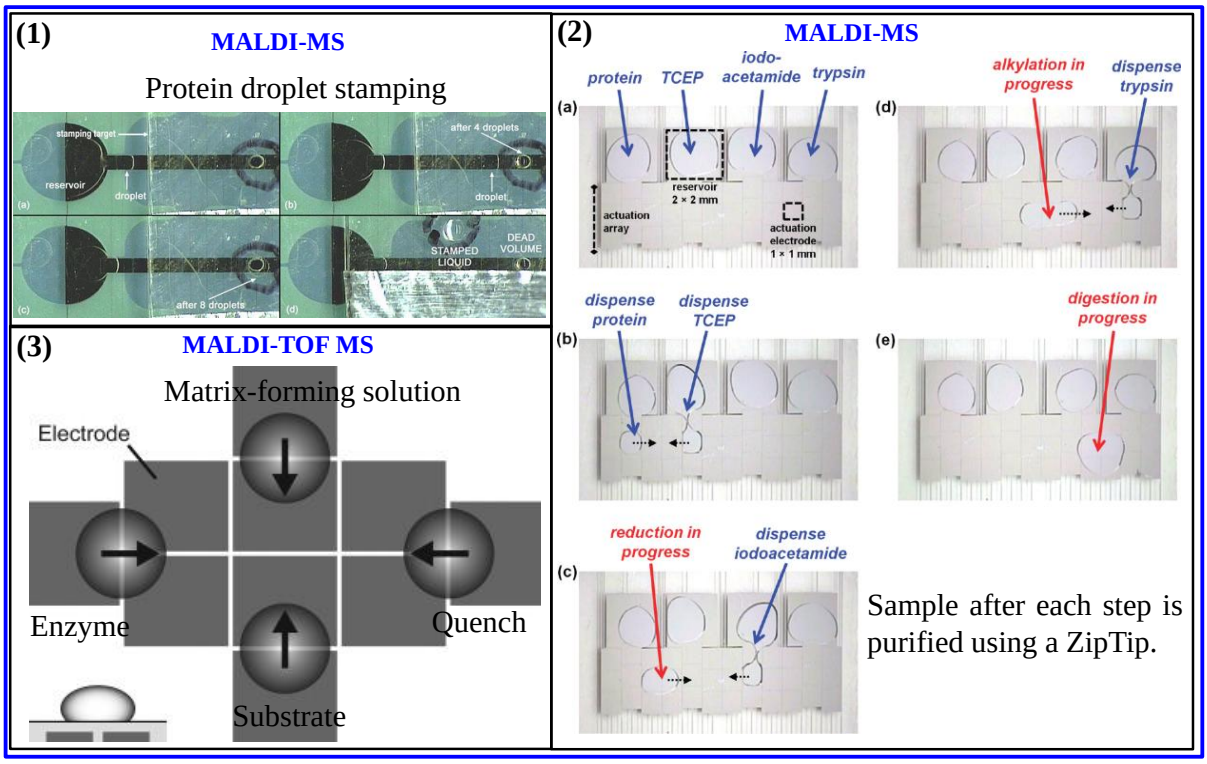

Figure 1.9 Taken-off-chip: (1) Protein droplet stamping (copy from [30]), (b) Implementing three proteomic sample processing, including reduction, alkylation and enzymatic digestion (copy from [64]), and (3) Pre-steady-state chemical kinetics (copy from [81]).

b) Dry-on-chip

In the prior work of **Garrell and Kim groups**, they demonstrated a critical step that the organic matrixes (required by MALDI) can be mixed with the peptides and/or proteins using EWOD technology (2004)[65]. Then, they integrated in-line sample purification for removing unwanted impurities which is important for the MALDI-MS signal (2004)[66]. A sample purification step is between the sample deposition and the matrix deposition (shown in **Figure 1.10(1)**). The rinsing process is performed in the following steps: a) after the sample is deposited and dried, passing a rinsing droplet over the dried pot, b) dissolving the impurities in this rinsing droplet, and c) removing this rinsing droplet. After solving the two key issues of interfacing EWOD with MALDI-MS, they proposed a EWOD-based system for analysis of peptides and proteins (2005)[67] (2006)[42].

Wheeler and Casper groups developed a single-plate EWOD device for the extraction and quantification of the sex steroid estrogen sample of 1μL, whose size is 1000 to 4000 times smaller than that required by conventional methods (shown in **Figure 1.10(2)**)

(2009)[69]. In addition, extensive pipetting, centrifugation, and drying processes required by conventional 5-6 hour hormone extraction techniques, can be replaced with the 10-20 min EWOD process. MS results confirm that the estradiol can be successfully extracted by the EWOD-driven chip.

Later, **Kim group** proposed a built-in heating function to locally heat droplet on a EWOD chip (shown in **Figure 1.10(3)**) (2010)[68]. To evaluate the feasibility of this system, they used relatively simple chemistries. The results demonstrate that the integrated heating function accelerates reaction rates and drying times in automatic proteomics sample processing.

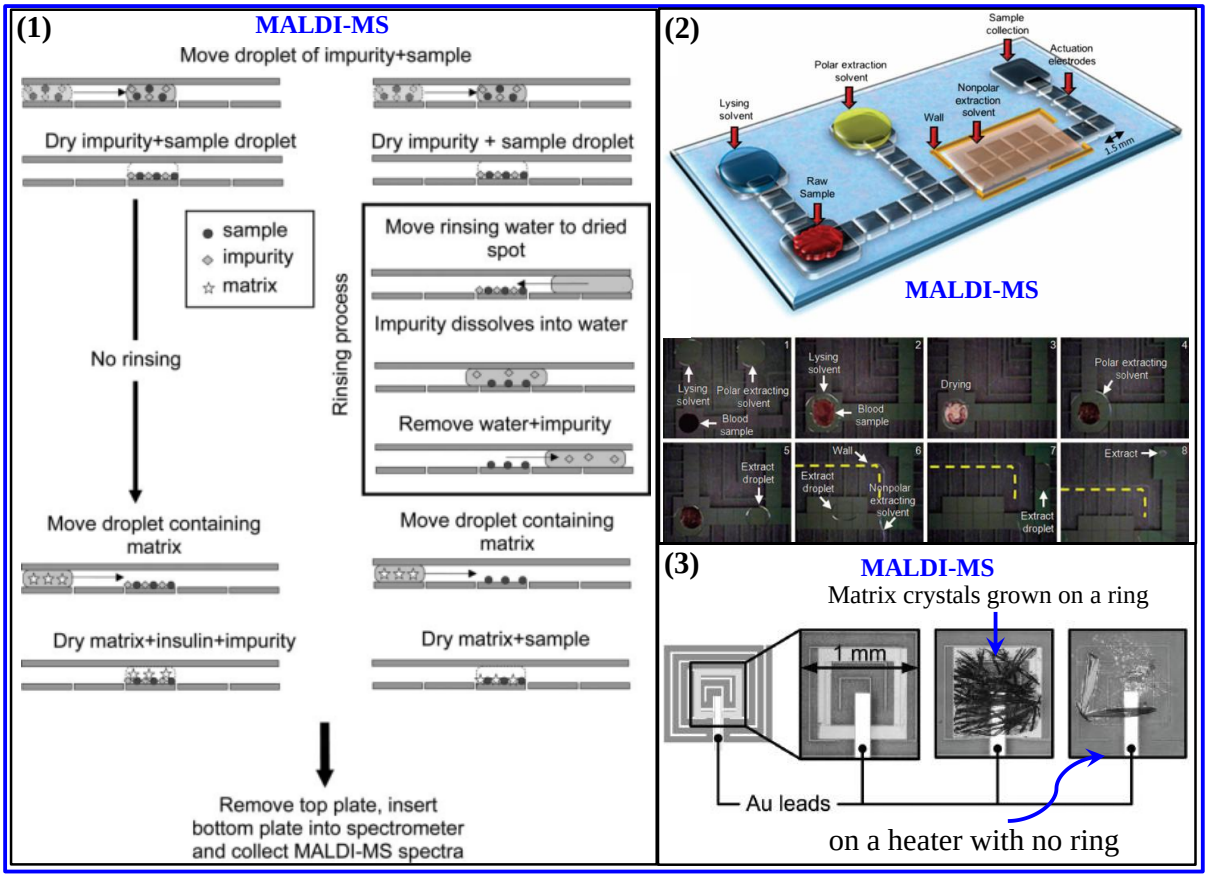

Figure 1.10 Dry-on-chip: (1) Purifying and analyzing of peptides and proteins (copy from [42]), (2) Extraction and quantification of the sex steroid estrogen (copy from [69]), and (3) Accelerate reaction rates and drying times by integrating heating function on EWOD platform (copy from [68]).

(2) Matrix-free

The previous section has demonstrated that EWOD chip can be coupled with off-line

MALDI-MS analysis. However, the use of matrix in the MALDI-MS technique presents several disadvantages [70]. These drawbacks are: (1) Analysis of low molecular weight compounds (<700 Da, *e.g.*, peptides) is limited due to the strong background generated by the organic matrix molecules; (2) Analysis of the biomolecules whose molecular weight (m/z) ranges from 1 to 6 kDa is required to reach a concentration (>0.33nmol/µL); (3) The displacement of the organic matrix is not easy to realize due to its viscosity and composition. Due to the matrix drawbacks listed above, it is necessary to develop of matrix-free MS technique.

Our group presented a EWOD system coupled to a surface-assisted desorption-ionization (SALDI) silicon nanowire-based interface for matrix-free desorption/ionization on silicon mass spectrometry (DIOS-MS) (shown in **Figure 1.11**) (2011)[70]. The top counter-electrode plate of this EWOD device is made of a patterned superhydrophobic/superhydrophilic silicon nanowire surface. A small amount of liquid can be deposited inside superhydrophilic pattern during the droplet displacement. This protocol can analyze a peptide (small molecule) mixture at concentration down to 10fmol/µL due to the absence of organic matrix molecules.

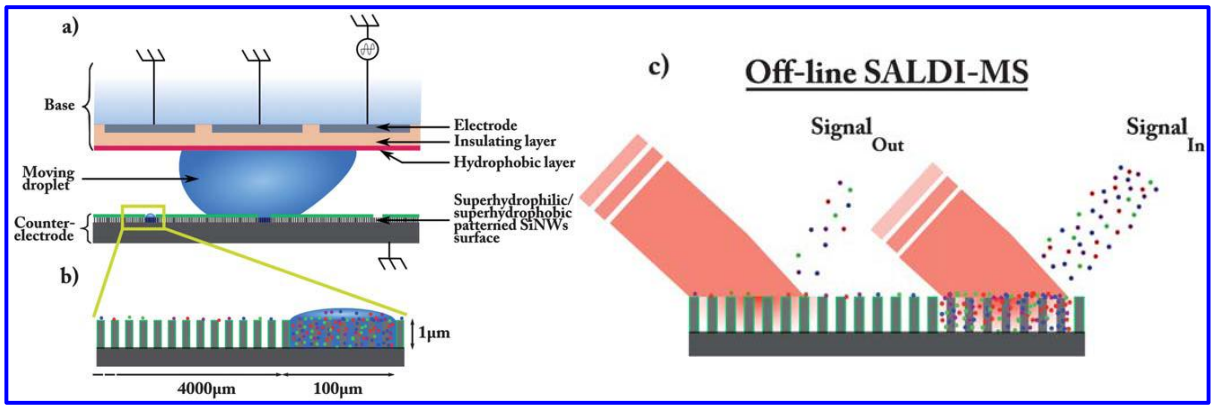

Figure 1.11 Matrix-free MS detection: analyze a peptide mixture at low concentration without organic matrix by adopting a SALDI silicon nanowire-based top plate (copy from [70]).

1.3.2.1.2. Optical detection

Optical detection offers multiple benefits including nondestructive operation mode and capability for rapid measurement by increasing the sensitivity of the assays [82][72].

(1) On-line detection

In on-line detection, biomolecular labeled with fluorescent dyes or quantum dots can be used as the detection principle with a light emitting diode (LED) and a photodiode (PD) or a fluorescence microscope; One can also find work where biomolecular are detected without labeling, for instance using surface plasmon resonance (SPR) imaging [82][75].

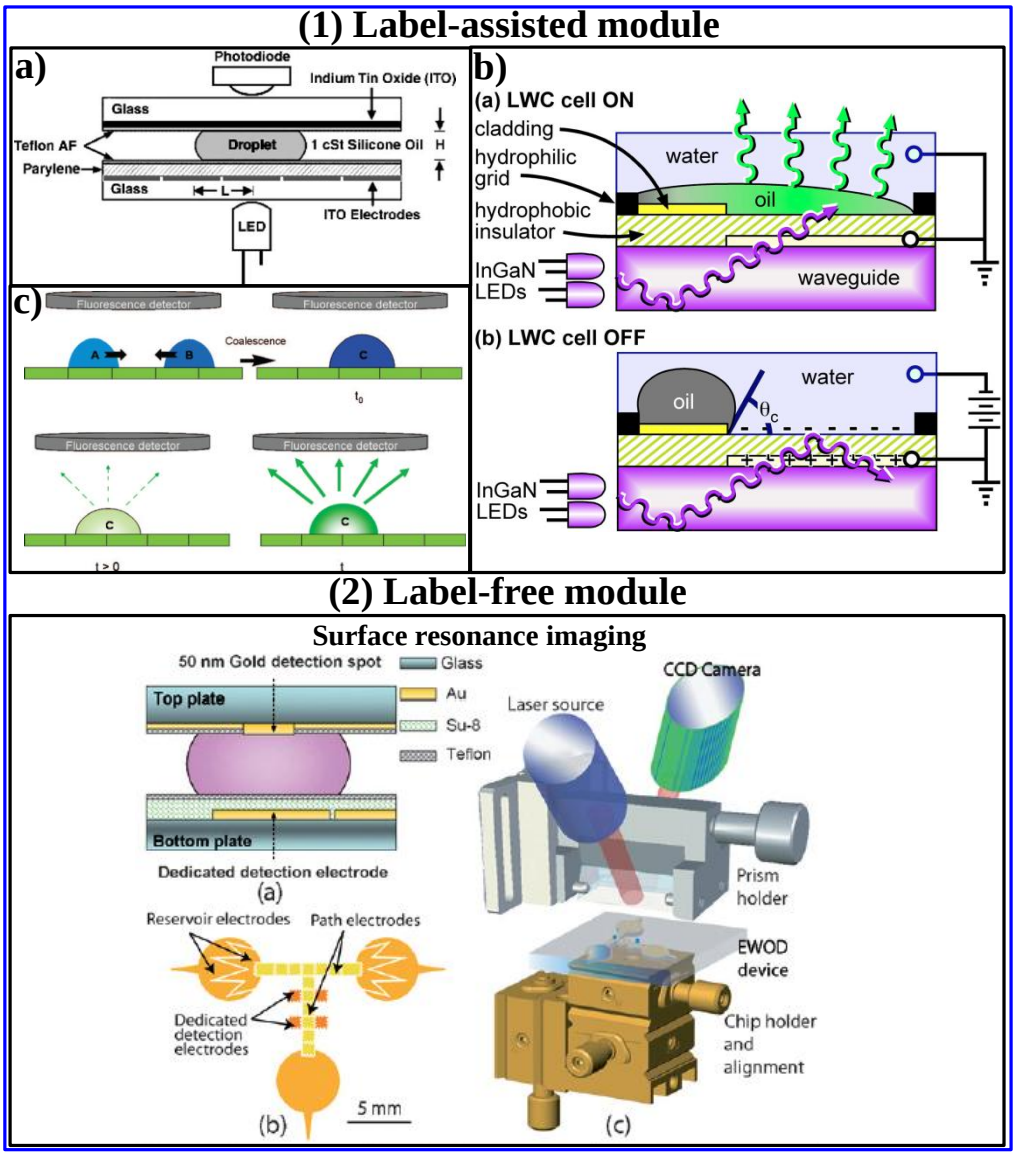

Figure 1.12.(1) Label-assisted on-line optical detection module: (a) Absorbance (copy from [72]), and (b-c) Fluorescence (copy from [73][74]); (2) Label-free on-line optical detection module: surface plasmon resonance (copy from [75]).

a) Label-assisted module

Various techniques have been used to couple EWOD-based DMF system to different types

of optical detection system. **Fair group** presented a EWOD-based platform for in vitro measurement of glucose using a colorimetric enzyme-kinetic method based on Trinder's reaction (2004)[72], shown in **Figure 1.12(1-a)**. Trinder's reaction is a diagnostic test used in medicine to determine the presence of glucose or glucose oxidase. The color change is detected using an absorbance measurement system consisting of a green light emitting diode (LED) and a photodiode (PD). The change of absorption can be correlated to the reaction rate, and is related to the glucose concentration. The collected data correlated well with the results obtained using a commercially available spectrophotometer with a detection limit of 9 mg/dL and 15 mg/dL, individually corresponding to dilution factor of 2 and 3.

Fluorescence labeling detection has high selectivity and sensitivity [82]. **Heikenfeld and Steckl** reported an intense switchable fluorescence system containing violet InGaN light-emitting diodes (LEDs) integrated on a EWOD device (shown in **Figure 1.12(1-b)**). Violet light propagates the layers whose refractive indices is greater than or equal that of the waveguide (n~1.46). The oil has a refractive index of ~1.46, which matches it to the index of waveguide substrate. Because the water has a lower refractive index (~1.33), violet light does not propagate through the water. Under conditions of zero applied bias to the water layer (OFF state), interfacial surface tensions cause the fluorescent oil to form a continuous film between the water and hydrophobic layers. In this OFF state, violet light from the waveguide propagates through the ITO ($n \approx 1.95$) and the hydrophobic insulator ($n \approx 1.5$), and penetrates the fluorescent oil layer. Conversely, in ON state, violet light is reflected and recycled back into the wave guide (2004)[73]. The device ON/OFF contrast ratio is about 20:1, with less than 100ms switching speeds.

Similar using labeling detection technique, **Marchand et al.** demonstrated that fluorescence can indeed be used for real-time monitoring of a fluorogenic Huisgen reaction in ionic liquids micro-reactors handled by EWOD technology (shown in **Figure 1.12(1-c)**) (2008) [74]. Such chemistry reaction starts from non-fluorescent reagents and the fluorescence signal of the mixed droplet is directly correlated to the generation of final produce, allowing simple real-time monitoring of the reaction.

b) Label-free module

Different from the above mentioned detection methods using labels, a label-free surface plasmon resonance imaging (SPRi) detection technique has emerged as an attractive alternative to real-time biomolecular interactions measurement. In this method, light is used to excite surface plasmon resonance which has evanescent character and is sensitive to refractive index changed at the metal-liquid interface. In this technique, the refractive light is recorded by a charge-coupled device (CCD) camera [83].

Malic et al. presented a EWOD-based platform coupled to a gold-coated SPRi chip (shown in **Figure 1.12(2)**) (2008)[75]. It employs a collimated illumination of the entire sensor surface through a prism and images the reflected beam on a CCD array detector. The different sample droplets can be transported over the chosen-size hydrophilic gold detection spot without remaining pinched. Because each concentration of samples with a self-refractive index is referring to a unique SPR peak, the reflected intensity (%R) traced as a function of time can show the kinetics of the events that take place at the surface of the chip. This chip enables *in-situ* monitoring of multiple reactions occurring at the surface of the chip without the use of label.

(2) Off-line detection: label-assisted

In off-line detection, DNA amplification via PCR can be analyzed by the gel electrophoresis technique, and the products of solution-phase chemical synthesis can be measured by ultraviolet-visible (UV) spectrophotometry (referring to absorption or reflectance spectroscopy). The two techniques are label-assisted.

Lee group reported a EWOD device integrated an on-chip PCR system with a programmable microprocessor and electrical components for measuring the temperature inside a PCR chamber (including a micro temperature sensor and two micro-heaters) (2006)[41]. The developed EWOD device is used to transport and to mix two droplets containing PCR reagent and cDNA samples (Dengue II virus), and then the mixture is pulled into the PCR chamber where the real-time temperature of PCR reagents can be obtained

precisely. The final PCR products are analyzed by using the **gel electrophoresis technique** (shown in **Figure 1.13(1)**). The total time for the PCR test is 55 minutes and the total sample volume consumed is 15μL.

Moon group demonstrate a novel EWOD-based device for drop-to-drop liquid-liquid micro-extraction (2011)[71]. Two immiscible droplets are merged and mixed for extraction, and finally phase separated. **UV absorption technique** is studied to measure dye concentrations of droplets. The device is placed on a separate holder integrated with a **UV spectrophotometer** (shown in **Figure 1.13(2-a)**), the sandwiched droplet can be aligned with the fiber optic. An **LED** with 650nm dominant wavelength is used as the light source. The source is suitable for aqueous dye (acid green 25).

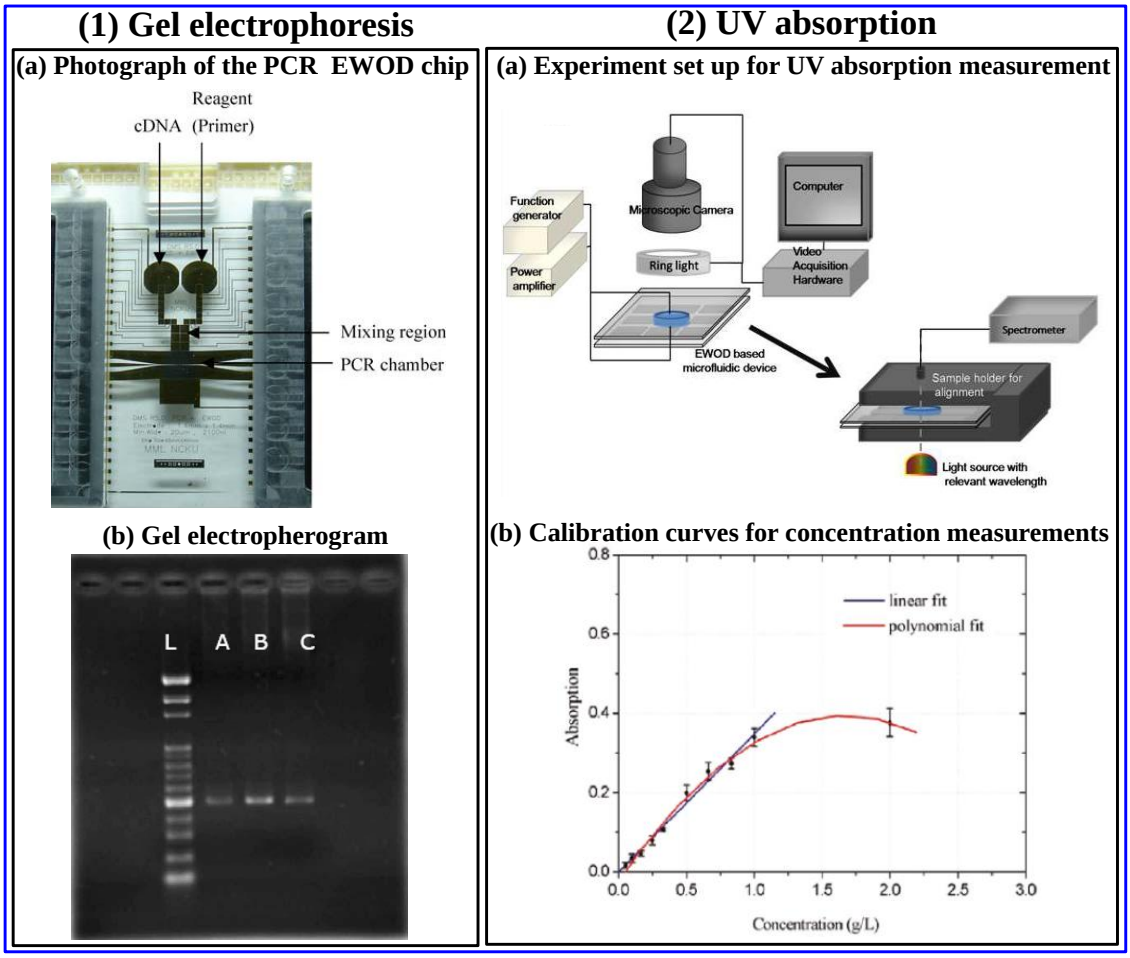

Figure 1.13 (1) Gel electrophoerogram (copy from [41]): a) the photography of the PCR EWOD chip, and (b) the gel electropherogram for Dengue-II virus cDNA detection (511 bps) after PCR amplification. (2) Label-free module (copy from [75]): (a) experiment set up, and (b) the calibration curves for concentration measurements.

1.3.2.1.3. Electrochemical detection

(1) Chemical synthesis

Electrochemical detection can be implemented without labeling by just integrating electrodes onto the device by microfabrication. Normally, there are three types of electrodes (the working electrode (WE), the auxiliary or contact electrode (CE), and a reference electrode (RE)), and the electric output results from an electron flow caused by the chemical reaction which takes place at the surface of the electrodes.

Marchand and Vaultier groups developed an EWOD-based tool without cover to perform solution-phase synthesis by using task-specific ionic liquids as soluble supports (2006)[76]. Two gold catenaries are integrated. The first catenary enables the polarization of the droplet and guides the droplet displacement. The second catenary is used as CE and also RE. The electrochemical measurement is performed between the first catenary (used as WE) and the second catenary (shown in **Figure 1.14-1(a)**). An ionic liquid droplet containing a given reagent is moved on the chip by EWOD and merged with the other ionic liquid droplet containing the other reagent. The reaction is carried out at room temperature for 1h by switching the actuation of electrodes. After incubation, the droplet is analyzed by electrochemical detection. It is also possible to take off the droplet with a micropipette, to dilute it and to inject it into the **high performance liquid chromatography (HPLC)** for separation and analysis.

Tuantranont group integrated a three-electrode electrochemical sensing system (consisting of Au working, Ag reference and Pt auxiliary wires) with a EWOD device for quantitative analysis of iodide (shown in **Figure 1.14-1(b)**) (2011)[77]. For iodide analysis, a droplet of KI solution and a droplet Tris buffer solution are moved and mixed by EWOD, and then the analytical performances of the mixture droplet were characterized by CV measurement at different concentrations ranging from 10 to 100µM. The total analysis time including droplet mixing and cyclic voltammetry (CV) measurement was approximately 12s, showing a promising potential for rapid chemical analysis.

(2) Bilayer lipid membrane formation

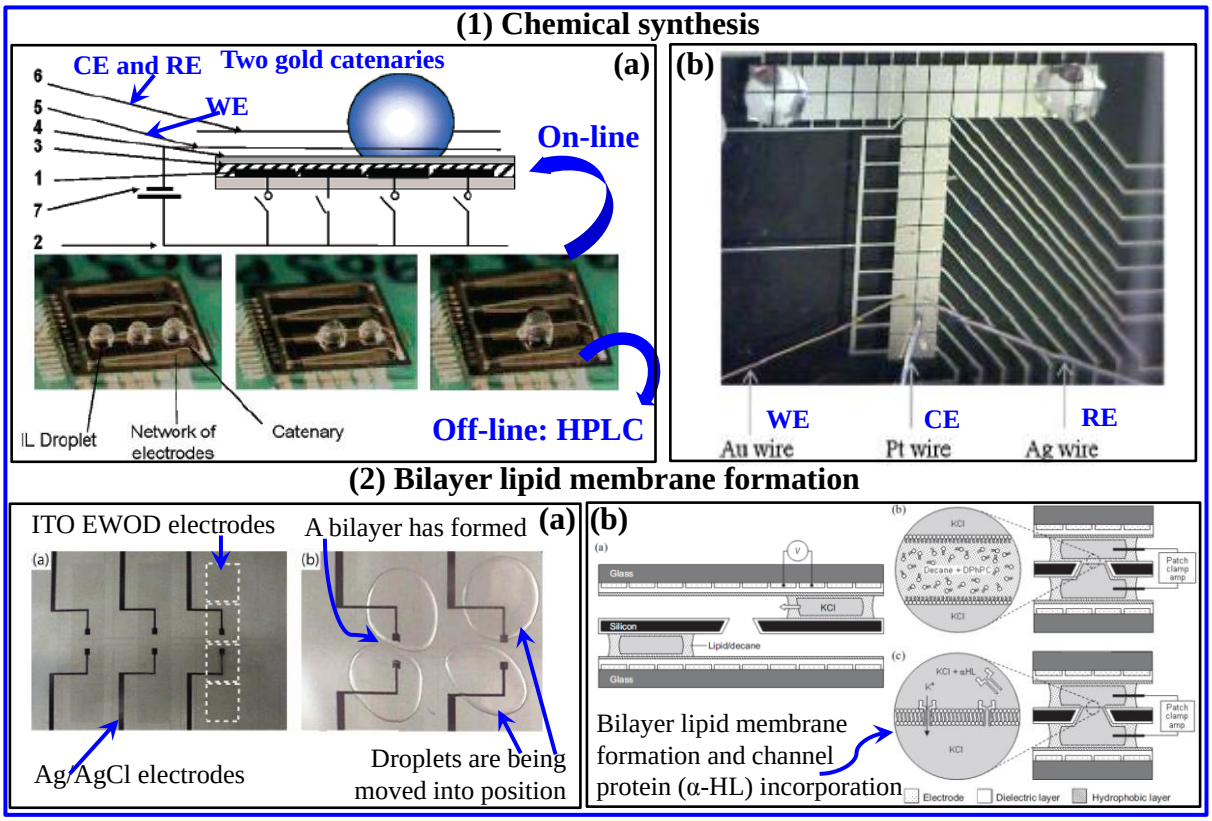

Figure 1.14 Electrochemical detection in (1) chemical synthesis by integrated electrodes and potentiostat (copy from [76][77]), and (2) artificial lipid bilayer formation by integrated electrodes and capacitor feedback patch-clamp (copy from [78][79]).

Poulos et al. proposed a magnetic microparticles-free device which combined three pairs of Ag/AgCl electrodes with underlying ITO EWOD electrodes for parallel formation and measurement of artificial lipid bilayer (shown in **Figure 1.14-2(a)**) (2009)[78]. Prior to use of the device, 0.5μL droplet of standard bleach is placed on the exposed silver electrodes for approximately 30s to create Ag/AgCl electrodes. 2–5μL aqueous droplets are pipetted on the device and immobilized by actuating ITO EWOD electrodes. After a monolayer of lipid molecules finish self-assemble at the aqueous-organic interface, the ITO EWOD electrodes are activated to move the droplets toward each other. When the electrodes are deactivated, a bilayer forms. The bilayer resistance and capacitance are measured, by using a capacitor feedback patch clamp amplifier and a low-noise acquisition system (connected to the Ag/AgCl electrodes). The measured membrane specific capacitance is approximately $0.36\mu F/cm^2$.

Fan group developed a sandwich device, including two opposite coplanar EWOD plates and a middle silicon plate holding an aperture with proper dimension and wettability for droplet interface bilayer formation (shown in **Figure 1.14-2(b)**) (2011)[79]. Two addressable encapsulated droplets in a bulk oil medium were placed above and underneath the middle silicon plate and individual driven by top and bottom EWOD electrodes. Droplet interface bilayer formation is monitored with a microscope and electrophysiological signal examinations (including the trans-membrane capacitance and the ion current) are performed by using Ag/AgCl elcetrodes and a patch clamp amplifier. The specific capacitance of the droplet interface bilayer (DIB) was 0.5μF/cm^2 (higher than the result of **Poulos et al.**) and the thickness of the DIB was calculated to be 6.8 nm.

1.3.2.2. Digital-to-Analog outlet interface

As mentioned in the previous section, a variety of on-line detection methods either optical or electrochemical techniques can be successfully coupling with EWOD chips. However, in mass spectrometry detection, samples are either manually pipetted onto the MALDI-MS substrate or the substrate is manually transported to mass spectrometer. These manual steps are slow and low efficiency. Though on-line optical or electrochemical techniques are widely used in biochemistry applications, but the detection signal carries no information about the chemical nature of the binding partner in solution which is available from MALDI-MS [84]. Thus, an interesting trend is to develop on-line MALDI-MS analysis coupling with EWOD-based device.

Coupling EWOD chip with on-line MS detection, there exist a wide-spread interest in intensifying the resolution and efficiency for analysis. For high-resolution analysis, an electrophoresis component for separating samples within channel or capillary should be coupled to MS [85]. Capillary electrophoresis (CE) coupled to mass spectrometry (MS) has become an increasingly employed technology on the component identification [86][87], because of its high resolving power, robustness and reproducibility, and acceptable time required for routine analysis. Thus, a Digital-to-Analog (D/A) outlet interface is developed to

couple with biochemical separation component prior to mass spectrometer.

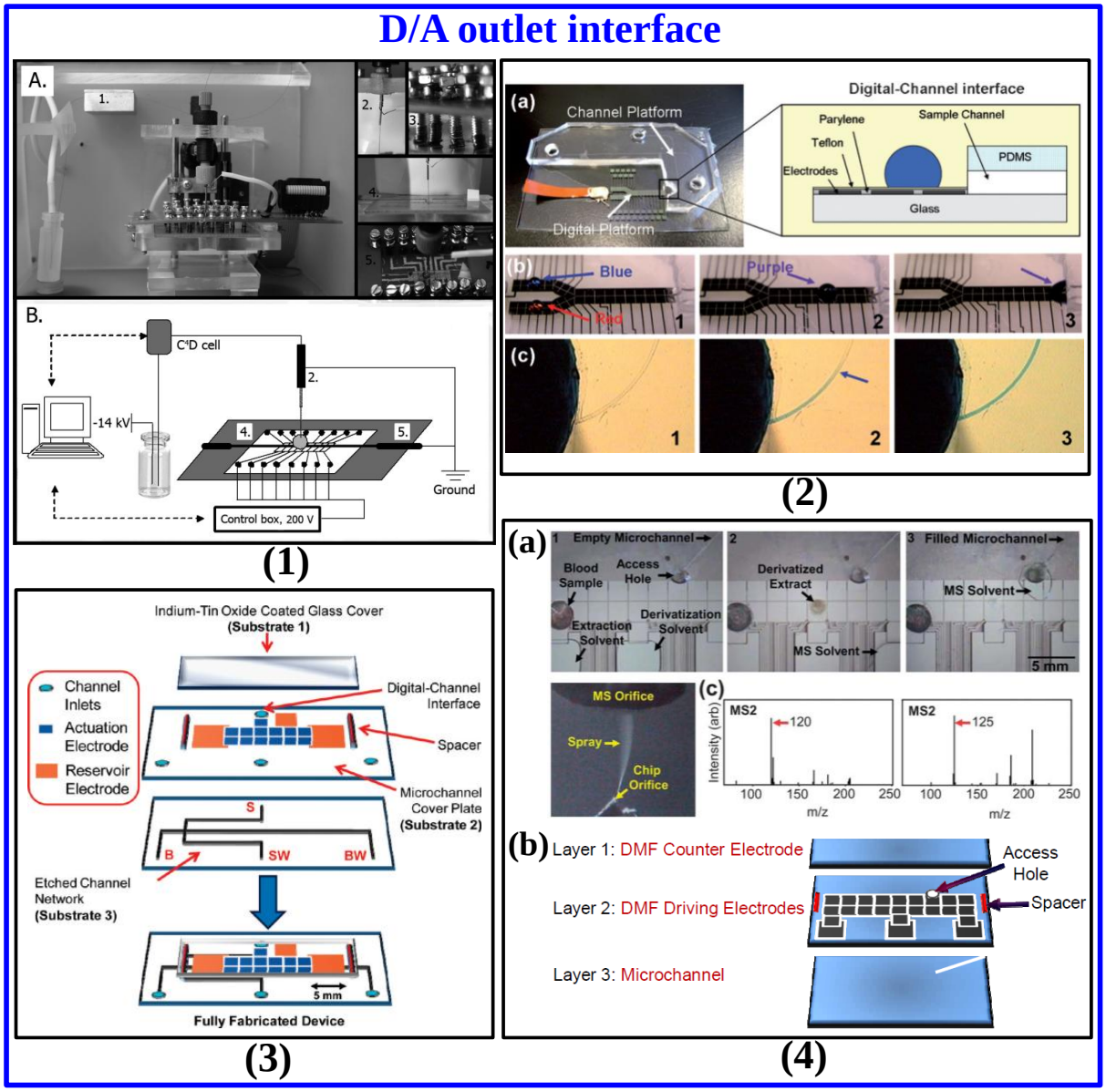

Figure 1.15 D/A interface module: (1)Interfacing the DMF sample into the portable CE analyzer (copy from [88]), (2)Hybrid digital-channel microfluidics device[89], (3)Multilayer hybrid microfluidics device (copy from [90]), and (4) Hybrid DMF-microchannel device for in-line analysis by mass spectrometry (copy from [51]).

Kaljurand group presented a sample introduction approach. Droplets containing sample and buffer solutions are successively transported by EWOD to the place under the vertical capillary electrophoresis (CE) inlet end. Then the mixture is separated by applying a high voltage between the grounded buffer droplet and CE outlet reservoir (shown in **Figure 1.15-1**) (2009)[88]. This method put forward a low-cost and rapid plan toward fully integrated on-line

sample processing and separation in biochemistry.

A similar EWOD-based DMF device coupling with CE was reported by **Wheeler group**. They developed a hybrid device comprising a single-plate EWOD platform for sample preparation and a network of PDMS microchannels for chemical separations (shown in **Figure 1.15-2**) (2009)[89]. In this hybrid device, droplets containing colored dyes are merged and mixed, then delivered to the interface by EWOD. Subsequently they are loaded into pre-filled channels by electrokinetics flow (an electrode is positioned such that it penetrated into the droplet at the interface), and followed by a separation using micellar electrokinetics chromatography (MEKC). However, the drawbacks of the hybrid devices are incompatibility with droplet dispensing from on-chip reservoirs and non-avoidance evaporation. In order to solve the above problems, this group improved the preliminary configuration and demonstrates a new multilayer design. In this new configuration, a two-plate EWOD structure is backside mated to a network of microchannels (shown in **Figure 1.15-3**) (2010)[90]. After completion of processing, samples can be transferred to the network of channels below for analysis by electrophoresis. Recently, this group developed of a strategy for forming EWOD with ‘nano-spray ionization’ mode to couple with electrospray ionization mass spectrometry (ESI-MS) (shown in **Figure 1.15-4**) (2008)[91][51][52]. The sample droplet is actuated to the access interface hole and filled the channel below by capillary action, and then is emitted for MS analysis by a nano-electrospray emitter. In microchannel electrophoresis, microchannels can separate samples fast with high resolution and efficiency. The coupling with MS detection allows the quantification of analytes related to genetic diseases in newborn blood samples.

1.3.3. Full interfaces integration

Full interfaces integration has two advantages. First, it can fully automatically process a sample. Second, it allows to reducing dead volume and thus the volume of the sample is reduced. The concept of ‘full interfaces integration’ is first proposed by **Fair group** (2003)[92]. But ‘full interfaces integration’ hybrid DMF chips still have not yet undergone the test of real implementation until recently when key technical difficulties have been solved. It

is classified into two groups (summarized in **Table 1.2**): (a) fully integrated hybrid EWOD chip (on-chip detection) and (b) fully integrated sample preparation unit (off-chip detection).

Table 1.2 Full interfaces integration module

#	Application	Medium	Inlet Interface		Outlet Interface		Group	Ref.
			Sample Load	Interface Unit	Sample Export	Detection		
Fully integrated hybrid EWOD chip								
1	Clinical applications	Oil-filled	A/D	Pre-stored in on-chip reservoirs	A loading hole in the top plate	D/D	On-line	Optical absorbance detection	Fair	[48]
2	PCR	Oil-filled	A/D	Pre-stored in on-chip reservoirs	A loading hole in the top plate	D/D	On-line	Optical fluorescence detection	Fouillet	[93]
3	Immunoassay	Oil-filled	A/D	Pre-stored in on-chip reservoirs	Loading ports in the top plate	D/D	On-line	Optical chemiluminescence	Advanced Liquid Logic Inc.	[40]
4	PCR						On-line	Optical fluorescence detection		[94]
Fully integrated sample preparation unit								
1	SPR	Air-filled	A/D	Automatic loading	Teflon coating capillary	D/A	On-line	Optical fluorescence detection	Patel	[50]
2	Online bioprocess monitoring	Air-filled	A/D	Automatic loading	Hydrophobic microchannel	D/A	Off-line	ELISA, and CE-MS	Our group	[53]
3	Online bioprocess monitoring				Superhydrophobic microchannel	D/A	Off-line			[54] [55]

1.3.3.1. Fully integrated hybrid EWOD chip: on-chip detection

Based on the prior period work, a fully integrated and reconfigurable hybrid DMF chip has been successfully presented by **Fair group** (shown in **Figure 1.16-1(a)**) (2004)[48]. This was the first time such high-levels of integration and automation have been realized from concept to a proof-of-concept. In the inlet interface part, samples are injected into on-chip reservoir through a loading hole in the top plate, and then droplet formation form the on-chip reservoir only via EWOD force. After separate samples are mixed on the main DMF part, colorimetric reactions are analyzed by using on-chip optical direction method. Similar work was done by **Fouillet group**. They developed an on-chip fluorescence detection hybrid EWOD chip, which integrates a thermal sensor, a Peltier element for temperature control, two lasers and a CCD camera (shown in **Figure 1.16-1(b)**) (2007)[93].

Advanced Liquid Logic Inc. demonstrated a EWOD-based cartridge with particular emphasis on reducing the time-to-result for immunoassays and DNA amplification applications (shown in **Figure 1.16-1(c)(d)**) (2009)[40] (2010)[94]. For the inlet interface

integration, samples are injected from ports mechanically drilled in the top plate and stored in the on-chip reservoirs; While, for the outlet interface integration, chemiluminescence measurement is implemented to enable real-time detection for PCR reaction. The flexibility and breadth of this cartridge makes it an ideal platform to address a wide range of problems in point of care testing.

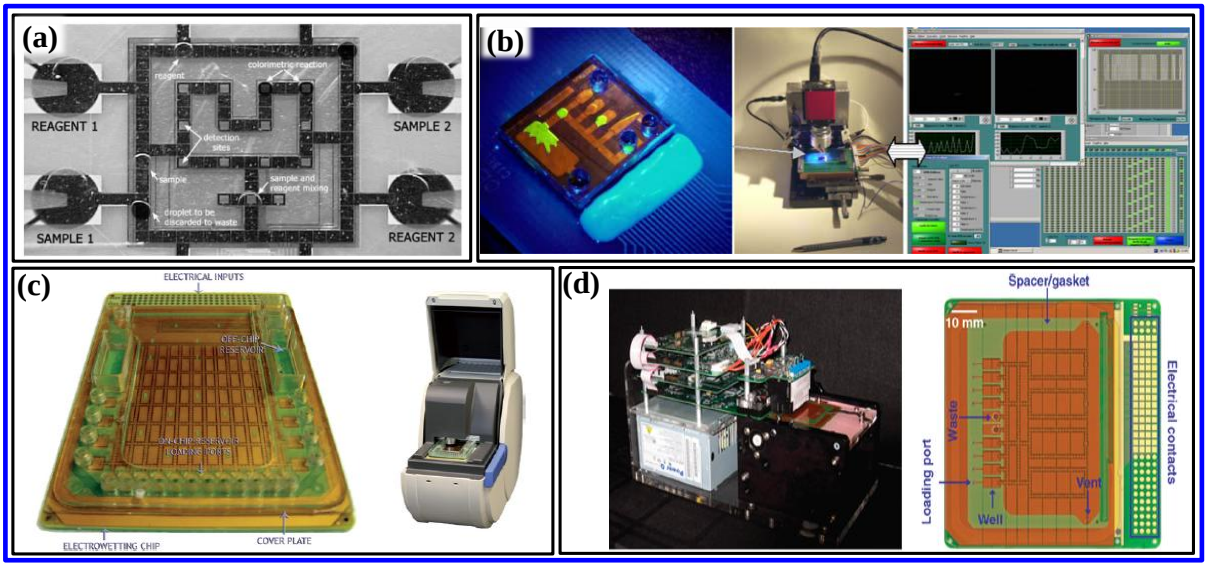

Figure 1.16 (a)High level schematic of EWOD protein droplet system (copy from [48]), (b)EWOD chip and associated instrumentation (copy from [93]), (c)A full assembled digital microfluidic platform (copy from [40]) and (d)Self-contained digital microfluidics PCR system (copy from [94]).

1.3.3.2. Fully integrated sample preparation unit: off-chip detection

When we started the work within the frame of this PhD thesis, we came to the conclusion that it would be desirable to leverage microfluidic designs into multiple applications, rather than specialize to a particular application or detection method. Thus, for achieving full interface integration, we decided to start the development of a flexible plug-in EWOD-based sample preparation unit. In our objectives, this device would work as a central fluid transceiver module (between upstream and downstream fluidic modules) in an integrated system. This full interface integration requires an A/D inlet interface where sample solution can be received and reformed into droplet format and a D/A outlet interface where analyte droplets can be collected to deliver out.

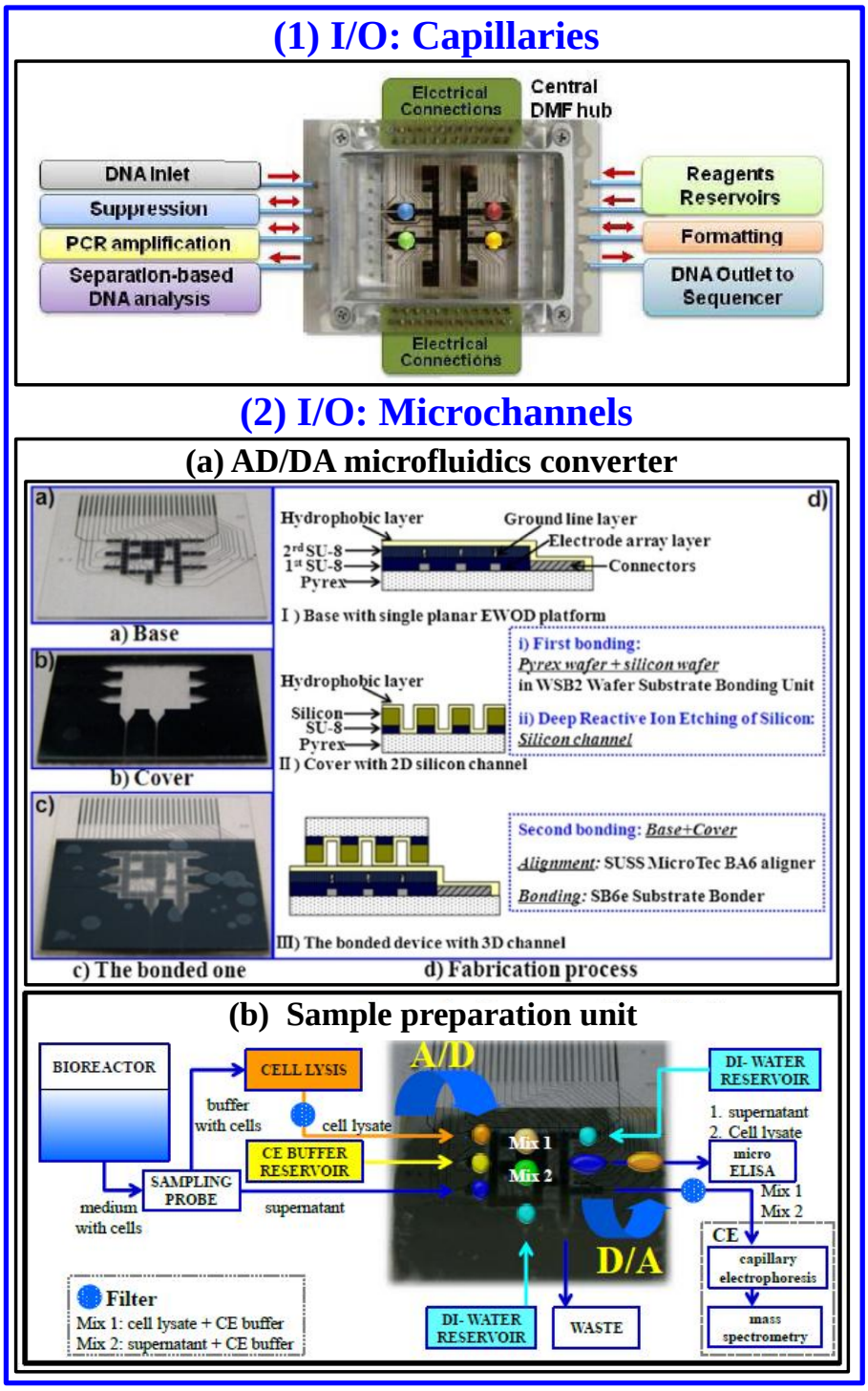

Figure 1.17 (1) Capillaries I/O: an integrated system of a digital microfluidics platform functions as a central hub using a capillary interface (copy from [50]); (2) Microchannels I/O: (a)AD/DA microfluidics converter (copy from [53]), and (b)Sample preparation unit in on-line bioprocesses monitoring (copy from [53][55]).

In the meantime, **Patel group** demonstrated a EWOD-based fluidic hub with capillary tubes to enable fluid transport between the EWOD main part and the external fluidic modules

(shown in **Figure 1.17(1)**) (2011)[50]. As inlet and outlet (I/O) interfaces, the capillary tubes are fixed in position between the substrates by ferrules. In inlet part, a dispensed spherical droplet is growing as sample liquid is pumped through the capillary. Once it grows to a threshold size, a droplet is created by actuating the receiving electrode and the neighboring electrode in sequence. In outlet part, separate sample droplets are automatically routed in succession via EWOD force to predefined 'parking spaces' and then are aspirated as a continuous liquid into capillary (connected to a syringe pump).

Similar, **our group** proposed an original approach integrating microchannles as the inlet and outlet interfaces. The device can: a) 'digital' preconditioning, b) simultaneously handling multiple liquid droplets, and c) well-controlled navigation of multiple samples to the different analysis/detection modules. We have developed two generations. Our preliminary AD/DA microfluidics converter successfully realized from concept to a proof-of-concept (shown in **Figure 1.17(2-a)**) (2011)[53], based on a three layers PSP (Pyrex-Silicon-Pyrex) configuration with hydrophobic liquid-solid interfaces. It is believed that this fabrication process can be used for various MEMS applications. However, our first device suffers from some key limitations (*e.g.*, droplet formation failure). To address these issues, our group demonstrated a second device (shown in **Figure 1.17(2-b)**) (2011) [54] (2012)[55]. It is made of a single-plate EWOD bonded to a silicon superhydrophobic top plate etched by DRIE to define inlets/outlets and the central samples conditioning area. This bilayer PS (Pyrex-Silicon) configuration has the added benefit of reducing applied voltage and facilitating the droplet generation due to little friction and tiny surface adsorption on superhydrophobic top plate. This prototype has been successfully used for 'digital' preconditioning samples taken from a yeast bio-reactor and then delivered to analytical modules either an enzyme-linked immunosorbent assay (ELISA) or a capillary electrophoresis (CE) device coupled with a mass spectrometry (MS). This method puts forward a new flexible and automatic plan toward full integrated on-line sample preconditioning, preparation and exporting.

1.3.4. Conclusion

Based on the integrated level of the interfaces, coupling EWOD chip to external fluidic modules is classified as inlet interface integration, outlet interface integration, and full interfaces integration.

1) In inlet interface, sample fluidic format is transferred from continuous-flow to droplet. Integration with inlet interface enables efficient sample loading on EWOD chip. Sample loading can be performed by: (a) filling from the loading hole in the top plate, (b) dispensing from a dosing system controlled by capacitance/impedance feedback, (c) loading through closed-channels where integrated EWOD electrodes, or (d) loading through virtual electrowetting channels.

2) Outlet interface is subdivided into Digital-to-Digital (D/D) module and Digital-to-Analog (D/A) module, due to the fluidic format of samples in post-processing. Several efforts are made to couple existing detection methods (mass spectrometry, optical detection, and electrochemical detection) and electrophoresis component.

3) Full interfaces integration is subdivided into fully integrated hybrid EWOD chip (on-chip detection) and fully integrated sample preparation unit (off-chip detection). High-levels of integration and automation have been realized in fully integrated hybrid EWOD chip. However, due to the special design, the scope of applications is limited. While, fully integrated sample preparation unit works as a central fluid transceiver module in an integrated system. This method put forward a new flexible plan toward fully integrated on-line sample preconditioning, preparation and exporting.

1.4. Summary

The aim of this Chapter is to understand the opportunities and limitations of EWOD-based DMF system, and focus on stating the desirable need for development of interfaces coupling to external fluidic modules. In the preceding part, we have dealt with the fundamental theory of electrowetting, analyzed the configurations of EWOD devices (two-plate closed and single-plate open configurations), and stated the basic EWOD fluidic operations (transport,

dispensing from on-chip reservoirs, splitting and merging, and mixing).

In the second part, we have presented the classification and pointed out the important of inlet and outlet interface integration on EWOD chip. Based on the integrated level of the interfaces, it is classified as inlet interface integration, outlet interface integration, and full interfaces integration. Among them, the full interfaces integration can fully automatically process the required operations from the sample loading to the sample detection. This method allows to reducing dead volume and thus the volume of the sample is reduced. Rather than specialize to a particular application or detection method, the fully integrated sample preparation unit leverages microfluidics designs into multiple applications. It provides a path toward realizing the true lab-on-a-chip.

In Chapter 2, we will present the design, fabrication and the validation experiments of our proposed EWOD-based sample preparation unit.

References

[1] G. M. Whitesides, "The origins and the future of microfluidics", *Nature*, vol. 442, pp. 368–373, 2006.

[2] D. Mark, S. Haeberle, G. Roth, F. von Stetten, and R. Zengerle, "Microfluidic lab-on-a-chip platforms: requirements, characteristics and applications", *Chem. Soc. Rev.*, vol. 39, pp. 1153–1182, 2010.

[3] S. Haeberle and R. Zengerle, "Microfluidic platforms for lab-on-a-chip applications", *Lab Chip*, vol. 7, pp. 1094–1110, 2007.

[4] P. S. Dittrich and A. Manz, "Lab-on-a-chip: microfluidics in drug discovery", *Nature Reviews Drug Discovery*, vol. 5, pp. 210–218, 2006.

[5] S.-Y. Teh, R. Lin, L.-H. Hung, and A. P. Lee, "Droplet microfluidics", *Lab Chip*, vol. 8, pp. 198–220, 2008.

[6] T. Thorsen, S. J. Maerkl, and S. R. Quake, "Microfluidic Large-Scale Integration", *Science*, vol. 298, pp. 580–584, Oct 2002.

[7] E. Verpoorte and N. F. De Rooij, "Microfluidics meets MEMS", *Proceedings of the IEEE*, vol. 91, no. 6, pp. 930 – 953, Jun 2003.

[8] N. Pamme, "Continuous flow separations in microfluidic devices", *Lab on a Chip*, vol. 7, pp. 1644–1659, 2007.

[9] B. Zheng, J. D. Tice, and R. F. Ismagilov, "Formation of Droplets of Alternating Composition in Microfluidic Channels and Applications to Indexing of Concentrations in Droplet-Based Assays", *Anal. Chem.*, vol. 76, pp. 4977–4982, 2004.

[10] L. Yobas, S. Martens, W.-L. Ong, and N. Ranganathan, "High-performance flow-focusing geometry for spontaneous generation of monodispersed droplets", *Lab on a Chip*, vol. 6, pp. 1073–1079, 2006.

[11] R. B. Fair, "Digital microfluidics: is a true lab-on-a-chip possible?", *Microfluidics and Nanofluidics*, vol. 3, pp. 245–281, 2007.

[12] M. Abdelgawad and A. R. Wheeler, "The Digital Revolution: A New Paradigm for Microfluidics", *Advanced Materials*, vol. 21, pp. 920–925, 2009.

[13] M. J. Jebrail and A. R. Wheeler, "Let's get digital: digitizing chemical biology with microfluidics", *Current Opinion in Chemical Biology*, vol. 14, pp. 574–581, 2010.

[14] G. Lippmann, "Relations entre les phénomènes electriques et capillaires" , Faculté des sciences de Paris, 1875.

[15] G. Beni and S. Hackwood, "Electrowetting displays", *Appl. Phys. Lett.*, vol. 38, no. 4, pp. 207–209, 1981.

[16] B. Berge, "Electrocapillarity and wetting of insulator films by water", *Comptes Rendus de l'Academie des Sciences Serie II*, vol. 317, no. 2, pp. 157–163, 1993.

[17] M. Vallet, B. Berge, and L. Vovelle, "Electrowetting of water and aqueous solutions on poly(ethylene terephthalate) insulating films", *Polymer*, vol. 37, no. 12, pp. 2465–2470, 1996.

[18] D. Brassard, L. Malic, F. Normandin, M. Tabrizian, and T. Veres, "Water-oil core-shell droplets for electrowetting-based digital microfluidic devices", *Lab on a Chip*, vol. 8, pp. 1342–1349, 2008.

[19] J. Berthier, *Microdrops and Digital Microfluidics*. William Andrew Publishing, 2008.

[20] J. Berthier, P. Dubois, P. Clementz, P. Claustre, C. Peponnet, and Y. Fouillet, "Actuation potentials and capillary forces in electrowetting based microsystems", *Sensors and Actuators A: Physical*, vol. 134, pp. 471–479, 2007.

[21] F. Li and F. Mugele, "How to make sticky surfaces slippery: Contact angle hysteresis in electrowetting with alternating voltage", *Applied Physics Letters*, vol. 92, no. 244108, pp. 1–3, 2008.

[22] J. H. Song, R. Evans, Y.-Y. Lin, B.-N. Hsu, and R. B. Fair, "A scaling model for electrowetting-on-dielectric microfluidic actuators", *Microfluidics and Nanofluidics*, vol. 7, pp. 75–89, 2009.

[23] K. Choi, A. H. C. Ng, R. Fobel, and A. R. Wheeler, "Digital Microfluidics", *Annual Review of Analytical Chemistry*, vol. 5, pp. 413–440, 2012.

[24] M. G. Pollack, A. D. Shenderov, and R. B. Fair, "Electrowetting-based actuation of droplets for integrated microfluidics", *Lab on a Chip*, vol. 2, pp. 96–101, 2002.

[25] Ui-Chong Yi and Chang-Jin Kim, "EWOD actuation with electrode-free cover plate", in *The 13th International Conference on Solid-State Sensors, Actuators and Microsystems*, Seoul, Korea, 2005, vol. 1, pp. 89– 92.

[26] S.-K. Fan, C. Hashi, and C.-J. Kim, "Manipulation of multiple droplets on N times;M grid by cross-reference EWOD driving scheme and pressure-contact packaging", in *IEEE Conf. Micro Electro Mechanical Systems (MEMS '03)*, 2003, pp. 694 – 697.

[27] J. Gong, S.-K. Fan, Chang-Jin, and C. J. Kim, "Portable digital microfluidics platform with active but disposable Lab-On-Chip", in *Micro Electro Mechanical Systems, 2004. 17th IEEE International Conference on. (MEMS)*, 2004, pp. 355 – 358.

[28] V. N. Luk, G. C. Mo, and A. R. Wheeler, "Pluronic Additives: A Solution to Sticky Problems in Digital Microfluidics", *Langmuir*, vol. 24, pp. 6382–6389, 2008.

[29] D. Chatterjee, B. Hetayothin, A. R. Wheeler, D. J. King, and R. L. Garrell, "Droplet-based microfluidics with nonaqueous solvents and solutions", *Lab on a Chip*, vol. 6, pp. 199–206, 2006.

[30] V. Srinivasan, V. K. Pamula, P. Paik, and R. B. Fair, "Protein stamping for MALDI mass spectrometry using an electrowetting-based microfluidic platform", *Proceedings of the SPIE*, vol. 5591, pp. 26–32, 2004.

[31] Y. Fouillet and J.-L. Achard, "Microfluidique discrète et biotechnologie", *Comptes Rendus Physique*, vol. 5, pp. 577–588, 2004.

[32] R. B. Fair, A. Khlystov, V. Srinivasan, V. K. Pamula, and K. N. Weaver, "Integrated chemical/biochemical sample collection, pre-concentration, and analysis on a digital microfluidic lab-on-a-chip platform", *Proceedings of SPIE*, vol. 5591, pp. 113–124, 2004.

[33] C. Cooney, C.-Y. Chen, M. Emerling, A. Nadim, and J. Sterling, "Electrowetting droplet microfluidics on a single planar surface", *Microfluidics and Nanofluidics*, vol. 2, pp. 435–446, 2006.

[34] M. Abdelgawad, S. L. S. Freire, H. Yang, and A. R. Wheeler, "All-terrain droplet actuation", *Lab on a Chip*, vol. 8, pp. 672–677, 2008.

[35] P. Y. Paik, V. K. Pamula, and K. Chakrabarty, "Adaptive Cooling of Integrated Circuits Using

Digital Microfluidics", *IEEE Transactions on Very Large Scale Integration (VLSI) Systems*, vol. 16, no. 4, pp. 432–443, Apr 2008.

[36] U.-C. Yi and C.-J. Kim, "Characterization of electrowetting actuation on addressable single-side coplanar electrodes", *Journal of Micromechanics and Microengineering*, vol. 16, pp. 2053–2059, 2006.

[37] M. Abdelgawad, P. Park, and A. R. Wheeler, "Optimization of device geometry in single-plate digital microfluidics", *Journal of Applied Physics*, vol. 105, no. 094506, pp. 1–7, 2009.

[38] J.-Y. Yoon, "Open-surface digital microfluidics", *The Open Biotechnology Journal*, vol. 2, pp. 94–100, 2008.

[39] E. M. Miller and A. R. Wheeler, "Digital bioanalysis", *Analytical and Bioanalytical Chemistry*, vol. 393, pp. 419–426, 2008.

[40] R. Sista, Z. Hua, P. Thwar, A. Sudarsan, V. Srinivasan, A. Eckhardt, M. Pollack, and V. Pamula, "Development of a digital microfluidic platform for point of care testing", *Lab Chip*, vol. 8, pp. 2091–2104, 2008.

[41] Y.-H. Chang, G.-B. Lee, F.-C. Huang, Y.-Y. Chen, and J.-L. Lin, "Integrated polymerase chain reaction chips utilizing digital microfluidics", *Biomedical Microdevices*, vol. 8, pp. 215–225, 2006.

[42] H. Moon, A. R. Wheeler, R. L. Garrell, J. A. Loo, and C.-J. "CJ" Kim, "An integrated digital microfluidic chip for multiplexed proteomic sample preparation and analysis by MALDI-MS", *Lab Chip*, vol. 6, pp. 1213–1219, 2006.

[43] J. K. Osiri, H. Shadpour, M. A. Witek, and S. A. Soper, "Integrated multifunctional microfluidics for automated proteome analyses", *Top Curr Chem*, vol. 304, pp. 261–294, 2011.

[44] I. Barbulovic-Nad, H. Yang, P. S. Park, and A. R. Wheeler, "Digital microfluidics for cell-based assays", *Lab Chip*, vol. 8, pp. 519–526, 2008.

[45] C. Y. Fan, Y. Tung, S. Takayama, E. Meyhöfer, and K. Kurabayashi, "Electrically Programmable Surfaces for Configurable Patterning of Cells", *Advanced Materials*, vol. 20, pp. 1418–1423, 2008.

[46] D. Witters, N. Vergauwe, S. Vermeir, F. Ceyssens, S. Liekens, R. Puers, and J. Lammertyn, "Biofunctionalization of electrowetting-on-dielectric digital microfluidic chips for miniaturized cell-based applications", *Lab Chip*, vol. 11, pp. 2790–2794, 2011.

[47] P. Y. Keng, S. Chen, H. Ding, S. Sadeghi, G. J. Shah, A. Dooraghi, M. E. Phelps, N. Satyamurthy, A. F. Chatziioannou, C.-J. C. Kim, and R. M. van Dam, "Micro-chemical synthesis of molecular probes on an electronic microfluidic device", *Proceedings of the National Academy of Sciences*, vol. 109, no. 3, pp. 690–695, Jan 2012.

[48] V. Srinivasan, V. K. Pamula, and R. B. Fair, "An integrated digital microfluidic lab-on-a-chip for clinical diagnostics on human physiological fluids", *Lab Chip*, vol. 4, pp. 310–315, 2004.

[49] M. J. Jebrail, M. S. Bartsch, and K. D. Patel, "Digital Microfluidics: A Versatile Tool For Applications in Chemistry, Biology and Medicine", *Lab on a Chip*, vol. 12, pp. 2452–2463, 2012.

[50] H. Kim, M. S. Bartsch,, R. F. Renzi, J. He, J. V. D. Vreugde, M. R. Claudnic, and K. D. Patel, "Automated sample preparation platform for next generation DNA sequencing using a digital microflidic hub", presented at the 15th International Conference on Miniaturized Systems for

Chemistry and Life Sciences, Seattle, Washington, USA, 2011, pp. 753–755.

[51] M. J. Jebrail, H. Yang, J. M. Mudrik, N. M. Lafrenière, C. McRoberts, O. Y. Al-Dirbashi, L. Fisher, P. Chakraborty, and A. R. Wheeler, "A digital microfluidic method for dried blood spot analysis", *Lab Chip*, vol. 11, pp. 3218–3224, 2011.

[52] S. C. C. Shih, H. Yang, M. J. Jebrail, R. Fobel, N. McIntosh, O. Y. Al-Dirbashi, P. Chakraborty, and A. R. Wheeler, "Dried Blood Spot Analysis by Digital Microfluidics Coupled to Nanoelectrospray Ionization Mass Spectrometry", *Anal. Chem.*, vol. 84, pp. 3731–3738, 2012.

[53] C. Wu, F. Bendriaa, F. Brunelle, and V. Senez, "Fabrication of AD/DA microfluidic converter using deep reactive ion etching of silicon and low temperature wafer bonding", *Microelectronic Engineering*, vol. 88, pp. 1878–1883, 2011.

[54] C. Wu, F. Brunelle, M. Harnois, and V. Senez, "Sample preparation unit for online bio-processes monitoring", in *Proceedings of the 15th International Conference on Miniaturized Systems for Chemistry and Life Sciences*, Seattle, Washington, USA, 2011, pp. 2034–2036.

[55] C. Wu, F. Brunelle, M. Harnois, J. Follet, and V. Senez, "An integrated hybrid microfluidic system for online bioprocesses monitoring: combining electrical lysis and EWOD sample preparation", in *Proceedings of the 25th International Conference on Micro Electro Mechanical Systems*, Paris, France, 2012, pp. 777–780.

[56] U.-C. Yi and C.-J. "CJ" Kim, "Soft printing of droplets pre-metered by electrowetting", *Sensors and Actuators A: Physical*, vol. 114, pp. 347–354, 2004.

[57] H. Ren, R. B. Fair, and M. G. Pollack, "Automated on-chip droplet dispensing with volume control by electro-wetting actuation and capacitance metering", *Sensors and Actuators B: Chemical*, vol. 98, no. B, pp. 319–327, 2004.

[58] H. Ding, S. Sadeghi, P. Y. Keng, S. Chen, G. J. Shah, C.-J. "CJ" Kim, and R. M. van Dam, "Accurate dispensing of volatile reagents on demand for EWOD chips", presented at the 15th International Conference on Miniaturized Systems for Chemistry and Life Sciences, Seattle, Washington, USA, 2011, pp. 227–229.

[59] F. Malloggi, S. A. Vanapalli, H. Gu, D. van den Ende, and F. Mugele, "Electrowetting-controlled droplet generation in a microfluidic flow-focusing device", *Journal of Physics: Condensed Matter*, vol. 19, no. 462101, pp. 1–7, 2007.

[60] J. Kedzierski, S. Berry, and B. Abedian, "New Generation of Digital Microfluidic Devices", *Journal of Microelectromechanical Systems*, vol. 18, no. 4, pp. 845–851, Aug 2009.

[61] M. Dhindsa, J. Heikenfeld, S. Kwon, J. Park, P. D. Rack, and I. Papautsky, "Virtual electrowetting channels: electronic liquid transport with continuous channel functionality", *Lab Chip*, vol. 10, pp. 832–836, 2010.

[62] A. Banerjee, E. Kreit, Y. Liu, J. Heikenfeld, and I. Papautsky, "Reconfigurable virtual electrowetting channels", *Lab Chip*, vol. 12, pp. 758–764, 2012.

[63] V. N. Luk and A. R. Wheeler, "A Digital Microfluidic Approach to Proteomic Sample Processing", *Anal. Chem.*, vol. 81, pp. 4524–4530, 2009.

[64] K. P. Nichols and Han J. G. E. Gardeniers, "A Digital Microfluidic System for the Investigation of Pre-Steady-State Enzyme Kinetics Using Rapid Quenching with MALDI-TOF Mass Spectrometry", *Anal. Chem.*, vol. 79, pp. 8699–8704, 2007.

[65] A. R. Wheeler, H. Moon, C.-J. "CJ" Kim, J. A. Loo, and R. L. Garrell, "Electrowetting-Based

Microfluidics for Analysis of Peptides and Proteins by Matrix-Assisted Laser Desorption/Ionization Mass Spectrometry", *Anal. Chem.*, vol. 76, pp. 4833–4838, 2004.

[66] A. R. Wheeler, H. Moon, C. A. Bird, R. R. Ogorzalek Loo, C.-J. "C. J. . Kim, J. A. Loo, and R. L. Garrell, "Digital Microfluidics with In-Line Sample Purification for Proteomics Analyses with MALDI-MS", *Anal. Chem.*, vol. 77, pp. 534–540, 2005.

[67] Hyejin Moon, A. R. Wheeler, R. L. Garrell, J. A. Loo, and Chang-Jin Kim, "On-chip sample preparation by electrowetting-on-dielectric digital microfluidics for matrix assisted laser desorption/ionization mass spectrometry", in *18th IEEE International Conference on Micro Electro Mechanical Systems, 2005. MEMS 2005*, 2005, pp. 859– 862.

[68] W. C. Nelson, I. Peng, G.-A. Lee, J. A. Loo, R. L. Garrell, and C.-J. "CJ" Kim, "Incubated Protein Reduction and Digestion on an Electrowetting-on-Dielectric Digital Microfluidic Chip for MALDI-MS", *Anal. Chem.*, vol. 82, pp. 9932–9937, 2010.

[69] N. A. Mousa, M. J. Jebrail, H. Yang, M. Abdelgawad, P. Metalnikov, J. Chen, A. R. Wheeler, and R. F. Casper, "Droplet-Scale Estrogen Assays in Breast Tissue, Blood, and Serum", *Science Translational Medicine*, vol. 1, no. 1 1ra2, pp. 1–6, Oct 2009.

[70] F. Lapierre, G. Piret, H. Drobecq, O. Melnyk, Y. Coffinier, V. Thomy, and R. Boukherroub, "High sensitive matrix-free mass spectrometry analysis of peptides using silicon nanowires-based digital microfluidic device", *Lab Chip*, vol. 11, pp. 1620–1628, 2011.

[71] P. A. L. Wijethunga, Y. S. Nanayakkara, P. Kunchala, D. W. Armstrong, and H. Moon, "On-Chip Drop-to-Drop Liquid Microextraction Coupled with Real-Time Concentration Monitoring Technique", *Anal. Chem.*, vol. 83, pp. 1658–1664, 2011.

[72] V. Srinivasan, V. K. Pamula, and R. B. Fair, "Droplet-based microfluidic lab-on-a-chip for glucose detection", *Analytica Chimica Acta*, vol. 507, pp. 145–150, 2004.

[73] J. Heikenfeld and A. J. Steckl, "Intense switchable fluorescence in light wave coupled electrowetting devices", *Applied Physics Letters*, vol. 86, no. 011105, pp. 1–3, 2005.

[74] G. Marchand, P. Dubois, C. Delattre, F. Vinet, M. Blanchard-Desce, and M. Vaultier, "Organic Synthesis in Soft Wall-Free Microreactors: Real-Time Monitoring of Fluorogenic Reactions", *Anal. Chem.*, vol. 80, pp. 6051–6055, 2008.

[75] L. Malic, T. Veres, and M. Tabrizian, "Two-dimensional droplet-based surface plasmon resonance imaging using electrowetting-on-dielectric microfluidics", *Lab Chip*, vol. 9, pp. 473–475, 2008.

[76] P. Dubois, G. Marchand, Y. Fouillet, J. Berthier, T. Douki, F. Hassine, S. Gmouh, and M. Vaultier, "Ionic Liquid Droplet as e-Microreactor", *Anal. Chem.*, vol. 78, pp. 4909–4917, 2006.

[77] C. Karuwan, K. Sukthang, A. Wisitsoraat, D. Phokharatkul, V. Patthanasettakul, W. Wechsatol, and A. Tuantranont, "Electrochemical detection on electrowetting-on-dielectric digital microfluidic chip", *Talanta*, vol. 84, pp. 1384–1389, 2011.

[78] J. L. Poulos, W. C. Nelson, T.-J. Jeon, C.-J. "CJ" Kim, and J. J. Schmidt, "Electrowetting on dielectric-based microfluidics for integrated lipid bilayer formation and measurement", *Applied Physics Letters*, vol. 95, no. 013706, pp. 1–3, 2009.

[79] Yi-Ying Lin, Ching-Wen Chen, Li-Chi Chen, and Shih-Kang Fan, "Formation of droplets interface bilayer by coplanar EWOD device", in *2011 IEEE International Conference on Nano/Micro Engineered and Molecular Systems (NEMS)*, 2011, pp. 964–967.

[80] H. Yang, V. N. Luk, M. Abelgawad, I. Barbulovic-Nad, and A. R. Wheeler, "A World-to-Chip Interface for Digital Microfluidics", *Analytical Chemistry*, vol. 81, pp. 1061–1067, 2009.

[81] M. J. Jebrail and A. R. Wheeler, "Digital Microfluidic Method for Protein Extraction by Precipitation", *Anal. Chem.*, vol. 81, pp. 330–335, 2009.

[82] L. Malic, D. Brassard, T. Veres, and M. Tabrizian, "Integration and detection of biochemical assays in digital microfluidic LOC devices", *Lab Chip*, vol. 10, pp. 418–431, 2010.

[83] A. H. C. Ng, U. Uddayasankar, and A. R. Wheeler, "Immunoassays in microfluidic systems", *Analytical and Bioanalytical Chemistry*, vol. 397, pp. 991–1007, 2010.

[84] P. L. Urban, A. Amantonico, and R. Zenobi, "Lab-on-a-plate: Extending the functionality of MALDI-MS and LDI-MS targets", *Mass Spectrometry Reviews*, vol. 30, pp. 435–478, 2011.

[85] W. Kolch, C. Neusüß, M. Pelzing, and H. Mischak, "Capillary electrophoresis–mass spectrometry as a powerful tool in clinical diagnosis and biomarker discovery", *Mass Spectrometry Reviews*, vol. 24, pp. 959–977, 2005.

[86] H. Mischak and J. P. Schanstra, "CE-MS in biomarker discovery, validation, and clinical application", *PROTEOMICS–Clinical Applications*, vol. 5, pp. 9–23, 2011.

[87] H. Mischak, J. J. Coon, J. Novak, E. M. Weissinger, J. P. Schanstra, and A. F. Dominiczak, "Capillary electrophoresis–mass spectrometry as a powerful tool in biomarker discovery and clinical diagnosis: An update of recent developments", *Mass Spectrometry Reviews*, vol. 28, pp. 703–724, 2009.

[88] J. Gorbatsova, M. Jaanus, and M. Kaljurand, "Digital Microfluidic Sampler for a Portable Capillary Electropherograph", *Anal. Chem.*, vol. 81, pp. 8590–8595, 2009.

[89] M. Abdelgawad, M. W. L. Watson, and A. R. Wheeler, "Hybrid microfluidics: A digital-to-channel interface for in-line sample processing and chemical separations", *Lab Chip*, vol. 9, pp. 1046–1051, 2009.

[90] M. W. L. Watson, M. J. Jebrail, and A. R. Wheeler, "Multilayer Hybrid Microfluidics: A Digital-to-Channel Interface for Sample Processing and Separations", *Analytical Chemistry*, vol. 82, pp. 6680–6686, 2010.

[91] S. L. S. Freire, H. Yang, and A. R. Wheeler, "A practical interface for microfluidics and nanoelectrospray mass spectrometry", *ELECTROPHORESIS*, vol. 29, pp. 1836–1843, 2008.

[92] R. B. Fair, V. Srinivasan, H. Ren, P. Paik, V. K. Pamula, and M. G. Pollack, "Electrowetting-based on-chip sample processing for integrated microfluidics", in *Electron Devices Meeting, 2003. IEDM 03 Technical Digest. IEEE International*, 2003, pp. 779–782.

[93] Y. Fouillet, D. Jary, C. Chabrol, P. Claustre, and C. Peponnet, "Digital microfluidic design and optimization of classic and new fluidic functions for lab on a chip systems", *Microfluidics and Nanofluidics*, vol. 4, pp. 159–165, 2008.

[94] Z. Hua, J. L. Rouse, A. E. Eckhardt, V. Srinivasan, V. K. Pamula, W. A. Schell, J. L. Benton, T. G. Mitchell, and M. G. Pollack, "Multiplexed Real-Time Polymerase Chain Reaction on a Digital Microfluidic Platform", *Anal. Chem.*, vol. 82, pp. 2310–2316, 2010.

2. DESIGN, FABRICATION, AND TEST OF A EWOD-BASED SAMPLE PREPARATION UNIT

Content

2.1. Introduction

The state-of-the-art of EWOD-based digital microfluidic has been given in the Chapter 1, where we have presented the classification and we have pointed out the important of fully integrated sample preparation unit. This chapter is devoted to the implementation of a EWOD-based digital microfluidic device for sample preparation. We present a work aiming at developing an analysis tool for the preparation of intra/extra cellular compounds of yeast cells, which is part of NANOBE project n°227243 supported by the E.U. (FP7). The accomplishment of this sample preparation unit is stated, from concept to a proof-of-concept. To fabricate the capabilities of this device, we have developed two generations based on a combination of EWOD functionalities and channel-based continuous microfluidic techniques.

In our first work, a three layers PSP (Pyrex-Silicon-Pyrex) configuration with hydrophobic liquid-solid interfaces has been employed (illustrated in **Table 2.1**). The fabrication has been based on deep reactive ion etching of silicon and low temperature full wafer adhesive bonding. The technology development includes an improvement of the bonding process in order to produce an adaptive strength of SU-8 bond, which not only ensures absence of debonding failures (during the silicon deep etching procedure and the subsequent dicing procedure), but also avoids the potential SU-8 overflow leakage into channels due to the bonding step. It is believed that the fabrication technology can be used in diverse MEMS applications. However, our preliminary device has suffered from a key limitation: the difficulty in droplet formation.

To address this limitation, we have developed a new sample preparation unit with a bilayer PS (Pyrex-Silicon) configuration with superhydrophobic liquid-solid interfaces (illustrated in **Table 2.1**). In our new design, the fundamental fluid operations (droplet formation, transport, merging and mixing, and delivery) have been validated. Finally, high speed camera has been used to observe water droplet transport, which is very useful for the understanding of the dynamic mechanism (*e.g.*, dynamic contact angle and instantaneous velocity).

Table 2.1 Comparison of the first generation device (AD/DA microfluidics converter) and second generation device (Sample Preparation Unit).

	(a) AD/DA microfluidics converter	(b) Sample Preparation Unit
3D	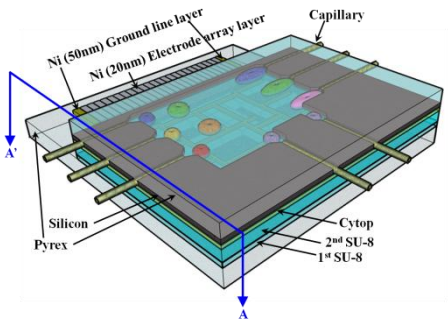	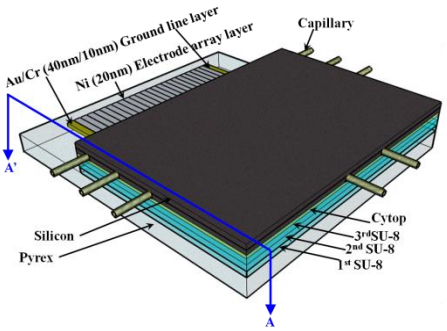
A-A'	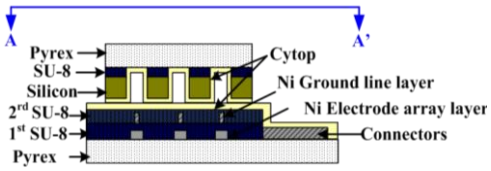	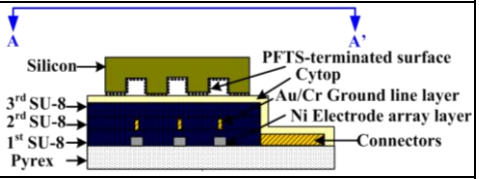
Device assembly	Adhesive bonding with patterned SU-8	Fixed by a homemade fixed mount
Property	Pyrex-Silicon-Pyrex configuration: ➢ Hydrophobic CYTOP cover ➢ Hydrophobic CYTOP base	Pyrex-Silicon configuration: ➢ Superhydrophobic PFTS cover ➢ Hydrophobic CYTOP base
	Limited fluidic operations: ➢ Fail in droplet formation from channels ➢ Successful transport ➢ Successful merging and mixing	Reproducibility fluidic operations: ➢ Successful droplet formation ➢ Successful transport and delivery ➢ Successful merging and mixing
	Higher driven voltage (190V)	Lower driven voltage (142V)
	The durability of the chip: small (<100 loops)	The durability of the chip: big (>400 loops)
	Velocity: low	Velocity: high
Merits	The fabrication process can be used for various MEMS applications.	The hybrid device can be used as 'fluidic transceiver' in an integrated system.

2.2. Concept of sample preparation unit

We propose a hybrid device, "sample preparation unit", integrating both AD interface and DA interface. **Figure 2.1** schematically illustrates the configuration of the sample preparation unit. The system consists of the following procedures: a) continuous preload of reagents, b) independently manipulation of several droplets, c) recombination and exportation of samples in channel-based continuous flow. On one side, 'digital' preconditioning by EWOD technology allows precise control of multiple reagents without the need of a complex network

of micro-valves. On the other side, 'continuous' format is ideal for interfacing to downstream analytical and detection instruments. The final layout of the hybrid device includes the design of the device configuration and sizing of the general features of the device.

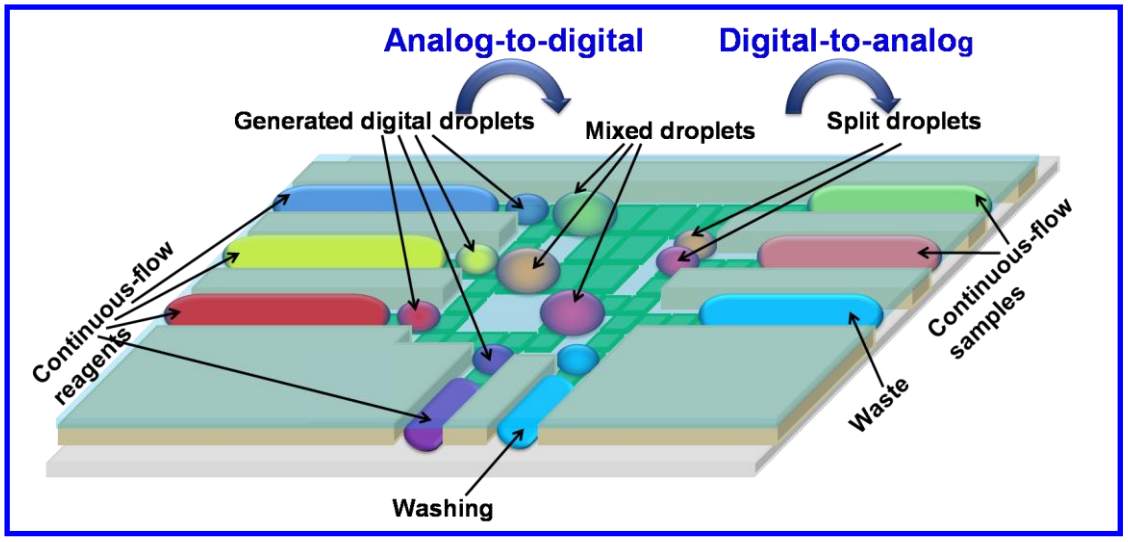

Figure 2.1 Schematic diagram of sample preparation unit: generating and manipulating droplets, and ensuring washing.

2.2.1. Design of the device configuration

In the two-plate configuration of EWOD systems, both plates have electrical wirings, which makes this configuration fairly complex for integration with other devices. Also in the single-plate configuration, there exist notable disadvantages: inevitable evaporation phenomenon and the lack of the capacity to dispense or split droplets. It is clear that the two-plate configuration and the single-plate configuration have their own advantages and disadvantages, and that these two configurations are in fact complementary.

Our interest is to develop a new parallel-plate configuration in which both configurations are combined. In our proposed parallel-plate configuration, a) the bottom plate is a EWOD platform which carries both the actuation and grounding electrodes and b) the top plate is an electrode-free cover which provides a network of microchannels.

2.2.2. Sizing of the general features of the device

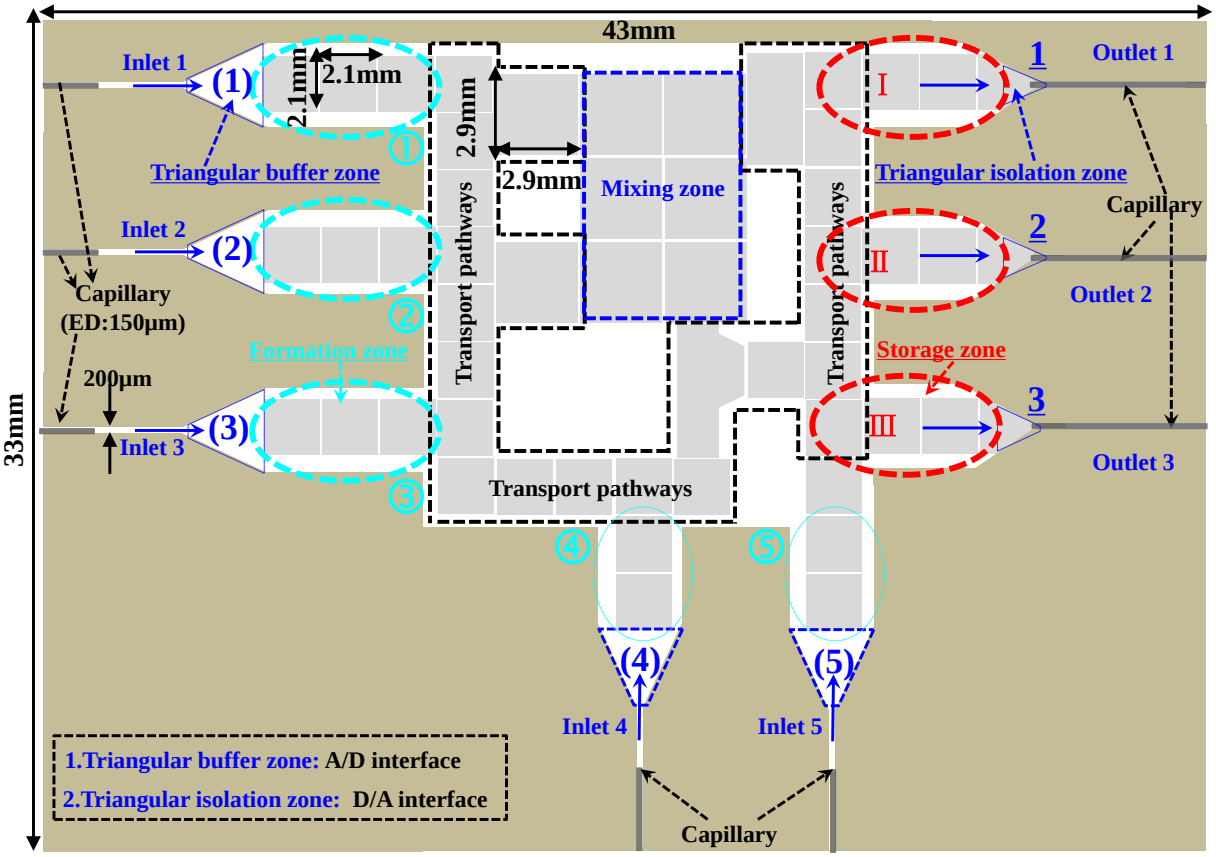

Figure 2.2 Schematic diagram of physical components architecture. Brown region is the top-view of the micro-channels wall.

The schematic diagram of physical components architecture (not including the electric connectors) is illustrated in **Figure 2.2**. The number of electric connectors is 26, 24 for connecting the actuation electrode network and 2 for connecting to the ground electrode. A LabVIEW program control a switch matrix to multiplexes an electrical square voltage to the actuation electrode network (50 electrodes). The actuation electrode network includes 40 standard electrodes (2.1mm*2.1mm) and 10 double-size electrodes (2.9*2.9mm). The width of microchannels is designed as 200μm to allow the insertion of the glass capillary (external diameter 150μm). The thickness of microchannels is 200μm (not shown in **Figure 2.2**). The architecture consists of 5 ***'droplet formation zones'*** isolated by the ***'triangular buffer zones'*** from the inlets, a central dual-channel ***'bus transportation pathway'***, a ***'mixing zone'***, 3 reprocessed ***'fluid storage zones'***, and 3 ***'triangular isolation zones'*** at the tip of outlet channels. The ***'triangular buffer zones'*** is used as analog-to-digital interface; while the

'triangular isolation zones' is used as digital-to-analog interface.

The fluid sample loading through the inlet channel can be extracted and created into several droplets in formation zone. The controllable volume of drop is determined by the size of standard electrode (2.1mm*2.1mm) and the minimum volume is 0.69μL (the details are presented in **Appendix A.1**). The extracted volume can be precise controlled by LabVIEW program (will be discussed in **Section 2.4.4.1**). In our design, 1μL is defined as an elemental volume. The droplet can be transported through the central dual-channel 'bus' to the mixing zone, and then can be merged and mixed with another droplet. After that, the mixture is transported to the object storage zone and exported from the outlet channel. The central 'bus' is designed to connect different zones, and it also can be used for merging and mixing operations or as additional storage buffer zone.

2.3. First generation: AD/DA microfluidics converter

2.3.1. Fabrication

For our specific chip design and applications, one additional issue had to be addressed. We need to select the material to form a 200μm thick channel structures (the thickness of channel is fixed according to the NANOBE project). Most of microfluidic structures predominantly are fabricated based on Si or SU-8. Both have specific advantages and disadvantages. Advantage of using SU-8 for thin closed channels and cavities is that it has the whole structure made out of one material only and it creates strong bonds for adhesive bonding with itself by cross-linking [1][2]. However, the fabrication of thick SU-8 has experienced severe problems such as cracks, distortions, or delaminations during the fabrication process and/or postservices, due to the large internal stress generated during the photolithography process [3]. In addition, thick SU-8 has to rely on UV glue for bonding, and the UV glue inevitably brings catastrophic overflow [4]. Here, we have to fabricate a 200μm thick channel structures, thus Si is preferable.

2.3.1.1. Materials

In our work, SU-8 is used as bonding intermediate layer, because of its good properties, such as photo-patternable, high mechanical strength, optical transparency, versatility, good adhesion on many different substrate materials and superior chemical stability[5][6]. Two-side polished 3-inch <100> Si wafers with 200µm thickness and 3-inch Pyrex wafers with 700µm thickness were employed. The photomasks were generated using a layout software (CleWin) and were printed on a chromium photomask. CYTOP® solution was prepared by mixing CYTOP CTL-809M with its associated solvent CT-solv 180 (1:10, v/v).

2.3.1.2. Device fabrication

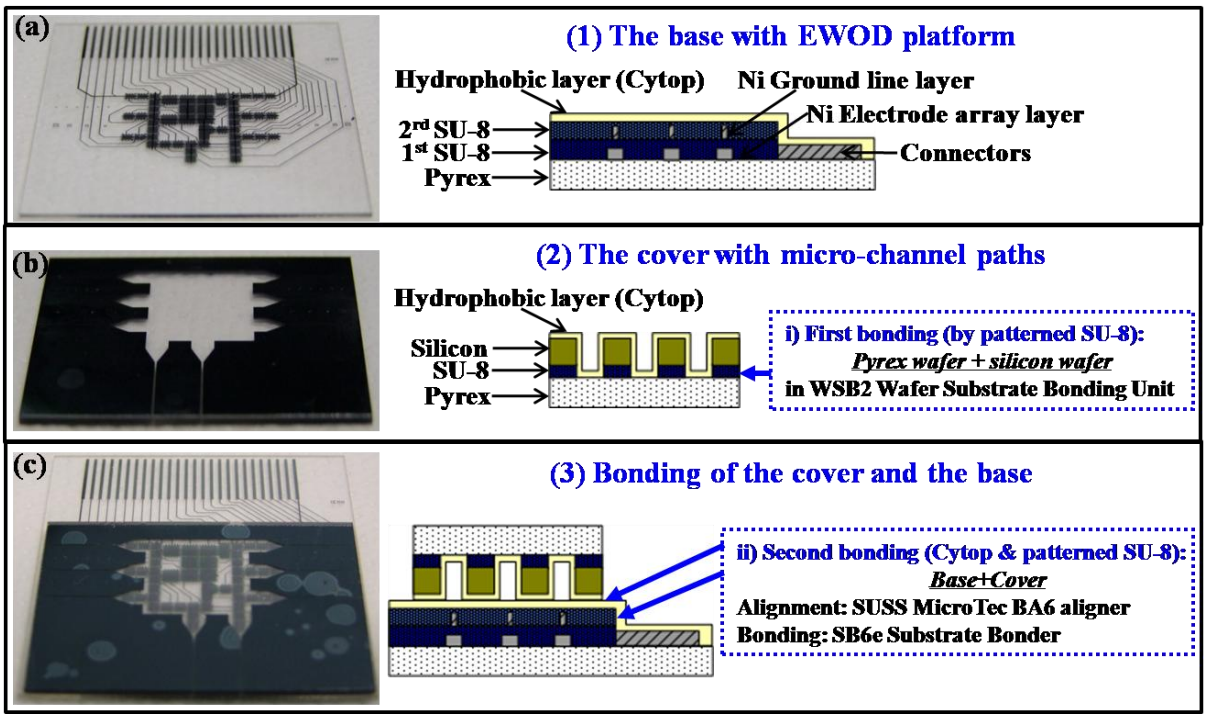

Figure 2.3 Photo pictures of (a) the base with EWOD platform, (b) the cover with micro-channel paths, and (c) the resulting bonded device. (1), (2), and (3) are schematic diagrams of the corresponding fabrication processes.

Our EWOD-based Hybrid Microfluidics Platform is made by the assembly of a single-plate EWOD platform (base) with electrode-free top plate including a network of micro-channel paths (cover) [7]. Using this configuration, two bonding processes are involved: a) the cover is based on the assembly of silicon and Pyrex wafers by adhesive bonding, then deep reactive

ion etching (DRIE) is used to define the micro-channel paths, b) the base and the cover bind with precise alignment. In order to achieve high-quality bonding results, the bonding process and parameters, as well as wafer-to-wafer alignment, must be precisely controlled.

The fabrication process consists of three steps (as shown in **Figure 2.3**): (a) the base with EWOD platform; (b) the cover with micro-channel paths; (c) the adhesive bonding of the base and cover.

(a) The base with EWOD platform

Since the experiment observation is from the backside of the bottom plate, optical transparency of electrodes is of crucial importance. Some transition metal films, when sufficiently thin, become transparent to light, still maintaining good electrical properties [8]. In the base fabrication, nickel is employed to form electrodes. After cleaning procedure, a first 20nm nickel layer is deposited on Pyrex substrate wafer by electron beam evaporation. Then, the nickel electrode array is photo-patterned and formed by using positive AZ1518 photo-resister. After, the first 1.5μm thick SU-8 film is spun coated, at 4500rpm with acceleration of 2000rpm/s for 30 seconds. With these parameters, the uniformity of SU-8 film thickness can be realized. To further crosslinking, hard bake at 180°C on a hot plate for 30 minutes is performed. Then, a second 50nm nickel layer (the ground line) is formed by lift-off technology.

The second SU-8 film has two functions: protecting the ground line layer and used as an intermediate bonding material. We have studied the effect of the second SU-8 thickness on the displacement of the conductive droplets. We have analyzed two different thicknesses (450nm and 1.5μm) and we have found that 1.5μm is the right thickness. After that, a CYTOP film is spun coated without soft bake. Finally, the crosslinking reactions are continued during the bond thermal treatment, obtaining strong adhesion. The fabrication methodology is outline in **Figure 2.4**.

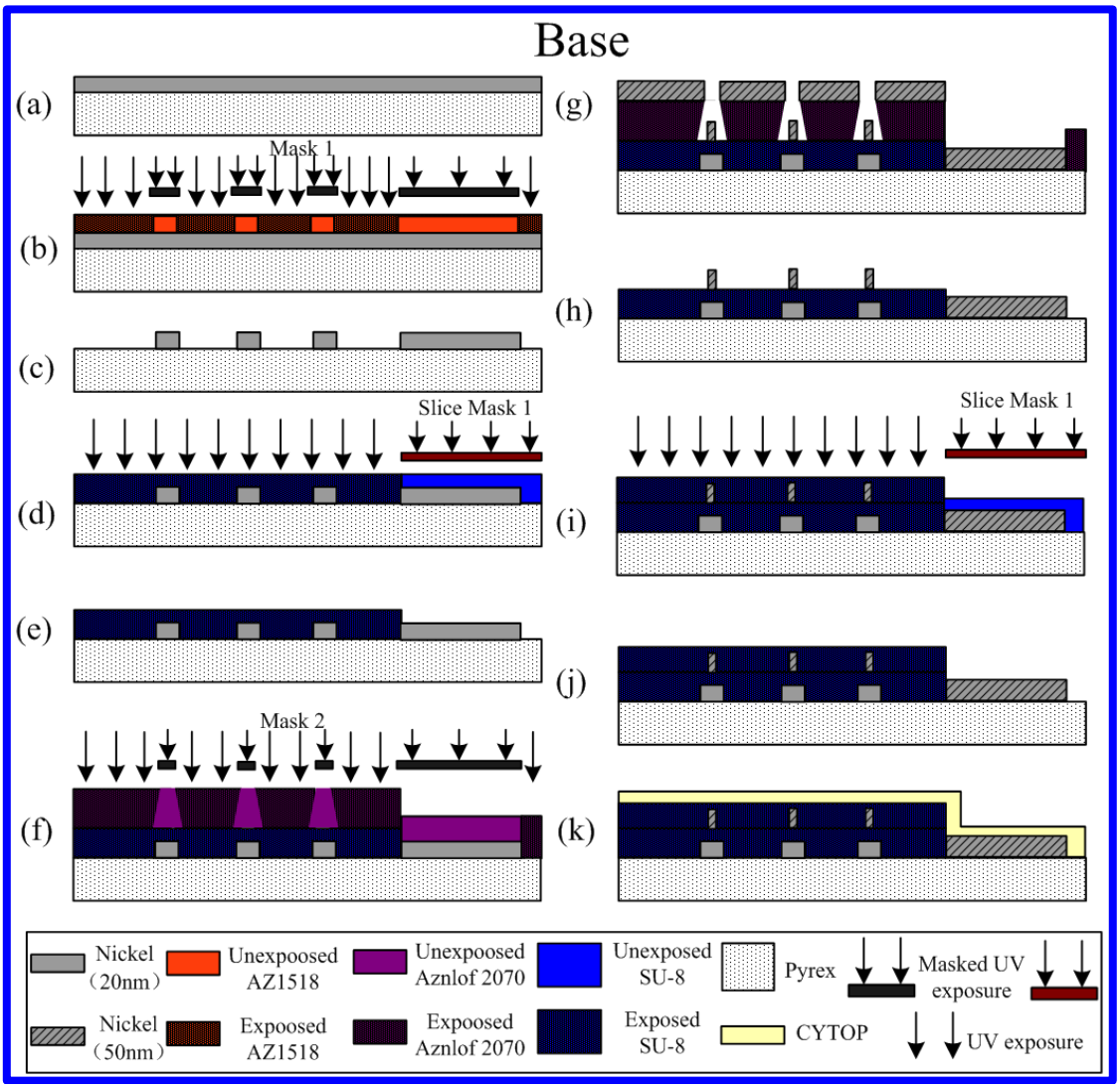

Figure 2.4 Outline of fabrication procedures used for the base: one electrode layer (Nickel), two dielectric layers (SU-8), one ground line layer (Nickel), and one hydrophobic layer (CYTOP). (a) start with a metallized (Nickel) substrate; (b) AZ1518 spin coating and pattern of the electrode layer with Mask 1; (c) development of AZ1518, etch of the unprotected Nickel layer in HNO_3 solution and then strip of AZ1518; (d) spinning of the first SU-8 layer (SU-8 2002) and expose of the first SU-8 layer with Slice Mask1 (a piece of red plastic sheet used to cover the area of connects); (e) development of the first SU-8 layer and hard bake at 180C° for 30 minutes; (f) AZnlof 2070 spin coating and pattern of the ground line layer with Mask 2; (g) second Nickel deposition after development of AZnlof 2070; (h) lift-off to form the ground line layer; (i) spinning of the second SU-8 layer (SU-8 2002 or SU-8 2000.5) and expose of the second SU-8 layer with Slice Mask1; (j) development of the second SU-8 layer (without hard bake); (k) hydrophobic (CYTOP) spin coating.

(b) The cover with micro-channel paths

Fabrication of the cover is based on the assembly of silicon and Pyrex wafers by SU-8 adhesive bonding. The fabrication methodology is outline in **Figure 2.5**. To obtain a good adhesion of the SU-8 film, both the Pyrex and the silicon wafers need a dehydrating treatment

on a hotplate at 200°C. Based on the process described for the first SU-8 dielectric layer in above section, a photolithographic patterned 1.5μm thick SU-8 layer is fabricated. Afterward, the two wafers are brought into contact and pressed against each other on a hotplate at 85°C for 10min. Finally, they are bonded in bonding machine (LOGITECH-WSB2 Wafer Substrate Bonding Unit).

Then, deep reactive ion etching (DRIE) of the silicon layer is used to define the micro-channel paths (inlet and outlet of the converter). A hard metal mask is one of the easier mask technologies to use for deep reactive ion etching of silicon. Commonly the metal mask is selected based on the ease of deposition and the relative inertness to the reactive process chemistry, which means selecting materials that do not form volatile fluorides [9]. Aluminum mask is commonly used and we have selected it in our work. First, we used Aznlof 2020 to pattern and to form the aluminum mask. H_3PO_4 aqueous solution is used to etch the aluminum (15min at 45°C), followed by rinsing with deionized water and drying under a stream of nitrogen. After that, the dry etching of silicon is carried out in a deep silicon etching system (Surface Technology System (STS) Deep Reactive Ion Etching (RIE) Etch System), separating into two distinct steps (passivation step and etching step) [10]. Here, SF_6/O_2 (O_2 being included to ensure the reactant species remain available to react with the silicon) and C_4F_8 are used as the etching and deposition gases, respectively. The deposition of passivation layer (2.2 seconds) and etching (3 seconds) take turns in the silicon etch process and the result etching speed is about 4.5μm/min. Thus, after 44 minutes (2 steps: 20min + 22min) deep silicon etching, 200μm depth channel can be made. After, the aluminum mask can be stripped in a H_3PO_4 aqueous solution at 45°C for 15min. The final step is spin coating of a thin hydrophobic layer (CYTOP).

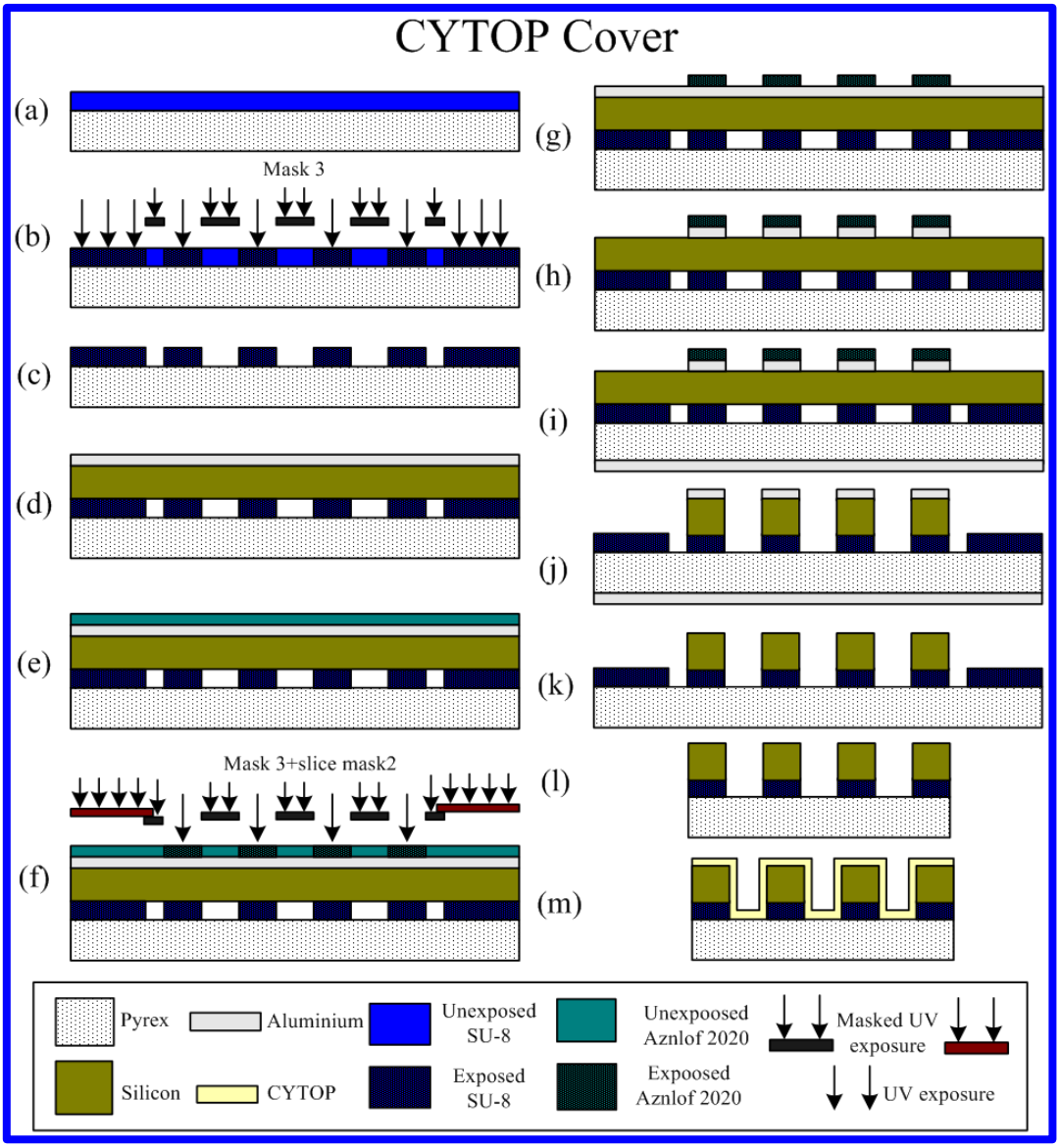

Figure 2.5 Outline of fabrication procedures used for the cover with micro-channel paths. (a) SU-8 2002 spin coating on Pyrex; (b) pattern of the structure SU-8 layer with Mask 3; (c) development of the structure SU-8 layer; (d) bonding of the Pyrex substrate with a metallized (Aluminum) silicon wafer; (e) AZnlof 2020 spin coating; (f) pattern of the hard mask (Aluminum layer) for deep reactive ion etching of silicon with Mask 3 and Slice Mask2 (a piece of red plastic sheet used to cover parts of Mask 3); (g) development of AZnlof 2020; (h) etch of the aluminum layer in H_3PO_4 solution at 45℃; (i) another aluminum deposition on the backside of the bonded wafer for avoiding helium leaking during deep reactive ion etching; (j) etch of the silicon layer in STS Deep RIE Etch System; (k) strip of both top and bottom aluminum layer in H_3PO_4 solution at 45℃; (l) dicing of the wafer with cut mark (dimension of cut: 4.4cm×3.4cm); (m) hydrophobic (CYTOP) spin coating.

(c) Bonding of the cover and base

Next, AD/DA converter is formed by adhesive bonding (outline in **Figure 2.6**), between "CYTOP" and "CYTOP&SU-8(no hard bake)" layers. Unlike the cover fabrication, the

assembly of the base and the cover must be controlled in precise alignment. This is accomplished with a cluster tool consisting of SUSS MicroTec BA6 bond aligner and SB6e substrate bonder.

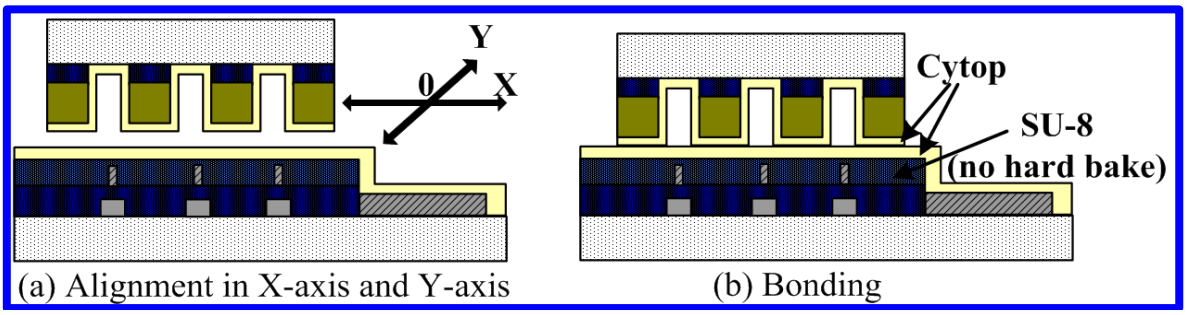

Figure 2.6 The assembly of the base and the cover: (a) precise alignment in both X-axis and Y-axis in SUSS MicroTec BA6 bond aligner, and (b) bonding in SB6e substrate bonder.

First, the base and the cover are aligned by BA6 bond aligner and then transferred to the bond chamber. Prior to contact, two heaters (bottom and top) start to heat until the two heaters have the same temperature of 85°C for 10min [11]. Subsequently, two heaters start to heat the wafers to a temperature of 110°C, applying a pressure of 2 bars for 30min.

2.3.2. Preliminary characterization

2.3.2.1. Characterization of device fabrication

The whole device fabrication process includes two wafer adhesive bondings using patterned SU-8: (a) the cover fabrication and (b) the assembly of the cover with the base.

(a) Cover fabrication

A major challenge in the cover fabrication is bonding. The most critical parameters to obtain a successful bonding are: (1) the bond strength: it should be strong enough to avoid de-bounding failure during deep reactive ion etching procedure in STS System and also the subsequent dicing of the wafer; (2) the overflow of SU-8: SU-8 overflow should not be significant during the pressure bonding procedure. Bonding parameters such as bonding pressure, bonding time, and dehydrating treatment can significantly impact the resulting bonding quality and defect density [2]. Prior to the bonding procedure, it is the dehydrating

process during which the two wafers are brought into contact and pressed against each other on hotplate. The dehydrating process is to enable moisture evaporation and prevent any void formation [12].

These parameters have been optimized and summarized in **Table 2.2**. When the bond pressure is high (3 bars), it is observed a catastrophic overflow leakage of SU-8 within channels. It suggests the bonding pressure should be decreased. Without change of the dehydrating treatment and bonding time, we have decreased the bonding pressure to 2 bars. The bonding is successful and without significant overflow. However, in the subsequent processes (deep reactive ion etching procedure in STS System), the two bonded wafers are de-bonded. It suggests the bonding strength is not enough. The bonding strength is strongly affected by the bonding time and dehydrating treatment. Thus, we increase the bonding time to 30 minutes in Test 3. However, the bonding strength is still not enough and de-bonding happens during the dicing of the wafer procedure. Then, we increase the dehydrating time to 10 minutes in Test 4, and the bonding is successful. Thus, the insufficient dehydrating can explain the failure of Test 3.

Table 2.2 Optimized bonding process parameters (SU-8:1.5μm; bonding temperature: 110°C)

#	Dehydrating treatment(min)	Bonding Time(min)	Bonding pressure(bar)	Results
Test 1	5	20	3	Fail: catastrophic overflow leakage
Test 2	5	20	2	Fail: de-bonding
Test 3	5	30	2	Fail: de-bonding
Test 4	10	30	2	OK

Furthermore, we have checked the level of the overflow, based on the bonding parameter in Test 4. **Figure 2.7** shows SEM cross-sectional images of the bonding interface between silicon wafer and Pyrex wafer (after DRIE procedure and the dicing procedure). Almost straight-line SU-8 boundary line is observed. It indicates that little SU-8 overflow has occurred within the micro-channel. The leakage SU-8 off the channel walls is probably generated by deep silicon etching. In photography (e), one can observe the presence of the SU-8 layer off the channel walls (4μm or 8μm). The different values maybe caused by lithography misalignment. However, this misalignment is non-critical and tolerable.

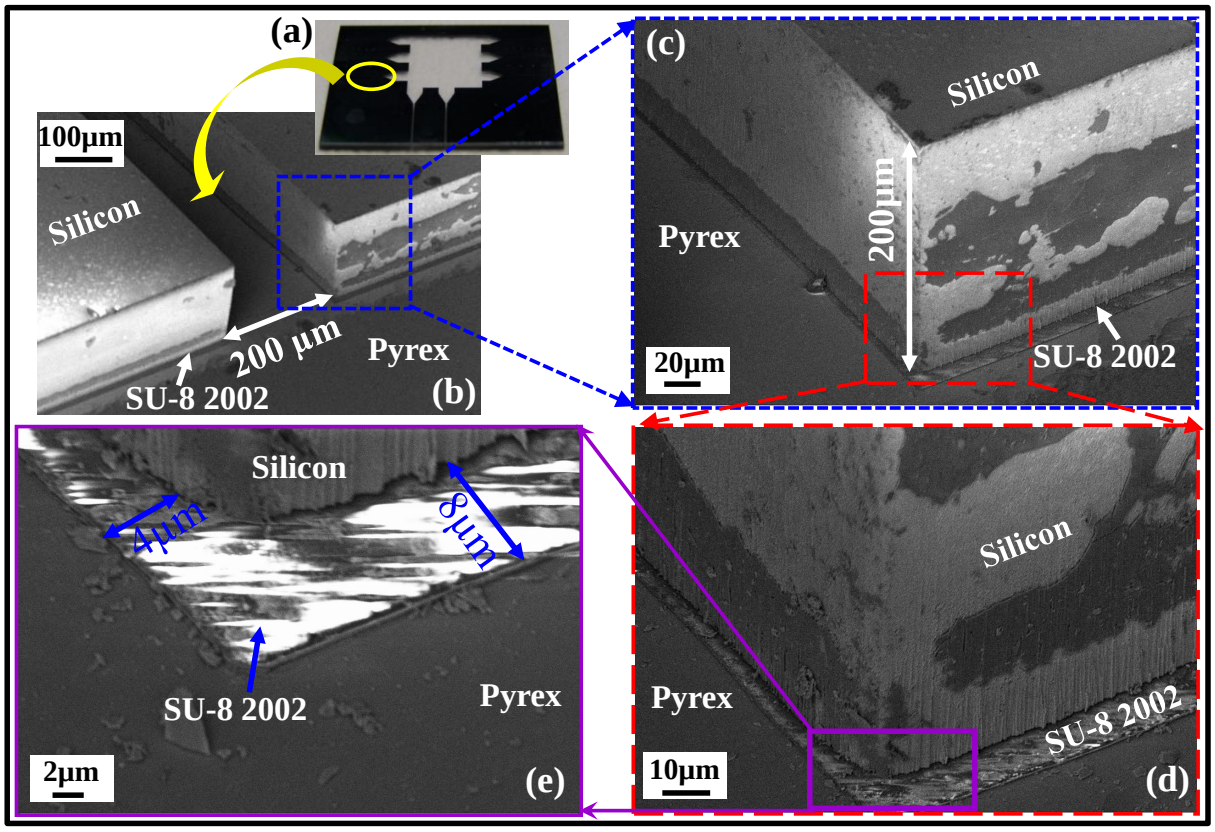

Figure 2.7 (a) Photo picture of the bonded top plate. (b)-(e) SEM images of the resulting bonding interface between silicon and Pyrex wafer with different magnifications.

All the results suggest that the bonding parameters in Test 4 are successful. Thus, in the assembly of the cover with the base, we also apply the same bonding parameters.

(b) The assembly of the cover with the base

In the assembly of the cover with the base, it is very critical to perform a perfect alignment to obtain good bonding results. We have checked the bonded device by using light microscope, and the results are shown in **Figure 2.8**. We have focused on three parts, two close to inlet (1-2) and one close to outlet. One can compare the design layer-out with the photography taken by optical microscope, and can observe a perfect alignment of the cover and the in all three parts.

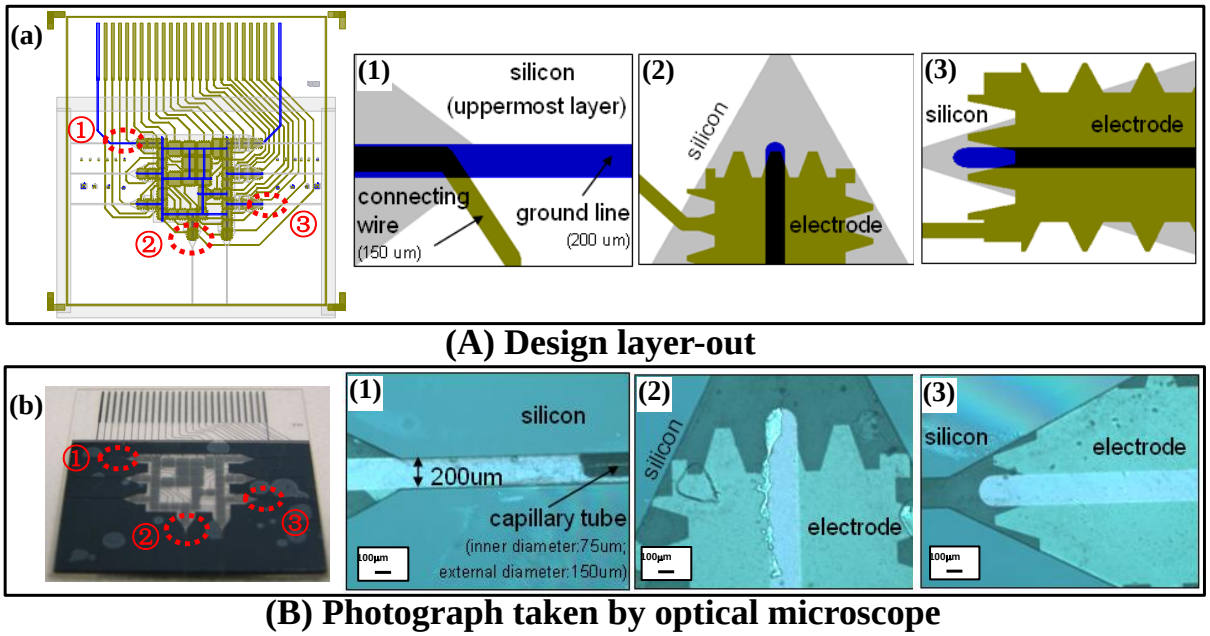

Figure 2.8 Comparison between the initial design layer-out (a) and the photograph taken by optical microscope (b). The design layer-out and the photography show the good alignment of the cover and the base, in two different parts close to inlet (1-2) and one part close to outlet (3).

2.3.2.2. First characterization of device performance

2.3.2.2.1. Contact angle hysteresis of the EWOD-based bottom plate

Regarding a droplet moving over a surface, the roughness is a very important parameter. The measure of contact angle hysteresis refers to a threshold resistance force to initial movement due to the surface roughness. Low contact angle hysteresis is preferred for efficient EWOD actuation. Thus, it is important to study the contact angle hysteresis. Thus, prior to verify the performance of the bonded device, we have measured the contact angle hysteresis of the EWOD-based bottom plate.

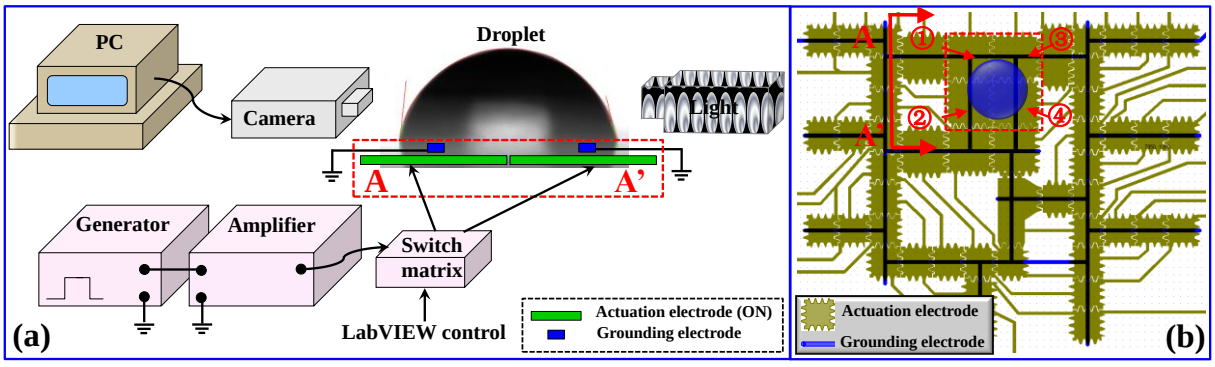

Figure 2.9 Schematic view of the experiment set up: (a) View of the experiment set up with electronics and monitoring, and (b) Top view of the used actuation electrodes.

From the contact angle versus voltage curve, the contact angle hysteresis can be extracted. **Figure 2.9** describes the set-up used for this experiment. A DI-water droplet (4µL) is positioned on four electrodes (2.9*2.9mm^2/each) belonging to the base of the device and the cover is removed. The measurement is performed using a KRŰSS Drop Shape Analysis System DSA100. A 1 kHz square-wave signal is applied between the ground electrode and the four actuation electrodes. The signal is created by a generator (CENTRRD-5MHz Function generator GF 265) and then amplified by an amplifier (TEGAM-High voltage Amplifier Model 2340).

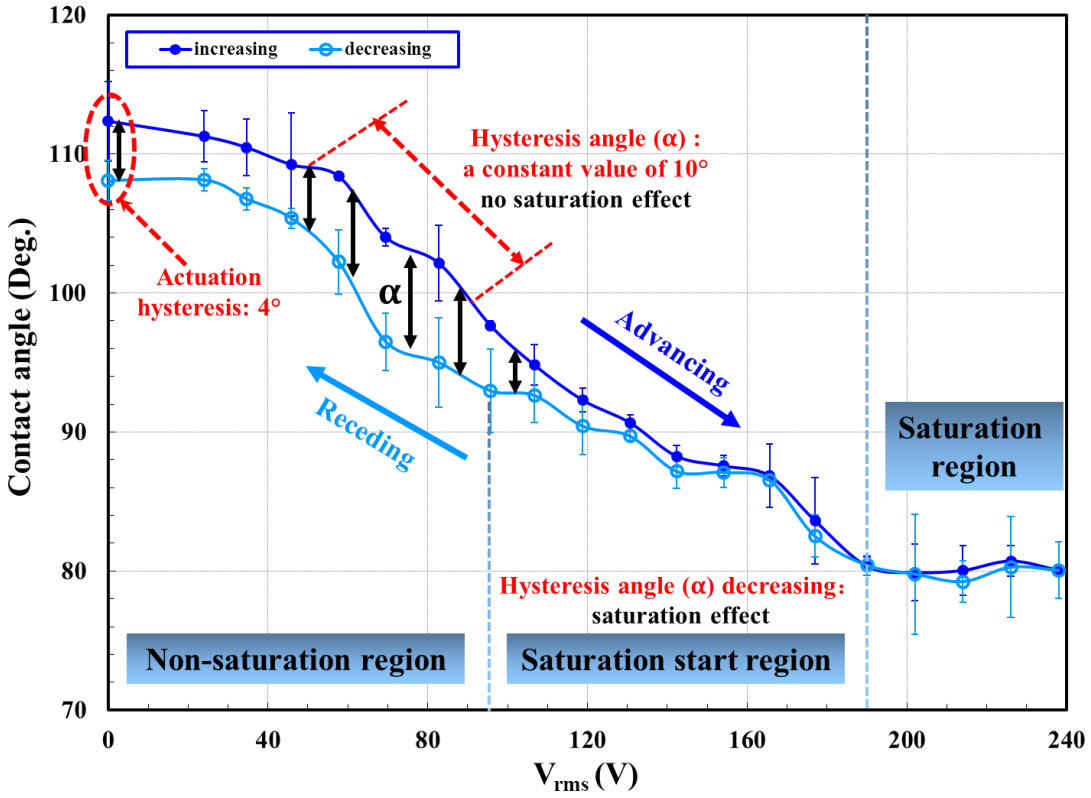

Figure 2.10 Performance parameters of the EWOD system through the measurement of the contact angle of a DI-water droplet (4µL) versus actuation voltage. The vertical shift between the advancing and receding curves defines the hysteresis angle (α).

In **Figure 2.10**, it is observed that the contact angle decreases from 112° to 80° when the voltage is increased from 0V to 190V. Above 190V, a well-known saturation phenomenon is observed, resulting in a marginal increase of the electrowetting effect. It is also noteworthy that, by reversing the direction of the voltage sweep, a complex hysteresis pattern is

evidenced. The contact angle increases up to 108° at the end of this cycle, meaning that the actuation hysteresis (*i.e.*: the variation of the contact angle at zero voltage after an excitation cycle) is equal to 4°. This actuation hysteresis characterizes the ageing and loading of the insulation layer. It reflects the trapped charged in or between the insulation layers. It is also observed that the contact angle saturation starts at 96V when the difference between the advancing and receding voltage branch gets smaller at high voltages. Finally, we can extract the contact angle hysteresis for low values of the voltage when there is no saturation effect. This contact angle hysteresis is found to be about 10°. Among all the results, it is believed that the bottom plate is feasible for EWOD actuation.

2.3.2.2.2. Primary fluidic operation experiments

(a) Droplet formation

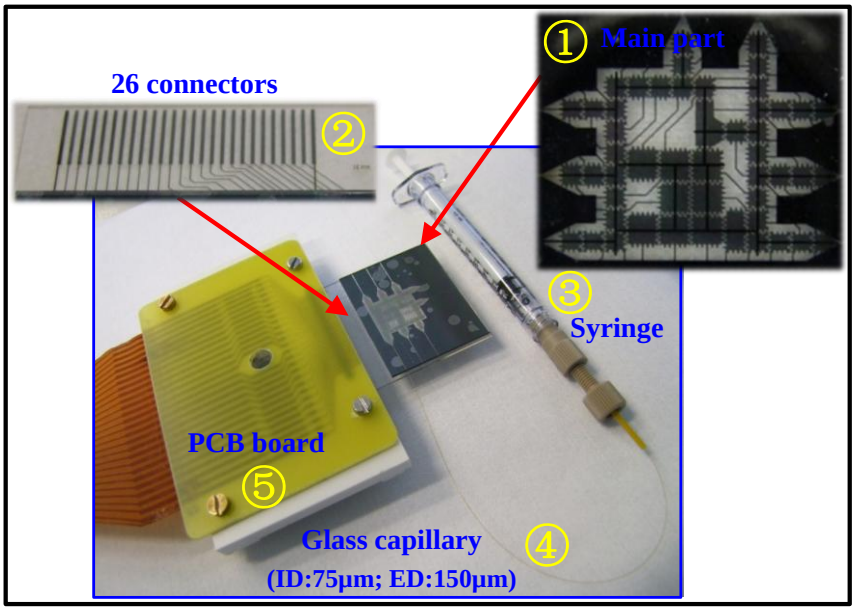

Figure 2.11 Schematic view of the experiment set up.

The schematic view of the experiment set up is shown in **Figure 2.11** and DI-water is used for the test. EWOD technology is used to generate the droplet and displace the droplet across the electrode row. The network of microchannels is manually filled with DI-water through a glass capillary by injection from a syringe. Small volumes of liquid extrude from the microchannels onto the electrode row. Switching of the different electrodes is controlled by

LabVIEW program. One can observe a pinching effect on the droplet that shrinks the liquid (illustrated in **Figure 2.12**). However, the pinching is not big enough to cut the liquid. By increasing the driving voltage, the droplet formation is still not possible. It can be explained that additional friction forces come from the channel side walls and also from the top plate. The additional friction forces act against the pinching mechanism so that the droplet cannot be extracted. On the contrary, when the capillary tube is directly connected to a neighboring electrode close to the actuated electrode, the generation of the droplet is possible (illustrated in **Figure 2.13(1)**).

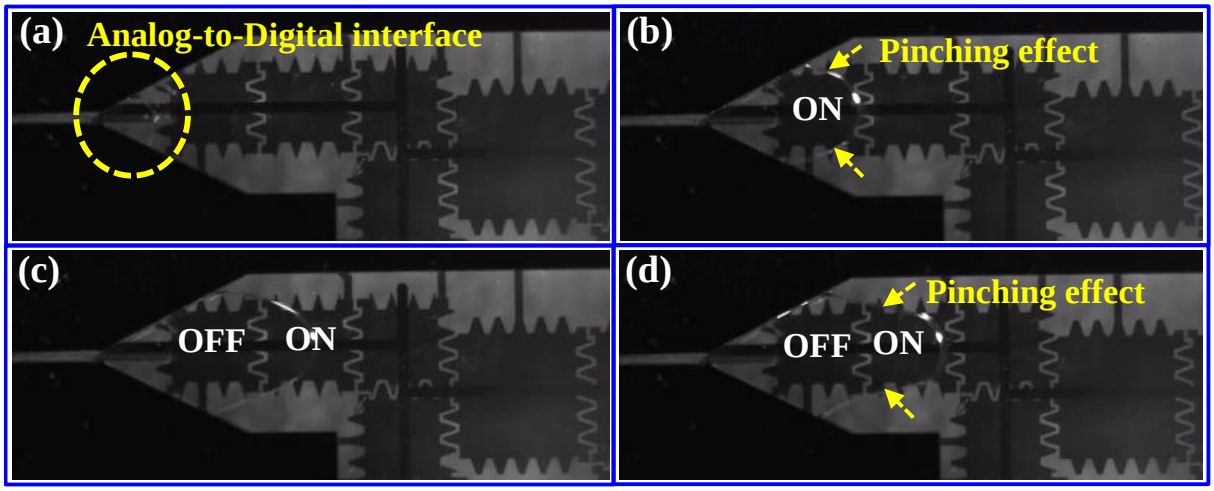

Figure 2.12 Picture sequences showing the motion of droplet formation: (a) The fluidic is loading through the glass capillary; (b) the first electrode on the electrode row is actuated and a pinching effect occurs; (c) the first electrode is switched off and the second electrode is switched on; (d) a pinching effect occurs.

However, this alternate method presents a major drawback: since the glass capillary is hydrophilic, the liquid is flowing back as the droplet growing. The effect of liquid flowing back makes the trouble in the droplet-volume control and also causes cross-contamination. This is the reason why an efficient analog-to-digital interface (micro-channels) has to be integrated in our design. Thus, in our next work will focus on how to achieve droplet formation by using the analog-to-digital interface.

(b) Droplet transport

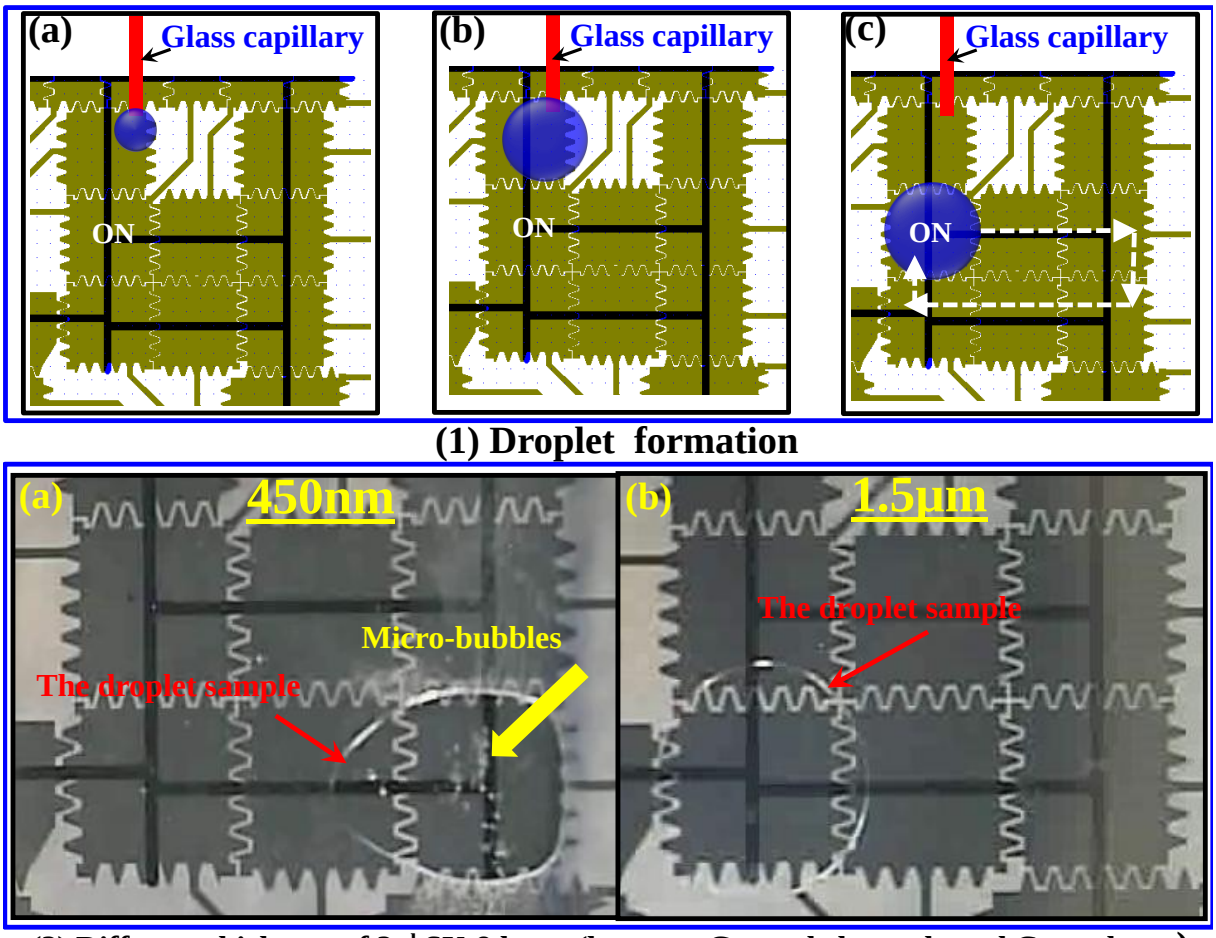

Figure 2.13 (1) Schematic diagram of creating a droplet from a glass capillary (inside diameter 75μm) and moving it under EWOD technology. The arrangement range of the capillary tip is the size of the neighbor electrode near the given actuated electrode. (2) Screen captures of the working device based on two different thicknesses of the second SU-8 layer: (a) 450nm under the driving voltage of 142V at 1 kHz and (b) 1.5μm under the driving voltage of 190V at 1 kHz.

Here, we focus on the basic operation of droplet transport. A droplet is extracted from a glass capillary and then transported along the direction of the activated electrode. The motion is carried on square loop rows of 6 double-size electrodes (see white path on **Figure 2.13-1(c)**). In the initial test, the bottom EWOD-based plate of the used device was fabricated with a 450nm SU-8 dielectric layer between the ground electrode and the CYTOP film. The droplet motion was under the driving voltage of 142V (12V for the magnitude of voltage in generator) at 1 kHz, with a switch time (*i.e.*, the voltage switching from one electrode to another) of 1 second. At the first loops (<5 loops), the droplet motion consisted of two parts: a)

quickly displacing from one electrode to another at the first part of the switch time period (1 second) and b) laying on the actuated electrode until the voltage switching to the adjacent electrode along the displacement direction. When the device was operated over 5 loops (5~10 loops), the second part of the droplet motion was not apparent, which suggested that the movement rate of the droplet became decreasing. In order to actuate the droplet at the same movement rate as the first 5 loops, we increased the driving voltage to 154V (13V for the magnitude of voltage in generator). However, for this higher voltage, one could observe electrolysis micro-bubbles (shown in **Figure 2.13-2(a)**). It can be explained by dielectric breakdown. Dielectric breakdown phenomenon is believed to be caused by the insulator accumulating charges at the hydrophobic surface [30][13]. Due to charging of the capacitor, the voltage drop through the dielectric layer becomes very high. As a consequence, a dielectric breakdown can be observed depending on the parameters of the set-up. The explanation is that pin-holes at the 2nd SU-8 dielectric layer (between the ground electrode and the CYTOP hydrophobic layer) may allow the liquid to come in contact with the electrode. As a result, the droplet undergoes electrolysis and the 2nd SU-8 dielectric layer is damaged, giving rise to a destructive malfunction of the EWOD device.

One solution is to increase the thickness of the 2nd SU-8 dielectric layer. We increased the 2nd SU-8 layer to 1.5μm and tested the droplet motion on square loop rows (shown in **Figure 2.13-2(b)**). Since the thickness increase, the required driving voltage was increased to 190V (16V for the magnitude of voltage in generator). We made a long course of 100 square loops and the droplet was successfully transported without dielectric breakdown. The results indicate that the thickness of the 2nd SU-8 dielectric layer is appropriate, at the expense of a high electrical potential. Thus, in the following work, the 2nd SU-8 dielectric layer thickness is set to 1.5μm.

2.3.3. Conclusion

In our first work, an original fabrication process has been successfully designed, employing deep reactive ion etching of silicon and low temperature wafer bonding. This technique has

ensured that the resulting structures exhibit the excellent adhesive bonding without misalignment and without de-bonding. Micro-channel paths have been created by deep reactive ion etching of the silicon layer. It is believed that the fabrication technology can be used in diverse MEMS applications. To characterize the chip performance, contact angle changes have been measured. After that, we have done preliminary validation tests on EWOD fluid operations. By modification of the thickness of the 2nd SU-8 dielectric layer from 450nm to 1.5μm, we succeeded in avoiding electrolysis due to dielectric breakdown. However, our preliminary device suffers from a key limitation: failure in droplet formation by using analog-to-digital microchannel interfaces.

To address this issue, we had attempted to use the surface superhydrophobic treatment on top cover plate. The advantages of superhydrophobic are apparent, witnessed by the large number of publications and diverse approaches every year. Due to the low contact angle hysteresis from the top cover plate, droplets can be moved at very low actuation potential. This is a very important point since nominal actuation levels should be far from the breakdown voltage. Hence the durability of the chip should be increased. In the next sections, electrowetting on textured superhydrophobic substrates is studied for our new generation device.

2.4. Second Generation: Sample Preparation Unit

2.4.1. Superhydrophobic top plate

2.4.1.1. Theory background

2.4.1.1.1. Different superhydrophobic states

The contact angle of a liquid on a solid surface depends on the roughness and the chemical homogeneity of the surface [14]. Depending on the value of the contact angle (CA), surface properties are determined as hydrophilic (CA<90°), hydrophobic (CA>90°), or superhydrophobic (water CA>150°) [15][16]. The behavior of a water droplet on a flat or rough surface is schematically shown in **Figure 2.14**. θ and θ* are the contact angles on flat

surface or rough surface, respectively. Surface roughness increases the wetting character: (a) $\theta^* > \theta$ when hydrophobic contact; and (b) $\theta^* < \theta$ when hydrophilic contact. The roughness plays a vital role to make any surface superhydrophobic. On a rough surface, two superhydrophobic models are illustrated in **Figure 2.14-b**. Water can either penetrate (Wenzel) into or be suspended (Cassie-Baxter) on the defects. The fundamental difference between the two models is the hysteresis value. In **Wenzel model**, the water droplet pins the surface in a wet-contact mode, and as a result, high CA hysteresis is observed. In contrast, in **Cassie-Baxter model**, the water droplet adopts a non-wet-contact mode on solid surfaces and can roll off easily owing to their low adhesive forces.

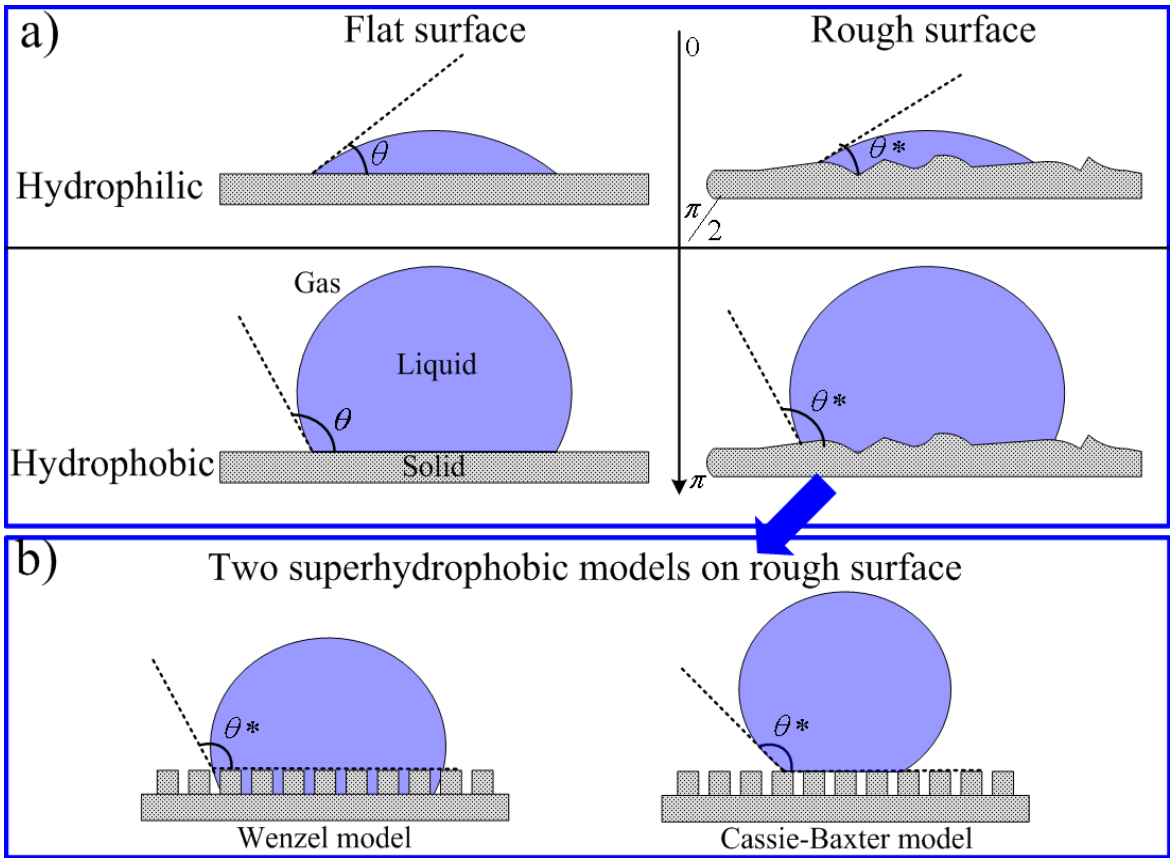

Figure 2.14 a) Contact of a liquid droplet on a flat/rough surface. b) Different behaviors of a liquid droplet on a superhydrophobic rough surface. θ and θ^* are the contact angles on flat surface or rough surface, respectively.

Jin et al. [17] proposed superhydrophobic aligned polystyrene (PS) nanotube films with a high CA and high adhesive properties, defined as 'Gecko' state. In this state, when the droplet is drawn, the volume change of the sealed air in the nanotubes induces the negative pressure

and results in producing an 'adhesive' force. Such a PS layer can be effectively used to transfer a water droplet from a superhydrophobic surface to a hydrophilic one. It is a special case of Wenzel model. In nature, lotus leave is one of the most famous examples occurring superhydrophobic surfaces, wherein a high CA and very low CA hysteresis are exhibited. Due to its hierarchical micro-scale rough structure (around 10μm scale) and nano-scale fine structure (around 100nm scale), self-cleaning effect is evident. Therefore, the superhydrophobic lotus-like state is a special case of Cassie-Baxter model. Indeed, superhydrophobic surfaces with different states have their own unique advantages in different aspects of fundamental research and technological applications. For example, the self-cleaning surface properties employs the 'Lotus' state, and transferring small-volume water droplet can utilize the 'Gecko' state.

2.4.1.1.2. Methods to prepare superhydrophobic surfaces

From a technological point of view, there are several possibilities to prepare artificial superhydrophobic surfaces. In practice, the approaches can be basically categorized into two directions: top-down and bottom-up approaches [16]. Top-down approaches encompass: a) lithographic technique and template-based technique by the use of a mask/master with the desired features [18][19], b) eletroless metal deposition (EMD) technique by scratching a silicon surface with catalytic metal particles[20][21][22], and c) plasma treatment of the surfaces with additional functions [23][24] depending on the type of gas, tetrafluomethane, ammonia, argon or oxygen. Bottom-up approaches involves mostly self-assembly and self-organization (*i.e.*, components spontaneously assemble in solution or the gas phase until a stable structure of minimum energy is reached). Contrary to the top-down approach, bottom-up methods include: a) chemical deposition [25], b) layer-by-layer (LBL) deposition [26], c) sol-gel methods [27], and d) colloidal assemblies [28]. Besides, there are also methods based on the combination of both approaches, especially useful for the creation of architectures with a lotus-like two-scale roughness [29].

2.4.1.2. Fabrication

As mentioned above, the eletroless metal deposition (EMD) technique for preparing superhydrophobic surface is based on: a) fabrication of silicon nanostructures (SiNSs) on a Si surface, and b) chemically modification of the prepared-SiNSs surface. The details are presented in **Appendix A.2**. This technique displays several advantages: taking place at relatively low temperature, and the dissolution reaction is independent of the doping type and level [20][21][30]. During silicon etching, large quantities of silver particles and dendrites are produced by the galvanic displacement reaction. Chemical dissolution of the silver structures in HNO_3/HCL aqueous at room temperature reveals highly oriented one-dimensional (1D) silicon nanostructures. By changing the reaction time or the concentration of the HF/$AgNO_3$ aqueous solution, SiNSs with different lengths and arrangements can be prepared. Increasing the etching time induces pore enlargement and inhomogeneity on the surface, due most likely to silver nanostructure coalescence [30].The technique is highly reproducible and can be easily applied for large area synthesis on wafer scale. In our work, the top cover plate is made entirely with silicon, thus we employed this preparation method to realize the superhydrophobic property of the cover plate.

(a) Channel network: deep reactive ion etching of silicon

First, the silicon wafer need to be rinsed with a HF (1% *i.e.* 0.525M) aqueous solution and then dried under a gentle stream of nitrogen. After cleaning procedure, a 500nm aluminum layer is sputtered on the full substrate wafer by using PULVE-Alliance DP650. Then, the aluminum channel network is photo-patterned and formed by using negative Aznlof 2020 photo-resister (at 2000rpm with acceleration of 1000rpm/s for 20 seconds). After that, etching of aluminum to form a hard mask for deep reactive ion etching at a H_3PO_4 aqueous solution at 45°C for 15 minutes, followed by rinsed with deionized water and dried under a stream of nitrogen. The next step is deep reactive ion etching of the silicon wafer with an etching speed (4.5µm/min) for about 44 minutes to achieve 200µm depth.

(b) Plasma etching

Typically, the chemical etching of the Al mask does not occur during the deep etch process.

However, the Al will still be physically sputter etched by the high energy ions in plasmas typically used for oxide etching [9]. The sputtered metal will redeposit onto the wafer surface. Any such re-deposition of Al metal onto the etching surface can result in 'micro-masking' residues and thus cause a very rough surface topography (shown in **Figure 2.15 (a)**). In order to eliminate the surface fluoropolymer 'nanoneedles', one hybrid plasma etching step (I. O_2 clean for 10min; II. CF_4+SF_6 for 10min) need to be added. In **Figure 2.15 (b)**, it is clearly shown that the residual is removed completely.

(c) Chemical etching

The cover plate consists of a highly doped silicon substrate [30][31][32][33]. First, the silicon wafer was degreased in acetone (for 5 minutes) and isopropyl alcohol (for 5 minutes), rinsed with deionized water (for 5 minutes) and then cleaned in a piranha solution (3:1 v/v mixture of concentrated sulfuric acid (H_2SO_4) with hydrogen peroxide (H_2O_2)) for 15 minutes, followed by re-rinsing with deionized water for 10 minutes. The clean substrate was immersed in a HF (10% *i.e.* 5.25M)-$AgNO_3$ (0.01M) aqueous solution at 54°C for 30min. The resulting surface was rinsed with deionized water and dried under a gentle stream of nitrogen. After that, the wafer was immersed in an aqueous solution of HCL-HNO_3-H_2O (1:1:1, v/v/v) at room temperature overnight (over 12 hours) to remove the silver nanoparticles and dendrites deposited during the chemical etching. As shown in **Figure 2.15 (c)**, the etched silicon sample results in a black and antireflective surface.

(d) Chemical surface termination

To achieve the superhydrophobic state, the silicon nanowire surface was chemically modified with an octadecyltrichlorosilane (OTS) or perfluorodecyl-trichlorosilane (PFTS) layer [30][31][32][33]. First the substrate was UV/ozone-treated (UV O Cleaner, Jelight Company, Inc., 4mW/cm^2 at 220nm) for 20 minutes to remove any organic contaminants on the surface and to generate surface hydroxyl groups. The surface was then reacted with an OTS solution ($4.22*10^{-3}$M) or a PFTS solution ($4.86*10^{-3}$M) in hexane for 4h at room temperature in a dry nitrogen purged glove box. The resulting surface was rinsed with hexane, dichloromethane (CH_2CL_2), and isopropyl alcohol (i-PrOH), and then dried under a gentle

stream of nitrogen. The OTS-terminated/PFTS-terminated surface displays a superhydrophobic character (shown in **Figure 2.15 (d)**) with a DI-water contact angle higher than 150°. A water droplet on both surfaces has a tendency to roll off (contact angle hysteresis is about 1°).

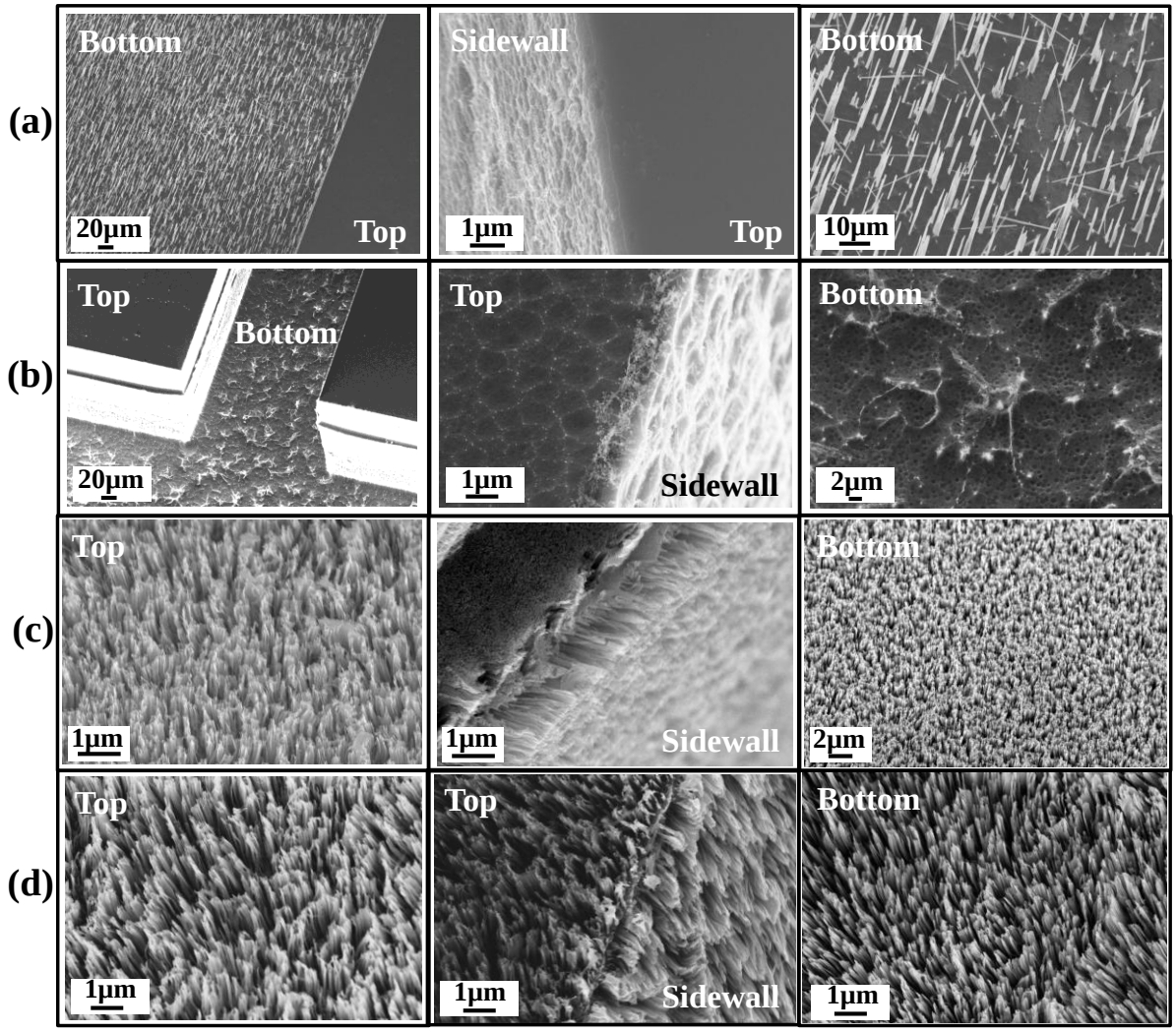

Figure 2.15 SEM images of the resulting surface after each fabrication steps: (a) after deep reactive ion etching, (b) after hybrid plasma etching, (c) after chemical etching, and (d) after chemical surface termination with PFTS. We do not show surface termination with OTS, since they look similar.

2.4.1.3. Surface functional material selection

In order to determine the scope of application of the two types of chemical terminations, we further characterized both the contact angle and hysteresis angle. The measurement was performed using a KRŰSS Drop Shape Analysis System DSA100. We chose some liquids for

test, which are typical used in EWOD-based bio-systems. For example, yeast cells are used extensively for protein production and genomics, phosphate buffer saline (PBS) is a buffer solution commonly used in biological applications (as it is isotonic and non-toxic to cells), and Pluronic F68 was used to reduce unspecific absorption of cells onto the EWOD chip. All the measurements were carried out at room temperature and ambient humidity. Each reported value in **Table 2.3** was the average value measured for three times.

Conductivities were measured using a conductivity meter (C533 Multi-Parameter Analyzer – Montreal Biotech Inc.). For each measurement, the temperature was stabilized. Contact angle and hysteresis angle were measured by dispensing 2µL droplet on a substrate mounted on a variable inclination/tilting stage. The deposited droplet was laid on the surface and formed a contact angle. By taken a picture from a side part camera, the left and right contact angles of the droplet were measured and the average value between them was set as the static contact angle (shown in **Figure 2.16**).

The hysteresis angle was measured by using the tilting stage of the DSA100. With this tilting stage, not only the sample was tilted, but also the whole instrument. This arrangement ensured the maximum utilization of the field of view at the tilt angle increases, because the video camera and sample are always in the same plane. The stage is controlled by software and inclined gradually until the droplet started sliding down the substrate, at which point a picture was taken by a side part camera consistent parallel to the stage. The advancing and receding contact angles of the droplet are measured. The calculated hysteresis angles on different substrates are summarized in **Table 2.3**.

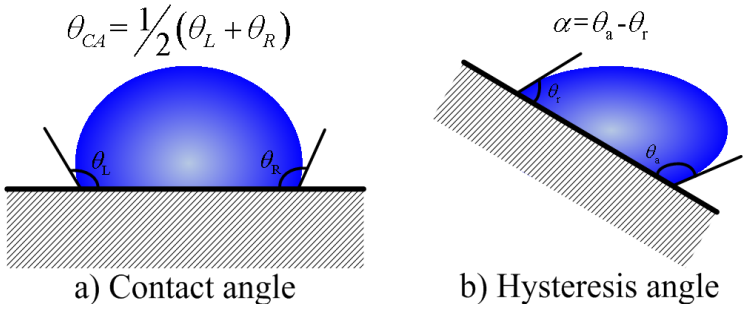

Figure 2.16 illustrated diagram describing the methodology for measuring a) the contact angle and b) the hysteresis angle.

Table 2.3 shows that OTS-termination and PFTS-termination top plates have similar

performances with a high initial static contact angle (>150°) and a low hysteresis (<5°) for all solutions, except for No. 4 solution (0.01% (w/v) Pluronic F68 in PBS (0.001M)). However, in case of No.4, OTS-termination has a catastrophic big hysteresis angle (~46°) which is much bigger than the one of PFTS-termination top plate (16°). Conversely, the hysteresis on CYTOP plate slightly decreases. The most probable explanation is that a low concentration of surfactants (Pluronic F68) as a solution additive can reduce unspecific absorption onto the surface. For No.4 solution, the contact angle on PFTS-termination top plate is still around 150°; while, the contact angle on OTS-termination top plate or CYTOP plate decreases about 10°.

Table 2.3 Static contact angle and hysteresis angle on different substrates: CYTOP coating base plate, OTS-termination and PFTS-termination top plates.

No.	Solution	Conductivity (mS/cm) @25°C	Contact angle			Hysteresis		
			CYTOP	OTS	PFTS	CYTOP	OTS	PFTS
1	DI-water	0.0002	112.88±2.18	154.32±2.08	152.01±0.18	11.67±1.48	2.27±0.91	2.00±0.35
2	10X-diluted PBS (0.001M)	1.88	110.37±0.80	151.4±0.23	153.32±1.17	11.27±1.59	4.57±0.76	2.5±0.62
3	No diluted PBS (0.01M)	13	109.68±0.29	152.28±1.99	153.28±0.28	19.57±3.02	4.9±0.17	2.33±0.55
4	0.01% (w/v) Pluronic F68 in 10X-diluted PBS	1.59	99.23±1.49	139.68±3.20	151.1±1.01	10.50±1.70	46.23±4.10	16.05±2.62
5	10^6 CFU/mL Yeast in 10X-diluted PBS	1.61	112.92±0.62	151.67±1.10	152.15±0.61	13.50±2.69	3.2±0.95	2.65±0.35
6	10^7 CFU/mL Yeast in 10X-diluted PBS	1.62	108.70±1.82	152.02±0.75	152.98±0.74	13.03±1.90	4.15±0.21	4.83±0.85

In conclusion, PFTS-termination plate shows the optimal results to our practical applications. In the later work, PFTS is selected as the chemical termination for the cover fabrication.

2.4.2. Device assembly: a homemade mount

Based on the same bonding process demonstrated in our previous work (**Section 2.3.1.2**), we succeeded in bonding the EWOD bottom platform with the superhydrophobic top plate showing good alignment. However, in practice during the operation of the microfluidics system, the hydrophobic coating degradation may appear gradually, resulting in pinning of the droplet on electrodes. While, the superhydrophobic top plate is far from being degraded. The superhydrophobic surfaces have apparent advantages on the contact angle and the hysteresis,

compared to hydrophobic coating surface (shown in **Table 2.3**). The different properties of bottom and top plates make us to reconsider the device assembly. Unlike the previous work, we developed a homemade fixed mount for fixing the two plates replacing the bonded process, which facilitates reuse of a given superhydrophobic top plate.

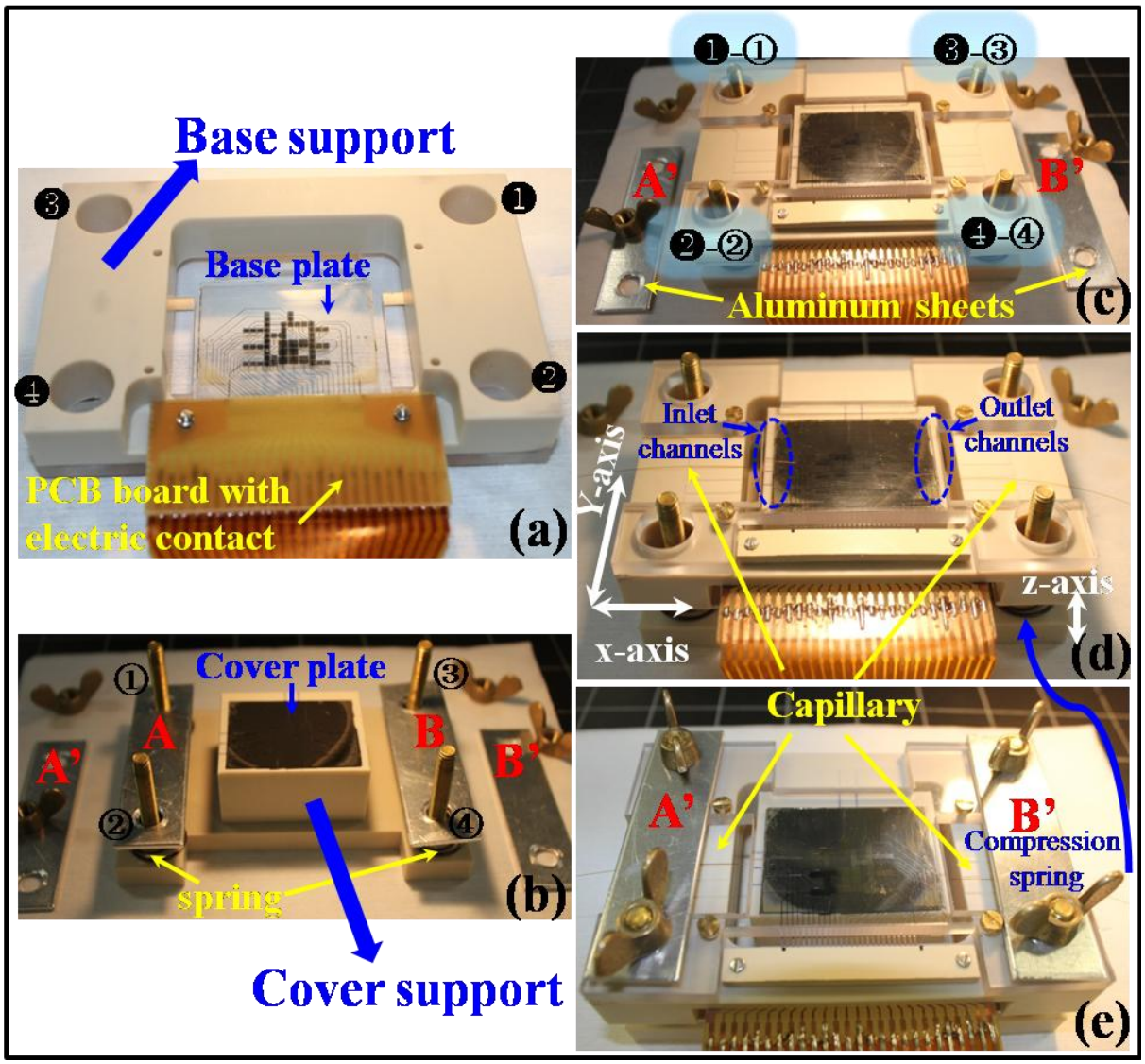

Figure 2.17 Schematic of the device assembly: (a) the base plate with the well electric contact; (b) the superhydrophobic cover plate on the support and two aluminum sheets on springs; (c) the base support faced to the cover support; (d) glass capillaries inserted into the inlet/outlet channels; (e) the two supports fixed by screws after the alignment accomplishment. Before screwing up the screws (*i.e.*, compression spring in Z-axis), the relaxed spring reserve a distance between the cover support and the base support, allowing the cover support and the base support alignment in X-axis and Y-axis.

As depicted in **Figure 2.17**, the bottom hydrophobic plate and the top superhydrophobic cover can be aligned and fixed by using our new prototype. In this strategy, fluidic operations

are carried out as usual. Furthermore, due to the four underneath spring, there is residual space to allow the base support to do X-axis and Y-axis alignments before screwing up the screws, which gives the chance for studying the extent of the 'triangular buffer zone' (L_1) (illustrated in **Figure 2.18**) on droplet formation.

2.4.3. Bottom EWOD platform further modification

Even if we show that the 2nd SU-8 dielectric layer is very useful in improving dielectric breakdown phenomenon (in the previous **Section 2.3.2.2.2**), one can still frequently observe dielectric breakdown during the use of the device. One possible explanation can be found in the technological process (*e.g.*, defaults in the substrate surface) [14]. Indeed, defects probably form during the lift-off process (shown in **Figure 2.4(h)**), where some tiny particles of nickel metal become reattached to the surface at a random location. It is very difficult to remove these particles, inducing defaults in the following SU-8 spin coating. As a result, the potential risk of dielectric breakdown increases. In order to avoid defaults of the 2nd SU-8 dielectric layer, chrome/gold (10nm/40nm) is used to replace nickel (50nm). It is observed that the phenomenon of metal particles reattached to the surface is much improved. Moreover, we add a 3rd SU-8 layer (1.5µm) above the 2nd SU-8 prior to CYTOP coating. We make two comparison tests on different device structures. The results are presented in **Table 2.4**.

For easier droplet movement, we use the working voltage which is slightly higher than the required minimum voltage, with a switch time (*i.e.*, the voltage switching from one electrode to another) of 1 second. In Test 1, we compare the influence of the top plate on droplet motion by using the same structure bottom plate. The devices are operated over a course of 100 back and force cycles on three electrodes. Droplet movement is more easily accomplished at the slightly higher working voltage. It is found that the actuation threshold voltage is much decreased by replacing CYTOP hydrophobic cover (#1) with PFTS-terminated superhydrophobic cover (#2), from 177V to 107V. The low hysteresis of the superhydrophobic PFTS-terminated cover (~2°) compared to the CYTOP cover (~11°) explains why the driving voltage is reduced in case of PFTS surface.

In Test 2, we compare the base structures having either a single-layer SU-8 (#2) or a bilayer SU-8 (#3) with both a CYTOP layer on top and a PFTS-terminated cover. The structure of #3 requires a higher actuation voltage. However, the increase is not significant. The droplet motion consisted of two parts: a) quickly displacing from one electrode to another at the first part of the switch time period (1 second) and b) laying on the actuated electrode until the voltage switching to the adjacent electrode along the displacement direction. When the device #2 is operated over the course of 100 cycles, the second part of the droplet motion is not apparent. Within 110 cycles, the droplet is pinned on the surface and cannot be displaced even by increasing the driving voltage. The most probable explanation of this failure is that the degradation of 2nd SU-8 layer becomes gradually apparent during the operations over 100 cycles. A consequence of this degradation is that droplet motion is prevented. Conversely, for the #3 device, it can be successfully operated over the 100 cycles. All results suggest that the bilayer SU-8 (instead of single-layer) underneath CYTOP layer can improve the degradation and cover any potential fabrication faults in 2nd SU-8 layer. Thus, this structure has been selected for our following work.

Table 2.4 Comparison of different structure combinations. A 1 kHz square-wave signal is created by a generator (CENTRRD-5MHz Function generator GF 265) and then amplified by an amplifier (TEGAM-High voltage Amplifier Model 2340). Threshold voltage is the required minimum driving voltage. Working voltage is slightly higher than threshold voltage for easier droplet movement. '-' corresponds undone tests.

#	Device structure		Threshold voltage (V)		Working voltage (V)		Operation (back and forth)	
	Top plate	Bottom plate	Generator	After amplifier	Generator	After amplifier	100 cycles	Over 100 cycles
1	CYTOP coating	20nm Ni/1.5μm SU-8/**50nm Ni/1.5μm SU-8/**20~30nm CYTOP	15	177	16	190	OK	-
2	PFTS termination		9	107	10	119	OK	Fail: pinning on the surface
3	PFTS termination	20nm Ni/1.5μm SU-8/**(10nmCr/40nmAu)/(1.5μm SU-8/1.5μm SU-8)**/20~30nm CYTOP	11	131	12	142	-	OK

2.4.4. Fluidic operations and Results

2.4.4.1. Droplet formation

Conversion of a continuous flow into discrete droplets is the most critical fluidic operation for our proposed sample preparation unit. The difficulties not only exist in droplet generation, but also in the lifetime of this function and in the accuracy on the volume of the resulting droplet. The protocols for the droplet formation are as follows:

(a) It is necessary to set an original point for triggering the LabVIEW program, because the extracted volume depends on the control sequences. The moment of the advancing of fluid reaches the tip of 'triangular buffer zone' is set as the original start point, illustrated in **Figure 2.18 (a)**.

(b) An electrical square voltage applied to the electrode network is controlled by our designed LabVIEW program. The uniform discretization time-step of the various operations performed by the LabVIEW program is defined as sequence time T_s. For the stability of the operations, the sequence time of the LabVIEW program is set as 0.5 second.

(c) The sample fluid is loaded by a peristaltic pump (ISM 936-ISMATEC) at a rate flow of 10μL/min according to the specialties of NANOBE integrated system (mentioned in **Chapter 3**).As the volume grows, the front of the fluid overlaps the first electrode (**Figure 2.18 (b)**).

(d) The 'Triangular buffer zone' is used as a 'cutting electrode'.

(e) According to the loading rate (10μL/min) and the sequence time of the LabVIEW program (0.5 second), it can be derived that each 1μL of sample is loaded in 6s and 12 sequence steps. Thus, an elemental droplet (1μL) can be generated in every 12 LabVIEW sequence steps.

(f) When the volume is about 1μL (at the 12^{th} sequence), the first electrode is switched on and the other electrodes are switched off. A pinching effect shrinks the liquid at the 'Triangular buffer zone' (used as the cutting electrode) and a neck forms in the 'Triangle buffer zone' (**Figure 2.18 (c)**). Theoretically, one droplet is cut with a desired

volume of 1μL and there is no dead "Tail" volume (**Figure 2.18 (d)**).

(g) The droplet is displaced by sequential actuation of the neighboring electrodes in sequence (**Figure 2.18 (e)-(f)**). At the meantime, the immediate rest of sample flow continues loading and the second droplet will be generated in the 24th sequence step.

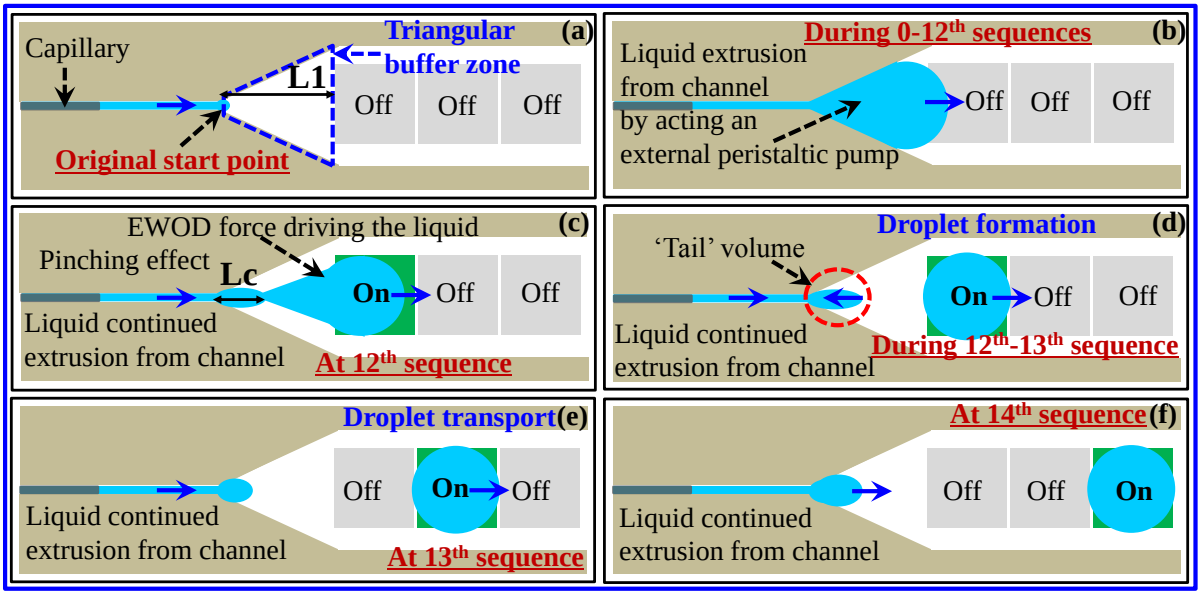

Figure 2.18 Droplet formation procedures: (a) the time when the advancing front of the fluid reaches the tip of the 'triangular buffer zone' is set as the original starting point for the control program, (b) the size of fluid is growing, (c) the first electrode is actuated and one droplet is formed (d), and (e-f) the droplet displacement by actuating neighboring electrodes in sequence. Energized electrodes are colored green and floating electrodes are colored grey. Brown region is the top view of the microchannel walls. L_1 is the extent of 'triangular buffer zone' (*i.e.*, the distance from the end of channel to the first electrode).

Successful droplet formation depends on the driving voltage and the size of the 'triangular buffer zone' (L_1, illustrated in **Figure 2.18**). The accuracy on the volume of the resulting droplet is impacted by the "Tail" volume, the loading flow rate of the peristaltic pump (S_P) and the time-step of the LabVIEW program (T_s). In the following sections, we discuss the parameters influencing droplet formation and the accuracy on the volume of the resulting droplet.

2.4.4.1.1. The success and reproducibility of droplet formation

It has been observed that the droplet formation depends on the electric voltage and the

distance between the first electrode and the end of the inlet silicon micro-channle (L_1). In this section, the process of droplet formation has been characterized by two different tests, illustrated in **Table 2.5**. Both tests are achieved twice. The time-step of the LabVIEW program (T_s) is set to 0.5 second. The loading flow rate of the peristaltic pump (S_P) is 10μL/min. Each elemental droplet (1μL) is designed to be generated in every 12 LabVIEW sequence steps.

Table 2.5 Influence of the driving voltage and the distance between the first electrode and the end of the inlet silicon micro-channel (*i.e.*, the dimension of 'triangle buffer zone') on droplet formation. Test 1 focuses on the influence of the driving voltage, while Test 2 focuses on the influence of the size of the cutting electrode (L_1). For the two tests, T_s=0.5s, S_P=10μL/min.

Test 1			**Test 2**	
L_1=2.2mm			**Effective driving voltage: 217V**	
Driving voltage (V)		Results	L_1 (mm)	Results
Generator	After amplifier			
5	135	Fail: pinching is not enough	1.0	Fail: pinching is inefficient
6	162	OK	1.6	Fail: low reproducibility of success
7	189	OK	2.1	OK
8	217	OK	2.2	OK
9	231	OK	2.3	OK
			2.6	OK: but the size of droplets is variable
			3.1	Fail: the advancing of fluid doesn't overlap the first electrode

In Test 1, the size of the cutting electrode (L_1) is fixed as 2.2mm, and we focus on the influence of driving voltage on droplet formation. The driving voltage is created in a generator (Tektronix AFG3021B) and then amplified in an amplifier (TEGAM-High voltage Amplifier Model 2340). We have tested five different magnitudes of voltage in generator: 5V, 6V, 7V, 8V, and 9V. Their corresponding effective voltages are 135V, 162V, 189V, 217V, and 231V, respectively. When the driving voltage is low (135V), it is observed that the pinching effect shrinks the sample at the 'Triangular buffer zone' and a neck forms; but the shrinking is not enough to cut the neck, which causes the failure in droplet formation. Increasing the voltage to 162V allows achieving the droplet formation. As the driving voltage increases, the pinching effect enhances and the droplet formation becomes easier. Thus, for L_1=2.2mm, the minimum voltage allowing droplet formation is 162V (6V for the magnitude of voltage in generator).

In Test 2, in order to eliminate the influence of the driving voltage on droplet formation, we

apply a relative higher voltage of 217V for test. Note that the standard dimensions of the electrodes are 2.1mm*2.1mm. We have studied several different values of L_1 and the results are as follows:

a) For the lowest one (1.0mm), the extracted fluidic part shows a weak shrinking and the pinching becomes inefficient.

b) When L_1 (1.6mm) is a little less than the size of the electrode (2.1mm), the droplet can be generated, but the reproducibility is low.

c) When the value of L_1 (2.1mm, 2.2mm or 2.3mm) is a little larger than or equals to the one of the electrode, the droplet formation is successful and very reproducible. **Figure 2.19** shows the motion of droplet formation when L_1 is 2.2mm. In photograph (2) the first electrode is actuated. In photograph (3-10) the sample moves to cover the electrode surface and is pinched in the 'triangle buffer zone'. In photograph (11), it is observed that the tail of the droplet just at the time of separation is retracted and adds to the droplet volume. In photography (12), one droplet is generated.

d) When the size of L_1 (2.6mm), the droplet formation is still successful and reproducible. But the size of droplets is variable. It is explained that when retracting after separation, the tail forces a supplementary volume of liquid into the already formed droplet; the 'tail' volume may produce variability in the droplet volume.

e) For the biggest one (3.1mm), the advancing of fluid doesn't overlap the first electrode until the first electrode switches to off-state, so that the droplet formation is failure.

According to the results of **Table 2.5**, a general rule can be obtained that the success and reproducibility of droplet formation are satisfactory when: a) the driving voltage is higher than 135V and b) the size of the cutting electrode (*i.e.*, the 'Triangle buffer zone') is a litter larger than or equals to the one of the electrode. In the following work, we determine L_1=2.2mm and the working voltage of 189V.

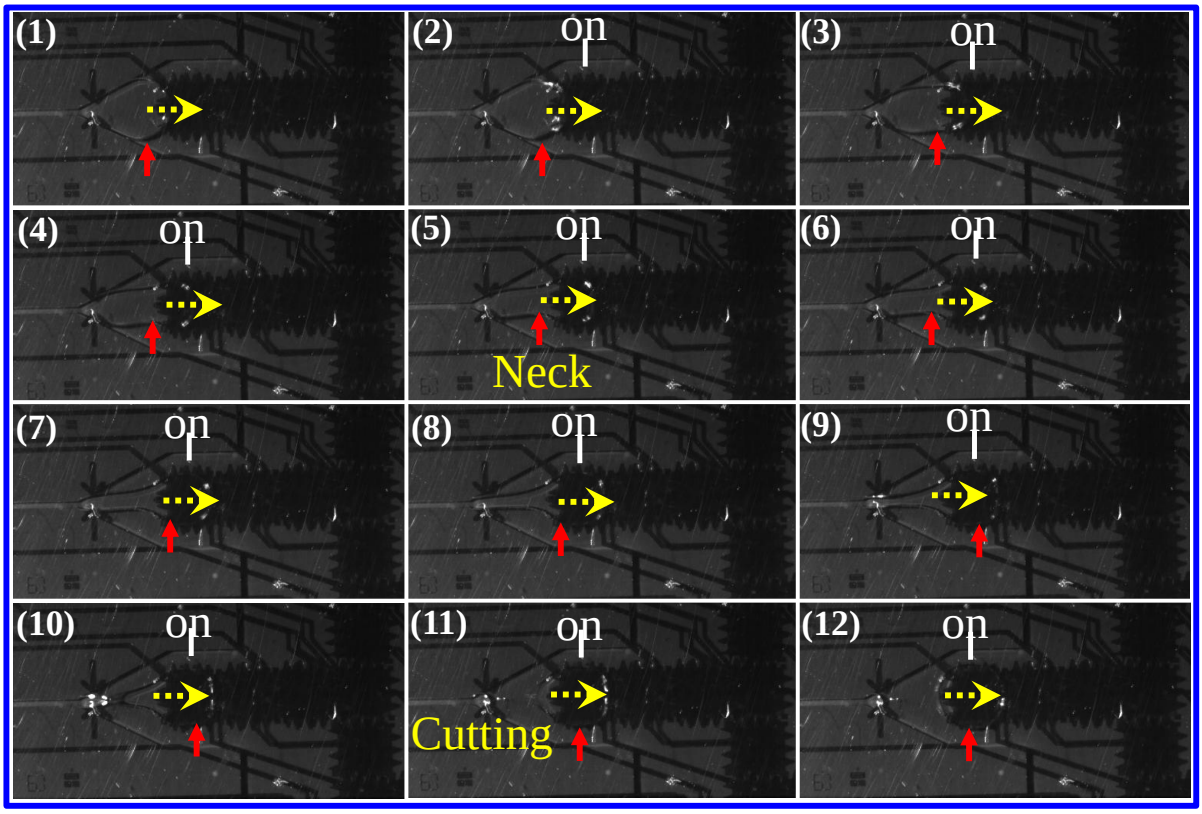

Figure 2.19 Picture sequences with a time step 2ms showing the droplet formation with an actuation voltage of 217V and L_1 of 2.2mm.

2.4.4.1.2. The accuracy of the resulting volume

In this section, we study the accuracy on the volume of the resulting droplet. Each elemental droplet (1μL) is designed to be generated in every 12 LabVIEW sequence steps. Thus, the theoretical volume of the resulting droplets (V_d) depends on the time-step of the LabVIEW program (T_s) and the loading flow rate of the peristaltic pump (S_P), and equals to

$$V_d = 12 \times T_s \times S_P \quad \textbf{(2.1)}$$

Under no dead "Tail" volume assumption (**Figure 2.18 (d)**), we test different loading flow rate of the peristaltic pump. The theoretical value of T_s is calculated by equation (2.1) based on the theoretical resulting volume of 1μL. The test results are summarized in **Table 2.6**. For a successful droplet formation, the maximum loading flow rate of the peristaltic pump is 25μL/min. When the loading flow rate is high (30μL/min), the droplet formation is failure. The reason of the failure is because that the calculated T_s (0.17s) is lower than the minimum

time (177ms, shown in the following **Table 2.7**) for switching the voltage from one electrode to another for the droplet movement.

Table 2.6 Influence of the loading rate on droplet formation. For all the tests, steps for each droplet (1μL) are 12, L_1=2.2mm, and the voltage is 189V.

#	V_d=1μL, Steps=12		Results
	S_p (μL/min)	T_s (second)	
1	5	1	OK
2	10	0.5	OK
3	20	0.25	OK
4	25	0.2	OK
5	30	0.17	Fail

Indeed, the "Tail" volume and the accuracy of the loading flow rate of the peristaltic pump have an influence on the accuracy of the resulting volume. In order to obtain the desired elemental droplet (1μL), we have tested three group values of T_s, 0.35s, 0.45s, and 0.50s. For each T_s, 15 extracted droplets are measured by using MacBiophotonics ImageJ software (shown in **Figure 2.20**). However, the results show that the resulting average volume of the droplet (1.113μL) is not the optimal value when the theoretical T_s of 0.5 second. One can observe that when T_s is 0.45s, the average volume of extracted droplets is 1.032μL and the coefficient of variation (CV %) is 6.7%. The volume is the closest value to the design elemental volume (1μL) among these three values. Thus, in the following work, the time-step of the LabVIEW program is set as 0.45s for the loading flow rate of 10μL/min.

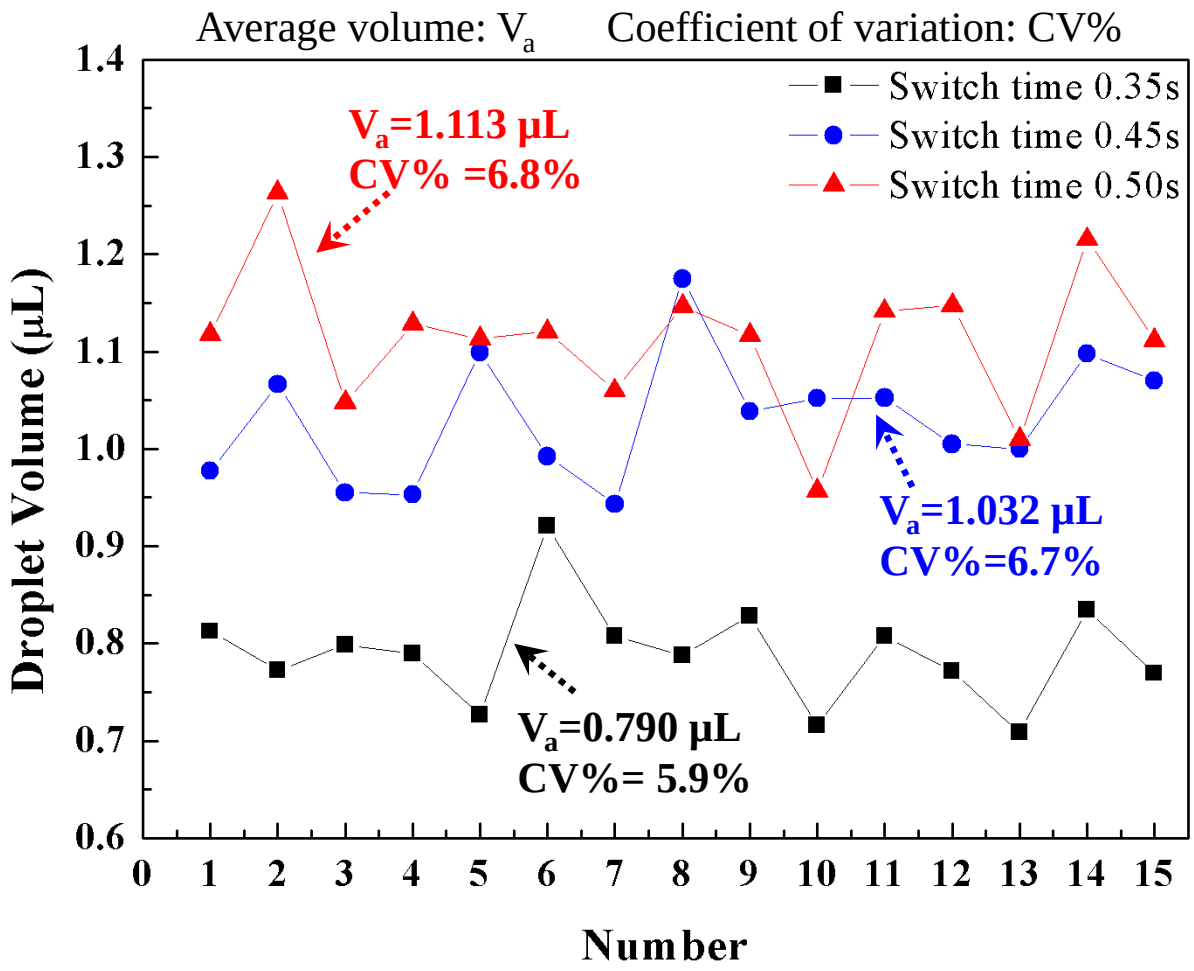

Figure 2.20 The volume reproducibility of the resulting droplets due to the variant of the flow rate of the peristaltic pump for three different time-step of the LabVIEW program (T_s). For all the tests, the theoretical loading flow rate is 10µL/min, L_1=2.2mm, and the voltage is 189V. Every data point represents the average measured value. V_a and CV % correspond the mean value and the coefficient of variation, respectively.

2.4.4.2. Fluidic delivery

To interface our device with external micro-analytical instruments, we have used microchannels at the end of the EWOD platform as the 'chip-to-world' interface, where samples can be recombined and exported in continuous flow. Delivery of the liquids from the microchannels can be described as follows (shown in **Figure 2.21**):

(1) Four elementary (1µL) droplets are gathered in the 'storage zone' and isolated to touch the capillary tip by the control of the 'triangular isolation zone'. The 'triangular isolation zone' is worked as a valve: a) when the voltage is applied to the EWOD electrode underneath the 'triangular isolation zone' (open-state), the droplets can touch the tip of the

glass capillary, and b) conversely (close-state), the droplets are isolated to the tip of the glass capillary.

(2) When the delivery program is triggered, EWOD force drives the liquid sample in contact with the tip of the capillary and the sample is extracted thanks to capillary effect and to the action of thanks to the external peristaltic pump.

(3) In order to increase the durability of the chip, electrodes within the outlet channel are sequentially deactivated. The control sequence of deactivation of the electrode is due to the delivery flow rate of the peristaltic pump. Take the delivery flow rate of 24µL/min as an example. 1µL of sample is exported in 2.5 second, namely 5 sequence steps, when T_s=0.5 second. Thus, each five sequences, one electrode is deactivated.

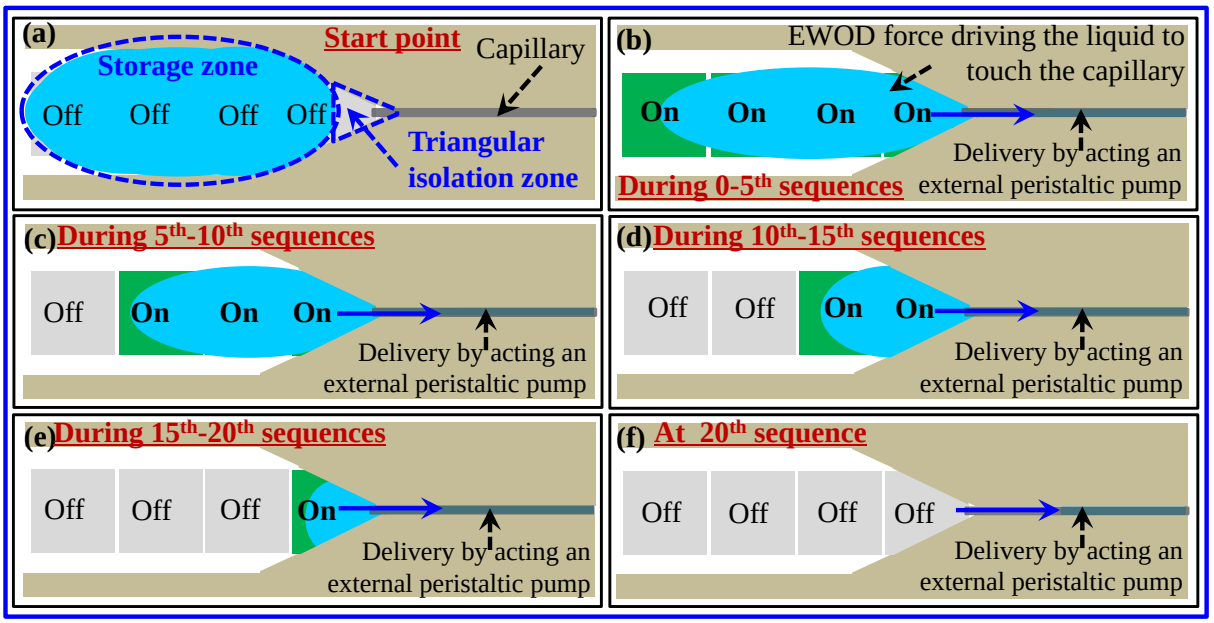

Figure 2.21 Procedure for delivery of liquids: (a) ready for export, (b) triggering of the delivery process, (c-f) programmed deactivated electrodes at the flow rate of 24µL/min. Energized electrodes are colored green and floating electrodes are colored grey. Brown region is the cross-section of the wall of the network of microchannels.

In **Figure 2.22**, one can observe that two droplets are already in the 'storage zone' (a). Two additional droplets are then carried out to this storage zone and merged with the first two droplets (b-c). The resulting sample (4µl) is then carried out to be in contact with the triangular zone and is ready for exportation (d-e). The delivery to the external module is

performed thanks to the peristaltic pump (f-i).

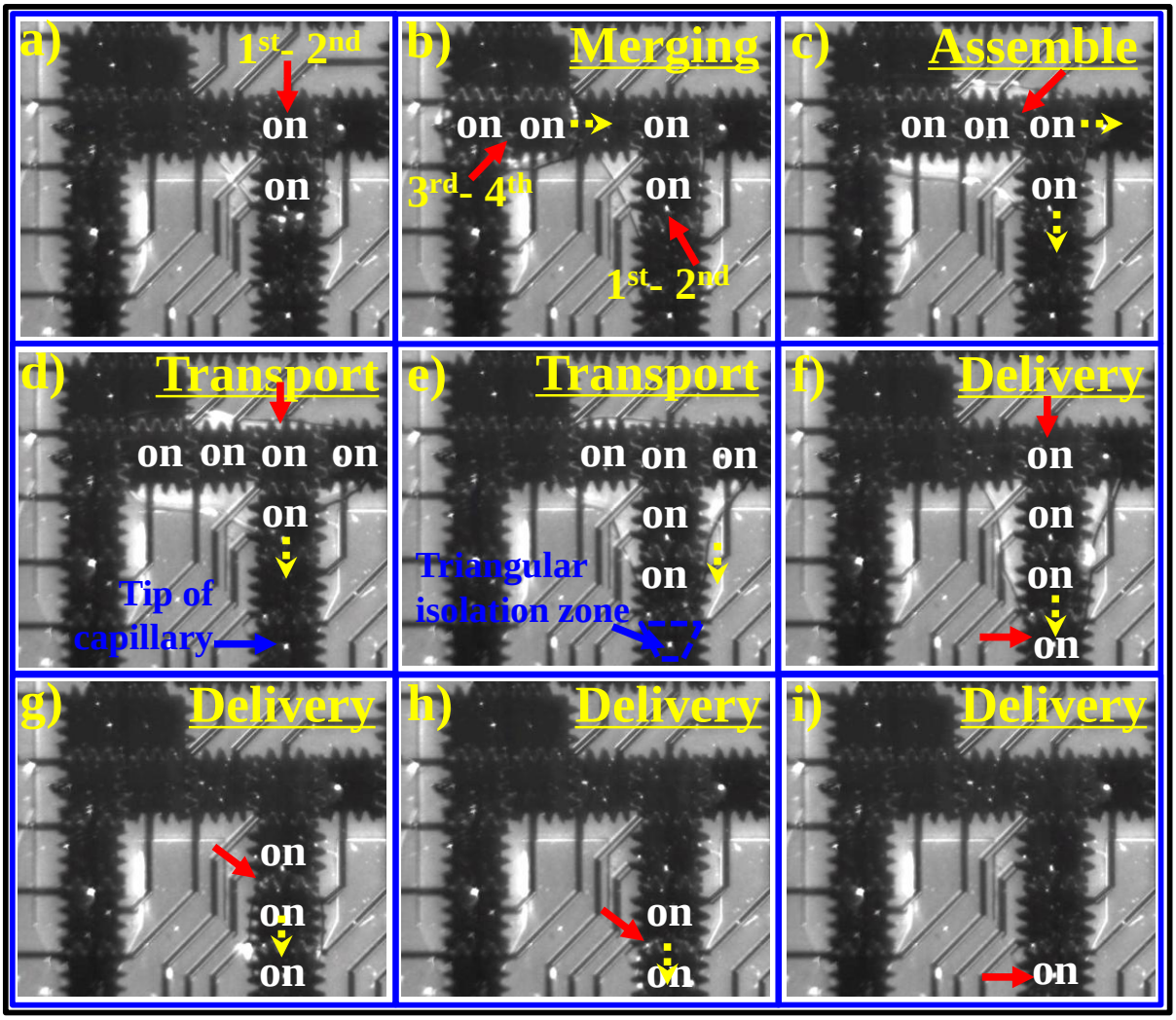

Figure 2.22 Sequential snapshots from the video records showing the delivery operation processing of the assembled analytes.

2.4.5. Conclusion

We have successfully developed a new sample preparation unit with a bilayer PS (Pyrex-Silicon) configuration with superhydrophobic liquid-solid interfaces. In our second design, the improvements are as follows:

a) By using PFTS-terminated cover, the voltage required to actuate the droplet was decreased, and thus the device's useful lifetime was extended.

b) A SU-8 bilayer structure underneath CYTOP layer reduce considerably the occurrence of dielectric breakdown and did not significantly increase the actuation voltage.

c) A homemade mount for fixing the two plates have successfully replaced the bonded process, facilitating reuse of a given superhydrophobic top plate and thus reducing the cost and fabrication time.

d) Fundamental fluid operations (droplet formation, transport, merging, and delivery) have been studied and successfully realized.

2.5. Droplet transport dynamics

The dynamics of the transport of the droplet has to be characterized to optimize the performances of our device. One of our main interests is to understand the friction resistance force from the electrode-free top plate on the motion velocity during the droplet transport. DI-water was applied for this purpose. High speed camera was used to observe water droplet transport, which is very useful for the displacement and velocity study of the receding and advancing fronts [34]. We have studied three cases: 1) no cover (used as the reference case of null influence from top cover plate), 2) a glass cover with CYTOP coating, and 3) a silicon cover with PFTS-termination.

2.5.1. Experimental set-up and protocol

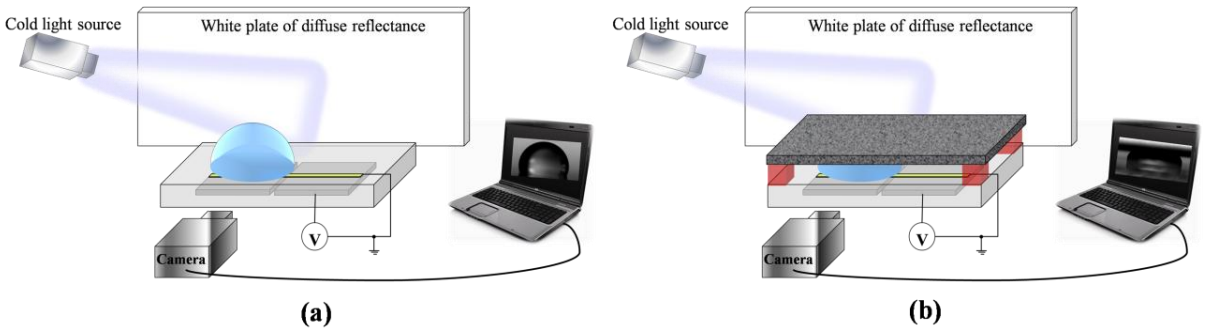

Figure 2.23 Schematic showing the test bench: (a) no cover plate, and (b) with a cover plate (CYTOP or PFTS-termination).

We have used a set-up where we can observe the droplet position with time. The experimental set-up is schematically represented in **Figure 2.23**. This set-up is composed of a high speed camera (Fastcam SA3 photron) capturing images at 4000 frame per second, cold

light source, white plate of diffuse reflectance, and the given devices (without cover, with CYTOP or PFTS cover) electrically connected to a power supply. To obtain the view of droplet profile and avoid the light-spot on the droplet body, the high-speed camera is places in plane with the substrate and the light was reflected from the backside white plate.

The chip was designed to transport 1μL droplet from the left electrode to the right electrode. Here, the CYTOP cover is a flat Pyrex wafer with a 20nm CYTOP coating (see the process used for the first version of our device with hydrophobic cover), and the PFTS cover is a chemical modified flat silicon wafer (see process used for the second version of our device with superhydrophobic cover). The cover and the EWOD platform base are fixed with a 200μm gap. Droplet transport is controlled by the electrode potential via a LabVIEW programmable switch control. The total test time is 0.4s, during the begin 0.2s the right electrode is actuated and then switched off.

2.5.2. Motion analysis

Based on high speed videos and the extracted series of pictures, the motion of the droplet can be analyzed. Here, the driven voltage for the three different configurations is 142V, 190V, and 142V, respectively. For the CYTOP cover case, the reason to energize the electrode with higher voltage (190V) is because under 142V the displacement of the water droplet from the first electrode to the second one is lower than the electrode pitch (2.1mm). It means that the water droplet stands on both electrodes at the end of the period (T_s).

2.5.2.1. No cover

A 142V–1kHz square-wave signal was applied between the ground electrode and the on-state driving electrode. The pictures taken from the film are processed with MacBiophotonics ImageJ software and are plotted in **Figure 2.24**. It illustrates the complete transport dynamics showing schematically the time-dependent variation in the droplet advancing and receding front in X-axis displacement and the instantaneous velocity. Before 27ms, the two electrodes are off-state (deactivated). From 27ms to 227ms, the left electrode is

on-state (activated) and the right electrode is off-state. After 227ms, both electrodes are deactivated.

(1) Elongation of the droplet

From 27ms to 32.5ms, only the advancing front of the droplet shows the movement with an increasing value in X-axis. In 2ms, the velocity of the advancing front reaches to 215 mm/s and then (from 29ms to 32.5ms) it slightly decreases to 180mm/s. As a result, elongation of the droplet along the axis of motion is evident. At 32.5ms, the receding front of the droplet stats to move and the distance between the advancing and the receding fronts is at the maximum value. The distance is elongated 37.5%, from the original 2.4mm to 3.3mm.

(2) Droplet movement

During 32.5ms to 33.5ms, the velocity of the receding front increases and reaches the same value as the one of the advancing front (180mm/s) at 33.5ms. To be noted that, from 33.5ms to 45.5ms, two curves of the velocity shows the similar change trend: first increasing and then decreasing. The maximum velocities of the advancing and receding front are 209mm/s and 254 mm/s, respectively. During this period, the velocity of the receding front is always bigger than the one of the advancing front. At 45.5ms, their velocities are the same value (30mm/s) and the distance between the advancing front and the receding front reaches a low value of 2.6mm at 45.5ms. From 45.5ms to 70ms, the velocity of the receding front first decrease from 30mm/s to 0 (at 47ms), then continuously reaches to a negative value of -50mm/s (at 57ms) and finally goes back to 0 (at 70ms). For the advancing front, the velocity first decrease from the 30mm/s to 0 (49ms), then continuously reaches to a negative value of -90mm/s (at 53ms) and finally goes back to 0 (at 70ms). This variation is also observed in graph (a): 1) the advancing and receding fronts with a peak in X-position are at 47ms and 49ms, respectively, and 2) the droplet shifts back and it totally covers the right electrode at 70ms. This ‘peak’ motion is due to the droplet inertia movement.

(3) Electric charge releasing

At 70ms, the droplet movement from the left electrode to the right one is finished. This suggests that the minimum switching time (T_s) for switching the voltage from one electrode to another is 43ms. From 70ms to 227ms, the droplet stays on the right electrode. The distance between the advancing front and the receding front is around 2.6mm. Finally, by deactivating electrode, the droplet recovers its initial diameter at 229ms.

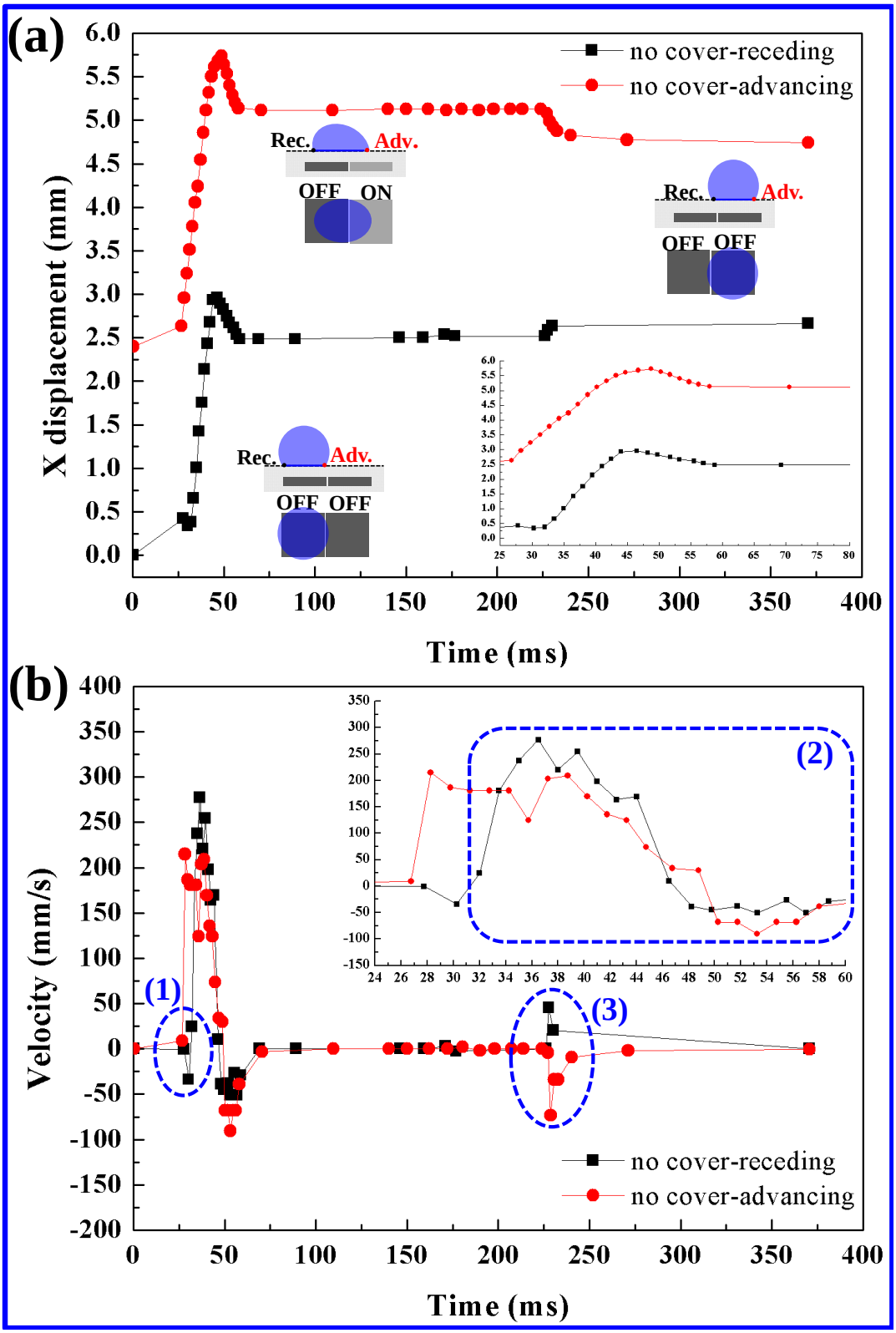

Figure 2.24 Results of the X displacement and of the instantaneous velocity of a DI-water droplet (1µL) as a function of time during a single transfer determined by image analysis in no cover configuration. (a) The displacement of the receding and advancing fronts of the droplet with respect to their initial position. (b) The instantaneous velocity of the receding and advancing fronts of the droplet. Every data point represents the average value among 6 frames (taken at 4000 fps).

In the following section, we focus on three phases (shown in **Figure 2.24**): the phase before initial droplet movement (1), the phase of droplet movement (2), and the final phase of electric charge releasing (3). Contact angle hysteresis is a reflection of a threshold resistance force to initial movement of a droplet from one metastable state to another on a surface [34][35][36]. At the moment when a droplet starts movement, the difference of the contact angle between the advancing and receding front is defined as contact angle hysteresis. We have measured the dynamic contact angle and the resulting hysteresis of the droplet under EWOD. The results of these three phases are illustrated in **Figure 2.25**.

In the phase before initial droplet movement (**Figure 2.25(1)**), elongation of the droplet along the X-axis of motion and shrinking of the droplet along the Y-axis are evident. One can observe that the advancing front of the droplet moves and the receding front pins on the surface. The contact angle of advancing ($\theta_{Badv.}$) on bottom plate quickly decreases from 112.8° to 65.5° in 0.5ms and then slightly decreases to 55.4° at 30.75ms. Whereas, from 26ms to 31ms, the contact angle of receding ($\theta_{Brec.}$) on bottom plate first slightly descends 15.5° (from 111.2° to 95.7°) and then drops to 80.7° at 30.75ms.

Figure 2.25(2) begins when the receding front starts to move at 32.5ms (1st picture). One can observe that: a) the droplet moves from the left to the right (1st picture to 4th picture), b) further displaces forward (5th picture to 8th picture), and c) finally moves backward (shown in 9th to 12th picture). At 32.5ms, the difference of the contact angle between the advancing and receding front, namely the hysteresis, is 17.7°. From 32.5ms to 47.7ms, $\theta_{Brec.}$ slowly descends to the lowest value of 55.7° (at 42.5ms) to be followed by a gradual increase to 62.9°; Similar, $\theta_{Badv.}$ first descends to the lowest value 58.3° and then ascends to 72.3°. The backward movement of the droplet is observed from 8th to 12th picture sequences. From 50ms (8th picture) to 57.5ms (11th picture), the contact angle of the advancing front drops to a value around 60°. In the following 2.5ms, it gradually rises back to 70° (12th picture). Whereas, the contact angle of the receding front gradually rise, but keeps bigger than the one of the advancing front.

The final phase of electric charge releasing is shown in **Figure 2.25 (3)**. At 227ms, the right

electrode is deactivated. In the following 2ms, the contact angle of advancing and receding contact angle both return back to approximately 110°. And, the distance between the advancing front and the receding front goes back to the original dimension (see 1st picture of **Figure 2.25(1-a)**).

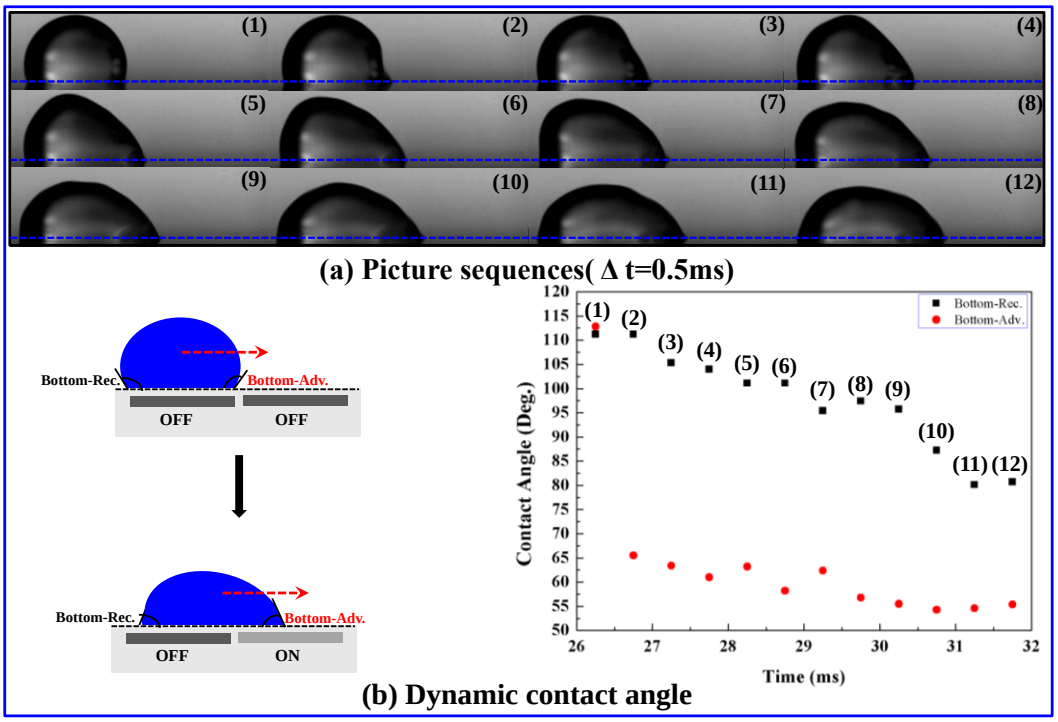

(1) With a time step 0.5ms to account for the phase before initial droplet movement

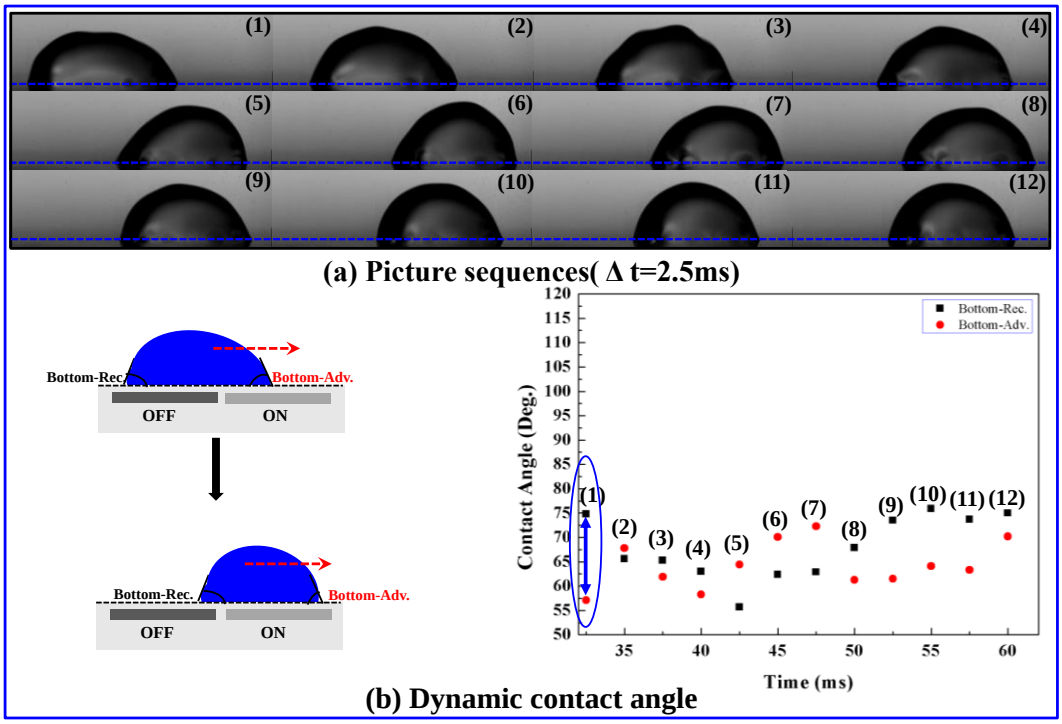

(2) With a time step 2.5ms to account for the phase of droplet movement

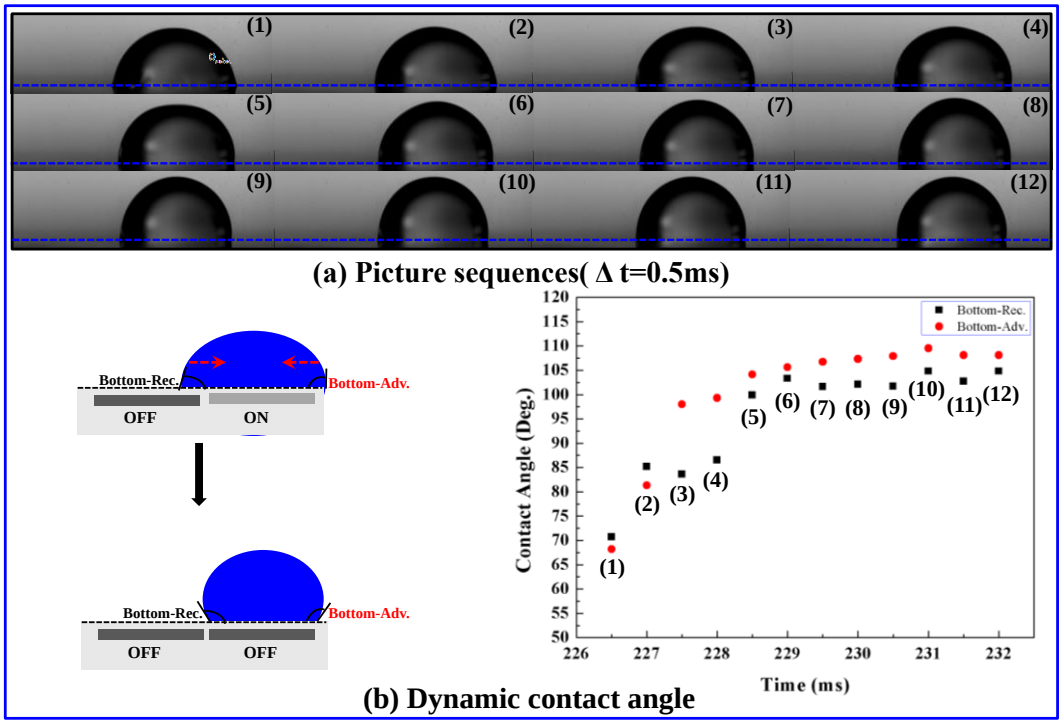

(3) With a time step 0.5ms to account for the phase of electric charge releasing

Figure 2.25 The motion of the droplet movement from left to right in three phases: 1) the phase before initial droplet movement, 2) the phase of droplet movement and 3) the phase of electric charge releasing. In every phase, picture sequences are extracted in (a) and the corresponding dynamic contact angle of the bottom plate are illustrated in (b).

2.5.2.2. CYTOP Pyrex cover

A 190V–1kHz square-wave signal was applied between the ground electrode and the on-state driving electrode. **Figure 2.26** illustrates the complete transport dynamics showing schematically the time-dependent variation in the droplet advancing and receding front in X-axis displacement and the instantaneous velocity. Before 17ms, the two electrodes are off-state (deactivated). From 17ms to 217ms, the left electrode is on-state (activated) and the right electrode is off-state. After 217ms, both electrodes are deactivated.

(1) Before the droplet initial movement

From 17ms to 22.5ms, only the advancing front of the droplet shows the movement with an increasing value in X-axis. In 5.5ms, the velocity of the advancing front increases to 64mm/s. As a result, elongation of the droplet along the axis of motion is evident. At 22.5ms, the receding front of the droplet stats to move and the droplet elongation is small (6%).

(2) Initial droplet movement

From 22.5ms to 45ms, two velocity curves changing trends are: a) the velocity of the advancing first increasing to the maximum value of 70mm/s at 24ms and then fast decreasing to 26mm/s at 45ms, and b) the velocity of the receding first increasing to the maximum value of 26mm/s at 26ms and then fluctuates between 18mm/s and 26mm/s. At 45ms, the velocity of the receding front and the one of the advancing are same (26 mm/s). From 45ms to 71ms, the velocity of the advancing decreases to 8mm/s (at 50ms) and then slightly drops to 6mm/s. Whereas, the velocity of the receding decreases to 12mm/s (at 54ms) and then slightly drops to 10mm/s. To be noted that, from 45ms to 71ms, the velocity of the receding front is always bigger than the one of the advancing front. This induces at 45ms the distance between the advancing and the receding fronts is at the maximum value. The maximum distance is elongated 16.7%, from the original 2.4mm to 2.8mm. After 45ms, the distance between the advancing front and the receding front continuously reduces, with a value of 2.6mm at 71ms.

(3) Constant movement and final electric charge releasing

From 71ms to 150ms, the velocities of the advancing front and the receding front are similar (8~10mm/s). As a result, the droplet is in constant movement and the distance between the advancing front and the receding front is around 2.5mm. After 150ms, both velocities start decrease. At 216.8ms, the droplet movement from the left electrode to the right one is finished. This suggests that the minimum switching time (T_s) for switching the voltage from one electrode to another is 199.8ms. The droplet inertia movement is not observed with a CYTOP cover configuration. Finally, by deactivating electrode, the droplet recovers its initial diameter at 219ms.

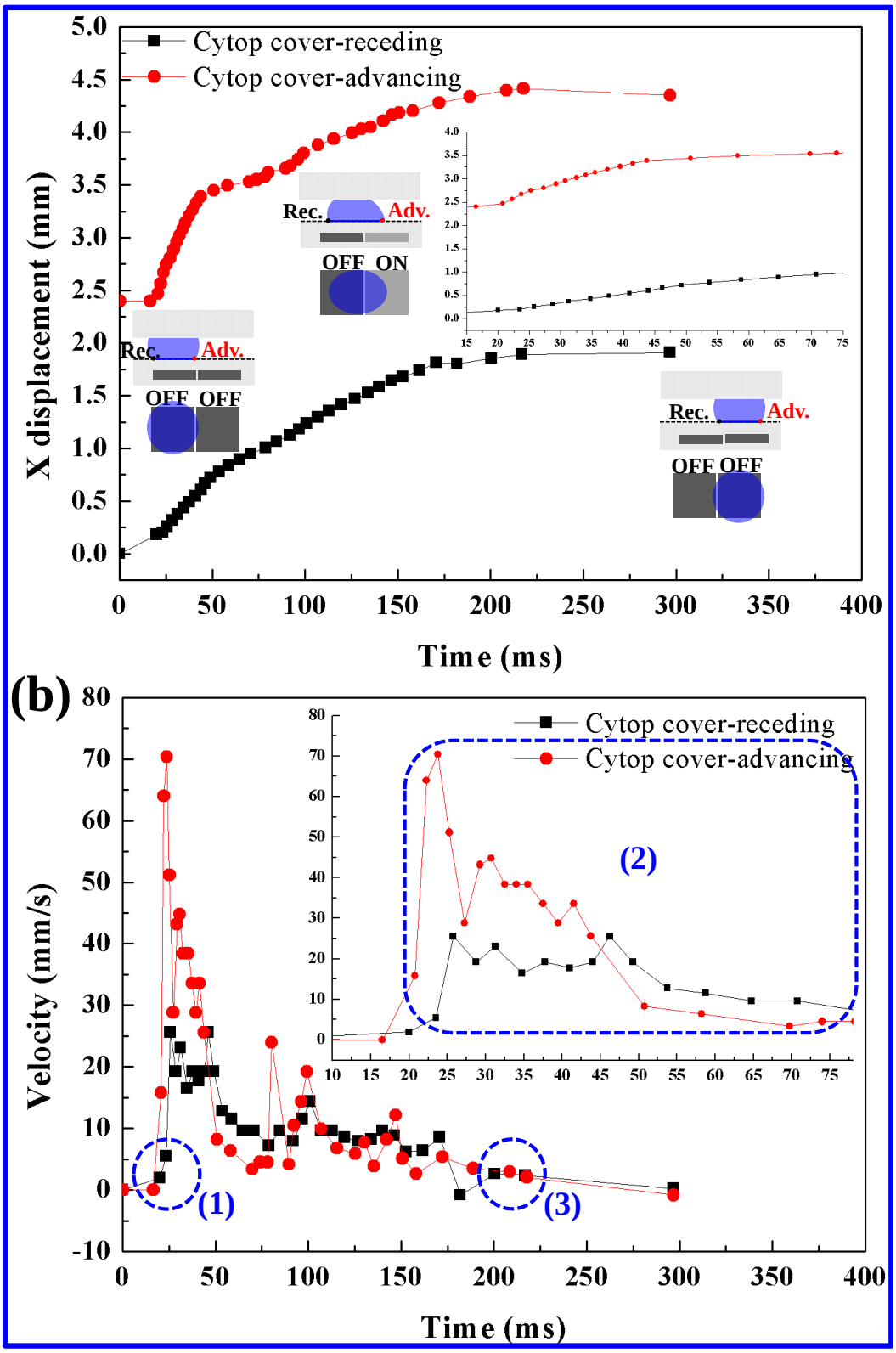

Figure 2.26 Results of the X displacement and of the instantaneous velocity of a DI-water droplet (1µL) as a function of time during a single transfer determined by image analysis with a CYTOP cover configuration. (a) The displacement of the receding and advancing fronts of the droplet with respect to their initial position. (b) The instantaneous velocity of the receding and advancing fronts of the droplet. Every data point represents the average value among 6 frames (taken at 4000 fps).

In the following section, we focus on three phases (shown in **Figure 2.26**): the phase before initial droplet movement (1), the phase of initial droplet movement (2), and final electric charge releasing phase (3).

In **Figure 2.27(1)**, elongation of the droplet along the X-axis of motion is evident. Before 22.5ms (12th picture), for the top plate, the contact angle of the advancing ($\theta_{Tadv.}$) and the receding front ($\theta_{Trec.}$) keep a value around 110°. Whereas, in the first 2ms, for the bottom plate, the contact angle of advancing ($\theta_{Badv.}$) and the receding front ($\theta_{Brec.}$) decrease 37.4° (from 108.4° to 71°) and 26.6° (from 108.4° to 81.8°), respectively. From 19ms to 22ms, $\theta_{Badv.}$ and $\theta_{Brec.}$ stabilize on a low value, approximately 72° and 82°, respectively. The receding front starts to move at 22.5ms. At this time, $\theta_{Trec.}$ quickly reduces to 100.6° and the variant value of the other three contact angles is small (<2°). One can observe that the hysteresis of the top plate and the bottom plate are 13.1° and 13.9°, respectively. This result indicates that the friction resistance comes not only from the bottom plate but also from the CYTOP cover during the droplet movement. It can explain the reason why the driving voltage (190V) in CYTOP cover configuration is higher than the one (142V) in no cover configuration.

Figure 2.27(2) shows initial droplet movement. From 27ms to 47ms, for both plates, the difference between the advancing and the receding front reduces. At 47ms (5th picture) the elongation of the droplet reaches the maximum value. After 47ms, the differences between the advancing and the receding front of both plates stabilize on a value of 5°~8°.

In **Figure 2.27 (3)**, at 217ms, the right electrode is deactivated. In the following 2ms, the contact angles of advancing and receding contact angle on the bottom plate and on the top plate return back to approach 103° and 107°, respectively. And, the distance between the advancing and the receding shrinks back to the original dimension (see 1st picture of **Figure 2.27(1-a)**).

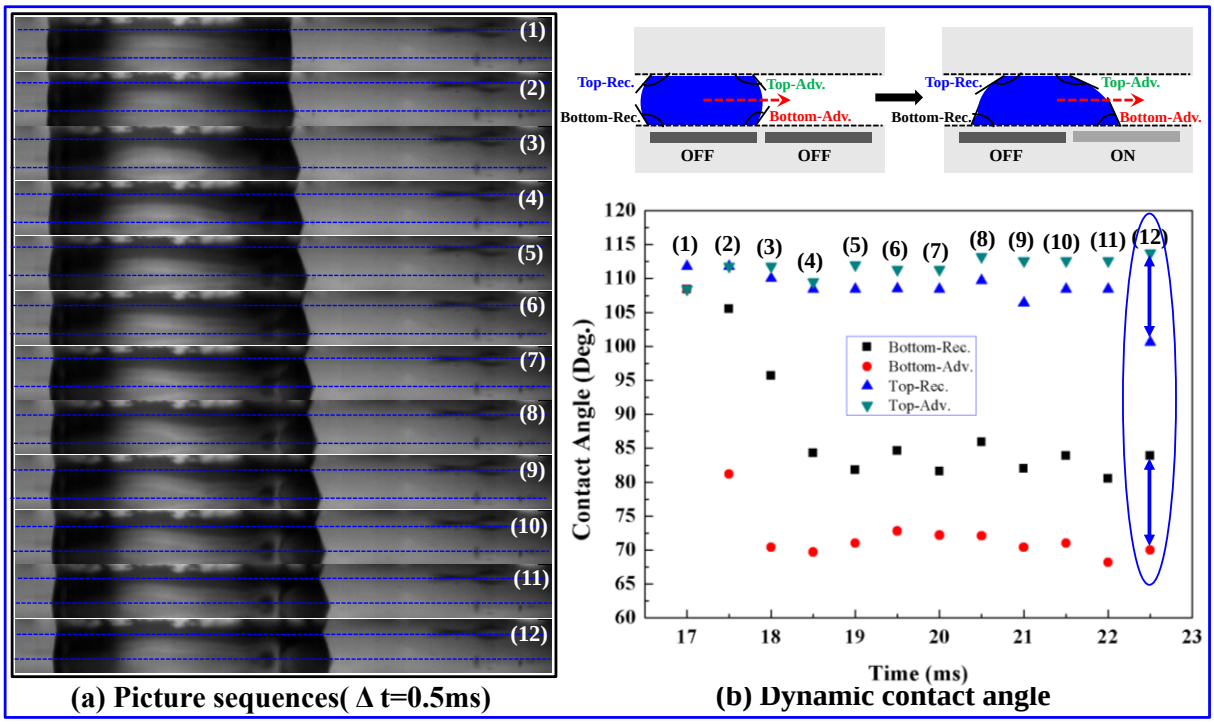

(a) Picture sequences(Δ t=0.5ms) **(b) Dynamic contact angle**

(1) With a time step 0.5ms to account for the phase before initial droplet movement

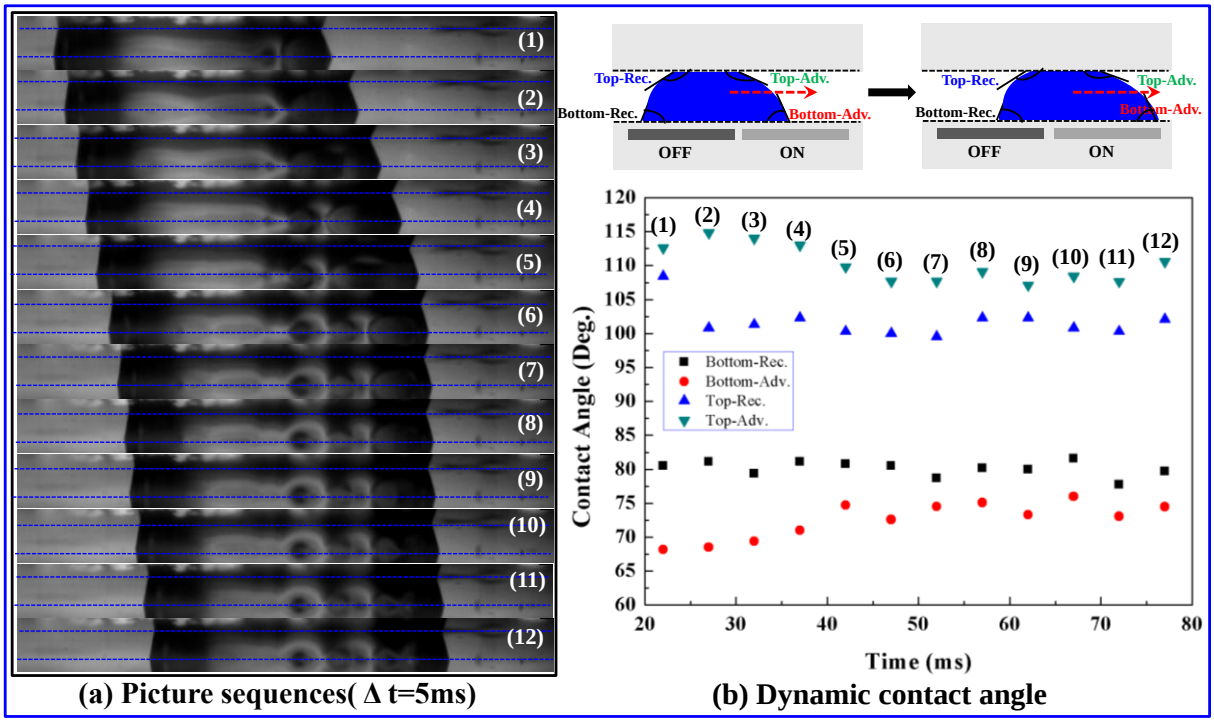

(a) Picture sequences(Δ t=5ms) **(b) Dynamic contact angle**

(2) With a time step 5ms to account for the phase of initial droplet movement

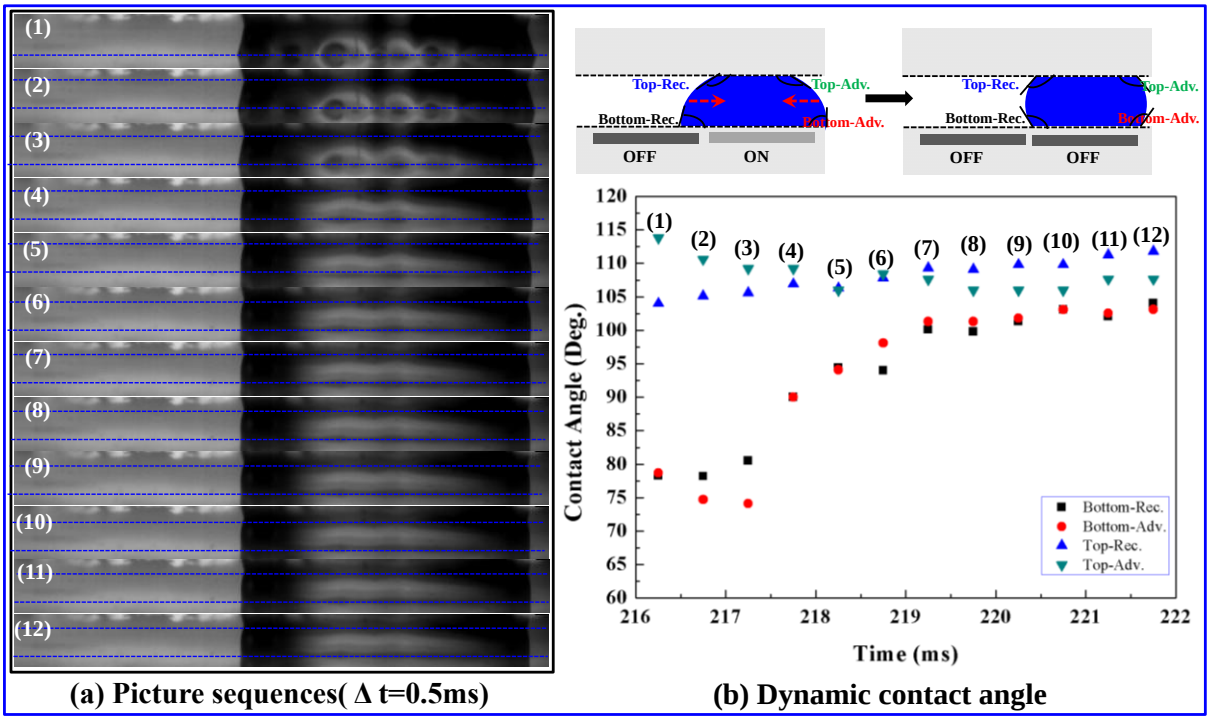

(a) Picture sequences(Δ t=0.5ms) **(b) Dynamic contact angle**

(3) With a time step 0.5ms to account for the phase of electric charge releasing

Figure 2.27 The motion of the droplet movement from left to right in three phases: 1) the phase before initial droplet movement, 2) the phase of initial droplet movement and 3) the phase of electric charge releasing. In every phase, picture sequences are extracted in (a) and the corresponding dynamic contact angle of the top plate and the bottom plate are illustrated in (b).

2.5.2.3. PFTS cover

A 142V–1kHz square-wave signal was applied between the ground electrode and the on-state driving electrode. **Figure 2.28** illustrates the complete transport dynamics showing schematically the time-dependent variation in the droplet advancing and receding front in X-axis displacement and the instantaneous velocity. Before 33ms, the two electrodes are off-state (deactivated). From 33ms to 233ms, the left electrode is on-state (activated) and the right electrode is off-state. After 233ms, both electrodes are deactivated.

(1) Before initial droplet movement

From 33ms to 37ms, only the advancing front of the droplet shows the movement with an increasing value in X-axis. The velocity of the advancing front increases to 133mm/s at 36ms and in the following 1ms slightly decreases to 130mm/s. One can observe that the receding front of the droplet stats to move at 37ms. At this time, the distance is elongated 16.7%, from

the original 2.4mm to 2.8mm.

(2) Initial droplet movement

From 37ms to 41ms, the velocity of the advancing fast decreases, yet the velocity of the receding increases. At 41ms, the velocity of the receding front and the one of the advancing are same (36mm/s). One can observe that the distance between the advancing and the receding front is at the maximum value at this time. The maximum distance is elongated 20.8%, from the original 2.4mm to 2.9mm. From 41ms to 54ms, the velocity curve of the receding is in vibrating change trend. The maximum velocity of the receding is appeared at 44ms with a value of 53mm/s. During this period, the velocity of the advancing slowly ascends. At 54ms, the two velocities are same with a value of 45mm/s. From 54ms to 80ms, both velocities decrease, but the velocity of the receding front is always bigger than the one of the advancing front. After 54ms, the distance between the advancing front and the receding front continuously reduces. At 79ms, the distance is approximately to 2.6mm

(3) Constant movement and final electric charge releasing

From 79ms to 93ms, the velocities of the advancing front and receding front are similar (~5mm/s). As a result, the droplet is in constant movement and the distance between the advancing front and the receding front is around 2.6mm. After 93ms, both velocities start decrease. At 210ms the droplet movement from the left electrode to the right one is finished, which suggests the minimum switching time (T_s) for switching the voltage from one electrode to another is 177ms. After deactivating the right electrode, the droplet recovers its initial diameter at 237ms.

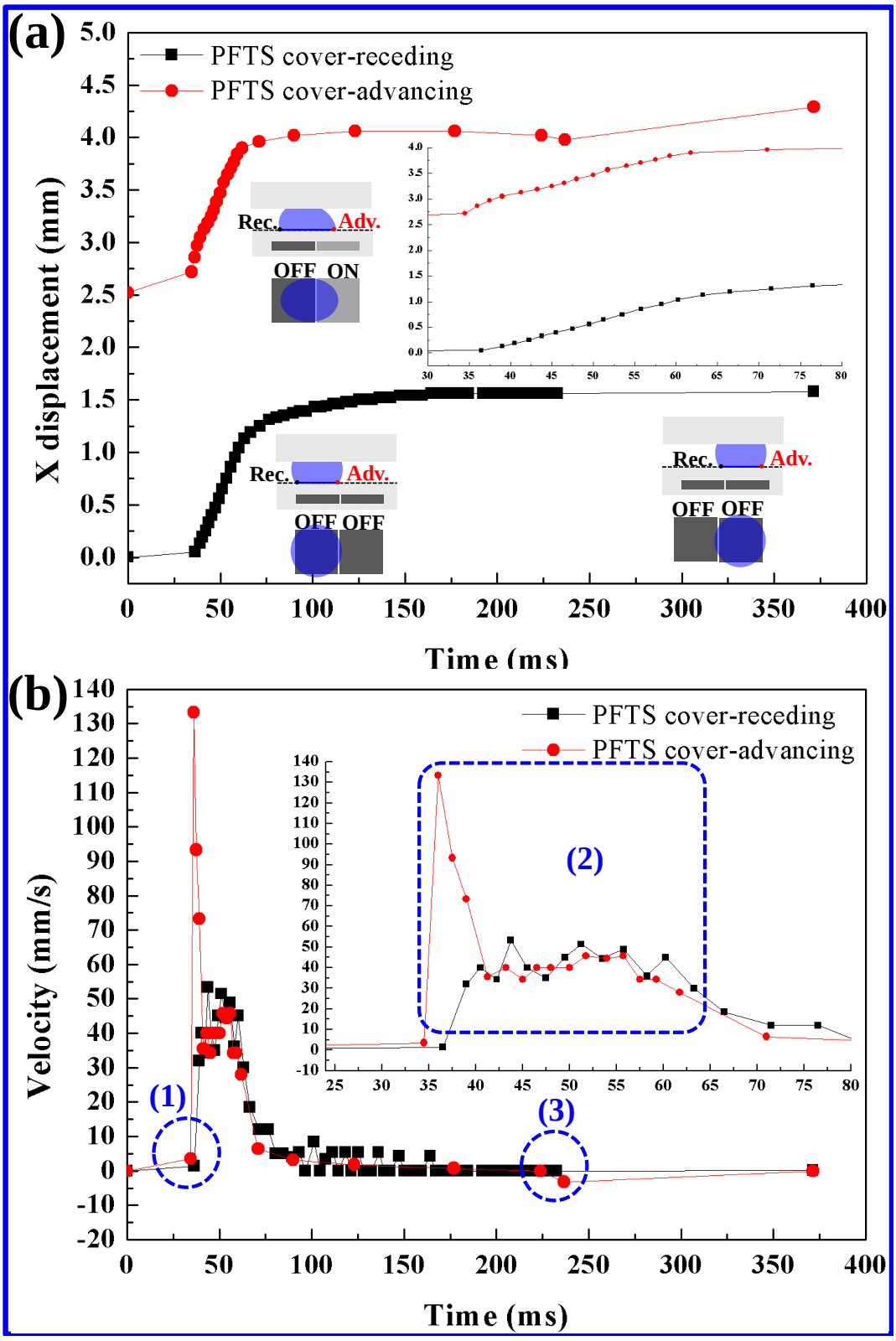

Figure 2.28 Results of the X displacement and of the instantaneous velocity of a DI-water droplet (1µL) as a function of time during a single transfer determined by image analysis in PFTS cover configuration. (a) The displacement of the receding and advancing fronts of the droplet with respect to their initial position. (b) The instantaneous velocity of the receding and advancing fronts of the droplet. Every data point represents the average value among 6 frames (taken at 4000 fps).

In the following section, we focus on three phases (shown in **Figure 2.28**): the phase before initial droplet movement (1), the phase of initial droplet movement (2), and final electric charge releasing phase (3).

In **Figure 2.29(1)**, elongation of the droplet along the X-axis of motion is evident. During this phase, the contact angle of the advancing ($\theta_{Tadv.}$) and the receding front ($\theta_{Trec.}$) on the top plate keep a value around 150°. For the bottom plate, from 33.5ms to 35.5ms, the advancing contact angle ($\theta_{Badv.}$) fast descends from 111.3° to 64.4° (in the first 0.5ms) and then slightly ascends to 72.9°; whereas, the receding contact angle ($\theta_{Brec.}$) keeps reducing from 110.7° to 79.7°. In the following 1.5ms, $\theta_{Badv.}$ and $\theta_{Brec.}$ slightly decrease (<1°). At 37ms (corresponding to 8th picture), the receding front starts to move. At this time, $\theta_{Badv.}$ and $\theta_{Brec.}$ reduces to 63.4° and 80°, respectively; whereas, $\theta_{Tadv.}$ and $\theta_{Trec.}$ are 145.6° and 146.3°, respectively. One can observe that the hysteresis of the top plate is 0.7° and the one of the bottom plate is 16.6°. It indicates that there is almost no friction resistance from the PFTS cover during the droplet movement.

Figure 2.29(2) shows the initial droplet movement. The contact angle of the advancing ($\theta_{Tadv.}$) and the receding front ($\theta_{Trec.}$) on the top plate still keep a value around 150°. Whereas, $\theta_{Badv.}$ and $\theta_{Brec.}$ fluctuate between 70° and 80°, and the difference between these two contact angle is lower than 10°.

In **Figure 2.29 (3)**, at 233ms, the right electrode is deactivated. At 237ms, the contact angles of advancing and receding contact angle on the top plate and on the bottom plate return back to approach 150° and 108°, respectively. One can also observe that the distance between the advancing and the receding shrinks back to the original dimension (see 1st picture of **Figure 2.29(1-a)**).

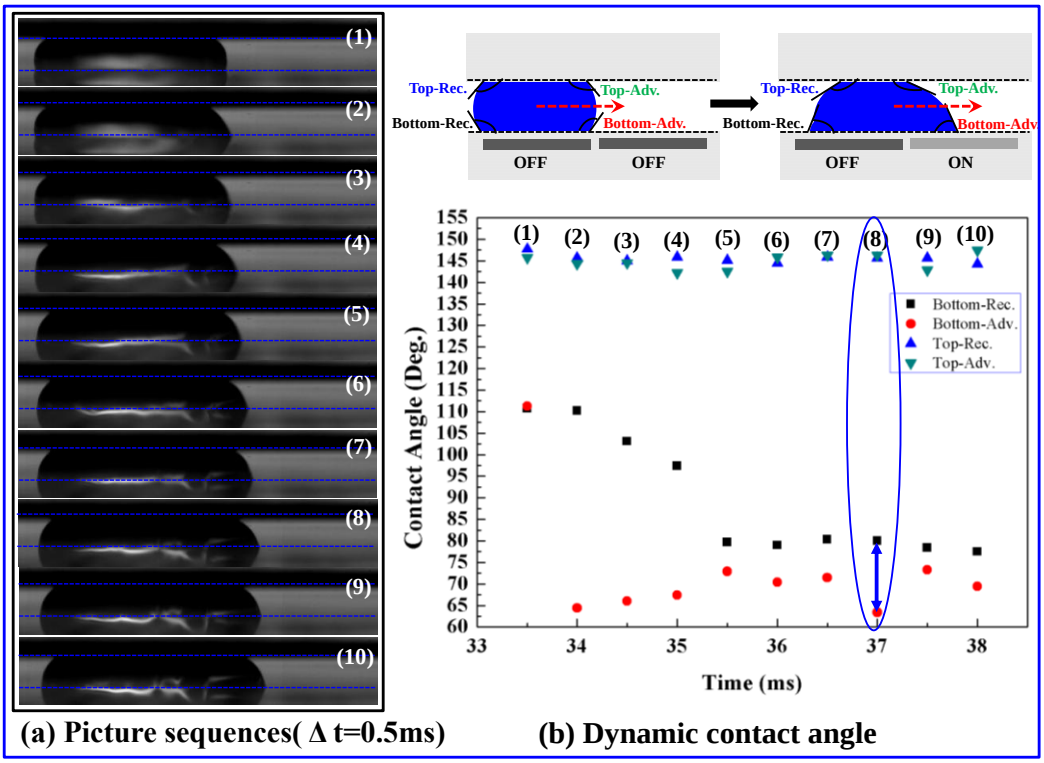

(1) With a time step 0.5ms to account for the phase before initial droplet movement

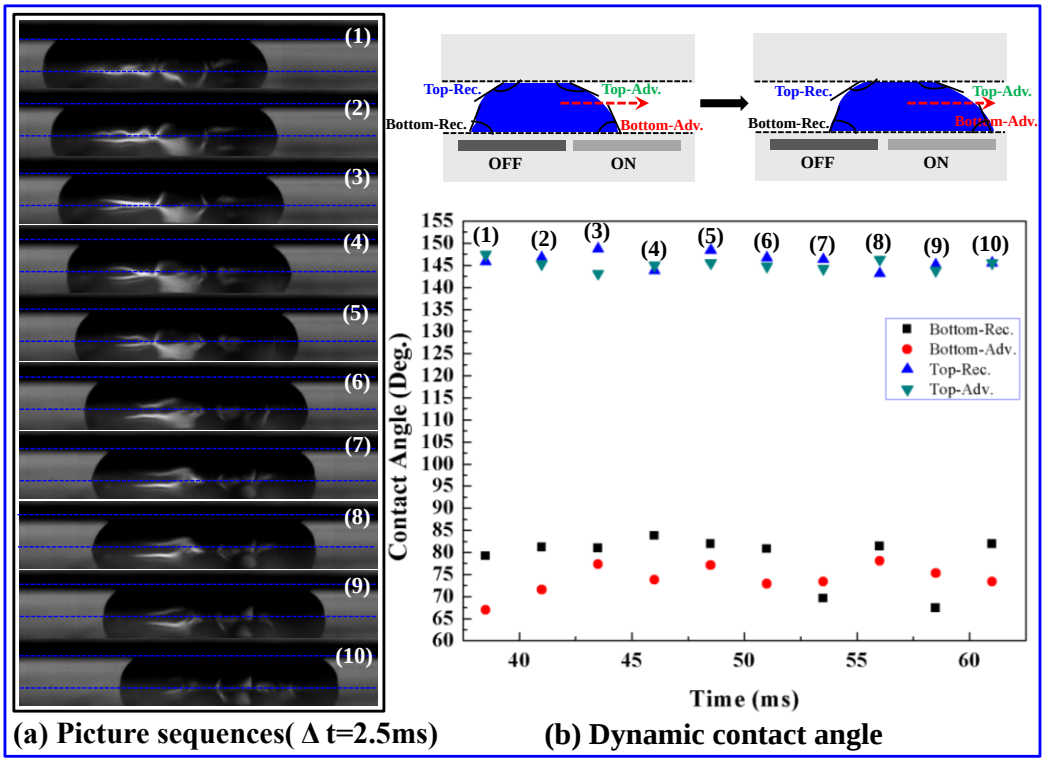

(2) With a time step 2.5ms to account for the phase of initial droplet movement

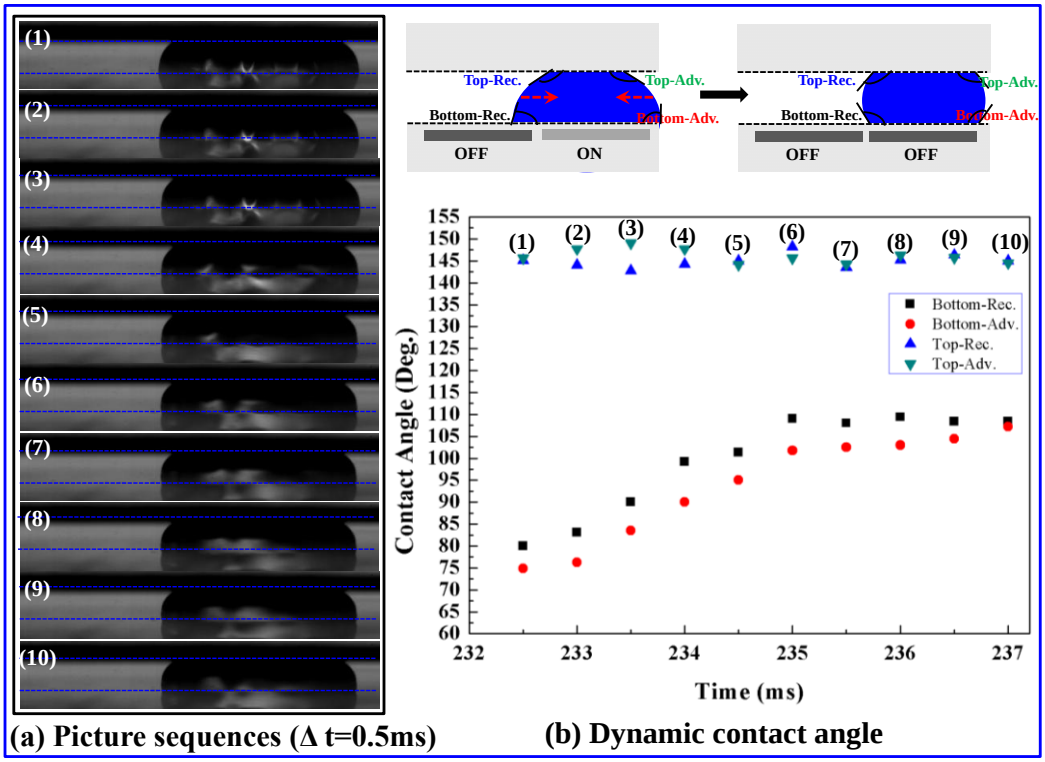

(3) With a time step 0.5ms to account for the phase of electric charge releasing

Figure 2.29 The motion of the droplet movement from left to right in three phases: 1) the phase before initial droplet movement, 2) the phase of initial droplet movement and 3) the phase of electric charge releasing. In every phase, picture sequences are extracted in (a) and the corresponding dynamic contact angle of the top plate and bottom plate are illustrated in (b).

Overall, the results of these three configurations (No cover, CTYOP cover, and PFTS cover) are summarized in **Table 2.7**. 'Maximum elongation' is the maximum value of the distance between the advancing front and the receding front on the bottom plate during the droplet movement. 'Minimum T_s' is the time for moving the droplet from the left electrode to the right one, which is used as the reference to set the T_s (switching the voltage from one electrode to another). During the droplet movement, the maximum value of the velocity for the advancing front and the receding front are also summarized. Besides, we have presented the consumption time (△Time) and the mean velocity, during the period of constant droplet movement (when the velocities of the advancing front and receding front are similar). Moreover, contact angle hysteresis is used to understand the resistance force to initial movement of the droplet.

We find that without cover, the droplet moves fastest and the maximum velocity is higher

than 200mm/s. The maximum elongation of the droplet is the biggest one (37.5%). The droplet completes the movement from the left electrode to the right one by using only 43ms. No constant movement is observed this configuration. For the CYTOP cover configuration, the droplet moves slowest. It takes a long period (79ms) of constant movement at a mean velocity of 8~10mm/s. The time for completing the whole movement from the left electrode to the right one is 199.8ms. For the PFTS cover configuration, the maximum velocity of the advancing and the receding is 133mm/s and 53mm/s, respectively. Compared to the 'CYTOP cover' configuration, it takes less time (14ms) for the constant movement and less time (177ms) for completing the whole movement.

On the bottom plate, the hysteresis is 17.7°, 13.9° and 16.6°, respectively for no cover configuration, CYTOP cover configuration and PFTS cover configuration. On the top plate, the PFTS cover (0.7°) gives much less resistance (approach to 0°) than the one with CYTOP cover (13.1°). It can explain the reason why the driving voltage in PFTS cover configuration is lower (142V) than the one (190V) in CYTOP cover configuration, but same as the one in no cover configuration.

Table 2.7 The results of these three configurations (No cover, CTYOP cover, and PFTS cover) under the voltage of 142V, 190V, and 142V, respectively.

#	X displacement and Velocity on bottom plate							Hysteresis	
	Voltage	Maximum elongation	Minimum T_s	Maximum Velocity		Constant movement			
				Advancing	Receding	△ Time	Mean Velocity	Bottom	Top
No cover	142 V	37.5%	43.0ms	209mm/s	254mm/s	No constant movement		17.7°	0°
CYTOP cover	190 V	16.7%	199.8ms	70mm/s	26mm/s	79ms	8~10mm/s	13.9°	13.1°
PFTS cover	142 V	20.8%	177ms	133mm/s	53mm/s	14ms	5mm/s	16.6°	0.7°

2.6. Summary

The purpose of this chapter is to describe the design, implementation and development of a hybrid microfluidics device for sample preparation. We have developed two generations of the device. In our first work, an original fabrication process has been successfully achieved, that can be ideally used in diverse MEMS applications. However, the preliminary

characterization results show some limits. To address this issue, a superhydrophobic technology has been employed for the top plate fabrication. Due to the low contact angle hysteresis of the top surface, the friction resistance on the surface is low during the droplet transport. The results of these preliminary experiments demonstrate that the sample preparation unit can achieve all the fluidic operations needed for the NANOBE system.

In **Chapter 3**, we will present the further validation experiments by using intra/extra cellular analytes of the genetically modified yeast cell strain (*saccharomyces cerevisiae*). We will show how the whole online bioprocess system work, including the LabVIEW control program description and the coupling experiments with different interface modules.

References

[1] J. Kedzierski, S. Berry, and B. Abedian, "New Generation of Digital Microfluidic Devices", *Journal of Microelectromechanical Systems*, vol. 18, no. 4, pp. 845–851, Aug 2009.

[2] S. Tuomikoski and S. Franssila, "Wafer-Level Bonding of MEMS Structures with SU-8 Epoxy Photoresist", *Physica Scripta*, vol. T114, pp. 223–226, 2004.

[3] B. Li, M. Liu, and Q. Chen, "Low-stress ultra-thick SU-8 UV photolithography process for MEMS", *Journal of Microlithography, Microfabrication, and Microsystems*, vol. 4(4), no. 043008, pp. 1–6, 2005.

[4] C.-H. Lin, G.-B. Lee, B.-W. Chang, and G.-L. Chang, "A new fabrication process for ultra-thick microfluidic microstructures utilizing SU-8 photoresist", *Journal of Micromechanics and Microengineering*, vol. 12, pp. 590–597, 2002.

[5] P. Svasek, E. Svasek, B. Lendl, and M. Vellekoop, "Fabrication of miniaturized fluidic devices using SU-8 based lithography and low temperature wafer bonding", *Sensors and Actuators A: Physical*, vol. 115, pp. 591–599, 2004.

[6] M. Agirregabiria, F. J. Blanco, J. Berganzo, M. T. Arroyo, A. Fullaondo, K. Mayora, and J. M. Ruano-López, "Fabrication of SU-8 multilayer microstructures based on successive CMOS compatible adhesive bonding and releasing steps", *Lab on a Chip*, vol. 5, pp. 545–552, 2005.

[7] C. Wu, F. Bendriaa, F. Brunelle, and V. Senez, "Fabrication of AD/DA microfluidic converter using deep reactive ion etching of silicon and low temperature wafer bonding", *Microelectronic Engineering*, vol. 88, pp. 1878–1883, 2011.

[8] D. S. Ghosh, L. Martinez, S. Giurgola, P. Vergani, and V. Pruneri, "Widely transparent electrodes based on ultrathin metals", *Optics Letters*, vol. 34, no. 3, pp. 325–327, Feb 2009.

[9] J. K. Bhardwaj, C. Welch, A. Barker, R. Gunn, L. Lea, and S. Watcham, "Advances in Deep Oxide Etch Processing for Mems - Mask Selection", in *Proceedings of the 5th Italian Conference — Extended to Mediterranean Countries (2000)*, 2000, pp. 300–307.

[10] P. T. Docker, P. Kinnell, and M. C. L. Ward, "A dry single-step process for the manufacture of released MEMS structures", *Journal of Micromechanics and Microengineering*, vol. 13, pp. 790–794, 2003.

[11] A. Ezkerra, L. J. Fernández, K. Mayora, and J. M. Ruano-López, "Fabrication of SU-8 free-standing structures embedded in microchannels for microfluidic control", *Journal of Micromechanics and Microengineering*, vol. 17, pp. 2264–2271, 2007.

[12] F. J. Blanco, M. Agirregabiria, J. Garcia, J. Berganzo, M. Tijero, M. T. Arroyo, J. M. Ruano, I. Aramburu, and K. Mayora, "Novel three-dimensional embedded SU-8 microchannels fabricated using a low temperature full wafer adhesive bonding", *Journal of Micromechanics and Microengineering*, vol. 14, pp. 1047–1056, 2004.

[13] Y.-Y. Lin, R. D. Evans, E. Welch, B.-N. Hsu, A. C. Madison, and R. B. Fair, "Low voltage electrowetting-on-dielectric platform using multi-layer insulators", *Sensors and Actuators B: Chemical*, vol. 150, pp. 465–470, 2010.

[14] J. Berthier, *Microdrops and Digital Microfluidics*. William Andrew Publishing, 2008.

[15] S. Wang and L. Jiang, "Definition of superhydrophobic states", *Advanced Materials*, vol. 19, pp. 3423–3424, 2007.

[16] X.-M. Li, D. Reinhoudt, and M. Crego-Calama, "What do we need for a superhydrophobic surface? A review on the recent progress in the preparation of superhydrophobic surfaces", *Chemical Society Reviews*, vol. 36, pp. 1350–1368, 2007.

[17] M. Jin, X. Feng, L. Feng, T. Sun, J. Zhai, T. Li, and L. Jiang, "Superhydrophobic aligned polystyrene nanotube films with high adhesive force", *Advanced Materials*, vol. 17, pp. 1977–1981, 2005.

[18] M. Sun, C. Luo, L. Xu, H. Ji, Q. Ouyang, D. Yu, and Y. Chen, "Artificial Lotus Leaf by Nanocasting", *Langmuir*, vol. 21, pp. 8978–8981, 2005.

[19] J. Feng, B. Huang, and M. Zhong, "Fabrication of superhydrophobic and heat-insulating antimony doped tin oxide/polyurethane films by cast replica micromolding", *Journal of Colloid and Interface Science*, vol. 336, no. 1, pp. 268–272, 2009.

[20] K. Q. Peng, J. J. Hu, Y. J. Yan, Y. Wu, H. Fang, Y. Xu, S. T. Lee, and J. Zhu, "Fabrication of single-crystalline silicon nanowires by scratching a silicon surface with catalytic metal particles", *Advanced Functional Materials*, vol. 16, pp. 387–394, 2006.

[21] K. Peng, H. Fang, J. Hu, Y. Wu, J. Zhu, Y. Yan, and S. Lee, "Metal-Particle-Induced, Highly Localized Site-Specific Etching of Si and Formation of Single-Crystalline Si Nanowires in Aqueous Fluoride Solution", *Chemistry – A European Journal*, vol. 12, pp. 7942–7947, 2006.

[22] G. Piret, H. Drobecq, Y. Coffinier, O. Melnyk, and R. Boukherroub, "Matrix-Free Laser Desorption/Ionization Mass Spectrometry on Silicon Nanowire Arrays Prepared by Chemical Etching of Crystalline Silicon", *Langmuir*, vol. 26, no. 2, pp. 1354–1361, 2010.

[23] S. Minko, M. Müller, M. Motornov, M. Nitschke, K. Grundke, and M. Stamm, "Two-Level Structured Self-Adaptive Surfaces with Reversibly Tunable Properties", *J. Am. Chem. Soc.*, vol. 125, pp. 3896–3900, 2003.

[24] J. Fresnais, L. Benyahia, and F. Poncin-Epaillard, "Dynamic (de)wetting properties of superhydrophobic plasma-treated polyethylene surfaces", *Surface and Interface Analysis*, vol. 38, pp. 144–149, 2006.

[25] E. Hosono, S. Fujihara, I. Honma, and H. Zhou, "Superhydrophobic Perpendicular Nanopin Film by the Bottom-Up Process", *J. Am. Chem. Soc.*, vol. 127, pp. 13458–13459, 2005.

[26] L. Zhai, F. Ç. Cebeci, R. E. Cohen, and M. F. Rubner, "Stable Superhydrophobic Coatings from Polyelectrolyte Multilayers", *Nano Lett.*, vol. 4, no. 7, pp. 1349–1353, 2004.

[27] T. Koga, M. Morita, H. Ishida, H. Yakabe, S. Sasaki, O. Sakata, H. Otsuka, and A. Takahara, "Dependence of the Molecular Aggregation State of Octadecylsiloxane Monolayers on Preparation Methods", *Langmuir*, vol. 21, pp. 905–910, 2004.

[28] T. Soeno, K. Inokuchi, and S. Shiratori, "Ultra-water-repellent surface: fabrication of complicated structure of SiO2 nanoparticles by electrostatic self-assembled films", *Applied Surface Science*, vol. 237, pp. 539–543, 2004.

[29] Q. Xie, J. Xu, L. Feng, L. Jiang, W. Tang, X. Luo, and C. C. Han, "Facile Creation of a Super-Amphiphobic Coating Surface with Bionic Microstructure", *Advanced Materials*, vol. 16, no. 4, pp. 302–305, Feb 2004.

[30] G. Piret, H. Drobecq, Y. Coffinier, O. Melnyk, and R. Boukherroub, "Matrix-Free Laser Desorption/Ionization Mass Spectrometry on Silicon Nanowire Arrays Prepared by Chemical Etching of Crystalline Silicon", *Langmuir*, vol. 26, no. 2, pp. 1354–1361, 2009.

[31] F. Lapierre, G. Piret, H. Drobecq, O. Melnyk, Y. Coffinier, V. Thomy, and R. Boukherroub, "High sensitive matrix-free mass spectrometry analysis of peptides using silicon nanowires-based digital microfluidic device", *Lab Chip*, vol. 11, pp. 1620–1628, 2011.

[32] G. Piret, Y. Coffinier, C. Roux, O. Melnyk, and R. Boukherroub, "Biomolecule and Nanoparticle Transfer on Patterned and Heterogeneously Wetted Superhydrophobic Silicon Nanowire Surfaces", *Langmuir*, vol. 24, pp. 1670–1672, 2008.

[33] K. Peng, Y. Wu, H. Fang, X. Zhong, Y. Xu, and J. Zhu, "Uniform, axial-orientation alignment of one-dimensional single-crystal silicon nanostructure arrays", *Angewandte Chemie International Edition*, vol. 44, pp. 2737–2742, 2005.

[34] R. Bavière, J. Boutet, and Y. Fouillet, "Dynamics of droplet transport induced by electrowetting actuation", *Microfluidics and Nanofluidics*, vol. 4, pp. 287–294, 2008.

[35] L. Gao and T. J. McCarthy, "Contact Angle Hysteresis Explained", *Langmuir*, vol. 22, pp. 6234–6237, 2006.

[36] W. C. Nelson, P. Sen, and C.-J. C. J. Kim, "Dynamic contact angles and hysteresis under electrowetting-on-dielectric", *Langmuir*, vol. 27, pp. 10319–10326, 2011.

3. SAMPLE PREPARATION UNIT FOR ONLINE BIOPROCESSES

MONITORING

Content

3.1. Introduction

The rapid development in biotechnology during the last few years was enhanced by progress in genetic engineering, and the advancement of bioprocess monitoring will play a crucial role to meet the future requirements of bioprocess technology [1][2]. Biotechnological processes are increasingly used for the production of chemicals, fuels and materials. The world market for non-food biotechnology-based products was €45 billion in 2006. Due to the economic needs and because of the complex nature of microbial growth and product formation in batch and fed-batch cultivations, the monitoring and control of bioprocesses represents an ever-increasing engineering challenge [2]. Advances in genome analysis, systems biology and synthetic biology now enable the engineering of cells as efficient hosts for production of a variety of compounds for various industrial sectors. Sustainability means that these bioprocesses need to be highly efficient and use minimal amount of resources. To achieve these goals, one needs to understand the performance of the production organism during the process, and be able to continuously monitor and control the process itself. The development of efficient bioprocesses is currently hampered by the lack of rapid, high-throughput analyzers. The increasing number of production organisms and bioprocesses sets demands for fast and versatile product measurement tools for applications ranging from strain screening to large-scale production. Overall, the requirements are to reduce the efforts needed for process development, running time and the cost from the initial idea to the production scale. Therefore, in the years to come, increasing focus has to be given to online techniques for process monitoring, driven by the industry's never-ending need for process optimization.

Improved bioprocess control, and faster organism development drives a need for a device system which fulfills the following requirements:

a) The ability to take rapid real-time measurements of product and biomarker levels during cultivation, thereby eliminating time-consuming manual analysis. Frequent measurements can be taken without sample storage.
b) A versatile analyte range, adjustable to measure various parameters and molecules

(including intra-cellular analytes) depending on the process. The analyte range to be measured by the system should be flexible with only changes to the method and without any changes to the system.

In this Chapter, we will demonstrate the sample preparation unit used for online bioprocess monitoring. First, a short introduction on the motivation and scope of the NANOBE project will be given. As in the central part of the whole integrated system, sample preparation unit is a key module which affects the success rate of the complete operation of the integrated system. Thus, the prior period work is to validate the sample preparation unit by using real samples needed in the final integrated test, including the movement feasibility and fluid operations. The operation procedures controlled by our homemade LabVIEW program will also be described. Then, coupling tests between the sample preparation unit and other modules will be presented. Finally, full analysis test cycles will be carried out with the integrated system.

3.2. Configuration of the NANOBE integrated system

The aim of the NANOBE project is to construct a versatile tool for real-time analysis of several compounds and biomarker in bioreactor processes. Automated sample handling for measurements of intra and extra-cellular analytes is of importance because some key biomarkers exist only inside cells. A small volume of samples has to be frequently withdrawn from a bioreactor, and the contents of the intracellular and extracellular products and biomarkers as well as culture conditions have to be measured within the system. This enables fully automated, online monitoring of bio-production processes for applications ranging from strain screening to large-scale production.

The flow diagram of the NANOBE integrated system and the responsible project partners for each fluidic module are shown in **Figure 3.1**.

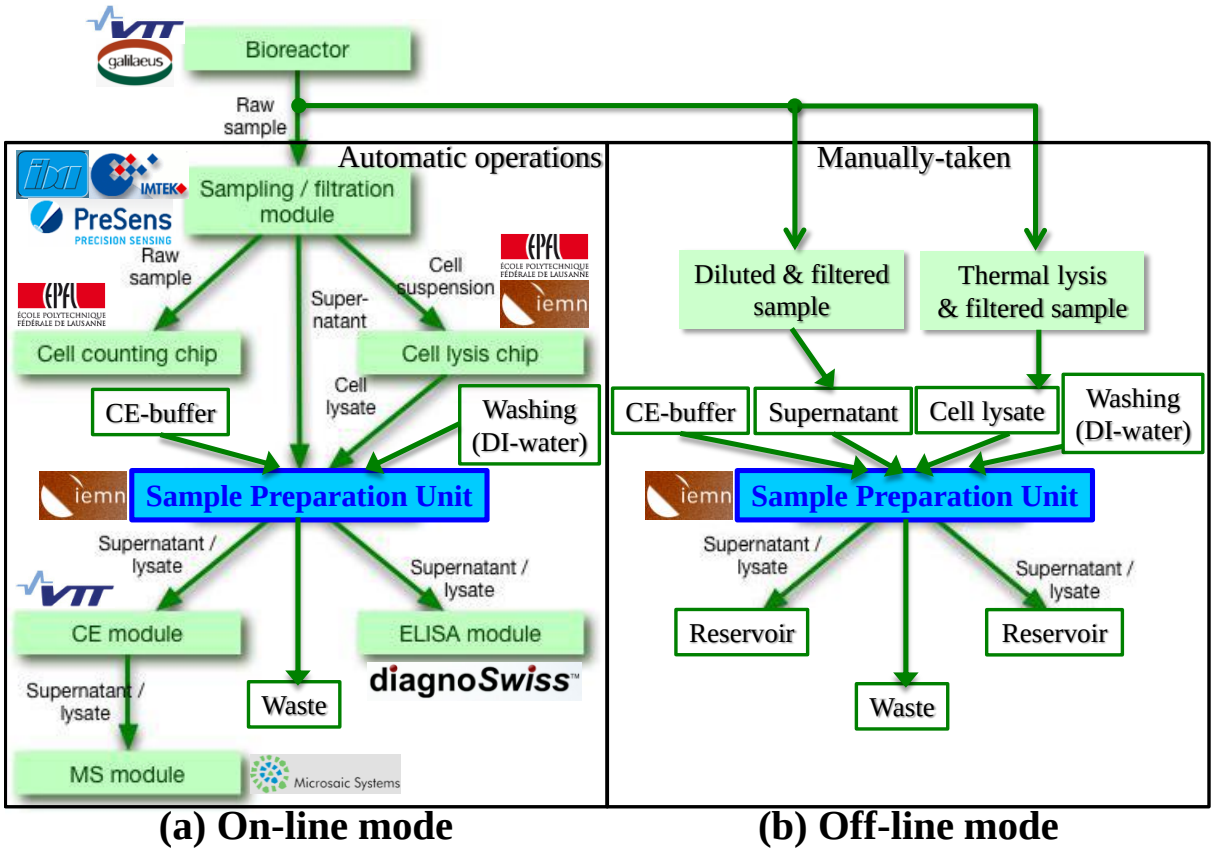

Figure 3.1 Flow diagram of the originally planned NANOBE integrated system: (a) On-line mode for experimental validation of integrated NANOBE system, and (b) Off-line mode for experimental validation of Sample Preparation Unit.

a) Off-line mode: experimental validation of Sample Preparation Unit

The separated intracellular and extracellular samples need to be distributed to different analysis components for the detection and measurement, which demands a device with a series of generic components (continuous-supply of reagents and samples, parallelization and individual manipulation of sample droplets on chip, and integration of an efficient digital-to-analog interface to couple with the outside world). Thus, the EWOD-based hybrid microfluidics device (shown in **Figure 3.2**) acts as a 'Sample Preparation Unit' in the bio-processes monitoring system. The EWOD technology enables precise volume definition and liquid mixing. Especially in NANOBE project, the ability to simultaneously handle multiple liquid droplets is extremely beneficial for well-controlled navigation of multiple samples to the different analysis modules. Besides the 'main' unit operations such as droplet merging and liquid mixing, fluidic A/D (continuous flow to droplets) and D/A (vice versa)

converters are implemented to allow connection of the sample preparation unit with upstream and downstream modules in which continuous flow is required.

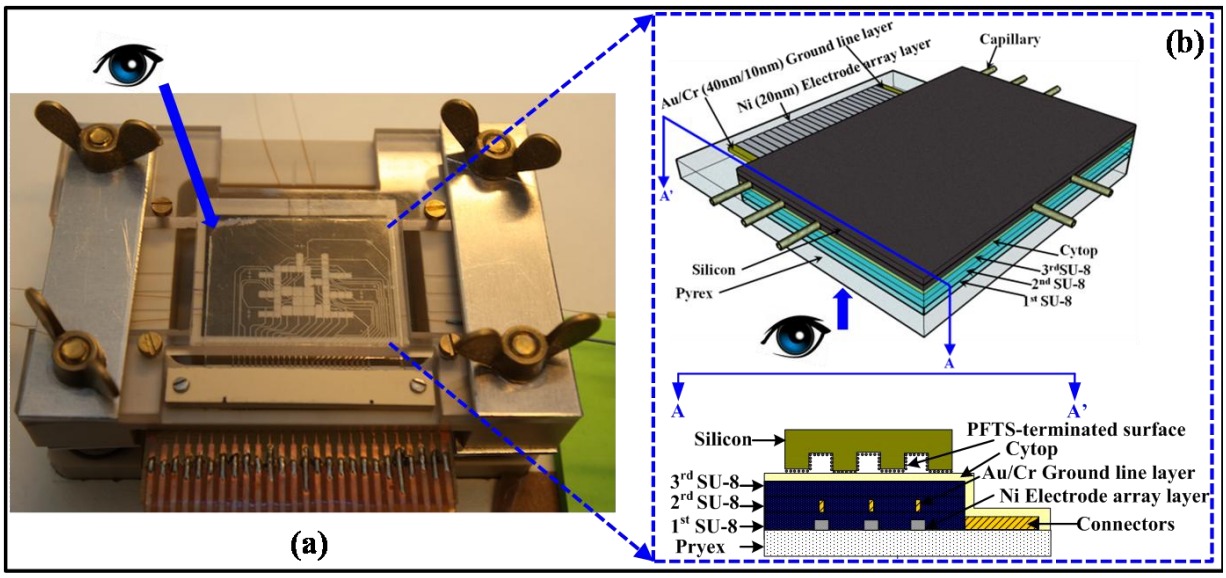

Figure 3.2 (a) The EWOD-based sample preparation unit (developed by IEMN) with electronic and fluidic connections and (b) A detailed scheme of the chip fabrication.

In off-line mode, cell samples are manually taken with a syringe at the same times as the automated sampling at the sampling/filtration module in on-line mode. Then, supernatant samples are separated from the cells, and cells are thermally lysed and filtrated. Prior work in Chapter 2 had shown that droplets of DI-water can be generated and handled (moved, merged, mixed, and delivered) in air by the sample preparation unit. Unlike the manipulation of DI-water, the transport of biological liquids usually suffers from sluggish movement of droplets and even dielectric breakdown. Since the sample preparation unit is in the central section of the integrated system, its performance on droplet manipulation affects the success of the complete operation of the NANOBE integrated system. Thus, prior to carry out the on-line integrated system, it is important to determinate the feasibility of the sample preparation unit.

In off-line mode, we have two objectives. The first is to validate the sample preparation unit by manipulating in air droplets of supernatant, cell lysate, and CE-buffer solutions (required in the NANOBE system). Based on the determined movable range of these solutions,

it is used to set the limit range of dilution rate in the sampling module. The second is to validate the fluidic operations (droplet formation, displacement, and delivery) of the sample preparation unit. Besides, the prepared samples exported from the sample preparation unit can be analyzed in the CE-MS module and ELISA modules and the off-line analysis results can be used for comparison with the on-line analysis results.

b) On-line mode: experimental validation of integrated NANOBE system

In on-line mode, a small amount of sample is taken from the bioreactor (provided by VTT and Galilaeus) into the sampling/filtration module (developed by IBA and IMTEK), where a) the cells are separated from the culture media and re-suspended in buffer solution, then the cells are lysed in the cell lysis module (developed by IEMN), and sorted and counted in cell counting chip (developed by EPFL); b) the supernatant is directly sent to the sample preparation unit (developed by IEMN). Ammonium formate is introduced and used as a buffer for CE-MS module. In the sample preparation unit, the cell lysate and the supernatant samples are divided into groups and are distributed to the downstream detection modules for sample analyses. After performing part of the sample preparation (*e.g.*, mixing with the appropriate buffer solution), the different samples are distributed to the downstream detection modules. Large molecules such as proteins or enzymes are analyzed in the ELISA module (developed by DiagnoSwiss), and other molecules are detected using the coupled CE-MS modules (developed by VTT and Microsaic Systems). In order to avoid cross-contamination between samples, it is necessary to wash electrodes and inlets/outlets between each analysis. Here, DI-water is used as the rinsing solution.

3.3. Off-line mode: experimental validation of Sample Preparation Unit

3.3.1. Working sample preparation

It is important to determinate the feasibility range of the solutions in the sample preparation unit, so that the sample preparation unit can cope with different analytes, different cell types and different cultivation conditions in the NANOBE system. However, only one application

example is to be focused on when testing the whole NANOBE system. Here, the genetically modified yeast cell strain (*Saccharomyces cerevisiae*) is cultivated in the bioreactor. Sample and bioreactor testing conditions are shown in **Table 3.1**.

Table 3.1 Conditions used in the bioreactor cultivations of the NANOBE integrated system for evaluation experiments.

Organism	*Saccharomyces cerevisiae* (genetically modified)
Culture medium	YNB (without amino acids) or YPD medium D-glucose BDH silicone antifoaming agent Immunoglobulin G (IgG) is spiked for experiments involving ELISA

In the Nanobe system test cultivations yeast (*Saccharomyces cerevisiae*) was grown on yeast nitrogen base without amino acids (YNB) or Yeast Peptone Dextrose (YPD) on the different time (3h, 8h and 24h). YPD is a complete medium for yeast growth, which contains yeast extract, peptone, bidest, water, and glucose or dextrose [3]. YNB is a base medium for preparation of minimal and synthetic defined yeast media. YNB contains ammonium sulphate but does not contain amino acids [4]. The composition of YPD and YNB are listed in **Appendix A.3**. The separated 'supernatant' solutions are then prepared in 1-fold, 10-fold and 100-fold diluted rate with DI-water.

The 'cell in buffer' solutions are the centrifuged cells (withdrew after 24 hours in yeast cultivation YPD or YNB) re-suspended in pure Phosphate Buffer Saline (PBS).

CE-buffer is prepared by dilution Ammonium formate solution (from Sigma, 10M in H_2O) 1000 times with water and the pH value is modified to 9 by adding a small amount of ammonium hydroxide.

Here, the working 'cell lysate' solutions are prepared by thermal lysis of yeast. Yeast strains (*Saccharomyces cerevisiae*) are harvested from Sabouraud agar and suspended in liquid Sabouraud at 90°C for 30 minutes. Cells are centrifuged at 3000g for 2min, the supernatant is discarded and yeasts are washed three times with (a) DI-water or (b) phosphate buffered saline (PBS) diluted 100-fold with water to reach the conductivity of 180µS/cm. Following the third washing, cells are resuspended either in DI-water or 100-fold diluted PBS. Cell concentration is manually adjusted with a haemocytometer to get a concentration of

$1*10^6$cells/mL or $1*10^7$cells/mL.

3.3.2. Experimental set-up

In off-line mode, the sample preparation unit is not yet connected to the bioreactor/cell lysis chip and the downstream analysis instruments (ELISA module and CE-MS module). Instead, the samples are loaded from reservoirs and then the processed samples are collected in collector reservoirs. The off-line experimental set-up is shown in **Figure 3.3**.

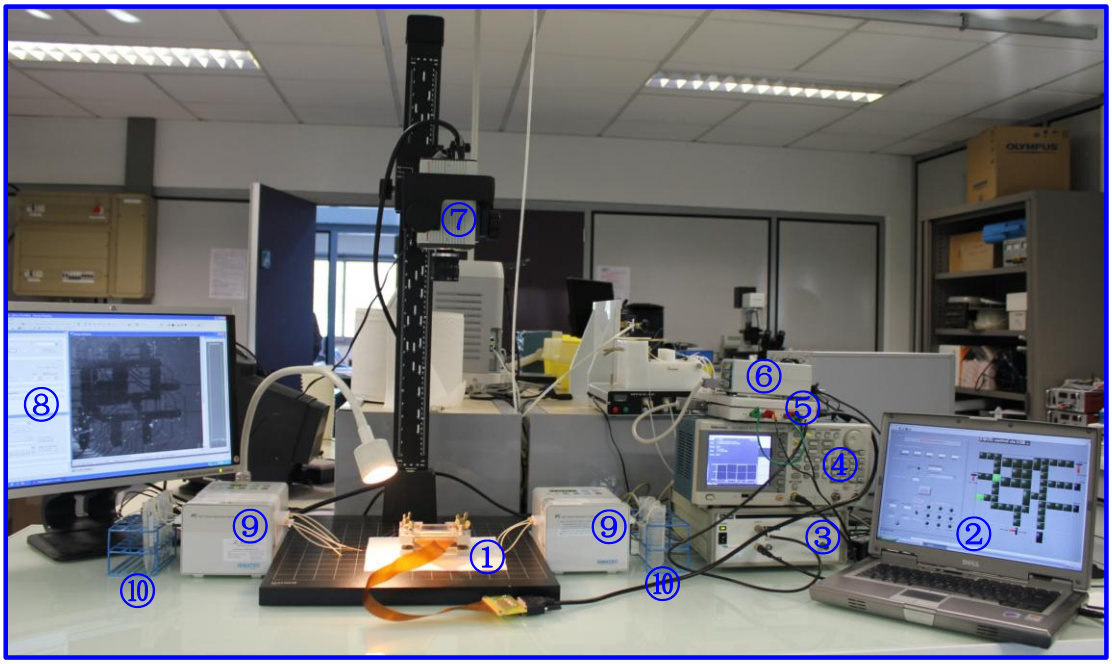

Figure 3.3 The off-line experimental set-up: 1) the sample preparation unit prototype, 2) LabVIEW software (2010 Version), 3) Single Channel High-voltage Amplifier (TEGAM-High voltage Amplifier Model 2340), 4) Function generator (Tektronix-AFG3021B), 5) Electric delay card, 6) USB Data Acquisition (DAQ) Unit 120 Channel Digital I/O, 7) High speed camera (ORCA-flash 2.8), 8) Monitoring screen, 9) Peristaltic pumps (ISM 936-ISMATEC) for samples loading to and exporting from the sample preparation unit, and 10) four sample reservoirs (supernatant, cell lysate, CE-buffer and DI-water) and three collector reservoirs (collected to ELISA outlet, CE-MS outlet, and Waste outlet).

The sample preparation unit has 5 inlets and 3 outlets. The fluids entering our sub-system are: i) the supernatant sample through inlet 1(IN1), ii) the capillary electrophoresis buffer (CE-buffer) through inlet 2 (IN2), iii) the cell lysate sample through inlet 3(IN3), and iv) De-Ionized (DI)-water samples though inlet 4 (IN4) and inlet 5 (IN5). They are pumped from

the different reservoirs. Outlet 1(OU1), Outlet 2(OU2), and Outlet 3(OU3) correspond to the CE-MS reservoir, the ELISA reservoir, and the waste reservoir, respectively. Horizontal connections to inlets/outlets are performed with glass capillaries which have 150µm external diameter and 75µm internal diameter. The advantage of these narrow capillaries is to reduce internal surfaces and thus to lower biomolecules loss due to surface bio-pollution. Their disadvantage is to have a higher hydrodynamic resistance that should be compensate by higher pressure gradient. The LabVIEW program synchronizes: a) fluidic operations (droplet formation, displacement, merging and mixing, and delivery) in the EWOD platform, and b) sample delivery through outlets thanks to the peristaltic pump (ISM936 - ISMATEC).

3.3.3. Software control

In this section, the operation protocol, the operation timeline during one cycle, the control programs and the control panel are presented.

3.3.3.1. Operation protocol

The operation protocol is as follows:

a) The inlet flow rate of the sample preparation unit

In NANOBE project, the completing online analysis cycle time (from sample uptake to detection) is planned in 20 minutes. According to this time limit, the flow rate of the supernatant sample through IN 1 and the cell lysate sample through IN3 are required at a high flow rate, namely 10µL/min. For simplifying the control, the flow rate of the CE-buffer sample and the DI-water sample are also fixed at 10µL/min.

b) The outlet flow rate of the sample preparation unit

In CE-MS module, the sample exported from the sample preparation unit to CE chip (prior to MS equipment) needs to be at a low flow rate of 2µL/min. The sample exported from the sample preparation unit to ELISA module is through a glass capillary which is placed on top of the wells of the microtiter-plate of ImmuSpeed^{TM} protocol. The sample droplet is fall into

the wells by gravity. Thus, we can set the flow rate of OU2 at a relative high flow rate (100μL/min) compared to the one of OU1. For the Waste outlet (OU3), we set the flow rate of OU2 at a high flow rate of 100μL/min.

c) Sample volume definition

The volumes of the supernatant sample and the cell lysate sample are defined by three-way valves actuation in the sampling/filtration module. During each cycle, 17μL of supernatant and 20μL of cell lysate samples are delivered to the sample preparation unit. The CE-buffer sample is used as the background electrolyte solution (BGE) for CE-MS module, because of its electrophoretic properties for CE and volatility for MS. Thus, 1μL sample (either supernatant or cell lysate) need to be pre-mixed with CE-buffer (1μL) in the sample preparation unit. 2μL of CE-buffer samples are delivered from the CE-buffer reservoir.

d) 'Digital' preconditioning in the sample preparation unit

Every unit droplet (~1μL) in the sample preparation unit is generated within 12 sequences in the LabVIEW program controlling. Each sequence time is set to 0.45 second.

e) Sample dispensing

For the 17μL of supernatant samples, the first 16μL samples are dispensed to the ELISA module, and the last droplet is mixed with another CE-buffer sample droplet (1μL). Then, the 2μL mixture samples (named Mix 1) are delivered to the CE-MS module. Similar, the first 16μL of the cell lysate samples are dispensed to the ELISA module and the 17^{th} droplet is mixed with 1 μL of CE-buffer sample. The 2μL mixture samples (named Mix 2) are then delivered to the CE-MS module. Excess cell lysate samples (3μL) are disposed to the 'Waste' outlet.

f) Washing

In order to avoid cross-contamination between function operation procedures, DI-water is

used for washing the internal surfaces (channel walls, top PFTS-termination superhydrophobic cover and bottom CYTOP hydrophobic layer) of the sample preparation unit and the inlet/outlet capillaries.

3.3.3.2. Operation timeline

The operation timeline of one cycle in the sample preparation unit is illustrated in **Figure 3.4(a)**. In order to increase the flexibility of the program control, we divided the different tasks into 10 individual operations, namely 'Supernatant', 'Mix 1', 'Wash ELISA', 'Wash CE', 'Cell lysate', 'Cell lysate (19^{th}) to Waste', 'Mix 2', 'Wash 1', 'Wash 2', and 'Wash 3'.

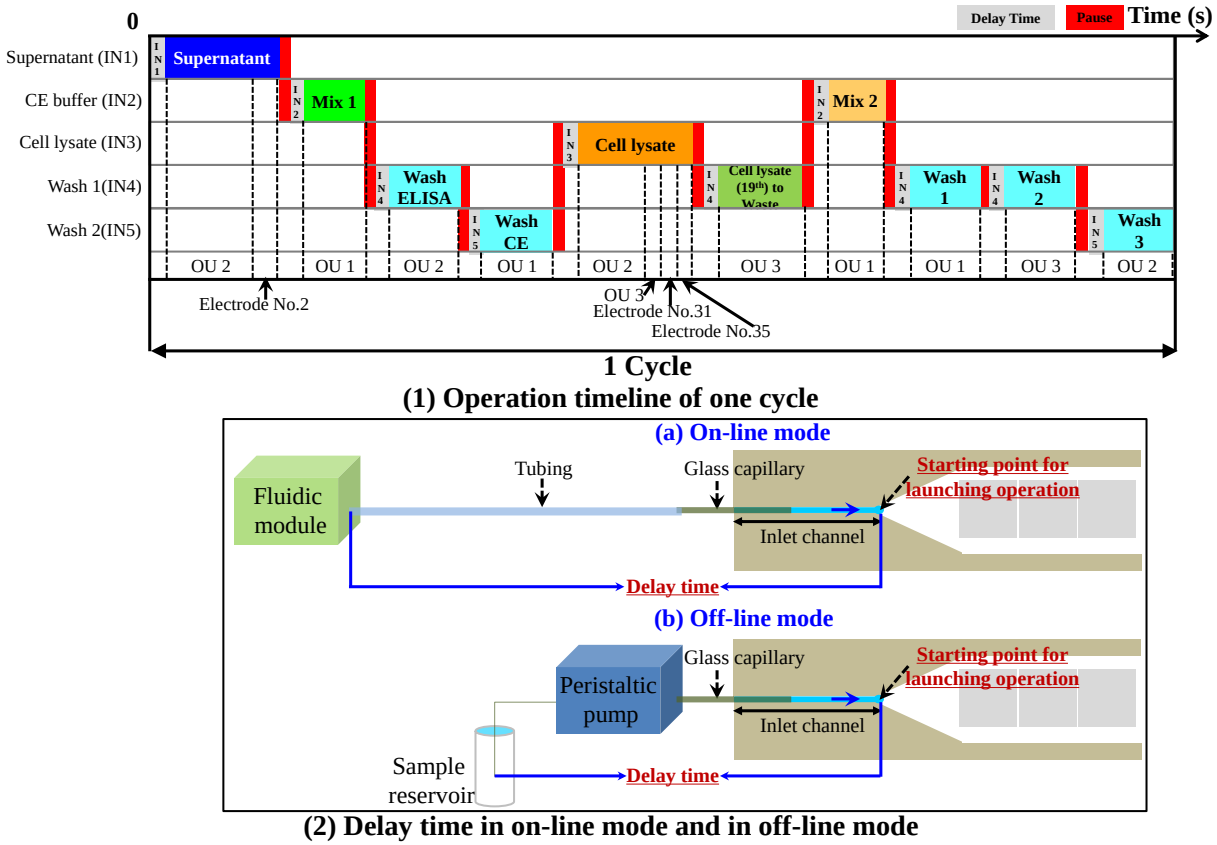

Figure 3.4 Operation timeline of one cycle performed in the sample preparation unit.

Before launching each operation, it exists a 'Delay time'. The 'Delay time' is depending on several parameters, such as the loading speed and the length of the tube/capillary. It is also various in the experimental modes (illustrated in **Figure 3.4(b)**). In on-line mode, 'Delay time'

is defined as the time that the sample is loaded from the outlet of the given upstream fluidic module to the end of one inlet channel of the sample preparation unit. In off-line mode, 'Delay time' is defined as the time that the sample is loaded from a sample reservoir to the end of one inlet channel of the sample preparation unit. In order to make our program compatible in both experimental modes, the 'Delay time' for each operation is individual set. When the operation is finished, there exists a 'Pause time' before starting the next operation. The 'Pause time' is defined as the time for fixing set-up or solving potential problems.

By this individual operation method, when a fault occurs in droplet manipulation, the program can be immediately stopped. After solving the problems (*e.g.*, the device replacement), it is possible to launch the same operation again instead of re-launching the whole program. For example, when dielectric breakdown happen during the 'Mix 2' operation, we can stop the program immediately. After fixing the problem, we launch the 'Mix 2' operation again without restarting from the first 'Supernatant' function operation.

3.3.3.3. Control program

The LabVIEW program consists of 10 individual operations for one cycle and we describe in the following these different operations.

1) Supernatant loading: 17µL of supernatant is loaded through inlet (IN 1) at 10µL/min with 225 time sequences, shown in **Figure 3.5(1)**. Every 12 sequences, one droplet of 1µL is generated and then displaced to the near-end of ELISA outlet. The first 16µL (16 droplets) are transferred to the ELISA modules (OU2). The last 17^{th} droplet is temporary stored on one electrode (No. 2) for the subsequent mixing process.

2) Mix1: Supernatant (17^{th} droplet) mixing with CE-buffer (1^{st} droplet): 1µL of CE-buffer is loaded through the control of three-way valve (V47) and mixed with the preload 17^{th} supernatant, and then delivered to CE outlet (OU1), shown in **Figure 3.5(2)**.

3) Wash ELISA: 2 droplets are loaded from IN4 by the control of three-way valve (V48) and are used for washing the path followed by the supernatant droplets, shown in **Figure 3.5(3)**.

4) Wash CE: 1 droplet is generated from IN5 by the control of three-way valve (V49) and used for washing the path followed by the mixture of supernatant and CE buffer, shown in **Figure 3.5(4)**.

5) Cell lysate load: 20µL lysate is loaded through IN3 at 10µL/min with 241 time sequences, shown in **Figure 3.5(5)**. The delivery of the beginning 16 droplets to the ELISA module is performed thanks to the peristaltic pump (100µL/min). The following 17^{th}-18^{th} droplets are directly transferred to Waste (OU3). Finally, the 19^{th} and 20^{th} droplets are temporary stored on the electrodes (No. 31 and No. 35, respectively) for the subsequent mixing and export process.

6) Waste cell lysate 19^{th}: in order to deliver the last cell lysate droplet, 1µL DI-water droplet is loaded from IN4 by the control of three-way valve (V48) and mixed with the lysate droplet and sent to the waste, shown in **Figure 3.5(6)**. Doubling of the volume (at least 2µL) is necessary to match the size of the droplet with the surface of some electrodes in the EWOD path.

7) Mix2: Cell lysate (20^{th}) mixing with CE-buffer (2^{nd}): 1µL of CE-buffer is mixed with the preload 20^{th} supernatant and then delivered to CE outlet, shown in **Figure 3.5(7)**.

8) Final washing (including Total wash 1, Total wash 2, and Total wash 3): 5µL DI-water (4µL and 1µL are generated from Wash 1 and Wash 2, respectively) to rinse all the electrodes and all the outlets, shown in **Figure 3.5(8-10)**.

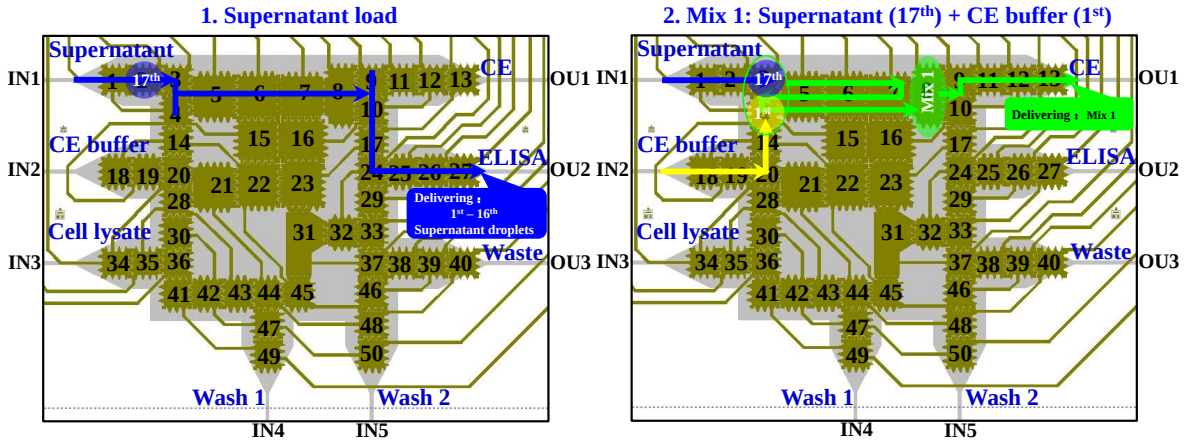

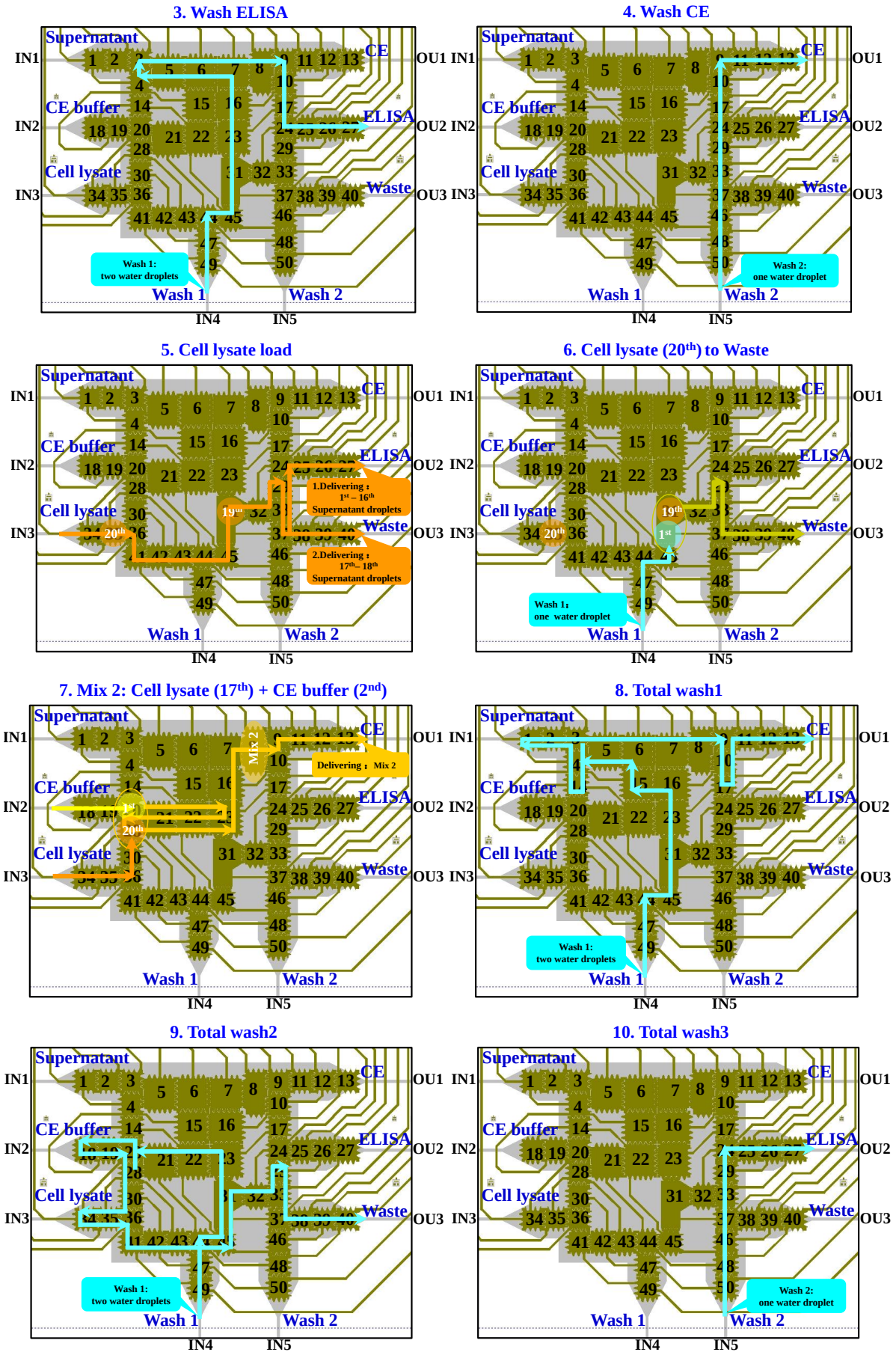

Figure 3.5 Operating sequences within each cycle

Table 3.2 shows a summary of one cycle performed in the sample preparation unit by the control program. The given details are: the port definition, the use of the three-way valve, the manipulated sample volume, the total sequences and the calculated time for each operation. Except delay times for each inlet and pause time between each function, the total time is less than 7 minutes. Thus, it meets the 20-minute performance time limit defined by the online analysis cycle.

Table 3.2 This table describes the different operations performed in the EWOD chip. '-' correspond to no use.

#	Operation	Inlet	Volume (µL)	Valve	Outlet	Sequences (step)	Time (second)
1	Supernatant loading	IN1	16	-	OU2	225	101.25
			1	-	Electrode No. 2		
2	Mix 1	IN2	1	47	OU1	41	18.45
3	Wash ELISA	IN4	2	48	OU2	55	24.75
4	Wash CE	IN5	1	49	OU1	29	13.05
5	Cell lysate load	IN3	16	-	OU2	241	108.45
			2	-	OU3		
			1	-	Electrode No. 31		
			1	-	Electrode No. 35		
6	Cell lysate (19th) to Waste	IN4	1	48	OU3	34	15.3
7	Mix 2	IN2	1	47	OU1	41	18.45
8	Total wash1	IN4	2	48	OU1	63	28.35
9	Total wash2	IN4	2	48	OU3	71	31.95
10	Total wash3	IN5	1	49	OU2	26	11.7
Total (except delay time of each inlet loading and pause time between each function)						**826**	**371.7sec. (6min11.7sec.)**

3.3.3.4. Control panel

The program consists of the control of electrode matrix control, the control of three-way valves, and the control of the pump. The LabVIEW contrl panel is shown in **Figure 3.6**. The details are explained in **Appendix A.4**.

a) Electrode matrix

As mentioned before, the 'delay time' is various in the experimental modes (the on-line mode and the off-line mode). In order to make our program compatible in both experimental modes, the '*DELAY TIMES FOR GENERATING(s)* (1)' for each inlet is individual set. Thus, the program waits for a given delay time (default '0') for each inlet before launching operation procedures.

This program can call 10 pre-saved procedures (corresponding to the operations in **Table 3.2**) in '*FUNCTIONS LAUNCHING* (2)', by selecting the function name in pull down *'Launch functions'* menu. The corresponding file name is shown in *'File corresponding'*. It is possible to repeat each procedure several times by setting the '*Number of the loops*' in (5). It also can adjust the '*SWITCH TIME(s)* (3)', which corresponds to the switching time from one procedure sequence to the next one. The program is trigged by pressing 'START' button (4). During the process, the value in the indicator '*Current sequences*' (in (5)) is increasing. In each sequence, the related electrodes indicators (9) are lighted.

It is able to reset the operations by press 'Reset button' (6). Also, at any moment, the program can be paused (7). Besides, the control can be automatic ('*Pause OFF*' in green) or manual ('*Pause On*' in red). In manual control, the procedure is continued by typing the corresponding '*Step by Step/Restart*' button (8). For example, in 'Supernatant loading' procedure, the procedure is continued by typing *'Supernatant'*. The control is changed back to automatic mode by shifting the 'Pause' button back to 'ON' and pressing one time of the corresponding '*Step by Step/Restart*' button.

b) Three-way valve

In the structure scheme of the integrated NANOBE system, the CE-buffer sample and cleaning fluids (DI-water) are introduced into the sample preparation unit thanks to a peristaltic pump (ISM936–ISMATEC). This pump (PM) has 8 channels (1 channel is used for the CE-buffer and 2 channels are used for DI-water fluids) that are not driven independently. As a consequence, it has been necessary to implement three-way valves (Electrovalve FLIPPER 4.5mm 3 channels TYPE 6650–BURKERT) in front of each channel to control the delivery of the corresponding liquids. The three-way valves (named V47, V48, and V49) are also performed by our home made LabVIEW program. In the 'open' status, the fluid is allowed to load into the inlets of the sample preparation unit; whereas, in the 'close' status, the fluid is transferred back to reservoirs. The statuses of valves are displayed in (10): (a) in 'open' status, the '*Chip*' lamp is in red, and (b) in 'close' status, the '*Tank*' lamp is in red.

c) Pump

The pump used for delivering samples is also controlled in our program. The working period of this pump is pre-setting. During the process, the status of the pump (11) is displaced, stopping in red lamp (*Stopped*) or working in green lamp (*Started*). When the pump is in working status, the corresponding outlet lamp (*CE/ELISA/WASTE*) in (12) is in blue.

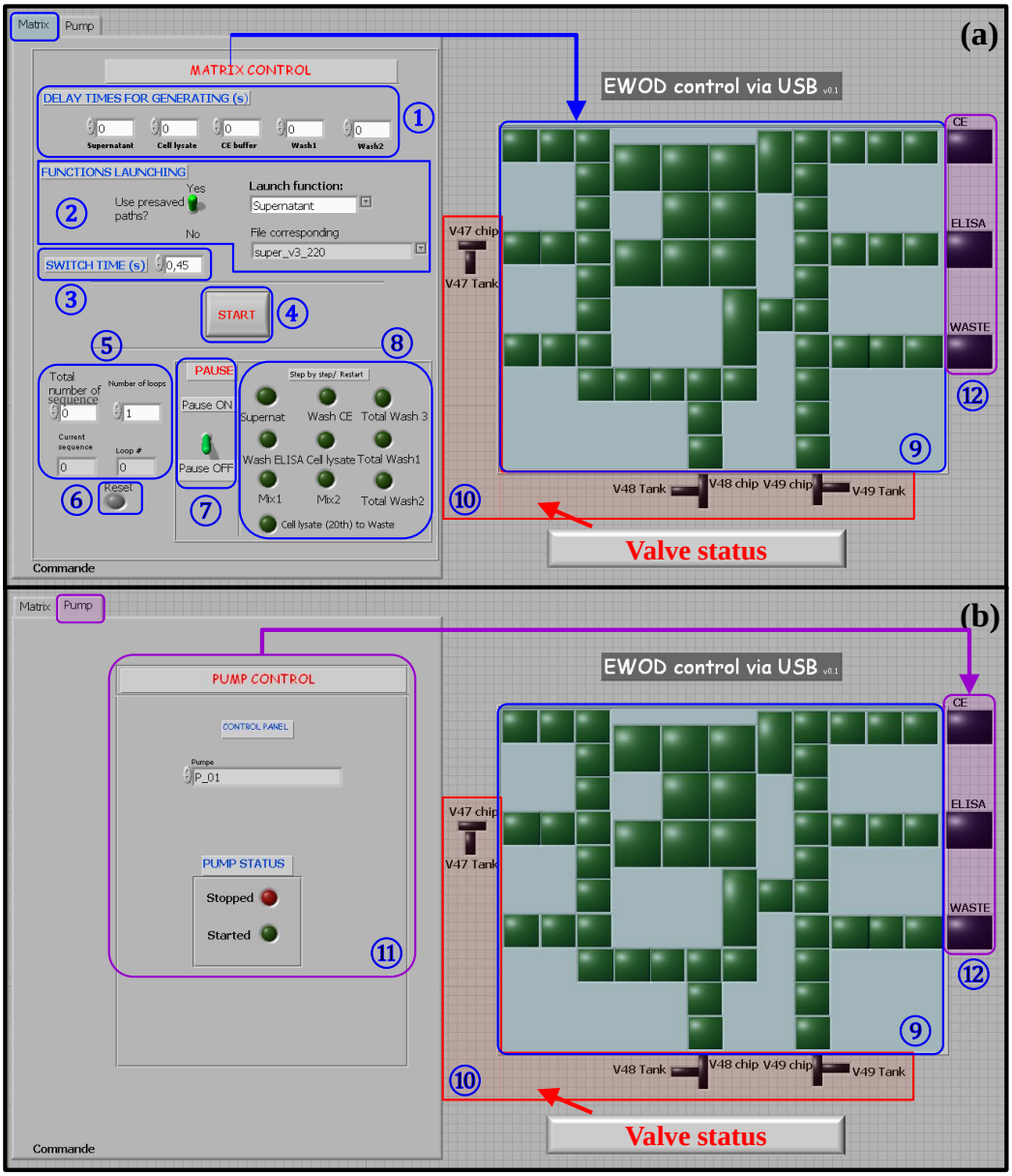

Figure 3.6 LabVIEW control panel: (a) control of EWOD electrodes and three-way valves, and (b) control of the peristaltic pump for delivery. ***(A) Matrix control:*** (1) DELAY TIMES FOR GENERATINGS; (2) FUNCTIONS LAUNCHING; (3) SWITCH TIME(s); (4) START; (5) SEQUENCE STATUS; (6) Reset; (7) PAUSE; (8) Step by step/Restart; (9) Electrode matrix. ***(B) The three-way valves (V47, V48, and V49) status:*** (10) showing the fluid loading to the inlets of chip or closing the gate to allow the fluid go back to tanks. ***(C) Pump control:*** (11) PUMP CONTROL; (12) LEDs: corresponding to outlet channels.

3.3.4. Results

3.3.4.1. Tests on different liquid sample

Table 3.3 Movement feasibility of various liquid samples at various dilution with DI-water ('1X': no dilution; '10X': (1:10 v/v); '100X': (1:100 v/v)). 'OK', 'Fail', and '-' respectively correspond to movable, unmovable or electrolysis, and undone experiments.) The concentration is the actual cell concentration of the sample when the sample is withdrawn and it can be used as characterization due to the change of supernatant composition during yeast fermentation.

#	Type	Cultivation Time/pH	Cultivation Medium / Buffer	Concentration (cfu/mL)	Results		
					1X	10X	100X
S-1	Supernatant	3[h]at25[°C]	YPD	1.00E+006	-	Fail	OK
S-2	Supernatant	8[h]at25[°C]	YPD	8.70E+006	-	Fail	OK
S-3	Supernatant	24[h]at25[°C]	YPD	1.48E+008	-	Fail	OK
C-1	Cell (cultivation in YPD) re-suspended in buffer	24[h]at25[°C]	PBS (0.01M)	1.48E+008	-	Fail	OK
S-4	Supernatant	3[h]at25[°C]	YNB	1.02E+006	Fail	OK	-
S-5	Supernatant	8[h]at25[°C]	YNB	5.08E+006	Fail	OK	OK
S-6	Supernatant	24[h]at25[°C]	YNB	6.00E+007	Fail	OK	OK
C-2	Cell (cultivation in YNB) re-suspended in buffer	24[h]at25[°C]	PBS (0.01M)	6.00E+007	Fail	Fail	OK
CL-1	Cell lysate	0.5[h]at90[°C]	DI water	1.00E+006	OK	-	-
CL-2	Cell lysate	0.5[h]at90[°C]	DI water	1.00E+007	OK	-	-
CL-3	Cell lysate	0.5[h]at90[°C]	PBS (0.0001M)	1.00E+006	OK	-	-
CL-4	Cell lysate	0.5[h]at90[°C]	PBS (0.0001M)	1.00E+007	OK	-	-
CB-1	CE buffer	pH=9	Ammonium formate	10 mM	OK	-	-
B-1	YNB	-	-	Pure	Fail	OK	OK
M-1	PBS	-	-	Pure (0.01M)	Fail	Fail	OK

Our first objective was to define the range of liquid samples that can be manipulated within our sample preparation unit. These liquid samples are: supernatant, cell re-suspended in buffer, cell lysate, and CE-buffer solutions. The experiments (summarized in **Table 3.3**) are performed under an applied voltage of $142V_{rms}$ which is switched from one electrode to the next one every 0.45 second. A liquid droplet is considered movable when it can be reversibly and repeatedly transported across three or more electrodes [5]. The 'movable' sample means that we succeeded in displacing the droplet 100 times back and forth on three successive electrodes. For the unmovable samples, we increased the voltage to actuate the droplet and three main cases were observed: (a) the droplet was stuck on the surface (no displacement possible), (b) the dielectric layer immediately experiences breakdown, or (c) the droplet can be displaced only during a few back and forth cycles and then electrolysis occurs. For (a) case, the high concentration of bio-species in the droplet made the droplet partially pinning on the

hydrophobic surface. For (b) and (c) cases, charges accumulate at the hydrophobic surface after several operations as the actuation voltage increase, and eventually the dielectric layer experiences catastrophic breakdown.

As shown in **Table 3.3**, for all supernatant solutions either cultivated in YPD or YNB medium, it is not possible to displace them without dilution. It is observed that the dilution rate of movable supernatant solutions in YPD and YNB are 100-fold and 10-fold, respectively. Thus, the feasibility range of supernatant solution cultivated in YNB is larger than the one cultivated in YPD medium. For cells re-suspended in pure phosphate buffered saline (PBS) buffer, whatever the original cultivation medium in YPD (#C-1) or YNB (#C-2), the successful displacement concentration is in 100-fold dilution. We have also tested pure YNB medium and PBS (0.01M) buffer solutions. It is observed that the dilution rate of movable YNB (#B-1) and PBS (#M-1) are 10-fold and 100-fold, respectively. Beside, we have observed that all cell lysate solutions and CE-buffer solution are movable.

Furthermore, the droplet displacement in the sample preparation unit has been quantified by two different tests, illustrated in **Table 3.4**. Both tests are achieved twice. In Test 1, 100 motion loops (back and forth displacement on three electrodes) of the supernatant samples for three concentrations of cells in the initial cultivation (#S-4, S-5, and S-6). Between each sample (three in total), we have performed a washing step by displacing a DI-water droplet on the three electrodes (10 motion loops). Thus, we can speculate that after the long duration use of the three test electrodes (100 back and forth): (a) there are few bio-fouling on the surface of the device or (b) DI-water washing in 10 motion loops is effective when there are a small amount of sample deposition on the surface. Further, in Test 2, these three supernatant samples (#S-4, S-5 and S-6) are displaced again (100 times back and forth motion), but without washing steps between each experience. We observed that the device is still workable after finishing all the three supernatant sample displacement with 100 back and forth. Thus, we decided to continue displacing the highest concentration sample (#S-6) with 100 back and forth and focus on finding the lifetime of the device. After 80 additional motion loops (380 in total), it is observed that the movement of the droplet becomes sluggish and from time to time

we can observe momentaneous pinning of the droplet. It is believed that the surface of the device is polluted. Characterization of the surface using laser desorption-ionization mass spectrometry was planned to clarify this result. However, due to lack of time, it was not performed. After that, we have displaced a DI-water droplet (10 motion loops) on the three test electrodes. For the first 5 loops, the movement of the DI-water droplet was slugging and we observed momentaneous pinning. After the first 5 loops, the movement was again normal. In order to show that the DI-water droplet performed an efficient cleaning of the three test electrodes, we have performed again 100 motion loops of sample (#S-6). As shown in **Table 3.4**, this last test was successful. The results show that DI-water can be used to wash the surface pollution and that 10 motion loops are enough to wash the electrodes.

Table 3.4 Two different tests based on movable solution concentrations. '10X': (1:10 v/v). 'OK' corresponds to movable.

#	Test 1				Test 2			
	Sample	Concentration (cfu/mL)	Loops	Results 10X	Sample	Concentration (cfu/mL)	Loops	Results 10X
1	S-4	1.02E+006	100	OK	S-4	1.02E+006	100	OK
2	DI-water	-	10	OK	S-5	5.08E+006	100	OK
3	S-5	5.08E+006	100	OK	S-6	6.00E+007	100	OK
4	DI-water	-	10	OK	S-6	6.00E+007	100	In the final 20 loops: sluggish movement
5	S-6	6.00E+007	100	OK	DI-water	-	10	In the first 5 loops: sluggish movement; In the rest loops: OK
6	DI-water	-	10	OK	S-6	6.00E+007	100	OK

In brief, the bio-contents of the bulk solution and diluted rate of the droplets are the key parameters to decide whether they are movable on the sample preparation unit. Too high concentration of biospecies or medium/buffer bulk solution in the droplet made the droplet displacement difficult or even impossible. The feasibility range of YNB is larger than the one of YPD. Thus, in the final on-line NANOBE integrated system tests, YNB is selected as the culture medium and the diluted rate of supernatant in sampling/filtration module is set as 10-fold. Also, the washing step by using DI-water is identified to be effective in 10 motion loops. Thus, in the NANOBE integrated system, DI-water is used to clean the sample preparation unit.

3.3.4.2. Fluid Operations

a) Droplet formation and displacement

Because the total volume sent to ELISA module (16µL) exceeds the outlet-channel capability of the sample preparation unit (4µL), it has to be divided into 4 groups (4µL/group). Each group is divided in 4 droplets of 1 µL. Each droplet follows the same path on the electrodes matrix. **Figure 3.7** illustrates the path followed by four of these droplets during the loading process. During the first 12 sequences, the supernatant sample fluid is loaded from the inlet channel. At the 12th sequence, the first electrode is actuated and the 1st droplet can be generated (shown in **Figure 3.7(a)**). Successive activation of one electrode to the adjacent one manipulates the 1st droplet along the direction of the activated electrodes. Similar, the 2nd droplet is formatted and then merged with the 1st one (shown in **Figure 3.7(d-e)**). Later, 3rd-4th droplet assembles with the 1st-2nd droplet within the outlet channels, and finally the group of four droplets is exported from the outlets in continuous format (shown in **Figure 3.7(j)**).

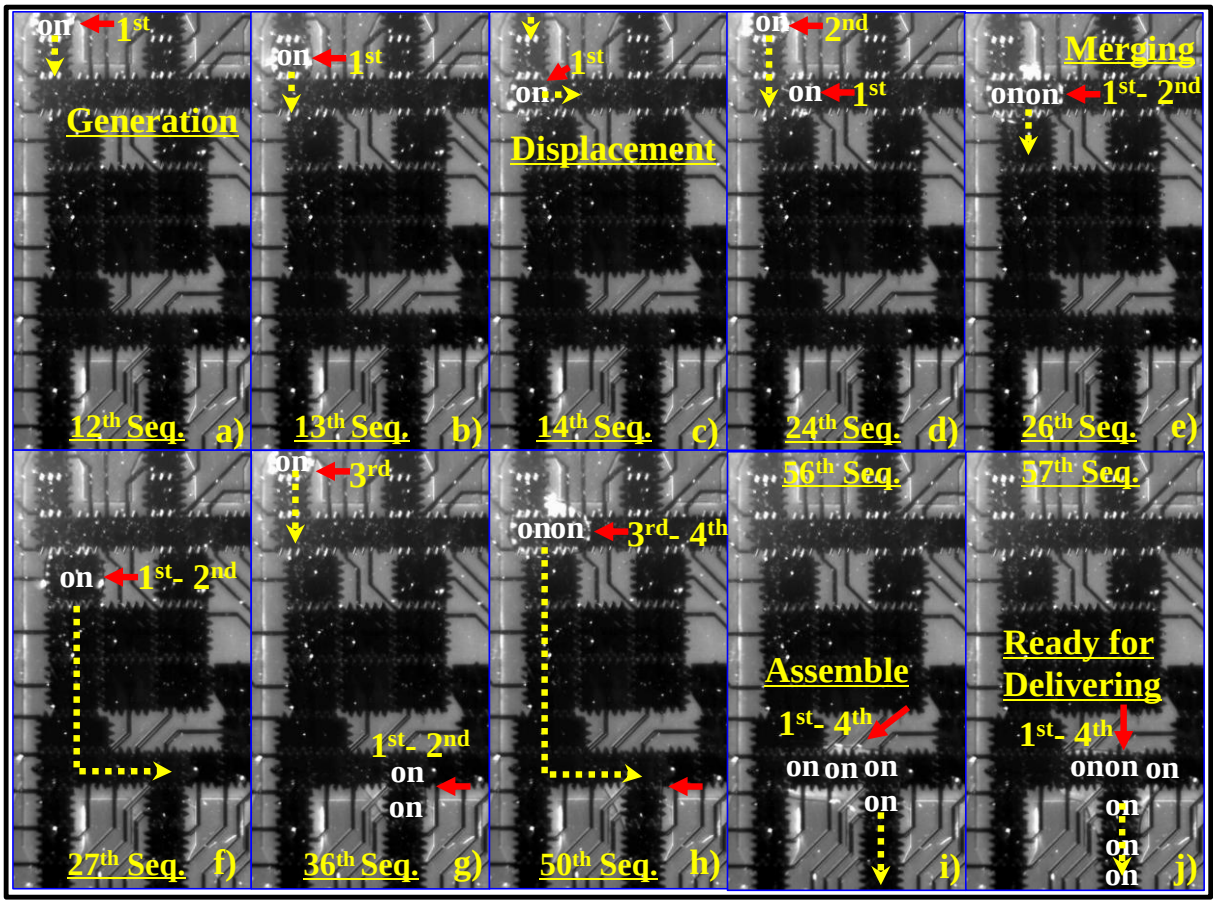

Figure 3.7 Sequential snapshots from the video records showing the operation processing of the supernatant (#S-4, shown in **Table 3.3**) loading.

With a similar procedure, 16µL of cell lysate are processed and exported to ELISA module (**Figure 3.8**).

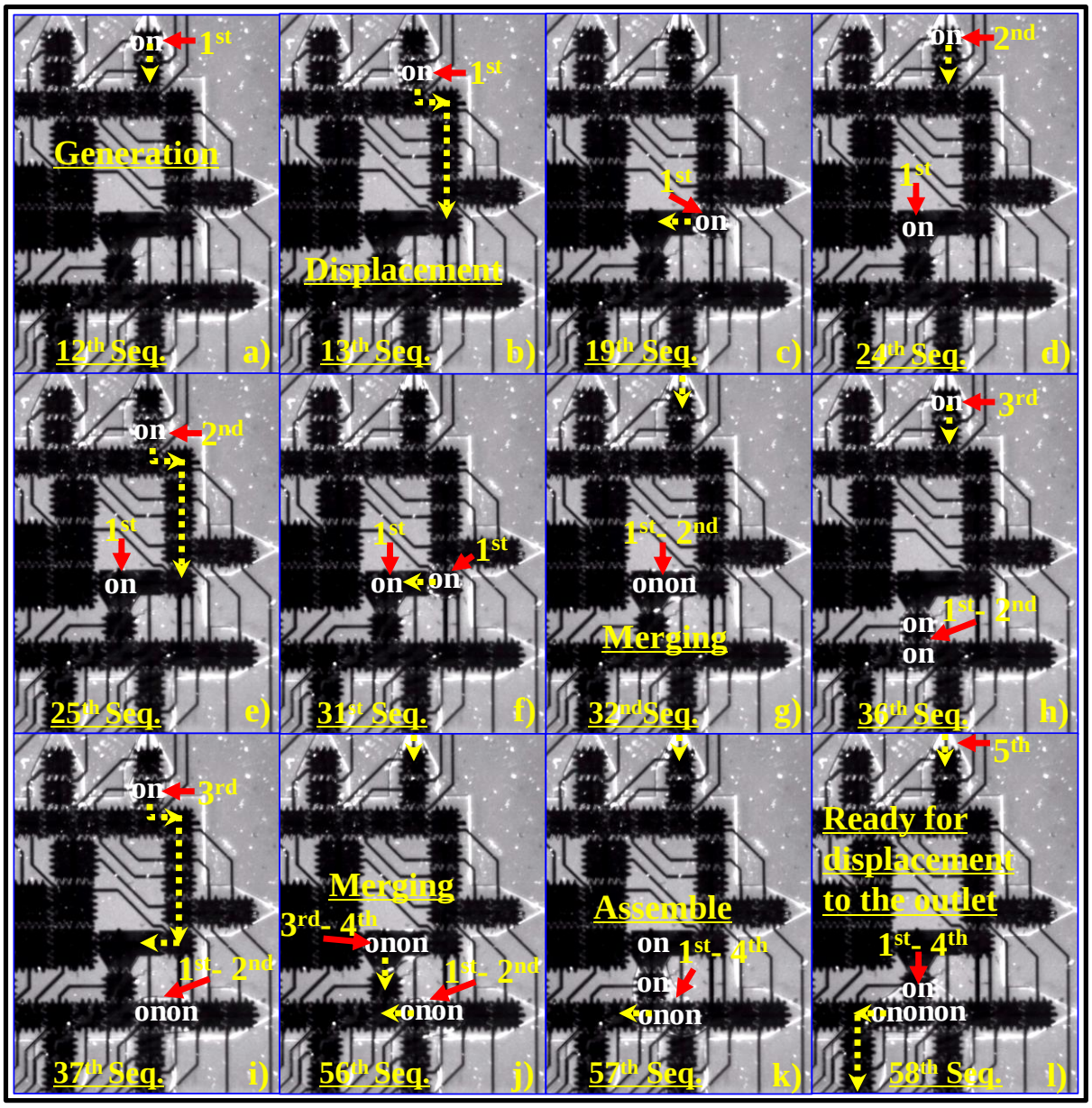

Figure 3.8 Sequential snapshots from the video records showing the operation processing of the cell lysate (#CL-1, shown in **Table 3.3**) loading.

b) Delivery

When the delivery program is triggered, EWOD force drives the sample fluid to become in contact with the tip of the capillary. The samples are then exported outside the sample preparation unit thanks to the activation of the external peristaltic pump. During this procedure, the four last electrodes in the outlet channel are deactivated one by one, in order to

prevent the breakdown of the dielectric at high voltage. We have tested different flow rate of the peristaltic pump, 24µL/min, 40µL/min and 100µL/min. For all the three flow rates, the time-step of the LabVIEW program (T_s) is set to 0.5 second. 1µL of sample can be successfully exported in 5 sequence steps (2.5 second) at the flow rate of 24µL/min, in 3 sequence steps (1.5 second) at the flow rate of 40µL/min, and within 2 sequence steps (1 second) at the flow rate of 100µL/min. **Figure 3.9** shows one of the successful delivery operations (at 24µL/min). During every five sequences, one droplet of 1µL can be exported. The total 4 droplets are exported in 10 second (20 sequences).

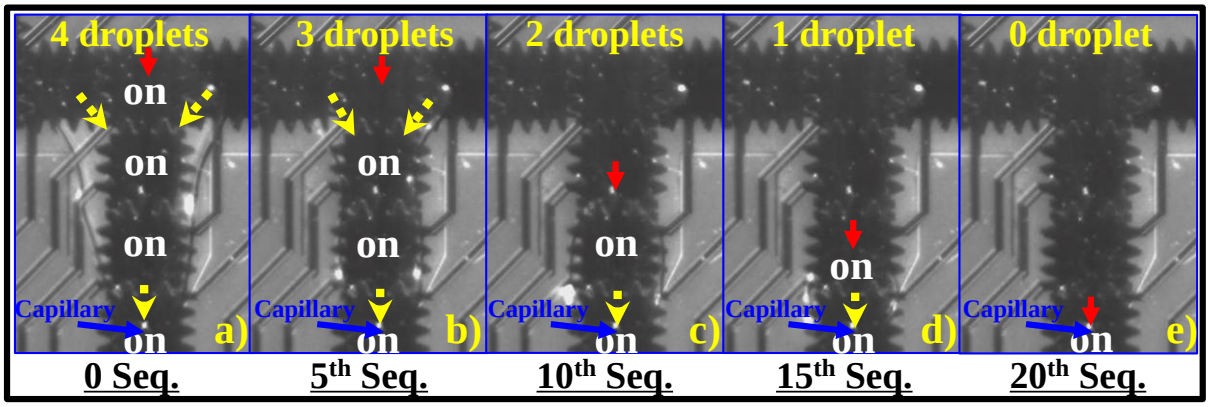

Figure 3.9 Sequential snapshots from the video records showing the delivery operation at 24µL/min at the end of the processing of the supernatant sample (the procedure is similar for the cell lysate sample).

c) Merging and mixing

Figure 3.10 presents the Mix1 procedure. One droplet of CE-buffer is formatted and then merged with the prepared supernatant droplet. Merging of the two droplets is a straightforward operation, whereas two aqueous droplets are displaced towards the same electrode and their coalescence is immediate. Then, the merged droplet is moved in a back and forth motion on a linear row of electrodes. After that, the mixture is transported to the outlet of CE and exported.

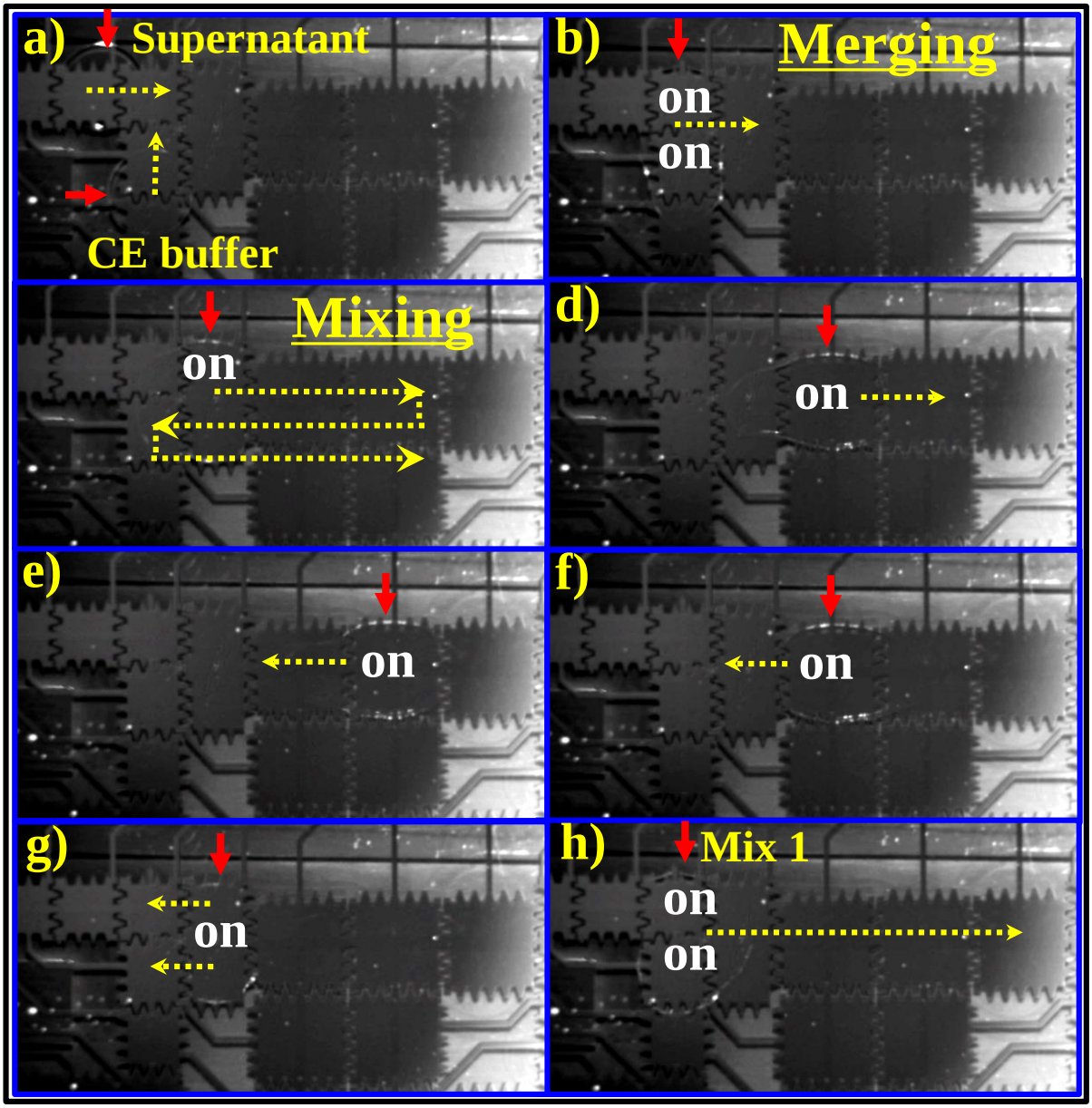

Figure 3.10 Sequential snapshots from the video records showing the Mix1 operation processing (No.6) of the cell lysate sample (#CL-1, shown in **Table 3.3**) mixed with the CE-buffer sample (#CB-1, shown in **Table 3.3**). a) Cell lysate is pre-loaded, then CE-buffer is loaded, b) Both droplets (1µL) are merged, c) to g) mix both liquids on larger electrodes, h) repeat set (b-e) and then ready to delivery to the outlet. Similar manipulations present in Mix2 operation processing.

3.3.5. Conclusion

The sample preparation unit was tested with real samples including cell lysate (with different cell concentration), supernatants (for different cell cultures), and the buffer used for CE analysis. The results confirmed that it is possible to handle all the types of fluids needed for final on-line integration test. Furthermore, the results of off-line validation experiments

confirm that the sample preparation unit is able to take in the samples (20µL of supernatant, 17µL of cell lysate and 2µL of CE-buffer) from reservoir at a flow rate of 10µL/min and divide the samples into several droplets (1µL). The formative droplets are properly transported by EWOD force along the predefined path under the LabVIEW programmed operating sequences. All operations can be done within 7 minutes in agreement with the operation protocol. Based on these experiment results, the applicability of the sample preparation unit is demonstrated and the final on-line test in the NANOBE integrated system can now be achieved.

3.4. On-line mode: experimental validation of the NANOBE system

The on-line mode tests of the integrated NANOBE system were done at VTT in collaboration with other partners. Our work is 'digital' preconditioning of sample liquids and well-controlled navigation of multiple sample droplets to the different analysis modules. Matching the flow conditions between the sample preparation unit and adjacent modules, and the interfaces managing are important for the integrated system to be successfully operated. Thus, prior to the whole integrated system test, it is necessary to develop the hardware coupling interfaces between the sample preparation unit and the adjacent modules.

3.4.1. Coupling with adjacent modules

3.4.1.1. Coupling with the Sampling/filtration module

The hardware development for the interface between the sampling/filtration module and the sample preparation unit was started without an additional peristaltic pump. However, the glass capillary (with the inner diameter of 75µm) connected between these two modules adds extremely high fluidic resistance to the entire fluidic system. Unfortunately, this aspect was not taken into account at the beginning of the project. As a result, a peristaltic pump (named M) is not able to overcome the fluidic resistance between the sampling/filtration module and the sample preparation unit. Therefore, an additional peristaltic pump is added to increase the

driving force at this interface, shown in **Figure 3.11**.

After, further adjustments in the timing of three-way valve and pump control, the sample supernatant can be reliably transported to the sample preparation unit. The supernatant volume is changed from the originally planned 17µL to 20µL. This change is imposed by the sampling/filtration module and its accuracy in volume definition. During this coupling test, it is observed that the timing of the supernatant sample from the outlet of the sampling/filtration module to the end of IN1 of the sample preparation unit (i.e., the delay time of IN1) is varied ±10 seconds. This variation is due to the compressibility of air plug surrounding the sample fluid. The accuracy of delay time setting is important for achieving automatic operation. Unfortunately, at the beginning of the project, this air plug was not taken into account in the off-line experimental mode where the sample is a continuous fluid filling the inlet capillaries. As a result, the arrival of the sample fluid front is monitored with eye and the operation of 'Supernatant' is trigged manually.

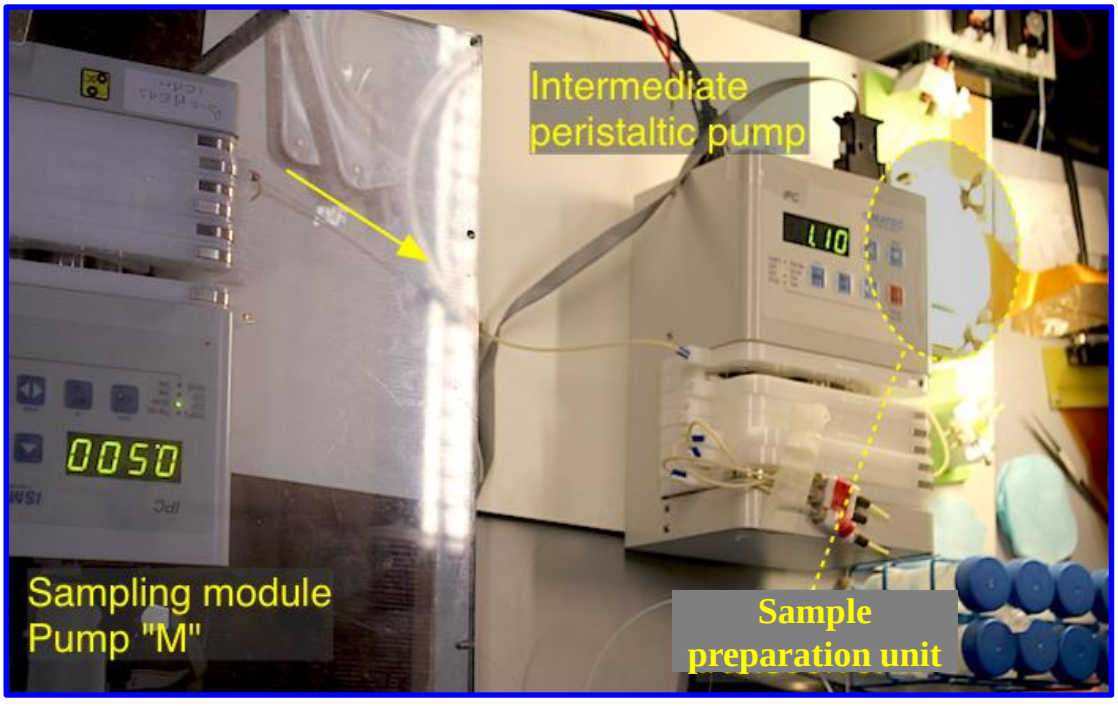

Figure 3.11 Physical interfaces between the sampling/filtration module and the sample preparation unit (*i.e.*, sample preparation unit) with an additional intermediate peristaltic pump.

Five analysis cycles are carried out for the coupling test. **Table 3.5** shows a summary of the interface function tests. The result shows that it is necessary to increase the theoretical

dilution ratio to 1:50 in the sampling/filtration module to be able to displace the droplets in the sample preparation unit electrodes. However, it was not possible to test if the initial liquid samples were the same as those tested for the off-line analysis neither if the dilution process performed in the sampling/filtration unit was enough accurate. Indeed, we did the off-line test (No.5), where the sample is manually taken from bioreactor and precisely diluted in 10-fold. The result of No.5 test confirmed that 10-fold diluted supernatant in YNB culture is feasibility and stabilization.

Table 3.5 Summary of tests between the sample/filtration module and the sample preparation unit.

#	Theoretical dilution ratio in Sampling/filtration module		Results
1	On-line mode	1:10	No: extremely viscous sample
2		1:20	No: sticky on the electrode
3		1:40	No: electric lysis existed at the end of droplet formation
4		1:50	Yes
#	**Real dilution ratio in Sampling/filtration module**		**Results**
5	Off-line mode	1:10	Yes: for several cycles

3.4.1.2. Coupling with Cell lysis module

The physical architecture of the integrated system components makes the length of the glass capillary between the sampling/filtration module and the cell lysis chip very long. Due to the presence of the other modules, it was not possible to reduce the distance between these two modules. The length of the glass capillary induced a significant increase in the pressure resistance between these two modules. The three-way valves used for flow switching in the sampling/filtration module are operated up to 1 bar. However, it is observed that a minimum pressure of 1 bar is required to drive continuous liquid flow into the cell lysis chip. Considering the fact that the sample is required to be transported as a plug embedded in air to avoid unwanted dilution and cross-contamination, it is clear that much higher pressure is required to successfully drive the cell sample from the sampling/filtration module into the cell lysis chip. Thus, it was decided that the cell lysis chip is not included in the online monitoring system for the final integrated testing.

3.4.1.3. Coupling with ELISA module

This section describes the coupling between the sample preparation unit and the micro-ELISA module. The coupled system is illustrated in **Figure 3.12**, where a peristaltic pump extracts the sample from the EWOD sample preparation unit and pumps it through a T-junction glass capillary maintained on a moving stage to ELISA module.

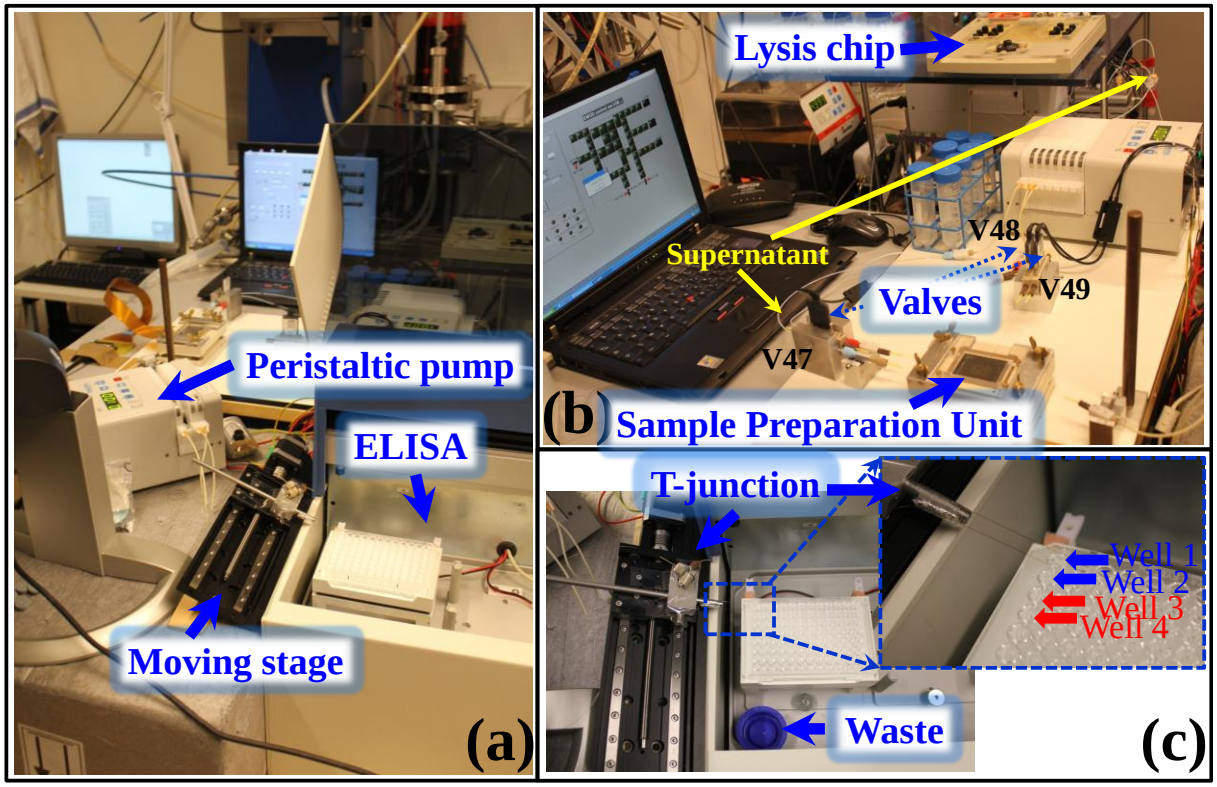

Figure 3.12 Picture of part of the online bioprocess monitoring system: (a) showing the interface between the sample preparation unit and ELISA modules, (b) the sample preparation unit with the three-way valves and lysis chip, (c) the moving stage and ELISA ImmuSpeed™ apparatus and the T-junction capillary ready to dispense in the collector.

The experiments are schematically illustrated in **Figure 3.13**. In graph (a), when ImmuSpeed™ is ready, the protocol begins in ImmuSpeed™-Software (developed by DiagnoSwiss) with the calibration of the assays. Then the master LabVIEW program (designed by IMTEK) sends a request to set the T-junction capillary. The moving stage allows moving the T-junction capillary above the well 1&2 of the collector ready for the dispensing of the first 2 samples (shown in graph (b)). Then the samples are collected in the well 1&2 of

the first row of a microtiter-plate of the ImmuSpeed™ prototype (shown in graph (c-e)). After finishing the dispensing, the T-junction capillary is placed back in the waste position (shown in graph (f)), which aims to prevent any collision with the pipetting heads of the robotic arm of ImmuSpeed™ (shown in graph (g)). Then; the detection of the first two samples is carried out in the ImmuSpeed™ system.

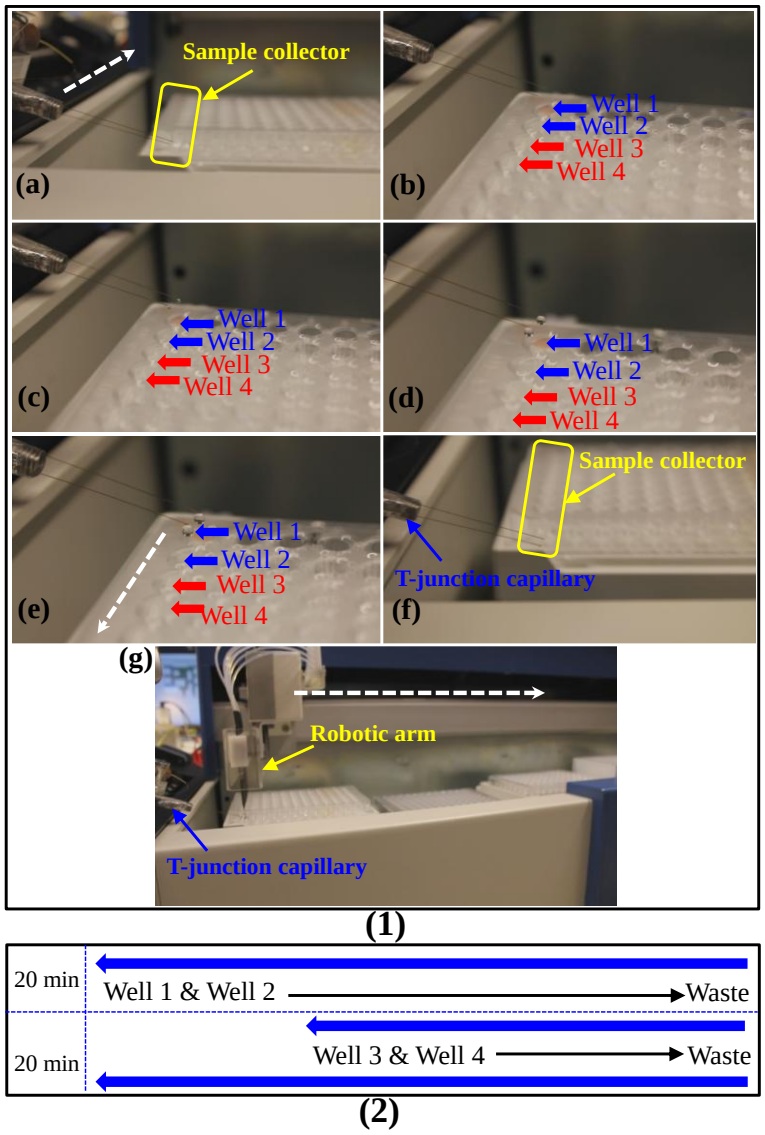

Figure 3.13 (1)Sequential snapshots from the video records showing the delivery of analytes from sample preparation to ELISA module in the first 20 minutes: (a) the original position (above the waste) of T-junction capillary, (b) T-junction capillary is moved to the target well 1&2 position of sample collector, (c)-(e) analyses are delivered and fell down to well 1&2 when the size of both two droplets are about 8μL, (f) after finishing the delivery, T-junction capillary is placed back above the waste, (g) the samples is transferred by the robotic head of the ImmuSpeed™ prototype. After 20 minutes, the next two samples are displaced into the well 3&4. (2) Schematic diagram of the movements of the stage for the filling of the 4 samples into collector wells in one analysis cycle (40 minutes) in ELISA module (Courtesy: Frédéric Reymond, Diagnoswiss and Junichi Miwa, IMTEK).

After the detection, the ImmuSpeed^{TM} system remains waiting until the dispensing of the next two samples in the well 3&4 of the collector. Then, the next two samples are then analyzed as the first two samples. This coupling test demonstrates that the sample preparation unit can be successfully coupled to the ELISA ImmuSpeed^{TM} platform.

3.4.1.4. Coupling with CE-MS module

In the original structure of NANOBE integrated system, ammonium acetate was planned to be used as the background electrolyte solution (BGE) for CE-MS module. However, this CE-buffer can clog (crystal formation) the CE chip and these crystals block the liquid flow to the MS. Thus, this CE-buffer is required to be carefully chosen to prevent this clogging. As a result, the CE-buffer was then changed to ammonium formate. However, the development was not completely ready before on-line analyses started. Thus, it was decided that CE-buffer was not added for CE-MS module for the final integrated testing.

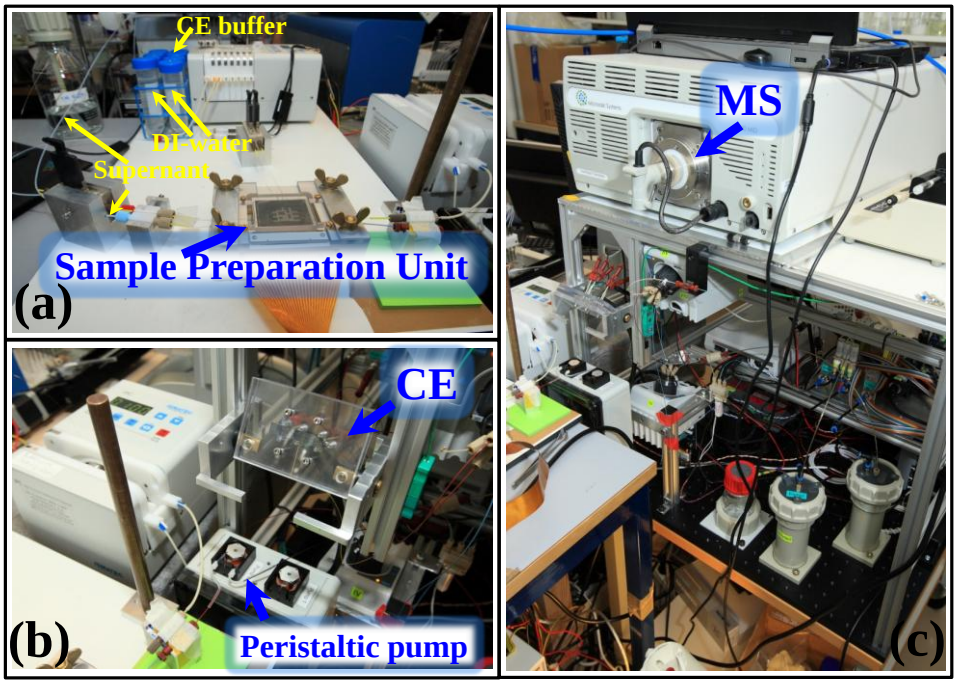

Figure 3.14 Picture of part of the online bioprocess monitoring system showing: (a) the sample preparation unit, the capillary providing supernatant from IBA sampling/filtration module and delivering the prepared sample trough the peristaltic pump (on right of the figure) to the capillary electrophoresis (CE) chip developed by VTT, b) the CE chip, c) the coupling between the CE chip and the mass spectrometer (MS) developed by MICROSAIC (Courtesy: Juha-Pekka Pitkänen, VTT and Peter Edwards, Microsaic).

The coupling system is illustrated in **Figure 3.14**, where the glass capillary at the outlet of the sample preparation unit is connected to the peristaltic pump via a short piece of polyether ether ketone (PEEK) tubing. Similar to the interface between the sampling/filtration module and the sample preparation unit, compressibility of air surrounding the sample plug introduces variation on the delay time needed to carry the sample from the sample preparation unit to the CE chip. Thus, the software triggering the sample preparation unit and the CE-MS module are performed manually. At the sample preparation unit, the arrival of the sample liquid front is monitored with the eye and the start control signal is initiated by hand. At the CE-MS module, the control software is triggered in the same way by hand when the sample droplet exported from the sample preparation unit enters into the tubing of the peristaltic pump.

For preliminary tests, the sample preparation unit is not yet connected to the bioreactor, the MS equipment is not yet connected to CE chip, and the supernatant samples have been replaced by DI-water and 10-fold diluted YNB solution. DI-water sample and 10-fold diluted YNB sample are alternately transported from EWOD sample preparation unit into the CE chip (*i.e.*, 4µL of DI-water, 4µL of 10-fold diluted YNB, 4µL of DI-water, 4µL of 10-fold diluted YNB, etc.). The validation of the coupling test was performed by recording the change of the conductivity measured by the CE conductivity detector when the two different samples were flowing through this detector. This test was successful and we have considered that the sample preparation unit and the CE chip can indeed be successfully connected.

3.4.2. Full integration test

Based on the results of the coupling tests, the complete NANOBE system has to be modified, as illustrated in **Figure 3.15**. As explained above, the high-pressure resistance of the silica capillary connections of the cell lysis chip and the limited pressure tolerance of the three-way valves used for flow switching prevent the use of the cell lysis chip in the online monitoring system for the final testing. Thus, the operations (#5, #6, and #7 in **Table 3.2**) are canceled. Moreover, according to the further modification of CE-MS module, the samples are not mixed with CE-buffer. Thus, the operation (#2 in **Table 3.2**) is also redundant. Overall,

the operations consist of: a) dispensing the supernatant sample to the CE-MS module and the ELISA module, and b) washing the electrodes and the outlet channels. For the operation of washing the surface of electrodes and the outlet channels, we have kept the operations (#8, #9, and #10 in **Table 3.2**).

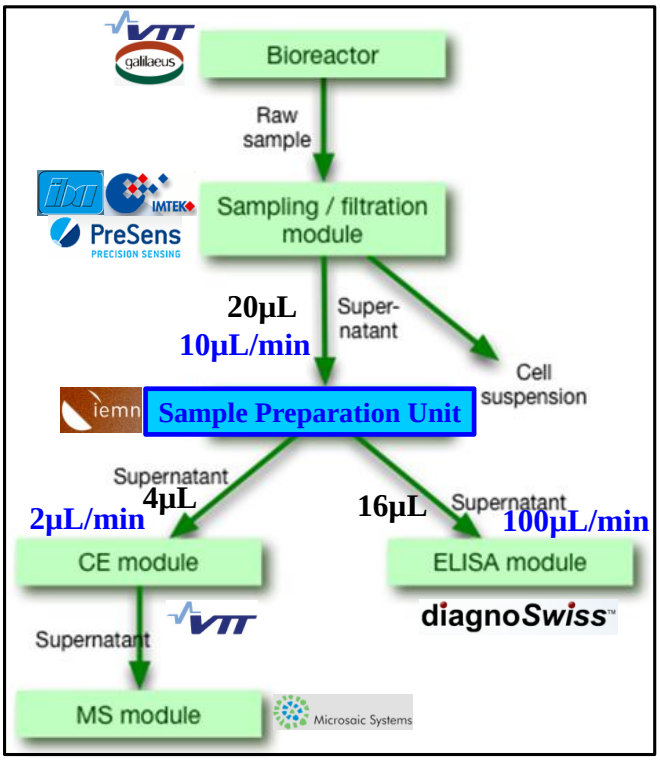

Figure 3.15 Configuration of the NANOBE integrated system.

For the operation of dispensing the supernatant sample to the CE-MS module and the ELISA module, it has been modified (shown in **Figure 3.16**). The dispensing operation is carried out in 260 sequences (117 seconds), a) the beginning 16µL send to ELISA module, and b) the rest 4µL send to CE-MS module. The washing procedure is simplified by repeating the supernatant loading procedure using DI-water. The modified analysis cycle was that: a) the sample was delivered to the sample preparation unit approximately 45mintes after automated sampling/filtration, b) the ELISA measurement and CE-MS analysis of the supernatant would finish at 60 minutes and 100 minutes after sampling/filtration, respectively.

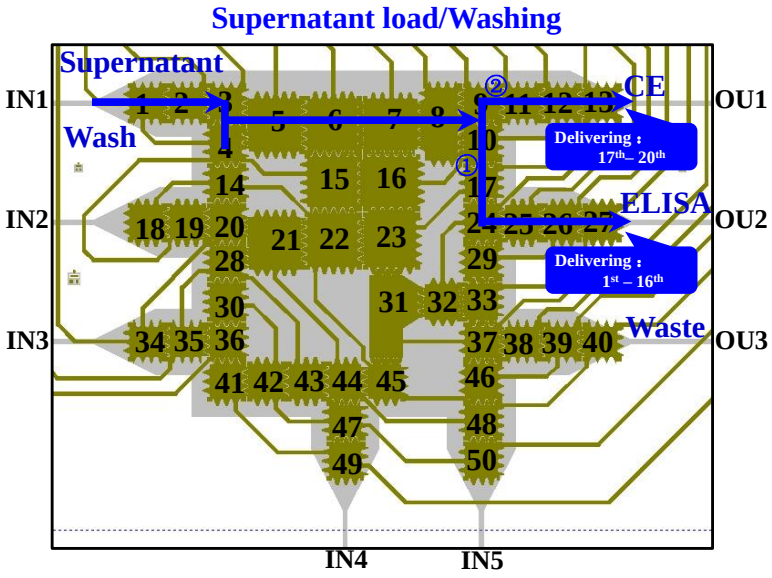

Figure 3.16 Modified operation processes.

Table 3.6 Summary of the integrated system function tests.

#	The success of different module operations				
	Sampling/filtration module (theoretical setting parameter 1:50)	Sample Preparation Unit	ELISA measurement	CE-MS module	
				CE separation	MS detection
1	Yes	Yes	No: software failure	Yes	No: clogged
2	Yes	No: electric lysis existed at the end of droplet formation	No: no sample	Yes	Yes
3	**Yes**	**Yes**	**Yes**	**Yes**	**Yes**
4	No: process time prolonged	No: extremely viscous sample	No: no sample	No: extremely viscous sample	No: no sample

In total, four analysis cycles have been carried out with the integrated system. The process steps in one analysis cycle includes: (a) preparation in the bioreactor, (b) sampling, splitting, transport and filtration in the sampling/filtration module, (c) sample preparation operations in the sample preparation unit, (d) analysis and detection in ELISA module and CE-MS module, and (e) the system washing. **Table 3.6** shows a summary of the integrated system function tests for each cycle.

There are two cycles (No.1 and No.3) in which the sample is successfully transported from bioreactor-sampling/filtration module to sample preparation unit and then sends to ELISA module and CE-MS module. However, in cycle 1, the sample reaches the inlet of the mass spectrometer but doesn't reach the detector due to clogging of the vacuum interface. The ELISA module also fails to proceed beyond the sample/bead conjugate incubation due to

software failure. Only No.3 cycle succeeds in: a) obtaining an electrochemical signal corresponding to an enzymatic reaction in ELISA module, and b) observing by-products in CE-MS analysis.

For the other two cycles (No.2 and No.4), dielectric breakdown and droplets pinning are observed. At the end period of cycle 2, one can observe that several electrodes in the sample preparation unit are damaged. In cycle 4, an unexpected viscous sample is transported from the sampling/filtration module to sample preparation unit in a relative long time. One possible explanation for the failure in these two cycles is that air bubble at one fluidic junction in the sampling/filtration module inducing inaccuracy in the sample dilution. This inaccurate sample dilution in the sampling/filtration modules induces change in conductivity and viscosity of the droplets as well as higher surface pollution. These modifications are known to generate dielectric breakdown and droplets pinning.

In order to determinate and quantify the sample effective resulting dilution rate in the sampling/filtration module, the manually-taken and diluted samples are detected by using ImmuSpeed^{TM} prototype in off-line mode. The manually-taken samples are either undiluted or diluted by DI-water with 10-fold or 20-fold dilution factor. Compared signal values between off-line mode (undiluted, 10-fold diluted, and 20-fold diluted) and on-line mode (No.3), the results suggest that the sample effective dilution rate in the sampling/filtration module is lower than 10-fold (about 7-fold), which is much far from the theoretical setting parameter of 1:50. This lower dilution rate makes the concentration of bio-species in the sample and the viscosity higher, out of the specifications of the sample preparation unit. The deviation of the real resulting dilution rate in sampling/filtration module can explain why we observed electrolysis in the sample preparation unit for the second analysis cycle and extremely viscous sample in the fourth analysis cycle.

Overall, only 2 cycles are successful, where the samples are automated taken from the bioreactor-sampling/filtration module to sample preparation unit and then deliver to ELISA module or CE-MS module. However, it demonstrates that the EWOD-based microfluidic device can be used in an on-line bioprocesses monitory system for sample preparation, from

sampling in a bioreactor to detection and analysis modules.

3.5. Summary

The aim of the NANOBE project is to develop a versatile tool for real-time analyzing of several compounds and biomarker in the bioreactor processes. Two different configurations of the system components are tested, off-line mode and on-line mode.

In off-line mode, the sample preparation unit is tested with real samples including cell lysate (with different cell concentration), supernatants (according to different cell cultures), and the buffer used for CE analysis. The determined movable range of these solutions is wide. Supernatant sample (cultivated in YNB medium) can be moved at a minimum dilution rate of 10-fold. All cell lysate solutions (either re-suspended in PBS (0.000M) or DI-water) can be movable without dilution at the high concentration of $1*10^6$ or $1*10^7$ cfu/mL. Also, the back ground electrolyte solution for CE-MS module (10mM ammonium formate, Ph 9) is possible to manipulate in the sample preparation unit. The results show that the sample preparation unit is able to handle with all the types of fluids needed for final on-line integration test. Furthermore, based on the movable solutions, the fluidic operations (droplet formation, displacement, and delivery) in the sample preparation unit are successfully demonstrated. The sample preparation unit was able to take in the samples (20µL of supernatant, 17µL of cell lysate and 2µL of CE-buffer) from reservoir at a flow rate of 10µL/min and divide the samples into several droplets (1µL). The formative droplets were properly transported by EWOD force along the predefined path under the LabVIEW programmed operations. All operations could be done within 7 minutes in agreement with the specifications. Thus, it is believed that the sample preparation unit can be used in the on-line integrated NANOBE system.

In on-line mode, prior to the whole integrated system tests, we have successfully developed the hardware coupling interfaces between the sample preparation unit and adjacent modules. 4 on-line analysis cycles are carried out with the final integrated system. However, only 2 cycles are successful, where a minute amount of sample with the volume of 20µL is

automated taken from the bioreactor-sampling/filtration module to sample preparation unit and then deliver to ELISA module and CE-MS module. The failure of the sample droplet displacement in the sample preparation unit is due to the deviation of the real resulting dilution rate in sampling/filtration module. However, it is successfully verified the feasibility of the sample preparation unit in: a) 'digital' preconditioning, b) simultaneously handling multiple liquid droplets, and c) well-controlled navigation of multiple samples to the different analysis/detection modules.

References

[1] K. Schügerl, "Progress in monitoring, modeling and control of bioprocesses during the last 20 years", *Journal of Biotechnology*, vol. 85, pp. 149–173, 2001.

[2] F. Clementschitsch and K. Bayer, "Improvement of bioprocess monitoring: development of novel concepts", *Microb Cell Fact*, vol. 5, no. 19, pp. 1–11, 2006.

[3] *http://en.wikipedia.org/wiki/YEPD*. .

[4] *http://openwetware.org/wiki/Composition_of_Yeast_Nitrogen_Base_(YNB)*. .

[5] D. Chatterjee, B. Hetayothin, A. R. Wheeler, D. J. King, and R. L. Garrell, "Droplet-based microfluidics with nonaqueous solvents and solutions", *Lab on a Chip*, vol. 6, pp. 199–206, 2006.

CONCLUSION AND PERSPECTIVE

1. Conclusion

In **Chapter 1** we give an overview of the-state-of-the-art in EWOD-based digital microfluidics. This review aims to illustrate the many efforts to struggle the compatibility of EWOD platform with other required fluidic elements by integrating inlet/outlet interfaces. In the first part, we have dealt with the fundamental theory of electrowetting, analyzed the configurations of EWOD devices (two-plate closed and single-plate open configurations), and stated the basic EWOD fluidic operations (transport, dispensing from on-chip reservoirs, splitting and merging, and mixing). In the second part, we have presented the classification and point out the important of inlet and outlet interface integration on EWOD chip. Based on the integrated level of the interfaces, we have proposed a classification depending on the type of interfaces: 1) inlet interface integration, 2) outlet interface integration, and 3) full interfaces integration. Among them, the full interfaces integration can fully automatically process the required operations from the sample loading to the sample detection. This method allows to reducing dead volume and thus the volume of the sample is reduced. Rather than specialize to a particular application or detection method, the fully integrated sample preparation unit leverages microfluidics designs into multiple applications. It provides a path toward realizing the true lab-on-a-chip.

The purpose of **Chapter 2** is to describe the design, implementation and development of a EWOD-based microfluidics device for sample preparation. We have developed two generation of the device. In our first design, namely AD/DA microfluidic converter, an original fabrication process has been successfully achieved, employing deep reactive ion etching of silicon and low temperature wafer bonding. This technique has ensured that the resulting structures exhibit the excellent adhesive bonding without misalignment and

de-bonding. The simple form of micro-channel paths is made by deep reactive ion etching of silicon. It is believed that the fabrication technology can be used in diverse MEMS applications. To characterize the chip performance, contact angle changes have been measured. After that, we have done preliminary validation tests on EWOD fluid operations. By modification of the thickness of the 2nd SU-8 dielectric layer from 450nm to 1.5µm, we succeeded in avoiding electrolysis due to dielectric breakdown. However, our preliminary device suffers from a key limitation: failure in droplet formation by using analog-to-digital microchannel interfaces.

To address this issue, we have used textured superhydrophobic substrates on top cover plate in our second design. The improvements are as following:

a) Due to the low dynamic contact angle hysteresis of superhydrophobic surface, droplets can be moved at very low actuation potential. This is a very important point since nominal actuation levels should be far from the breakdown voltage. Hence the durability of the chip is increased.

b) A bilayer structure with SU-8 underneath CYTOP layer can reliably prevent dielectric breakdown and does not significantly increase the actuation voltage.

c) A mounting platform have been used for fixing the two plates, replacing the bonded process, facilitates reuse of a given superhydrophobic top plate. Thus, this fixing method economizes the cost and fabrication time.

d) Fundamental fluid operations (droplet formation, transport, merging, and delivery) can be successfully realized.

We have discussed the parameters influencing the droplet formation and the accuracy of the droplet volume. The successful droplet formation depends on the driving voltage and the distance from the end of the inlet channel to the first electrode (*i.e.*, L_1). It is observed that the threshold voltage for successful droplet formation is 162V (6V for the magnitude of voltage in generator). When the distance from the end of the inlet channel to the first electrode (L_1=2.1mm, 2.2mm or 2.3mm) is a little larger than or equals to the size of the electrode (2.2mm), the droplet formation is successful and very reproducible. The volume of the

resulting droplet is impacted by the time-step of the LabVIEW program (T_s) and the loading flow rate of the peristaltic pump (S_P). Indeed, the loading flow rate of the peristaltic pump is not accurate to 10μL/min (prescribed loading flow rate in NANOBE project). It has a small fluctuation scope. We have tested three group values of T_s, 0.35s, 0.45s, and 0.50s. One can observe that when T_s is 0.45s, the average volume of extracted droplets is 1.032μL and the coefficient of variation (CV %) is 6.7%. The volume is the closest value to the design elemental volume (1μL) among these three values. Thus, in the following work, the time-step of the LabVIEW program is set as 0.45s for the loading flow rate of 10μL/min.

Besides, high speed camera is used to observe water droplet transport, which is very useful for the displacement and velocity study of the receding and advancing fronts. It is observed that the PFTS terminated superhydrophobic cover gives much less resistance (0.7°) than the one (13.1°) from CYTOP cover. It can explain the reason why the driving voltage in PFTS cover configuration is lower (142V) than the one (190V) in CYTOP cover configuration.

In **Chapter 3**, the 'Sample Preparation Unit' is validated in NANOBE integrated system for online bioprocesses monitoring. Two different architectures of the NANOBE system components are tested, off-line mode and on-line mode.

In off-line mode, the sample preparation unit is tested with real samples including cell lysate (with different cell concentration), supernatants (according to different cell cultures), and the buffer used for CE analysis. The range of concentration of these solutions for which the droplet can be handled by our EWOD technology is wide. Supernatant sample (cultivated in YNB medium) can be moved at the dilution rate as low as 10-fold. All cell lysate solutions (either re-suspended in PBS (0.0001M) or DI-water) can be moved without dilution at the high concentration of $1*10^6$ or $1*10^7$ cfu/mL. Also, the back ground electrolyte solution for CE-MS module (10mM ammonium formate, Ph 9) can also be manipulated in the sample preparation unit. The results show that the sample preparation unit is able to handle all the types of fluids required for final on-line integration test. Furthermore, based on the movable solutions, the fluidic operations (droplet formation, displacement, and delivery) in the sample

preparation unit are successfully demonstrated. The sample preparation unit is able to take in the samples (20μL of supernatant, 17μL of cell lysate and 2μL of CE-buffer) from reservoir at a flow rate of 10μL/min and divide the samples into several elemental droplets (1μL). The formative droplets are properly transported by EWOD force along the predefined path under the LabVIEW programmed operating sequences. All operations can be done within 7 minutes in agreement with the specifications. Thus, it is believed that the sample preparation unit can be used in the on-line integrated NANOBE system.

In on-line mode, prior to the whole integrated system tests, we have successfully developed the hardware coupling interfaces between the sample preparation unit and adjacent modules. Four on-line analysis cycles have been carried out with the final integrated system. However, the inaccurate sample dilution (around 7-fold dilution) in the sampling/filtration module exceeds the standard movable range of solutions (minimum 10-fold dilution) for the sample preparation unit. Thus, only 2 cycles have been successful, where a minute amount of sample with a volume of 20μL is automated taken from the bioreactor-sampling module to sample preparation unit and then deliver to ELISA module and CE-MS module. However, it is successfully verified the feasibility of the sample preparation unit in: a) 'digital' preconditioning, b) simultaneously handling multiple liquid droplets, and c) well-controlled navigation of multiple samples to the different analysis/detection modules.

2. Future work and perspectives

Future works include two parts, optimization of the sample preparation unit and further development of the integrated NANOBE system.

2.1. Optimization of the sample preparation unit

For the optimization of the sample preparation unit, the work should focus on the following areas:

(1) Integration of superhydrophobic surface treatment on the bottom EWOD platform

In this thesis, the integration of nano-structured superhydrophobic treatment on the top

plate of the EWOD-based sample preparation unit can: a) decrease the force of friction from top plate during droplet displacement and b) improve the device lifetime due to the decreased driven voltage. Also, it achieved the A/D fluidic conversion operation (*i.e.*, droplet formation). The advantages of integration of the superhydrophobic property are obvious. Thus, the optimization should now integrate superhydrophobic surface treatment on the bottom EWOD platform.

(2) Integration a feedback monitoring system to automatic trigger the LabVIEW program

The software triggering of the sample preparation unit is performed manually. The arrival of the sample liquid front is monitored with the eye and the start control signal is initiated by hand. Thus, the optimization should also integrate a feedback monitoring system to automatically trigger the LabVIEW control program.

(3) Quantization analysis of the DI-water washing efficiency on the surface

The tests to validate the washing efficiency of DI-water have been done. The results show that DI-water can be used to wash the surface pollution and a minimum of 10 motion loops are necessary. However, the efficiency of the DI-water washing is not qualitatively analyzed. Thus, the optimization should quantify the effects the DI-water washing efficiency.

2.2. Further development of the integrated NANOBE system

Considering that the dilution ratio of the supernatant sample in the sampling module is yet to be quantitatively evaluated, the outcome is encouraging for further development of the system. Improvements in robustness and accuracy of sample handling are keys for achieving constant operation for online monitoring over the full duration of fermentations. Besides, it is important to develop the NANOBE system so that it can cope with different analytes, different cell types and different cultivation conditions.

APPENDIX

Content

A.1. The controllable droplet volume

The controllable volume of the drop is determined by the size of standard electrode (2.1mm*2.1mm). The minimum volume is 0.69μL (illustrated in **Figure 1(1)**), where the radius of the droplet sandwiched between two plates (R) equals to half of the width of the square electrode (e). Below this value, the droplet cannot overlap the adjacent electrodes so that the EWOD device is out-of-work. When the droplet just covers the whole electrode, the radius of the droplet (R) equals to $^{e}/_{\sqrt{2}}$. At this state, the volume of droplet is 1.39μL (illustrated in **Figure 1(3)**). The target volume (1μL) in our work (illustrated in **Figure 1(2)**) is between these two states, where the radius of the droplet (R) are between $^{e}/_{2}$ and $^{e}/_{\sqrt{2}}$.

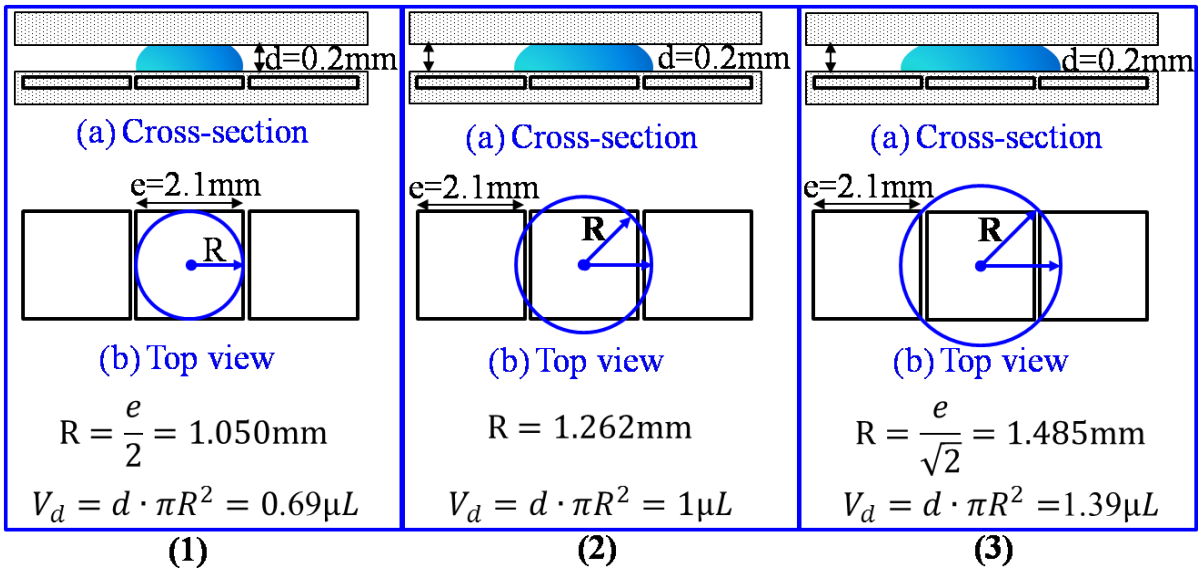

Figure 1 The controllable volume of drop determined by the size of standard electrode: (1) the minimum volume, (2) the targeted elemental volume (1μL), and (3) the volume when the droplet just covers the whole electrode. R, d, e are the radius of the droplet sandwiched between two plates, the thickness between two plates, and the square electrode width, respectively.

A.2. Formation Mechanism of silicon nanostructures (SiNSs)

In our work, the method to prepare artificial superhydrophobic surface is referred to the work done by Peng et al. [1][2] and the work done by Piret et al. [3]. The method is eletroless metal deposition (EMD) on silicon from HF/$AgNO_3$. The fabrication process consists of: a) obtaining silicon nanostructures (SiNSs) of different lengths and arrangements by galvanic

displacement reaction of crystalline silicon in $HF/AgNO_3$ aqueous solution, b) chemical dissolution of the silver structures in HNO_3/HCL aqueous solution at room temperature, c) covering the prepared-SiNSs by a thin silicon oxide layer after exposure to ambient conditions, and d) chemically modifying the SiNSs surface with an octadecyltrichlorosilane (OTS) or perfluorodecyl-trichlorosilane (PFTS) layer. Finally, the OTS- or PFTS-terminated SiNSs display a superhydrophobic behavior (CA~160°).

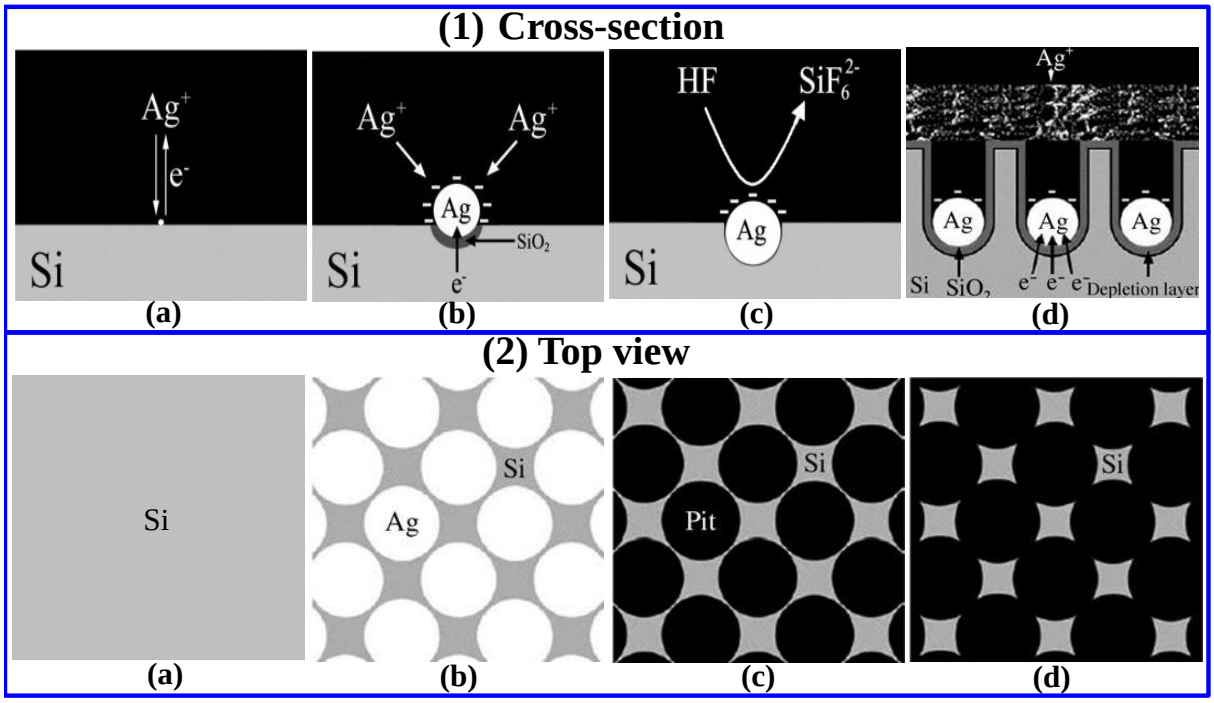

Figure 2 Schematic representation of the formation of vertically aligned SiNSs on a Si surface in aqueous $HF/AgNO_3$ solution (Copy from [1][2]): (1) Cross-section and (2) Top view. (a) Ag nucleation, (b) Ag particle growth and induced local excess oxidation, (c) Ag-induced pit, and (d) formation of SiNSs due to further sinking of the Ag particles.

The working principle is the galvanic displacement reaction. Simultaneous electrochemical processes occur on the Si surface exposed in $HF/AgNO_3$ solution. Surface Si atoms are oxidized (**Equation (2)**) and supply the electrons for the Ag^+ reduction (**Equation (1)**). The reaction of Si atoms oxidization occurs underneath Ag nanoparticles.

$$Ag^+ + e_{VB}^- \rightarrow Ag^0 \quad (1)$$

$$Si^0 + 2H_2O \rightarrow SiO_2 + 4H^+ + 4e^- \quad (2\text{-a})$$

$$SiO_2 + 6HF \rightarrow H_2SiF_6 + 2H_2O \quad (2\text{-b})$$

Figure 2 presents the formation of vertically aligned SiNSs on a Si surface in aqueous $HF/AgNO_3$ solution. In the initial stage of Ag deposition, Ag^+ ions in the vicinity of the silicon surface capture electrons from the valence band (VB) of Si (show in **photography (a)**). The Ag nuclei grow into larger particles as more Ag ions are deposited (show in **photography (b)**). As many electrons required by Ag ions reduce, local oxidation occurs and SiO_2 is produced underneath these Ag nanoparticles. Shallow pits immediately form underneath the Ag nanoparticles, due to the etching of SiO_2 by the HF solution. Then, Ag particles enter the forming pits (show in **photography (c)**). The subsequent chemical dissolution of thin Si pore walls enlarges the pores and lead to merging of nearest-neighbor pores. Finally, after sufficient etching time, a high density of one-dimensional Si nanostructure remains on the silicon surface (show in **photography (d)**).

A.3. Composition of YPD and YNB

A.3.1. Yeast Nitrogen Base (YNB)

Yeast Nitrogen Base (YNB), per liter [4]

- Biotin 2 µg
- Calcium pantothenate 400 µg
- Folic acid 2 µg
- Inositol 2000 µg
- Niacin 400 µg
- p-Aminobenzoic acid 200 µg
- Pyridoxine hydrochloride 400 µg
- Riboflavin 200 µg
- Thiamine hydrochloride 400 µg
- Boric acid 500 µg
- Copper sulfate 40 µg
- Potassium iodide 100 µg
- Ferric chloride 200 µg
- Manganese sulfate 400 µg
- Sodium molybdate 200 µg
- Zinc sulfate 400 µg
- Potassium phosphate monobasic 1 g
- Magnesium sulfate 500 mg
- Sodium chloride 100 mg

- Calcium chloride 100 mg
- Final pH 4.5 before addition of Ammonium sulfate (5 g/L)
- Final pH 5.4 after addition of Ammonium sulfate (5 g/L)
- Difco 0919-15 Yeast nitrogen base w/o amino acids 100g
- Difco 0335-15 Yeast nitrogen base w/o amino acids and ammonium sulfate 100g

A.3.2. Yeast Peptone Dextrose (YPD)

- 10 g/L Yeast Extract (BD Bacto)
- 20 g/L Peptone (BD Bacto)
- 20 g/L D-glucose

A.4. LabVIEW Program Guide

A.4.1. How it works globally

The NANOBE project demands to do a certain number of biological analyses. This program calls 10 different operations corresponding to a particular analysis and which occur in the following order:

1) Supernatant: 16µL has to be delivered to ELISA outlet
2) Mix 1: one droplet (Supernatant + CE buffer) of 2µL to CE outlet
3) Wash ELISA: 2µL water droplet is used to wash the path and exported from ELISA outlet
4) Wash CE: 1µL water droplet is used to wash the path and exported from CE outlet
5) Cell lysate: 16µL has to be delivered to ELISA outlet
6) Cell lysate (19^{th}) to Waste: the 19^{th} cell lysate droplet has to be delivered to Waste outlet
7) Mix 2: one droplet (Cell lysate + CE buffer) to CE outlet
8) Total Wash 1: 2µL water droplet is used to wash the path and exported from CE outlet
9) Total Wash 2: 2µL water droplet is used to wash the path and exported from Waste outlet
10) Total Wash 3:1µL water droplet is used to wash the path and exported from ELISA outlet

It is possible to repeat the whole loop in the same order and also to repeat each function.

A.4.2. Starting the program

1) Choose the function by launching *"Launch function"*. The default value of this command is *"Supernatant*" because it is the first function in the NANOBE process.

2) The button '*Use presaved paths*" is needed to put on "*Yes"* (green), which is also the default value for this command.

3) The value of the switch time for electrodes can be changed. The default value is *0.45s*.

4) Pressing the *"Start"* button, the program will automatically launch the process. One can see the indicators *"File corresponding*" (which the path loaded) and *"Total number of sequences"* changing.

5) During the process the value in the indicator *"Current sequence"* is increasing. One step corresponds to a different state of the electrodes (that is to say to a switching step of 0.45s)

A.4.3. End of a Function

1) When the value of the total number of sequences is reached, a *message* appears to the operator asking him or her to *prepare the next function*. It follows the predefined order. For example, at the end of Supernatant operation, the message is "Prepare Mix 1". At the end of Mix 1 operation the message will be "Prepare Wash ELISA" etc. It enables the operator to have time between 2 operations.

2) One can see at the end of each operation the command *"Launch function"* changing automatically and taking the value of the next function in the order (Supernatant is changed automatically into Mix 1)

3) However, to launch the next operation, the operator has to press the button "Start" again.

A.4.4. Pause a Function

At any moment you can put the process on pause.

1) Put the Pause button on "Pause ON" (red). This will fix the process. The default value of this button is "Pause OFF" (green).

2) Then, you can continue the process manually using the buttons “Step by Step”. It will change manually the state of the electrodes. Each function has its own step by step button.

3) To be noted that, it is not possible to use the step by step buttons if the process is not on pause.

4) If the operator wants to restart the automatic process, he or she has to put the pause button on “Pause OFF” and press one time on the corresponding “Step by Step/Restart” button.

A.4.5. Delay times setting

It exist some delay times to loading the sample from the upstream fluidic module to the sample preparation unit, until the related inlet channel of the sample preparation unit is filled. The delay time is depending on several parameters, for example the speed of pumps and the length of capillary connecting between the two modules.

1) One can set the delay time for each operation using the appropriate command.

2) This delay time corresponds to the time of sample loading from the outlet of upstream module to the end of the related Inlet channel of the sample preparation unit. The program will wait before launching the operation.

A.4.6. Pump control

A peristaltic pump (ISM 936-ISMATEC) is controlled for the delivering at the outlets.

1) The pump is started automatically at the right moment for the different periods of delivering.

2) One can see the status of the pump in the program (if it is stopped or started)

3) One can also command the pump.

4) The LEDs blue will be activated during the periods of delivering

References

[1] K. Q. Peng, J. J. Hu, Y. J. Yan, Y. Wu, H. Fang, Y. Xu, S. T. Lee, and J. Zhu, "Fabrication of single-crystalline silicon nanowires by scratching a silicon surface with catalytic metal particles", *Advanced Functional Materials*, vol. 16, pp. 387–394, 2006.

[2] K. Peng, H. Fang, J. Hu, Y. Wu, J. Zhu, Y. Yan, and S. Lee, "Metal-Particle-Induced, Highly Localized Site-Specific Etching of Si and Formation of Single-Crystalline Si Nanowires in Aqueous Fluoride Solution", *Chemistry – A European Journal*, vol. 12, pp. 7942–7947, 2006.

[3] G. Piret, H. Drobecq, Y. Coffinier, O. Melnyk, and R. Boukherroub, "Matrix-Free Laser Desorption/Ionization Mass Spectrometry on Silicon Nanowire Arrays Prepared by Chemical Etching of Crystalline Silicon", *Langmuir*, vol. 26, no. 2, pp. 1354–1361, 2010.

[4] *http://openwetware.org/wiki/Composition_of_Yeast_Nitrogen_Base_(YNB)*.

PUBLICATION

1. **C. Wu**, F. Bendriaa, F. Brunelle, and V. Senez, "Fabrication of AD/DA microfluidic converter using deep reactive ion etching of silicon and low temperature wafer bonding", *Microelectronic Engineering*, vol. 88, pp. 1878–1883, 2011.

2. **C. Wu**, F. Brunelle, M. Harnois, and V. Senez, "Sample preparation unit for online bio-processes monitoring", in *Proceedings of the 15th International Conference on Miniaturized Systems for Chemistry and Life Sciences*, Seattle, Washington, USA, 2011, pp. 2034–2036.

3. **C. Wu**, F. Brunelle, M. Harnois, J. Follet, and V. Senez, "An integrated hybrid microfluidic system for online bioprocesses monitoring: combining electrical lysis and EWOD sample preparation", in *Proceedings of the 25th International Conference on Micro Electro Mechanical Systems*, Paris, France, 2012, pp. 777–780.

4. R. Dufour, **C. Wu**, F. Bendriaa, V. Thomy, and V. Senez, "Analog to Digital mcrofluidic converter", presented at the Proceedings of the 2009 European COMSOL Conference, Milan, Italy, 2009.

Résumé

Ce travail présente la conception, la fabrication et le test d'une unité de préparation d'échantillons utilisant une approche originale combinant les microfluidiques digitale et continue. L'avantage du préconditionnement 'numérique' est d'éviter l'introduction d'un réseau complexe de micro-vannes pour manipuler les échantillons, tandis que le format 'continu' en entrée et sortie de l'unité permet de coupler facilement ce dispositif avec des composants microfluidiques situés en amont et en aval. Nous avons travaillé sur deux procédés de fabrication. Le premier comprend un tricouche PSP (Pyrex-Silicium-Pyrex) pour lequel les interfaces liquide-solide sont de nature hydrophobe. Un procédé original de collage thermoplastique a été optimisé qui est suffisamment générique pour être utilisé dans d'autres procédés MEMS. Cependant, les résultats des caractérisations ont montré que bon nombre des échantillons ne pouvaient pas être manipulés. Pour résoudre ce problème, nous avons développé un procédé bicouche PS (Pyrex-silicium) où les interfaces liquide-solide sont de nature superhydrophobe suite à une nanotexturation du silicium par traitement chimique. Grâce à la faible hystérésis, la résistance de friction et la pollution biologique sont largement réduites ce qui permet la manipulation de liquides complexes. Cette technologie a été employée pour fabriquer une unité microfluidique dédiée à de la préparation d'échantillons issus de bioprocédés à base de levures. Ces échantillons préparés sont ensuite analysés soit par une méthode immuno-enzymatique (ELISA) soit par une analyse par spectrométrie de masse précédée par une étape de séparation par électrophorèse capillaire.

Mots-clés: Microfluidique, Electromouillage sur diélectrique, Unité microfluidique de préparation d'échantillons, Superhydrophobe, Bioprocédés

Abstract

This work presents the concept, fabrication technology and characterization of a sample preparation unit using an original approach coupling channel-based continuous and electrowetting-on-dielectric (EWOD)-based digital microfluidics. The major advantage of 'digital' is the accurate control of multiple reagents without the need of a complex network of microvalves, while unprocessed and reprocessed 'continuous' format is ideal for coupling with upstream and downstream microfluidic devices. We have developed two generations. In our first work, a three layers PSP (Pyrex-Silicon-Pyrex) configuration with hydrophobic liquid-solid interfaces was employed. An original adhesive wafer bonding technique has been optimized that is sufficiently generic to be used in diverse MEMS processes. However, the preliminary characterization results have shown that most real samples used in bioprocessing could not be handled by this first prototype. To address this issue, we have developed a bilayer PS (Pyrex-Silicon) configuration with superhydrophobic liquid-solid interfaces made by chemical nanotexturation of silicon. Thanks to the low contact angle hysteresis of this superhydrophobic surface, the friction resistance and bio-adsorption on the surface were largely reduced allowing transport of real complex liquids. Finally, this prototype has been successfully used for preconditioning samples taken from a yeast bio-reactor and then delivered to analytical modules either an enzyme-linked immunosorbent assay (ELISA) or a capillary electrophoresis (CE) device coupled with a mass spectrometry (MS).

Keywords: Microfluidic, Electrowetting on Dielectric, Sample preparation unit, Superhydrophobic, Bioprocesses monitoring